DETAILED DESIGN

RANKINE-CYCLE POWER SYSTEM WITH ORGANIC-BASED WORKING FLUID AND RECIPROCATING EXPANDER FOR AUTOMOBILE PROPULSION

VOLUME II – APPENDICES

Prepared for

Division of Advanced Automotive Power Systems Development
Environmental Protection Agency
Ann Arbor, Michigan

Prepared by

Thermo Electron Corporation
Research and Development Center
101 First Avenue
Waltham, Massachusetts

Report No. 4134-71-72

DETAILED DESIGN

RANKINE-CYCLE POWER SYSTEM WITH ORGANIC-BASED WORKING FLUID AND RECIPROCATING EXPANDER FOR AUTOMOBILE PROPULSION

Edited by:

Dean T. Morgan, Program Manager

Prepared by: Rankine Power Systems Department

Edward F. Doyle, Manager
Robert J. Raymond, Expander Development
Ravinder Sakhuja, Heat Exchanger Development
Herb Soini, System Integration and Packaging
William Noe, Controls Development
Chi Chung Wang, Performance Analysis
Andrew Vasilakis, Combustor Development
Luco DiNanno, Feedpump and Rotary Shaft Seal Development

Thermo Electron Corporation
Research and Development Center
85 First Avenue
Waltham, Massachusetts 02154

Prepared for:

Division of Advanced Automotive Power System Development
Environmental Protection Agency
Ann Arbor, Michigan

Contract No. EHS 70-102

Work Performed: May 6, 1970 - November 5, 1971

Report Issued: May 5, 1972

TABLE OF CONTENTS

TABLE OF CONTENTS (continued)

TABLE OF CONTENTS (continued)

APPENDIX I

ANALYSIS OF
MECHANICAL VALVE GEAR

A. MASS AND INERTIA OF VALVE COMPONENTS

1. Inner Valve

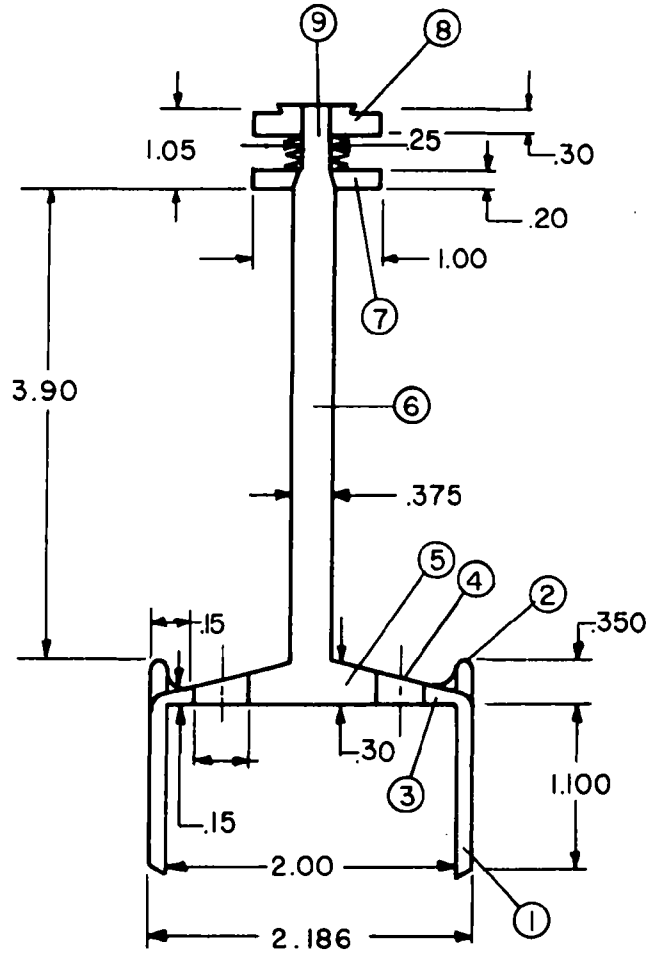

Volumes

1. $= (\pi/4)\ (2.186^2 - 2.00^2)(1.1) = .67266\ in^3$

2. $= (\pi/4)\ (2.186^2 - 1.886^2)(.35) = .33580\ in^3$

3. $= (\pi/4)\ (2.00^2 - 1.00^2)(.15) = .35343\ in^3$

4. $= -(4)\ (\pi/4)(.50^2)(.20) = -.15708\ in^3$

5. $= (\pi/4)(1.00^2)(.25)$ $= .19635\ in^3$

6. $= (\pi/4)(.375)^2(3.90)$ $= .43074\ in^3$

7. $= (\pi/4)(1.00^2 - .25^2)(.20)$ $= .14726\ in^3$

8. $= (\pi/4)(1.00^2 - .25^2)(.30)$ $= .22089\ in^3$

9. $= (\pi/4)(.25^2)(1.05)$ $= .05154\ in^3$

Total Volume = $2.25159\ in^3$

Mass = $(.283)(2.25159)$

$= .6372$ lbm

2. Outer Valve

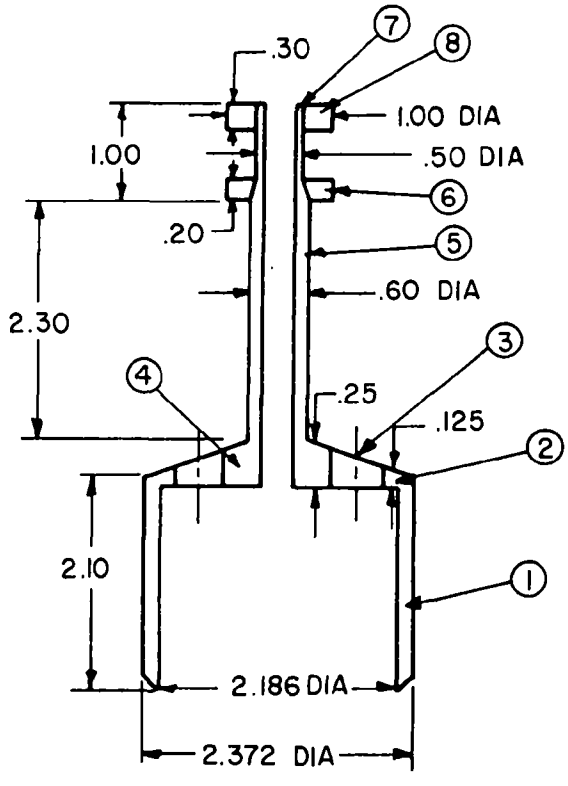

Volumes

1. $= (\pi/4)(2.372^2 - 2.186^2)(2.10) = 1.3983\ in^3$

2. $= (\pi/4)(2.00^2 - 1.00^2)(.125) = .2945\ in^3$

3. $= -(\pi/4)\ 4\ (.50)^2(.20) = -.1571\ in^3$

4. $= (\pi/4)(1.00^2 - .38^2)(.25) = .1680\ in^3$

5. $= (\pi/4)(.60^2 - .38^2)(2.30) = .3895\ in^3$

6. $= (\pi/4)(1.00^2 - .38^2)(.20) = .1344\ in^3$

7. $= (\pi/4)(.50^2 - .38^2)(1.00) = .0829\ in^3$

8. $= (\pi/4)(1.00^2 - .38^2)(.30) = .2016\ in^3$

Total volume = $2.5121\ in^3$

Mass = .7109 lbm

3. Cam Follower

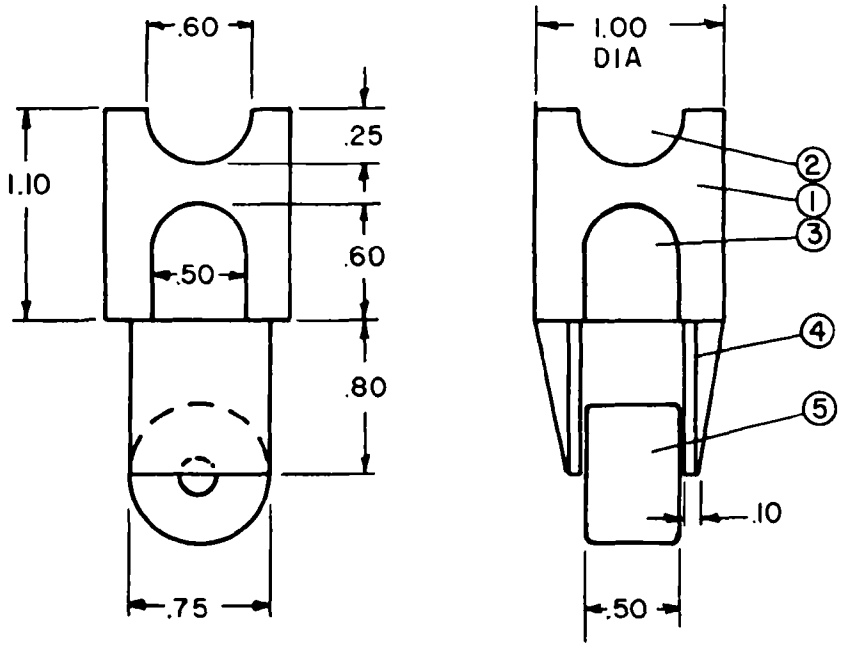

Volumes

1.	$= (\pi/4)(1.00)^2(1.1)$	$= .8639\ in^3$
2.	$= -(\pi/2)(.25)^3(4/3)$	$= -.03273\ in^3$
3.	$= -(\pi/4)(.5)^2(.35) - (\pi/2)(.25)^3(4/3)$	$= -0.10145\ in^3$
4.	$= (2)(.10)(.80)(.75)$	$= .1200\ in^3$
5.	$= (\pi/4)(.75)^2(.50)$	$= .22089\ in^3$

Total Volume = $1.0706\ in^3$

Mass = .3030 lbm

4. Springs

Two springs, 0.25 in.wire diameter 1.50 in spring O. D.

0.187 in. wire diameter, 1.00 in. spring O. D.

Approximately 6 coils in each spring

Volume

$$= 6\left[(1.5\pi)\left(\frac{\pi}{4}\right)(0.25)^2 + (\pi)\left(\frac{\pi}{4}\right)(0.187)^2\right]$$

$$= 1.9057\ in^3$$

Mass = .5393 lbm

5. Push Rod Adjustor and Ends

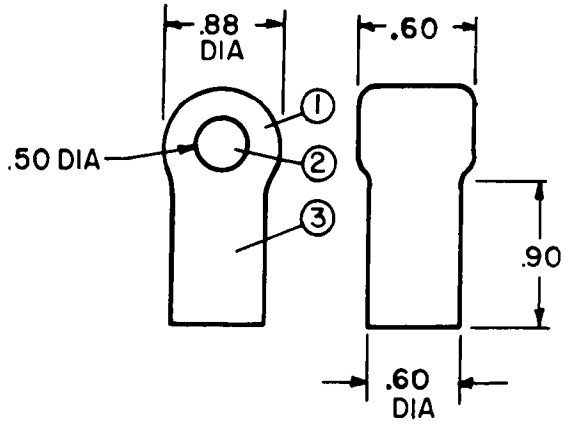

Volumes

1. $= (\pi/4)(.88)^2(.60)$ $=$ $.3649\ in^3$

2. (P_{in}) $= (\pi/4)(.50)^2(1.2)$ $=$ $.2356\ in^3$

3. $= (\pi/4)(.60)^2(.90)$ $=$ $.2543\ in^3$

Total Volume $= .855\ in^3$

Mass $= .242$ lbm

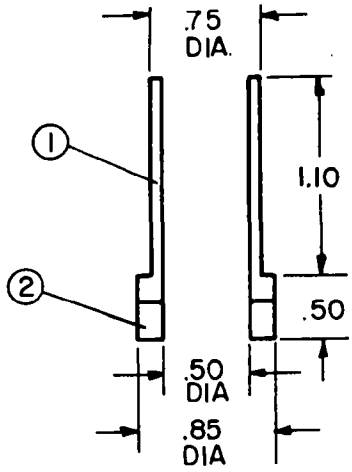

Volumes

1. $= (\pi/4)(.75^2 - .50^2)(1.10) = .2700 \text{ in}^3$

2. $= (\pi/4)(.85^2 - .50^2)(.50) = .1856 \text{ in}^3$

Total Volume = $.4556 \text{ in}^3$

Mass = .1289 lbm

6. Valve Spring Retainers

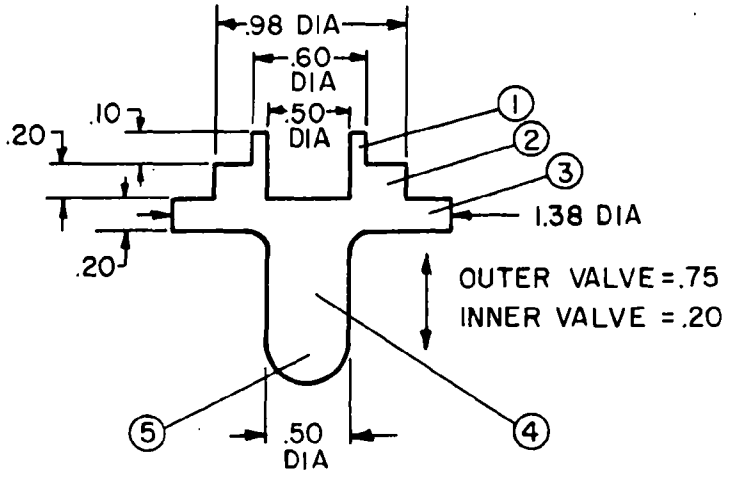

a. For Inner Valve

Volumes

1. $= (\pi/4)(.60^2 - .50^2)(.10) = .00864 \text{ in}^3$

2. $= (\pi/4)(.98^2 - .50^2)(.20) = .11159 \text{ in}^3$

3. $= (\pi/4)(1.38^2)(.20) = .29914 \text{ in}^3$

4. $= (\pi/4)(.50)^2(.20) = .03927 \text{ in}^3$

5. $= (\pi/4)(.25)^3(4/3) = .03272 \text{ in}^3$

Total Volume = $.4914 \text{ in}^3$

Mass = .1391 lbm

b. For Outer Valve

Volumes

1. = .00864 in^3

2. = .11159 in^3

3. = .29914 in^3

4. = $(\pi/4)(.50)^2(.75)$ = .11045 in^3

5. = .03272 in^3

Total Volume = .5625 in^3

Mass = .1592 lbm

7. Push Rods

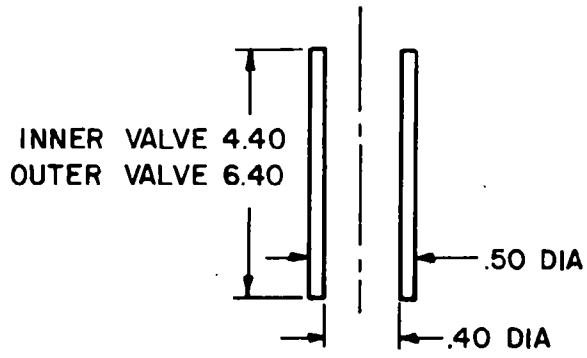

(a) For Inner Valve

Volume = $(\pi/4)(.50^2 - .40^2)(4.40)$ = .3110 in^3

Mass = .088 lbm

(b) For Outer Valve

Volume = $(\pi/4)(.50^2 - .60^2)(6.40)$ = .4524 in^3

Mass = .128 lbm

8. Rockers

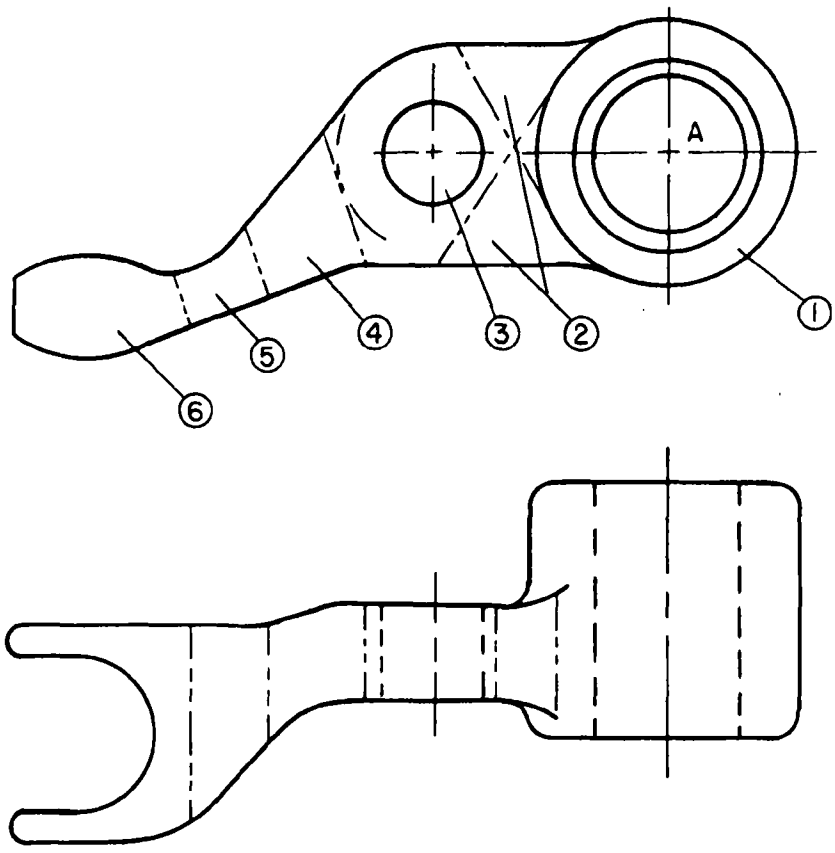

Second Moment of Inertia about A:

$$1.\ I = \frac{\pi}{2}\ \rho L \left[R_o^4 - R_i^4\right] = \left(\frac{\pi}{2}\right)(0.283)(1.3)\left[(0.75)^4 - (0.38)^4\right]$$

$$= .1708\ \text{in}^2\ \text{lbm}$$

$$2.\ I = (M)(d^2) = \left[\frac{(0.3)(0.5)}{2}\right](2)\ (0.50)(0.283)(0.9)^2$$

$$= .0172\ \text{in}^2 - \text{lbm}$$

3. $I = \left[\pi (.5)^2 \frac{(.5)(.283)(.5^2)}{2} - \pi (.25)^2 \frac{(.5)(.283)(.25)^2}{2} \right]$

$+ (1.2^2)(\pi)(.5^2 - .25^2)(.283)(.5)$

$= .1330 \text{ in}^2 - \text{lbm}$

4. $I = (.3)(.55)(.5)(.283)(1.85)^2$

$= .0799 \text{ in}^2 - \text{lbm}$

5. $I = (.5)(.3)(.5)(.283)(2.3)^2$

$= .1347 \text{ in}^2 - \text{lbm}$

6. $I = (.9)(.4)(.3)(2)(0.283)(3.2^2)$

$= .6260 \text{ in}^2 - \text{lbm}$

Total inertia about A:

$= 1.162 \text{ in}^2 - \text{lbm}$

9. Effective Mass at Cam

a. Due to valve

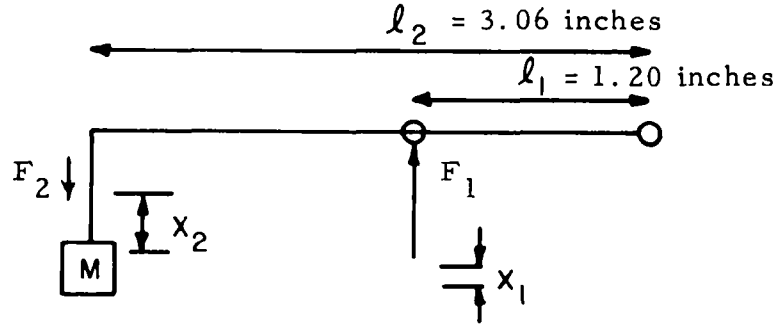

$$X_2 = \left(\frac{\ell_2}{\ell_1}\right) X_1$$

$$\ddot{X}_2 = \left(\frac{\ell_2}{\ell_1}\right) \ddot{X}_1$$

$$F_2 = M\ddot{X}_2 = M\left(\frac{\ell_2}{\ell_1}\right) \ddot{X}_1$$

$$F_2 \ell_2 = F_1 \ell_1$$

$$F_1 = F_2\left(\frac{\ell_2}{\ell_1}\right) = M\left(\frac{\ell_2}{\ell_1}\right)^2 \ddot{X}_1$$

Therefore, at Cam

$$M_{eff} = M_{valve}\left(\frac{\ell_2}{\ell_1}\right)^2$$

b. Due to Rocker Arm

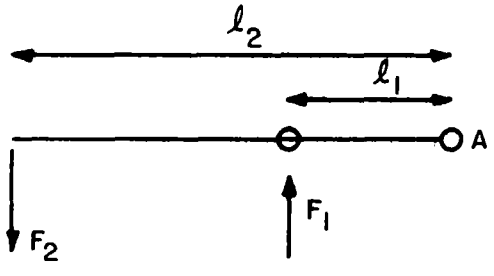

$$\tau = I\alpha$$

$$\tau = F_1 \ell_1 , \quad \ddot{X}_1 = \ell_1 \alpha$$

$$F_1 \ell_1 = \frac{I \ddot{X}_1}{\ell_1}$$

$$F_1 = \frac{I}{\ell_1^2} \ddot{X}_1$$

Therefore at Cam

$$M_{eff} = \frac{I}{\ell_1^2}$$

TABLE I-1

CAM AND RAMP CHARACTERISTICS FOR DOUBLE INLET VALVE

Cam θ, Degrees	Event θ Degrees	V x 10^{+4} in/ Degree^2	V x 10^{+3} in/ Degree^2	Cam θ X x 10^3, in.	Valve Lift, in	Cam θ, Degrees	Event θ Degrees	A x 10^{+4} in/ Degree^2	V x 10^{+3} in/ Degree^2	Cam θ X x 10^{+3}, in.	Valve Lift, in.
0		.00	.00	.00	0	46	31	-.40	3.723	101.109	.240
1		.20	.0075	.0025	0	47	32	-.44	3.681	104.811	
2		.50	.0425	.0256	0	48	33	-.47	3.636	108.469	.259
3		.77	.1058	.0981	0	49	34	-.49	3.588	112.081	
4		.96	.1940	.247	0	50	35	-.51	3.538	115.643	.277
5		1.02	.2935	.4901	0	51	36	-.53	3.486	119.155	
6		1.05	.3973	.8353	0	52	37	-.55	3.432	122.613	.295
7		1.02	.5010	1.285	0	53	38	-.57	3.376	126.017	
8		.96	.6005	1.836	0	54	39	-.60	3.317	129.363	.312
9		.70	.6840	2.480	0	55	40	-.63	3.256	132.649	
10		.30	.7350	3.192	0	56	41	-.655	3.191	135.873	.329
11		.00	.7500	3.936	0	57	42	-.68	3.125	139.031	
12		.00	.7500	4.686	0	58	43	-.705	3.055	142.120	.345
13		.00	.7500	5.436	0	59	44	-.73	2.984	145.140	
14		.00	.7500	6.186	0	60	45	-.755	2.909	148.086	.360
15	0	.00	.7500	6.936	0	61	46	-.78	2.833	150.957	
16	1	.20	.7600	7.691	.0019	62	47	-.80	2.754	153.750	.374
17	2	1.00	.8200	8.481	.0039	63	48	-.825	2.672	156.463	
18	3	1.70	.955	9.369	.0062	64	49	-.85	2.589	159.093	.388
19	4	2.20	1.150	10.42	.0089	65	50	-.875	2.502	161.639	
20	5	2.50	1.385	11.689	.0121	66	51	-.90	2.414	164.097	.401
21	6	2.68	1.644	13.203	.0160	67	52	-.92	2.323	166.465	
22	7	2.78	1.917	14.984	.0205	68	53	-.94	2.230	168.741	.413
23	8	2.81	2.197	17.040	.0258	69	54	-.96	2.135	170.923	
24	9	2.82	2.478	19.378	.0317	70	55	-.98	2.038	173.009	.424
25	10	2.80	2.759	21.996	.0384	71	56	-1.00	1.939	175.000	
26	11	2.70	3.034	24.893	.0458	72	57	-1.00	1.839	176.885	.433
27	12	2.52	3.295	28.057	.0539	73	58	-1.01	1.738	178.673	
28	13	2.16	3.529	31.469	.0626	74	59	-1.01	1.637	180.361	.442
29	14	1.50	3.712	35.090	.0718	75	60	-1.01	1.536	181.947	
30	15	0.85	3.830	38.860	.0814	76	61	-1.02	1.435	183.433	.450
31	16	.45	3.895	42.722	.0913	77	62	-1.02	1.333	184.816	
32	17	.22	3.928	46.634	.1012	78	63	-1.02	1.231	186.098	.457
33	18	.12	3.945	50.570	.1113	79	64	-1.02	1.129	187.277	
34	19	.05	3.954	54.519	.1213	80	65	-1.02	1.027	188.355	.463
35	20	0	3.956	58.474	.131	81	66	-1.02	.925	189.330	
36	21	-.05	3.954	62.429	.142	82	67	-1.02	.823	190.204	.467
37	22	-.08	3.947	66.379	.152	83	68	-1.02	.721	190.975	
38	23	-.12	3.937	70.321	.162	84	69	-1.03	.618	191.644	.471
39	24	-.16	3.923	74.251	.172	85	70	-1.03	.515	192.211	
40	25	-.20	3.905	78.165	.182	86	71	-1.03	.412	192.674	.474
41	26	-.23	3.884	82.059	.192	87	72	-1.03	.309	193.035	
42	27	-.27	3.859	85.930	.201	88	73	-1.03	.206	193.292	.475
43	28	-.31	3.830	89.774		89	74	-1.03	.103	193.447	
44	29	-.34	3.797	93.588	.221	90	75	-1.03	.000	193.498	.476
45	30	-.37	3.762	97.367							

c. For Outer Valve Train

$$M_{eff} = .7109(2.55)^2 + .3030 + .5393 + .242 + .1289 + .1592 + .128 + 1.162\left(\frac{1}{1.2^2}\right)$$

(Outer Valve; Cam Follower; Springs; Push Rod Adjuster; Push Rod End; Valve Spring Retainer; Push Rod; Rocker Arm)

$$= 6.93 \text{ lbm}$$

d. Inner Valve Train

$$M_{eff} = .6372(2.55^2) + .3030 + .5393 + .242 + .1289 + .1391 + .088 + 1.162\left(\frac{1}{1.2^2}\right)$$

$$= 6.29 \text{ lbm}$$

B. PRESSURE FORCES ON VALVES

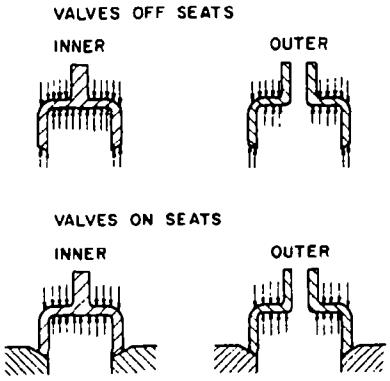

The inlet vapor pressure is 700 psia. For estimating the pressure forces, 700 psi is assumed across the valves to allow for the highest possible loading on the valve drive.

1. Pressure Forces on Valves when Off Their Seats

$$\text{Outer valve} = (.60^2 - .38^2)(\pi/4)(700) = 118.53 \text{ lbf}$$

$$\text{Inner valve} = (.38^2)(\pi/4)(700) = 79.39 \text{ lbf}$$

2. Pressure Forces on Valves Whilst on Their Seats

$$\text{Outer Valve} = (\pi/4)(2.372^2 - 2.186^2)(700) - 118.53$$

$$= 347.57 \text{ lbf}$$

$$\text{Inner Valve} = (\pi/4)(2.186^2 - 2.000^2)(700) - 79.39$$

$$= 348.67 \text{ lbf}$$

C. CAM DESIGN CHARACTERISTICS AND ESTIMATE OF SPRING SIZES

1. Cam Design Characteristics

The cam and ramp characteristics are summarized in Table I-1 for the cam-driven valves.

$$\frac{1}{\rho_{cr}} = \frac{1}{R}\left(\frac{A_{max}}{R} - 1\right)$$

For ease of cam manufacture, ρ_{cr} should be negative or ∞.

If ρ_{cr} were allowed to become positive by increasing the forward acceleration, it would mean a concave radius on the cam, increasing the cost of manufacture considerably. This effectively sets an upper limit to A_{max}.

$$\rho_{cr} = \infty \text{ if } A_{max} = R$$

Thus, the upper limit of

$$A_{max} = \frac{1.0 \text{ in.}}{(57.3)^2} = 3.046 \times 10^{-4} \text{ in./o}^2.$$

From the cam curve, $A_{max} = 2.82 \times 10^{-4}$ in./o^2

The value of ρ_{cr} for the actual cam curve is:

$$\frac{1}{\rho_{cr}} = 1\left[\left(\frac{2.82 \times 10^{-4}}{1}(57.3)^2 - 1\right)\right]$$

$$\rho_{cr} = -13.5 \text{ inches}$$

The value of ρ corresponding to A_{min} is:

$$\rho_{min} = \frac{(R + L)^2}{R + L + A_{min}}$$

$$= \frac{(1.0 + 0.20)^2}{1.0 + 0.2 - (-1.03 \times 10^{-4} (57.3)^2)}$$

$$= .936 \text{ inch}$$

Since $r < .936 < R$, ρ_{min} is satisfactory where r is the cam roller radius, the maximum cam angle, ϕ_{max}, should be less than 30°.

$$\phi_{max} = \tan^{-1} \left(\frac{2}{2R + L}\right) (V_{max})$$

From cam curve, $V_{max} = 3.956 \times 10^{-3}$ in/°

$$\phi_{max} = \tan^{-1} \left(\frac{2}{2.0 + 2.0}\right) (3.956 \times 10^{-3}) (57.3)$$

$$= 11.64°$$

Therefore $\phi < 30°$.

2. Estimate of Spring Size

$$F_{spring, max} = \text{Pressure Force} + [(M_{eff}) | A_{min} | (RPM^2)]$$

Pressure Forces

Outer Valve = 118.53 lbf

Inner Valve = 79.39 lbf

Mass

Outer Valve Train = 6.93 lbm

Inner Valve Train = 6.39 lbm

Taking the case of the outer valve train (as this will require higher spring force) at an expander speed of 1800 RPM:

$$F_{spring, max} = 2.55 (118.53) + 6.93 \left[\frac{(1800)(360)}{60}\right]^2 \left[\frac{1.03 \times 10^{-4}}{(12)(32.2)}\right]$$

$$= 302.3 + 215.5$$

$$= 517.8 \text{ lbf}$$

$$F_{spring, min} = 302.3 \text{ lbf}$$

Spring force required ≈ 302.3 to 517.8 lbf

An amount of overforce is also required to ensure that the valve train follows the cam. The springs in the drawing of Figure 5.15 are steel and have the following characteristics:

Outer spring rate = 700 lbf/inch

Inner spring rate = 500 lbf/inch

Lift = .20 inch

Compression at Zero Cam Lift = .30 inch

Spring travel is from .30 to .50 inch relative to uncompressed spring position. This range is within the allowable spring travel range. The spring force varies from 360 to 600 lbf and gives the necessary overforce. There is space available for slightly more powerful springs if follower jumping is observed.

D. FORCES AND STRESSES IN THE SYSTEM

1. Maximum Cam Stress

The maximum cam stress occurs when the valves are lifted off their seats. The force due to pressure forces on the valve is:

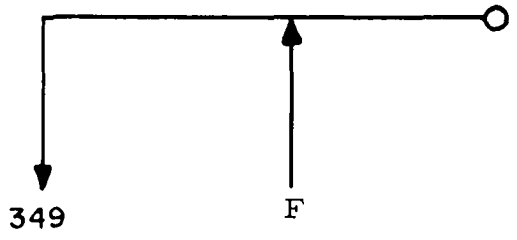

$F = (2.55)(349)$ lbf.

The force on the cam will have the spring force added to the pressure force:

$$F_{cam} = (2.55)(349) + 360$$

$$= 1250 \text{ lbf.}$$

$$\text{Hertz Stress} = \left\{ \frac{(.35)(1250)}{.5} \left(\frac{\frac{1}{R} + \frac{1}{r}}{\frac{1}{E_{cam}} + \frac{1}{E_{roller}}} \right) \right\}^{1/2}$$

Cam and Roller are of steel. Cam radius = R at pick-up position. Thus,

$$\text{Hertz Stress} = \left(\frac{\frac{(.35)(1250)}{.5} \quad \frac{1}{1.0} + \frac{1}{.5}}{\frac{1}{15 \times 10^6}} \right)^{1/2}$$

$$= 218,322 \text{ lbf/in}^2.$$

Max. allowable stress = 250,000 lbf.

2. Buckling Length of Push Rods

Maximum force in push rods = 890 lbf.

$$P_{crit} = \frac{\pi^2 EI}{\ell^2}$$

$$\ell = \left(\frac{\pi^2 EI}{P_{crit}} \right)^{1/2}$$

$$= \left[\frac{\pi^2 (30 \times 10^6)}{890} \frac{\pi}{64} (.5^4 - .4^4) \right]^{1/2}$$

$$= 24.5 \text{ inches}$$

The maximum push rod length is approximately 7 inches.

3. Bending Stress in the Rocker Arm

Maximum bending moment is where the push rod pivots on the rocker arm.

Bending moment = 349 x 2

= 700 inches lbf.

$\sigma_x = \frac{My}{I}$; $I = \frac{bh^3}{12} - \frac{bd^3}{12}$; h = 2y; d = diam. of push rod pin hole.

$$\sigma_x = \frac{(700)(.55)}{\frac{.5(1.1)^3}{12} - \frac{5.5^3}{12}}$$

$$= 7662 \text{ lbf/in}^2$$

The recommended maximum bending stress in the extreme fibre for a machine part subject to alternating loads is 15000 lbf/in^2.

Stresses due to maximum forward acceleration are extremely low due to the pressure force which virtually accelerates the valve by itself reducing the force throughout the remainder of the valve train.

4. Maximum Stress in Valve Stems

Maximum Force ≃ 350 lbf.

Inner Valve:

$$\sigma = \frac{1}{\pi/4\ (.25)^2} \times 350 = 7130 \text{ lbf/in}^2.$$

Outer Valve:

$$\sigma = \frac{1}{\pi/4\ (.60^2 - .50^2)} \times 350 = 4051 \text{ lbf/in}^2$$

5. Stresses at Valve Stem to "Bell" Transition

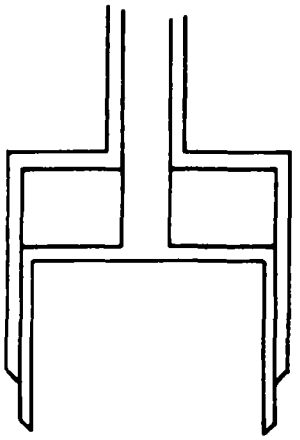

Treat these as a circular plate with the central hole clamped and supported. The outer edge R is prevented from rotation and is supporting a total load F evenly distributed around its periphery.

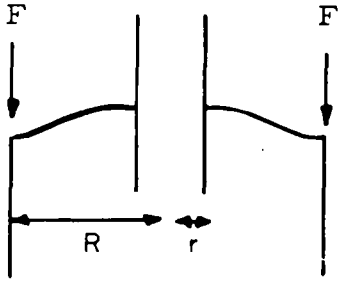

$$W_{max} = \mu \left(\frac{PR^2}{Et^2}\right)$$

$$S_{max} = \nu \left(\frac{P}{t^2}\right)$$

The coefficients μ and ν are obtained from tables as a function of R/r.[1]

a. Outer Valve

$2r = .600$; $2R = 2.372$; $R/r \simeq 4.80$;

$\mu = .11$; $\nu = 1.1$;

Max. force = 350 lbf; $S_{max} = 10,000$ psi

$$10000 = \frac{(1.1)(350)}{t_{min}^2}$$

$t_{min} = .196$ inch

b. Inner Valve

$2r = .38$; $2R = 2.186$; $R/r = 5.76 = .12\nu = 1.20$;

Max. force = 350 lbf; S_{max} use = 10,000 psi

$\mu = 0.12$ $r = 1.2$

$$10000 = \frac{(1.2)(350)}{t^2}$$

$t_{min} = .205$ inch

The stress varies across the transition as illustrated below:

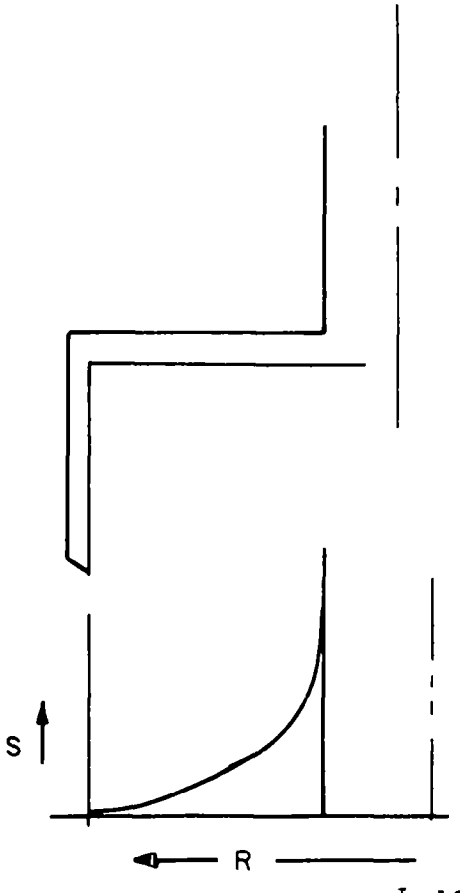

The maximum stress occurs at the stem with the stress decreasing exponentially with distance from the stem. Hence, at least .200 inch thickness is required at the stem, but the thickness can be reduced and holes can be used away from the stem as illustrated below:

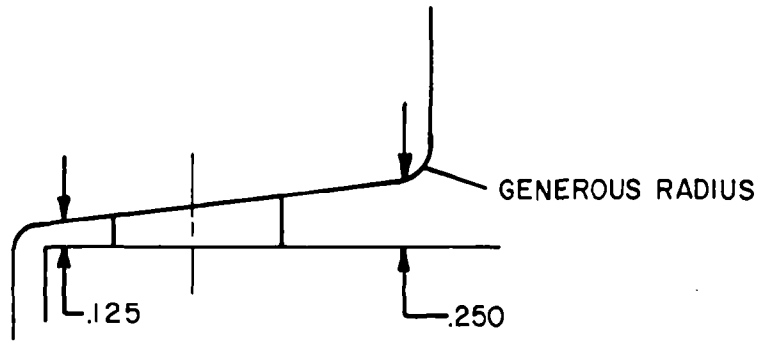

6. Tolerances and System Set-up, Valve Stem Leakage

a. Valve Stem Leakage

From analysis of leakage by the valve stems, a diametral clearance of .0003 inch results in a leakage of 15 lbm/hr, which is acceptable.

b. Tolerance on Inner Valve Stem Where Outer Valve Stem is in Collets

The tolerance on the inner valve stem must be increased at this point from .0003 to .002 inch so that compression of the outer stem by the cones on the collets does not lock the two stems together.

c. Clearance Between Rocker Arm and Valve Stems

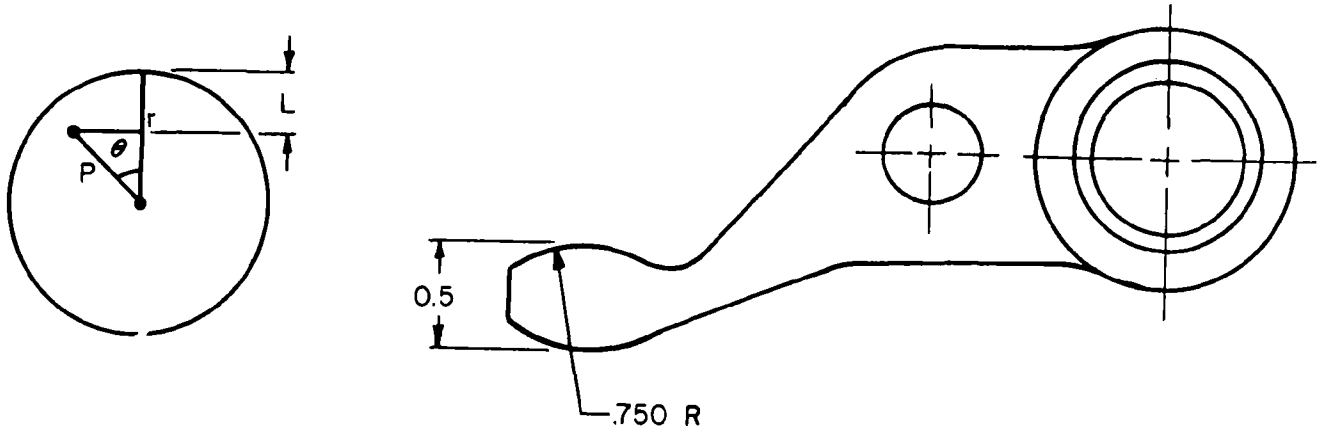

Length of rocker arm = 3.2 inches

Valve travel ≈ .50 inch

Angle moved through by arm ≈ $\frac{.50}{3.2}$ radius

$= 8.95° \approx 9°$

$\phi = \pm 4.5°$ if center ϕ = position at center of travel of valve.

$h = r - p \cos \phi = \pm .00154$

Clearance required = 2h

$= \pm .00308$ inch minimum

REFERENCES FOR APPENDIX I

1. Roark, R. J., Formulas for Stress and Strain, 3rd Ed., McGraw-Hill Book Company, Inc., New York, N. Y., 1954.

APPENDIX II

FIVE-CYLINDER AXIAL FEEDPUMP

A. INTRODUCTION

The conceptual design report of June 1970 [1] recommended the following design features of the feedpump in an organic reciprocating Rankine-cycle engine for automotive applications:

- The pump should be a piston type because of the high discharge pressure and high efficiency requirements.

  The pump should be variable displacement. Although pumping work at the system design point represents only about 5% of the expander output, the pump work at high shaft speeds and low expander power output can easily exceed the required road load power if a fixed displacement pump is used. This power loss would represent a severe system efficiency penalty and a variable-displacement pump must be used.

- At least five cylinders are needed to prevent cavitation of the intake flow in the suction line due to pressure pulsations.

- A wobble plate design is preferred from the standpoints of packaging, weight and vibration.

- The variable displacement control should be directly actuated from the driven foot pedal. This control would, of course, interrelate with the expander speed sensor and the maximum intake ratio control. (This control concept was subsequently changed.) The axial feedpump designed and tested in the execution of this phase of the project is a prototype component incorporating the above features as far as practically possible.

B. FEEDPUMP DESIGN

1. Required Performance

The performance initially required from the feedpump is given below:

Fluid: Thiophene

Pressure Differential: 600 psi

Maximum Flow: 16.2 gpm

Speed range for maximum flow: 800 - 2000 rpm

Displacement: 0 - 100% variation over speed range

Subsequently, this performance requirement was modified to reflect the change of working fluid from Thiophene to Fluorinol-85 and vehicle performance specifications from an intermediate to a full size sedan. At the time of these changes, the test pump had already been fabricated. With Fluorinol-85, the volume flow rate is less so that the test pump is oversized for this fluid.

Overall efficiency on the order of 75 - 80% was an objective, along with a minimum subcooling requirement.

2. Conceptual Design

The conceptual design study[1] recommended the use of a diesel injection-type pump employing helical undercuts in rotatable pistons to effect the variable displacement. Early study on this project showed that this design would be costly due to the extremely small diametral clearances necessary to limit blowby leakage. As seen in Figure II-1, piston rings are not adaptable to the helical undercut type of piston; thus, clearance sealing must be employed on the

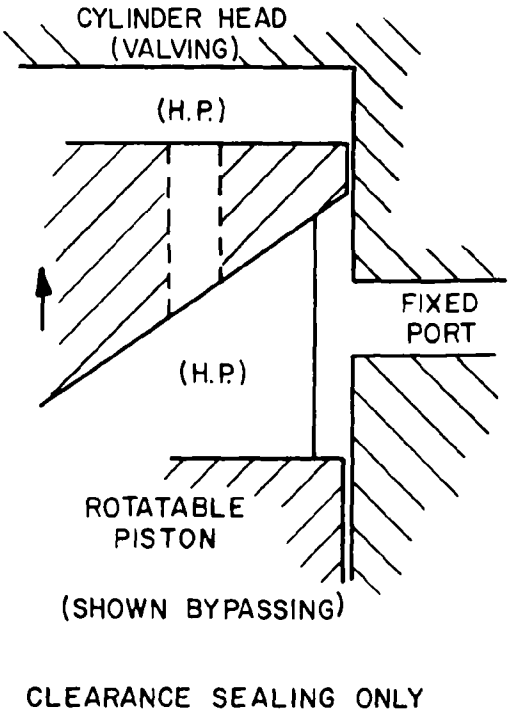

Figure II-1. Rotatable Undercut Piston.

pistons. An estimate of fluid leakage through an annular slit representing the piston-cylinder geometry from Bird[1] gives:

$$Q = \frac{2}{3} \frac{(\Delta P)\, B^3 W}{\mu L},$$

where Q = volumetric leakage rate

ΔP = pressure drop across slit

$2B$ = radial clearance of slit

W = width of slit

L = length of slit

μ = fluid viscosity

Using a Weatherhead hydraulic pump as a check, the above formula predicts 2% leakage past the piston of that pump when it pumps hydraulic oil with a viscosity of 20 cp at 3000 psi. This leakage rate is reasonable and was consistent with the Weatherhead pump performance.

For thiophene, $\mu_{Cp} \approx \frac{1}{75} \mu_{oil}$, and the calculated leakage rate is presented in Table II-1 as a function of radial clearance. These leakage rates are based on a leak path approximately 0.4 inch long and a piston diameter of 1.75 inches. The small clearance required for reasonable leakage is not acceptable.

3. Test Pump Design

Having rejected the rotating undercut piston as a means of achieving variable displacement, the selection of an alternative means was the first step in the test pump design. Partial delivery and variable stroke were both considered at some length. The partial

TABLE II-1

CALCULATED PUMP BLOWBY LEAKAGE RATES
AS FUNCTION OF RADIAL PISTON CLEARANCE

Radial Clearance (in)	Leakage (gpm)	Fraction of Pump Rate (%)
0.001	16.	≈ 100.
0.0005	2.	13.
0.00025	0.25	1.5

delivery technique has the simplicity of a constant stroke motion, but produces noticeable pressure fluctuations in the discharge manifold. Variable stroke can be achieved in a wobble plate pump by varying the angle of the wobble plate. This invariably means that the wobble plate does not rotate, but that the pistons and cylinders do, necessitating a wear plate cylinder head with a sliding seal between the intake and exhaust ports. Due to the low viscosity of the thiophene, this type of seal was considered impractical, since the leakage would be high and the efficiency would be low. Moreover, the appreciable force required to vary the wobble plate angle was deemed excessive for driver foot pedal control of the pump displacement.

The partial delivery variable displacement concept was thus adopted as the design. This meant that the piston stroke was constant, and that only a part of the piston displacement was delivered to the exhaust port through the exhaust valve. The remainder of the displacement would either be returned internally to the pump intake, or be delivered through a bypass valve or port to a low-pressure line (such as the condenser) outside the pump. If the undelivered displacement was returned to the pump intake, an internal, closed flow loop would exist within the pump when the engine power requirement was small. Since the pump, closely coupled to the expander, would be warm relative to the working fluid, the fluid in this closed loop would be heated, resulting in cavitation and deterioration in pump performance. Thus, the bypass flow for the test pump was not returned internally in the pump, and an external bypass flow was used for handling undelivered displacement.

The complete upstroke of the piston is comprised of two parts: a delivery or pumping part, and a bypass part. The order in which pumping takes place is significant. Pumping from the bottom dead center (BDC) piston position means that pumping starts at zero piston velocity. If, on the other hand, the action is first to bypass and then to pump, the pumping is initiated at some finite piston velocity, with a resultant rapid acceleration of the fluid to be pumped. This rapid acceleration is only produced by very high pressure pulses in the cylinder, which cause noisy operation. Therefore, to minimize pump noise, the pump-bypass mode of partial delivery (rather than bypass-pump) was used in the design as demonstrated in Figure II-2. An axially movable cylinder block was chosen as the control member to govern the degree of bypassing. This type of displacement control is used in the line of industrial hydraulic pumps manufactured by The Weatherhead Company of Cleveland, Ohio. The basis of this scheme is shown in Figure II-3.

Figure II-4 is an assembly drawing of the final test pump design. The pump is a five-cylinder wobble plate design having 1.875" diameter bore and 0.40" nominal stroke. Spring-loaded poppet-type valves are used for both intake and exhaust. The intake valve is located in the piston and the exhaust valve is located in the cylinder head. The bypass valve action is accomplished by the motion of the piston over a port in the slidable cylinder block. Since the variable displacement pumping feature of the test pump is of prime interest, this feature is described in detail below.

The intake, bypass and exhaust ports are shown in Figure II-4. The bypass and intake manifolds are annular depressions in the pump

casing (1), while the exhaust manifold is cast into the exhaust valve cover plate. Fluid is admitted into the cylinder through the intake valve during the piston downstroke. This intake valve is opened under the combined effects of pressure differential across the valve and valve inertia. The valve is closed at BDC by spring force and valve inertia.

Figure II-4 shows the cylinder block positioned for minimum delivery and the piston at BDC. Note that as the piston is moved toward TDC by the rotation of the wobble plate on the shaft, the middle ring on the piston, the flow control ring, opens the bypass port within the piston to the bypass manifold in the cylinder block. As shown, bypassing begins at the start of the piston upstroke. However, if the cylinder block were moved closer to the exhaust valve cover plate (4), the piston would start pumping at BDC and deliver fluid through the exhaust valve until the flow control ring entered the bypass passage in the cylinder block.

Spherical bearings are used on both ends of the rods, connecting the pistons to the reaction plate (5). The reaction plate does not rotate, being restrained by the cam follower (36) which oscillates in the stop (12). Needle bearings are used everywhere other than the spherical bearings on the connecting rods. Flooded crankcase and splash lubrication are both possible. A lip type shaft seal is used to prevent lubricant loss from the crankcase. The working fluid system is sealed from the lubricant system by Rulon rings used for the bottom piston ring. O-rings on the sliding cylinder block and a metal bellows on the displacement control also prevent mixing of the lubricant and working fluid systems.

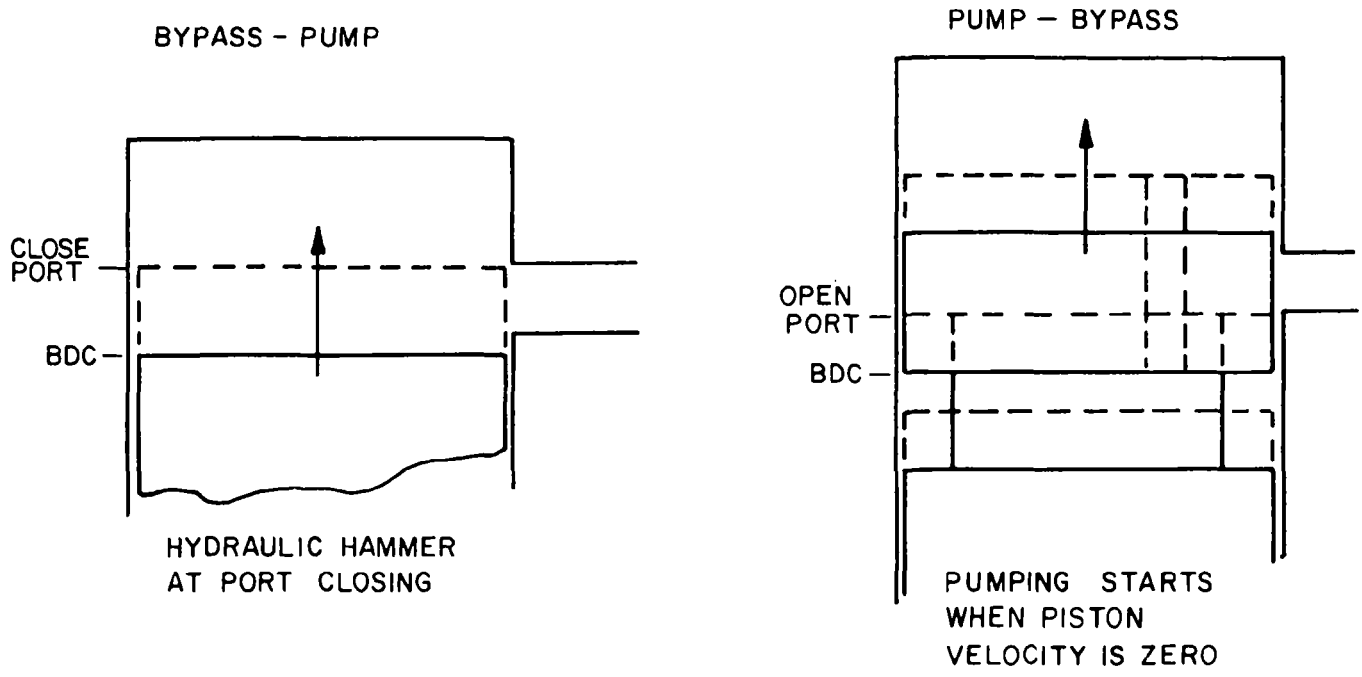

Figure II-2. Bypass-Pump and Pump-Bypass Sequences.

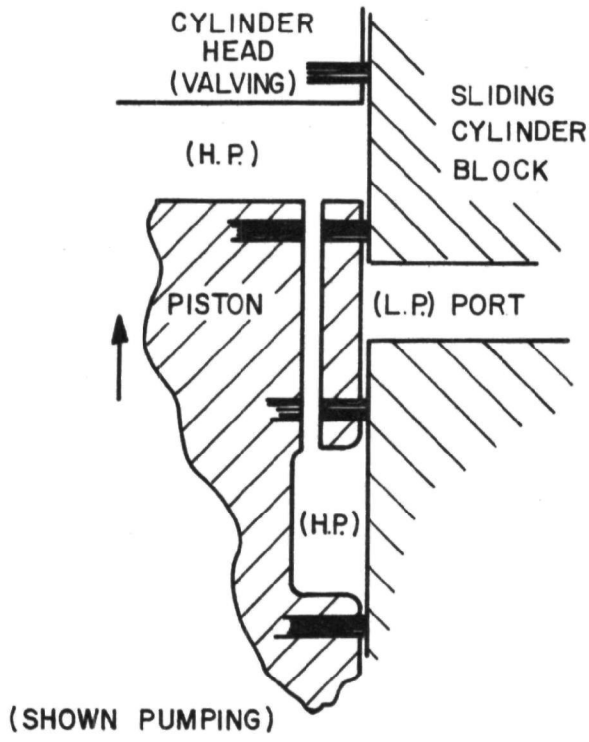

Figure II-3. Final Pump Apparatus.

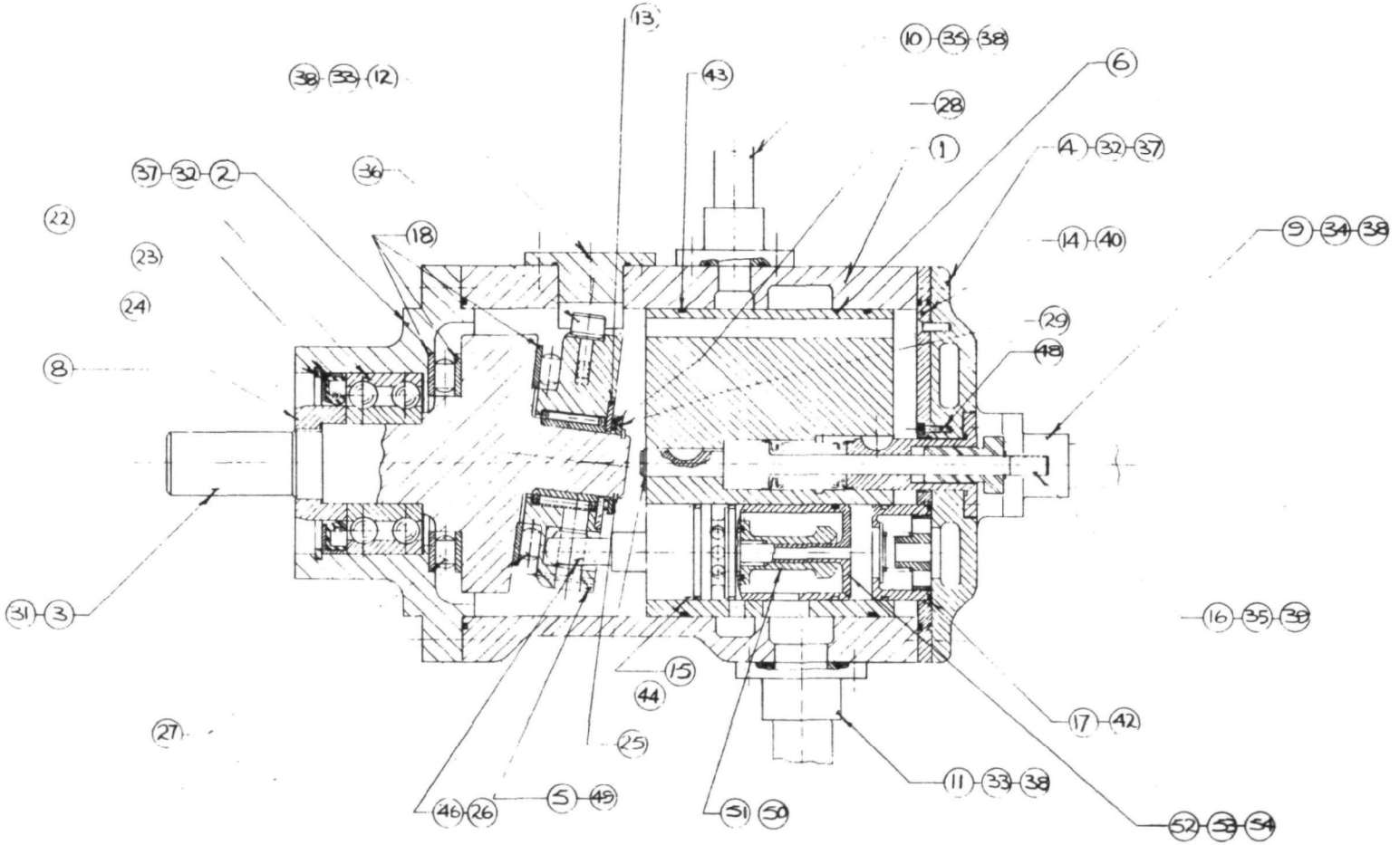

Figure II-4. Feedpump Assembly.

C. TEST RESULTS

Testing of the five-cylinder axial feedpump was conducted on the feedpump test loop facility described in Section 5.1.2 of this report. During the initial phase of testing, design changes were made in both the bearings and the valves.

The spherical bearings used on the reaction plate end of the connecting rod failed prematurely. This problem was corrected by rotating the reaction plate rod end bearing by 90° to the position shown in Figure II-4 so that the load would be taken radially instead of axially. The rated radial bearing capacity is several times the axial bearing capacity. This change proved satisfactory and no additional bearing problems were encountered during the test program.

Erratic valve action was encountered during the initial tests. This erratic behavior resulted in very low volumetric efficiency, large pressure transients in both the suction and discharge lines, and very noisy pump operation. Because of this difficulty, both intake and exhaust valves were redesigned. The discharge valve was changed from a guided spring-loaded poppet valve to a simple spring-loaded flat washer, as shown in Figure II-4. It is believed that the valve guide in the original design prevented proper seating of the valves.

Originally, a piston ring seal was used on the intake valve stem and the stem was much larger in diameter than the final design shown in Figure II-4. The valve was redesigned to reduce the stem diameter and increase the area on which the inlet pressure acted on the valve. The piston ring seal was eliminated with the smaller diameter stem,

since leakage from the inlet port to the bypass port was negligible with the small pressure differential that exists. These changes reduced the friction on the intake valve and increased the opening forces.

After the described changes were made, a series of test runs was performed. These results are presented in Figures II-5 to II-7, in which the volumetric efficiency and overall pump efficiency are shown as a function of outlet pressure, inlet pressure, shaft speed, and percent of maximum flow rate for variable delivery runs. Figures II-5 and II-6 present data for the pump in the full delivery position, while Figure II-7 presents data on variable delivery.

Figure II-5 shows that volumetric efficiency at full delivery decreases from over 95% at 200 psi to just over 85% at 600 psi outlet pressure. At 600 psia outlet pressure, the volumetric efficiency increases slightly with increasing rpm. The overall efficiency is a weak function of both outlet pressure and rpm in the range tested varying from about 62% to 70%.

Figure II-6 shows the effect of inlet pressure on the pump efficiencies at full delivery. The volumetric efficiency increases slightly with inlet pressure and with rpm. The overall efficiency is a weak function of both inlet pressure and rpm at fixed outlet pressure, and varies from approximately 65% to 70%.

The pump operated smoothly and quietly at the full delivery position. The data in Figures II-5 and II-6 were all for the full delivery position, and extend only to 800 rpm, since the system does not require full delivery at pump speeds above 800 rpm.

Figure II-7 presents the results for partial delivery. The overall efficiency is shown to be a very strong function of the fraction of flow rate delivered. The overall efficiency drops more rapidly at higher rpm and is almost directly proportional to the fraction of flow rate delivered. These results suggest that the pump losses are almost constant for fixed rpm and outlet pressure.

The pump was noisy when operated at partial delivery and large suction and discharge pressure transients occurred. These pressure transients were expected, since the flow delivered by one cylinder stops before the next cylinder starts to pump at less than 40% of full delivery for a five-cylinder pump. The extent of the noise and pressure pulsation problem was greater than anticipated however. In an actual system, the boiler and condenser would provide some accumulator effect to help reduce these problems; however, additional accumulators would probably be required on both the inlet and outlet lines. The pump was operated above 800 rpm only briefly due to the noise and pulsation problems, since large accumulators were not available on the pump test loop.

D. CONCLUSIONS

The test on the five-cylinder axial pump indicated a number of problems with this design approach. The main problems can be summarized as follows:

- Low overall efficiency at partial delivery, resulting in reduction in system efficiency under low-power conditions.
- Noise and pressure pulsation at partial delivery.

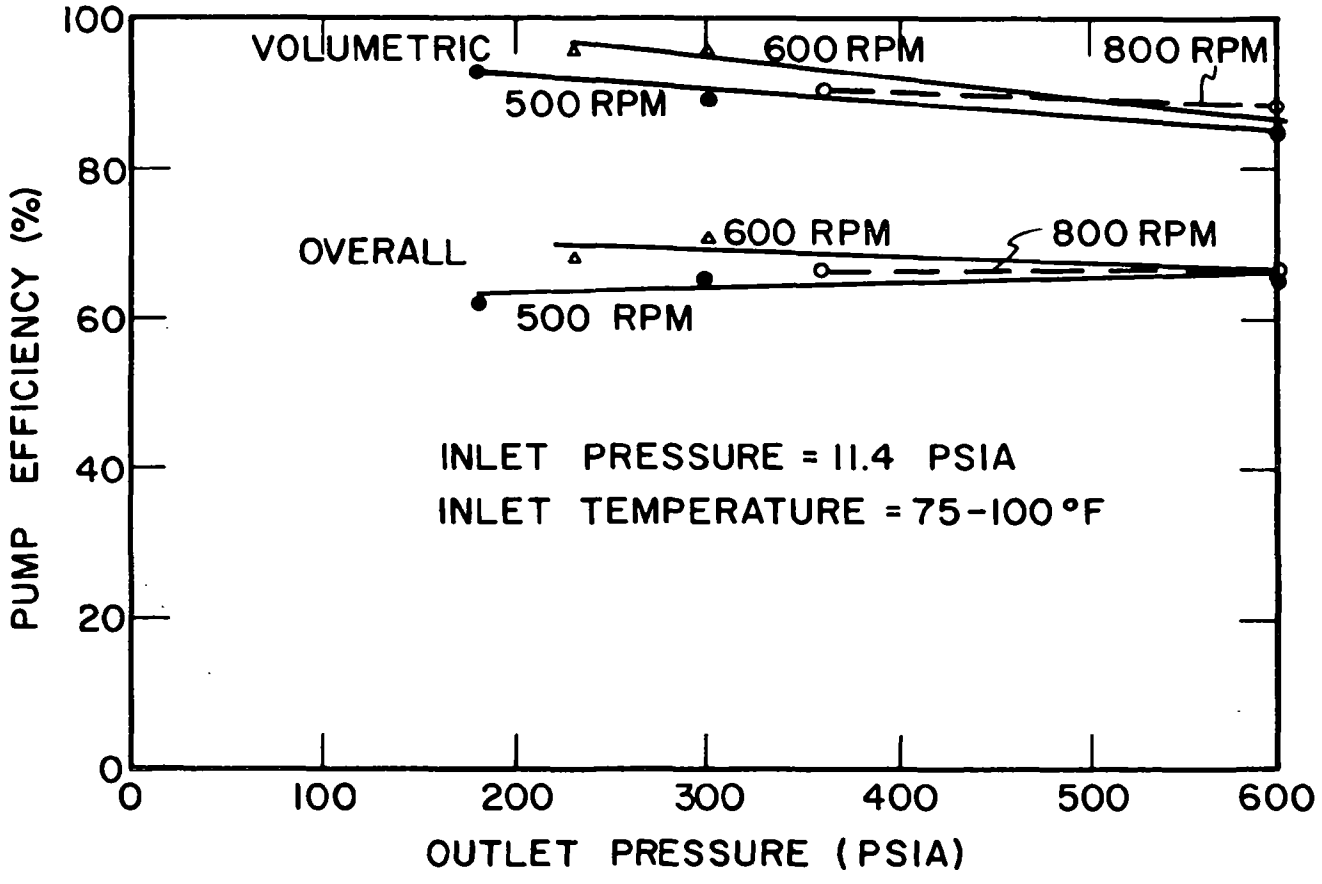

Figure II-5. Pump Efficiency vs. Outlet Pressure for Axial Pump (Full Delivery).

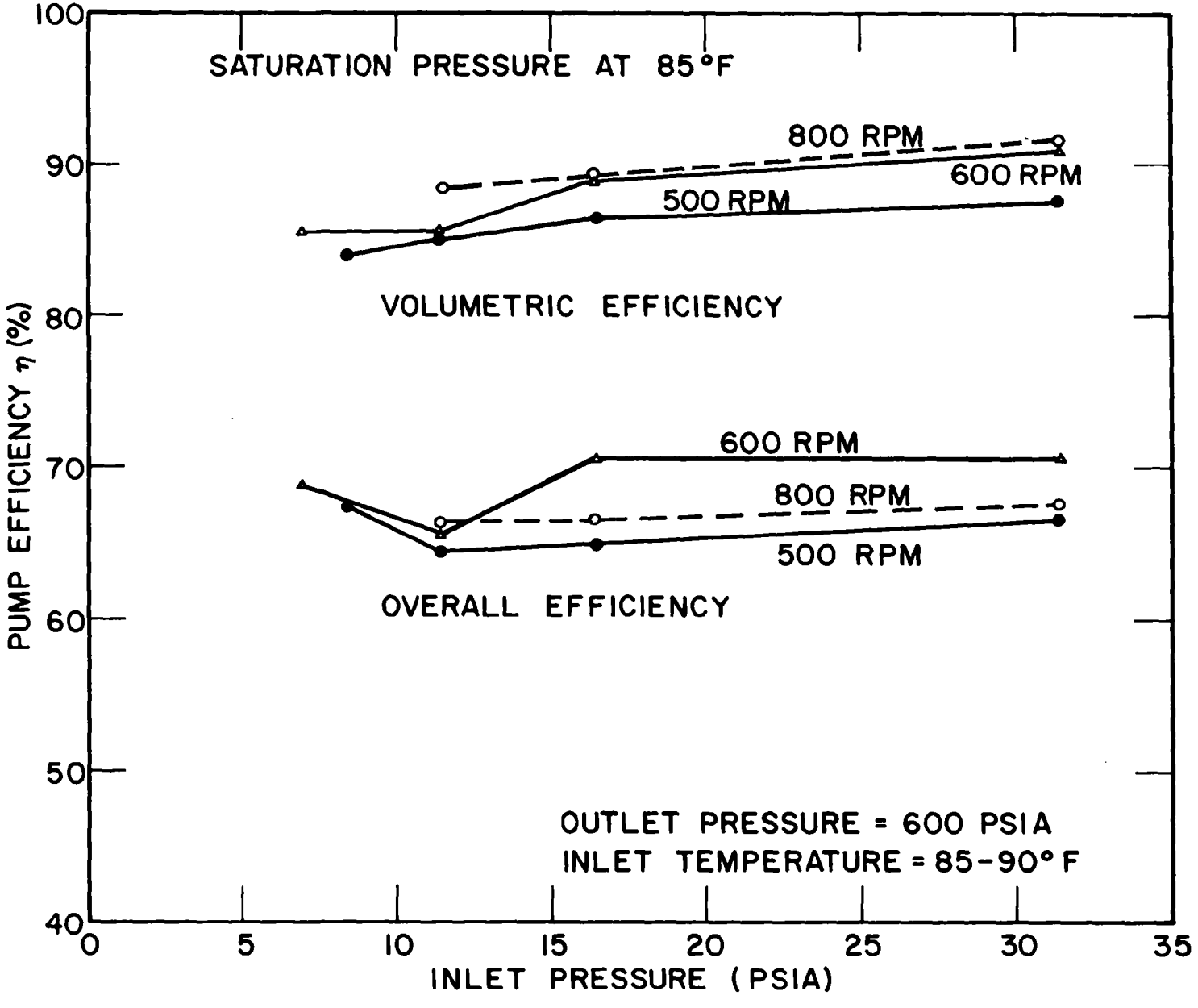

Figure II-6. Pump Efficiency vs. Inlet Pressure for Axial Pump (Full Delivery).

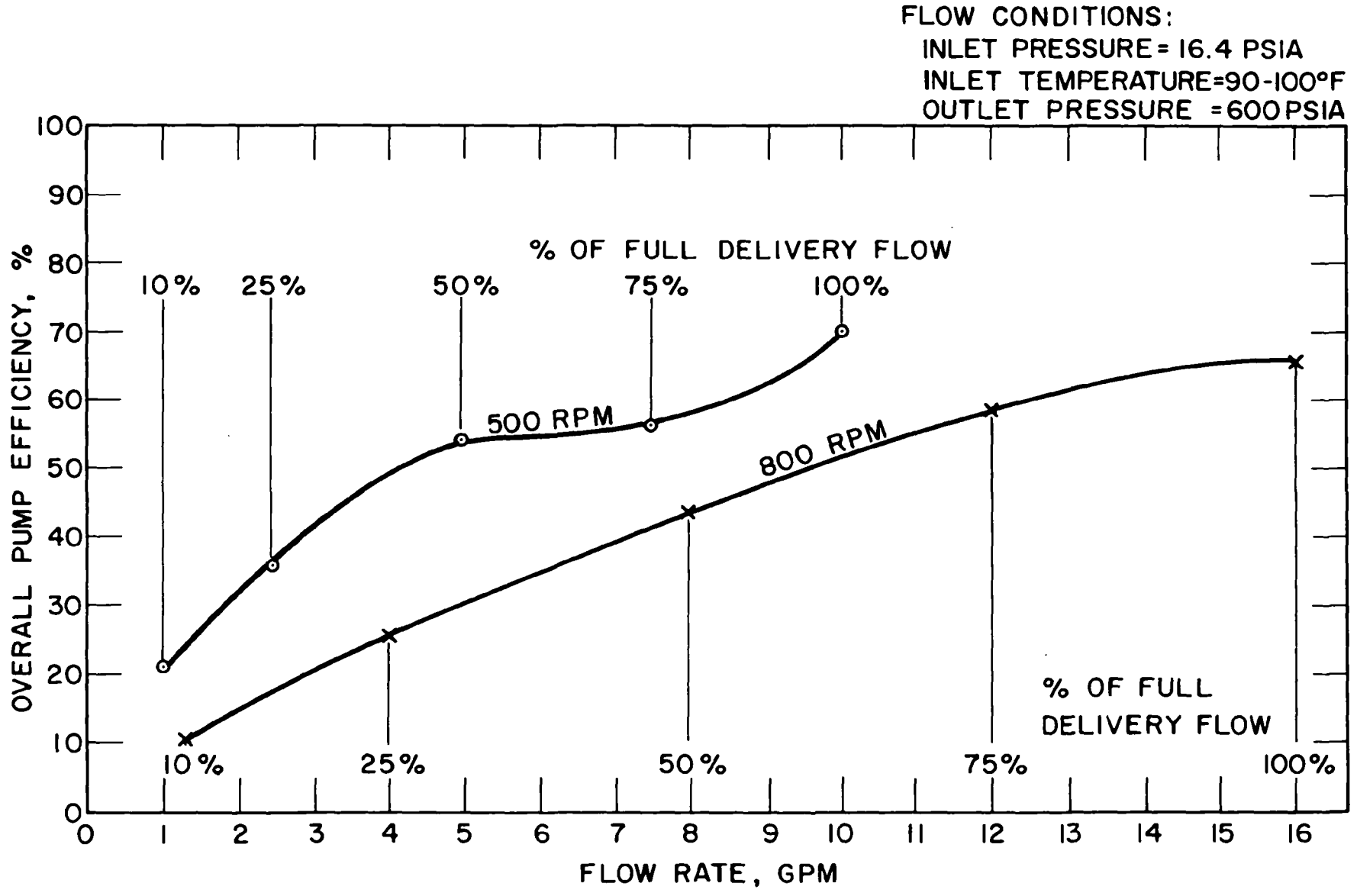

Figure II-7. Overall1Efficiency of Pump at Partial Delivery.

Two additional problems occur in the design. Friction from the additional piston rings required for the bypass port results in lower overall efficiency. The intake valve design is more difficult for a variable delivery design than for a variable displacement design. In a variable delivery design, the full displacement flow passes through the intake valve. At the maximum shaft speed, approximately half the displacement flow rate is all that is ever required. Since the valve must pass twice the required flow rate, it must have four times the area that a variable displacement pump would require. This design problem is compounded when the bypass port must go through the intake valve. The bypass port must be able to pass the full displacement flow rate. If the bypass port is too small, it contributes to lower pump efficiency at partial delivery, particularly at higher shaft speeds.

Two deficiencies of the variable delivery pump summarized above can be overcome with a true variable displacement pump. Therefore, the pump development was redirected to the development of a variable displacement radial pump as described in Section 5.1.2 of this report.

APPENDIX III

ROTARY SHAFT SEAL

A. INTRODUCTION

An automotive Rankine-cycle system requires at least one rotary shaft seal for transmission of the power from the expander to the driveline of the automobile. During system operation, the internal system pressure at the seal can be above atmospheric pressure so there is a tendency for working fluid to leak from the system. During system shutdown, the internal system pressure is less than atmospheric pressure and there is a tendency for air to leak into the system. While both leakage rates must be controlled, air in-leakage is the most serious for the following reasons:

a. The presence of oxygen in the system accelerates thermal decomposition of the lubricant and working fluid and tends to oxidize the system components.

b. Non-condensable gases collect in the condenser during system operation and degrade the condenser performance.

c. The normal family automobile spends most of its life shut down. Thus, assuming a 10 year life with 100,000 mileage and average vehicle speed of 33 mph, the car would have an operating time of 3030 hours and a shutdown time of 84,600 hours over its lifetime, a ratio of 28 hours of shutdown for every hour of operation. The crankcase is thus at subatmospheric pressure over most of the system life.

The seal approach followed positively prohibits leakage of air into the system and of working fluid from the system. As illustrated conceptually in Figure III-1, a double seal is used with pressurized

oil buffer fluid between the two seals. Since the oil buffer pressure is set above the internal system (or crankcase) pressure at the seal, the only leakages possible are leakage of the buffer fluid into the system through the inboard seal and leakage of the buffer fluid out to the atmosphere through the outboard seal. The buffer fluid used is the lubricating oil used in the system. This approach has been used on the 5-1/2 hp Rankine-cycle systems developed at TECO with very satisfactory operation.

Since some slight leakage of this buffer fluid into the crankcase and to the atmosphere is inevitable and the magnitude of these leakages is the prime factor in determining the suitability of a particular seal design for the TECO Rankine-cycle system. The leakage rate goals for evaluating a seal were established as a maximum of 2/3 pint/1000 hours of operation total buffer leakage and a maximum of 1/2 pint/1000 hours operation through either the inboard or outboard seal. The leakage rates in the shutdown condition were demonstrated to be much less than when the seal was operating so that the emphasis in the testing was primarily on measurement of the operating leakage rates. It should be noted that leakage through the outboard seal in the system will be collected and stored in the expander rear housing rather than being allowed to drain onto the ground.

The objective of the testing was to demonstrate the availability of a rotary shaft seal for use in the automotive-size Rankine-cycle system which has a 3-inch diameter power shaft from the expander. The two seal designs chosen for test are both of the mechanical face seal type - one manufactured by Chicago Rawhide Manufacturing Company, Chicago, Illinois and the other manufactured by Crane Packing Company,

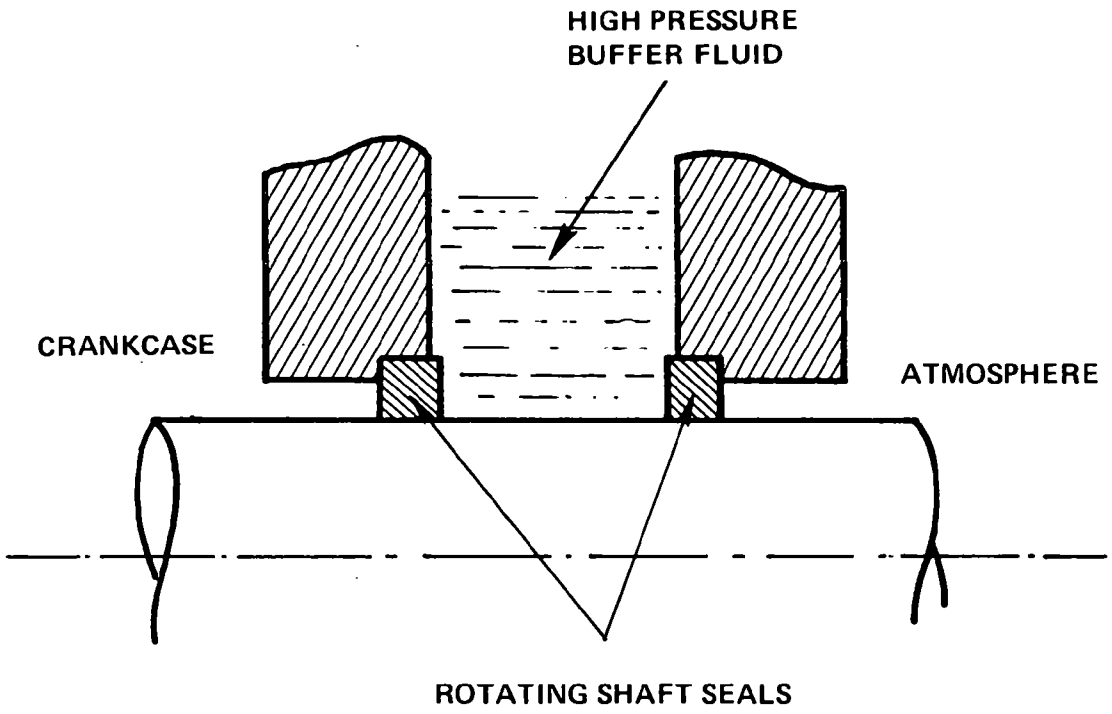

Figure III-1. Double Shaft Seal Concept.

Chicago, Illinois. The selection of these seals was a result of the vendor recommendations and the small shaft seal testing which had previously been performed at Thermo Electron Corporation.

B. SEALS

The seals used in this experiment are both of the type generally termed as face seals or axial mechanical seals. This type of seal forms a running seal between flat, precision-finished surfaces. The sealing surfaces are usually located in a plane at right angles to the shaft. The rubbing faces are held in contact by forces which are parallel to the shaft. Although face seals have different design details, they all have the following basic elements:

a. Rotating seal ring
b. Stationary seal ring
c. Spring-loading device
d. Static seal

Test data obtained at Thermo Electron on smaller shaft diameter seals of the same type demonstrated interest and capability of the two vendors, and current usage of similar seal designs commercially led to the selection of the two particular seal types for the test program as described below.

1. Chicago Rawhide Face Seal

This double face seal, as shown in Figure III-2, consists of a single mating ring made of 440 C stainless steel. This seal ring rotates with the shaft and is lapped on both axial faces. Two cartridges containing the graphite rings and the spring-loading device make up the stationary seal rings. A spring washer or belleville spring is

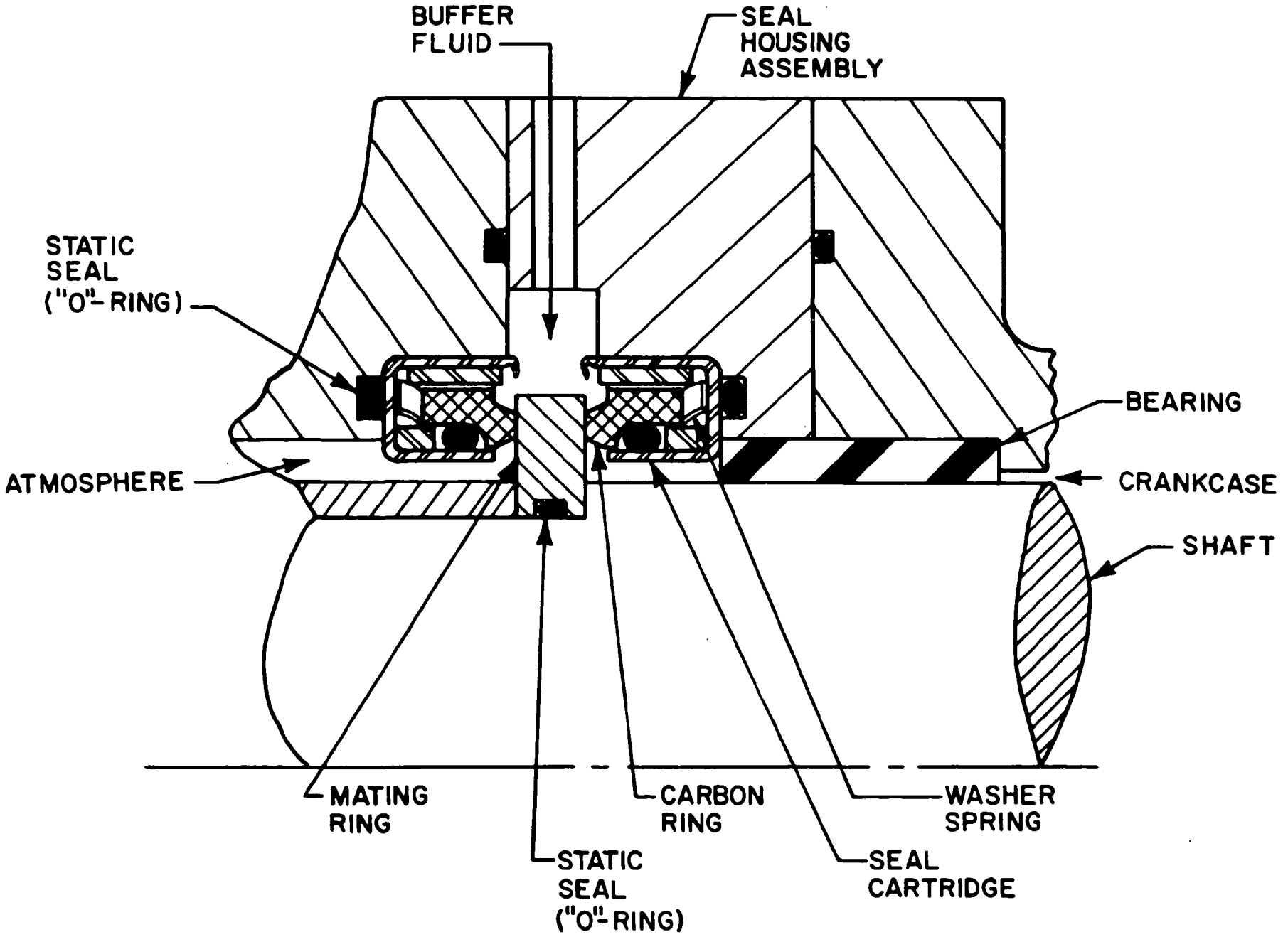

Figure III-2. Chicago Rawhide Double Face Seal.

used to keep the lapped sealing faces closed in this particular seal configuration. A photograph of the major seal elements is shown in Figure III-3. The shaft has a 3-inch diameter and the total seal thickness is 1-1/4 inches.

2. Crane Face Seal

There are two separate mating rings used in this seal design (see Figures III-4 and III-5). In this case, the metal mating rings are precision finished only on the contact side of the ring. The mating rings are the stationary seal while the carbon rings constitute the rotating seal elements. A single compression spring provides the loading on the contact faces. The spring is located between the two carbon rotating seal rings and exerts force on both contact faces. Figure III-5 shows a drawing of the seal arrangement and assembly. The seal thickness for a 3-inch diameter shaft is 2-1/8 inches.

The carbon rings (washers) are the rotating seal rings in this design, and the drive between the washer and the shaft is accomplished by a positive pre-load of the rubber diaphragm on the shaft by the drive ring. As can be seen in Figure III-6, the washer or carbon seal ring and the washer retainer are interlocked by corresponding dents in each part. The retainer in turn has fingers interlocking with notches on the drive ring, thereby providing the positive drive of the carbon seal ring.

C. TEST STAND DESCRIPTION

Four test stands were constructed for testing of the seals under simulated operating conditions. Two test stands were used for each

Figure III-3. Photograph of Major Elements of Chicago Rawhide Seal.

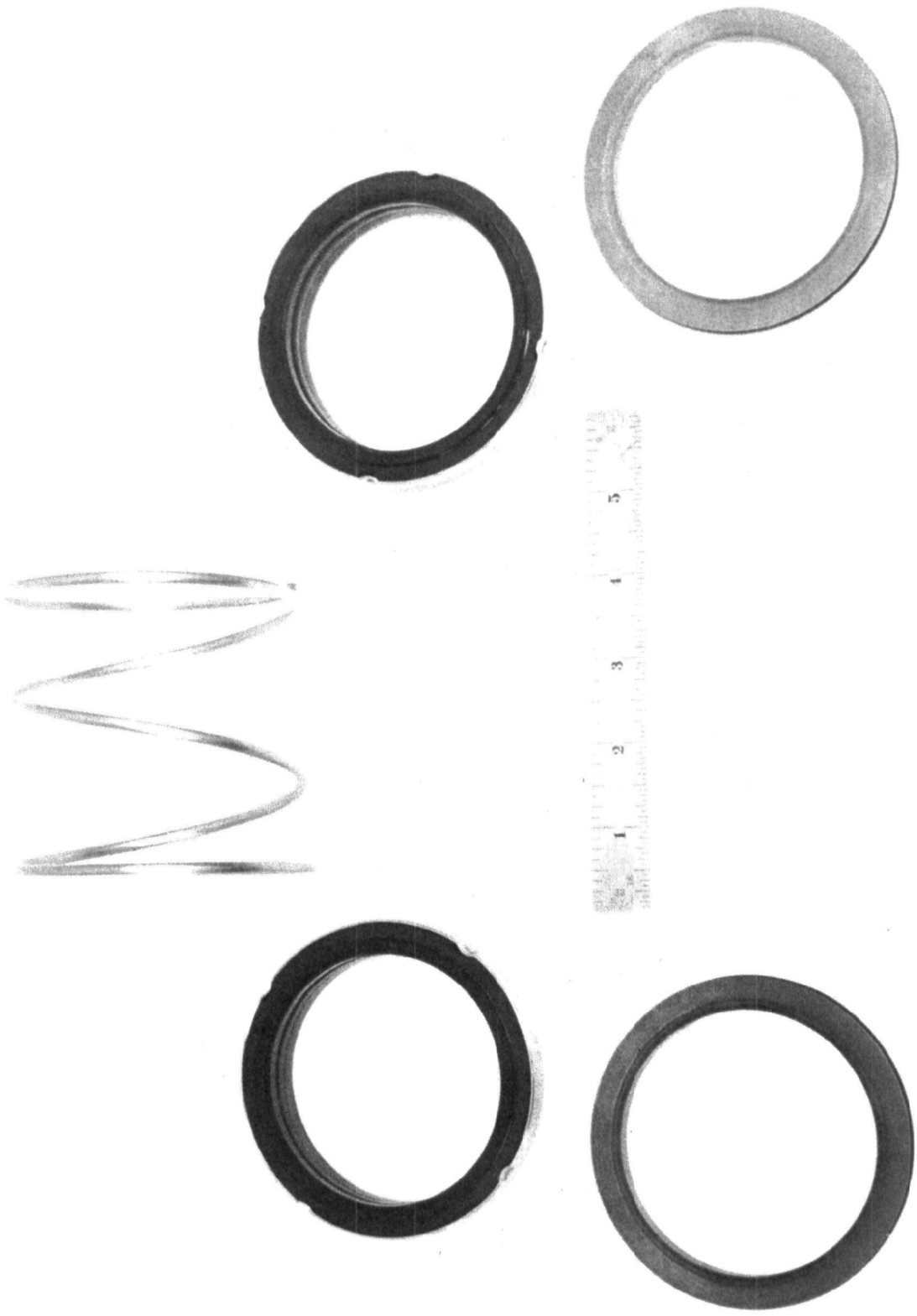

Figure III-4. Photograph of Main Elements of Crane Seal.

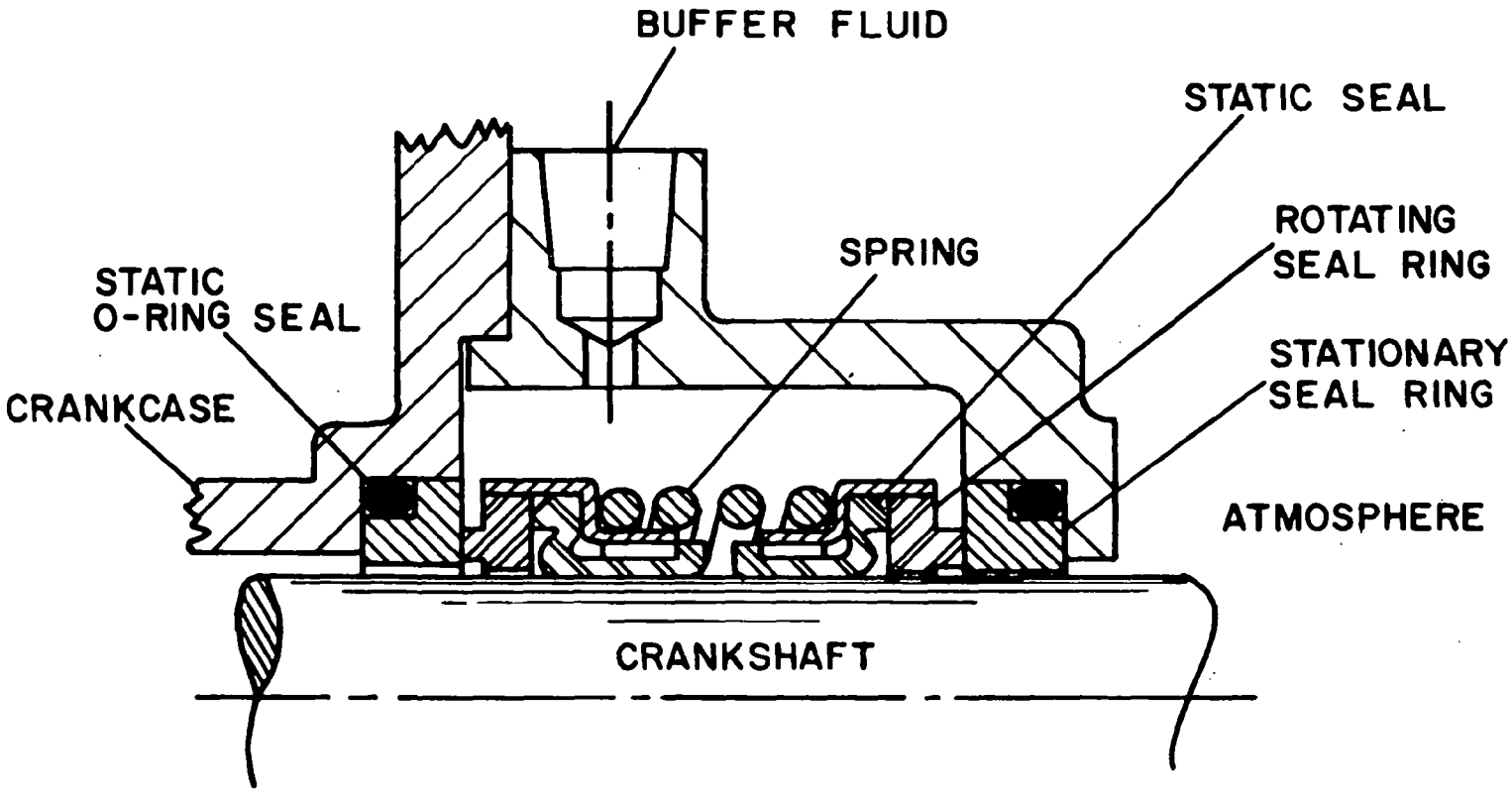

Figure III-5. Crane Double Face Seal.

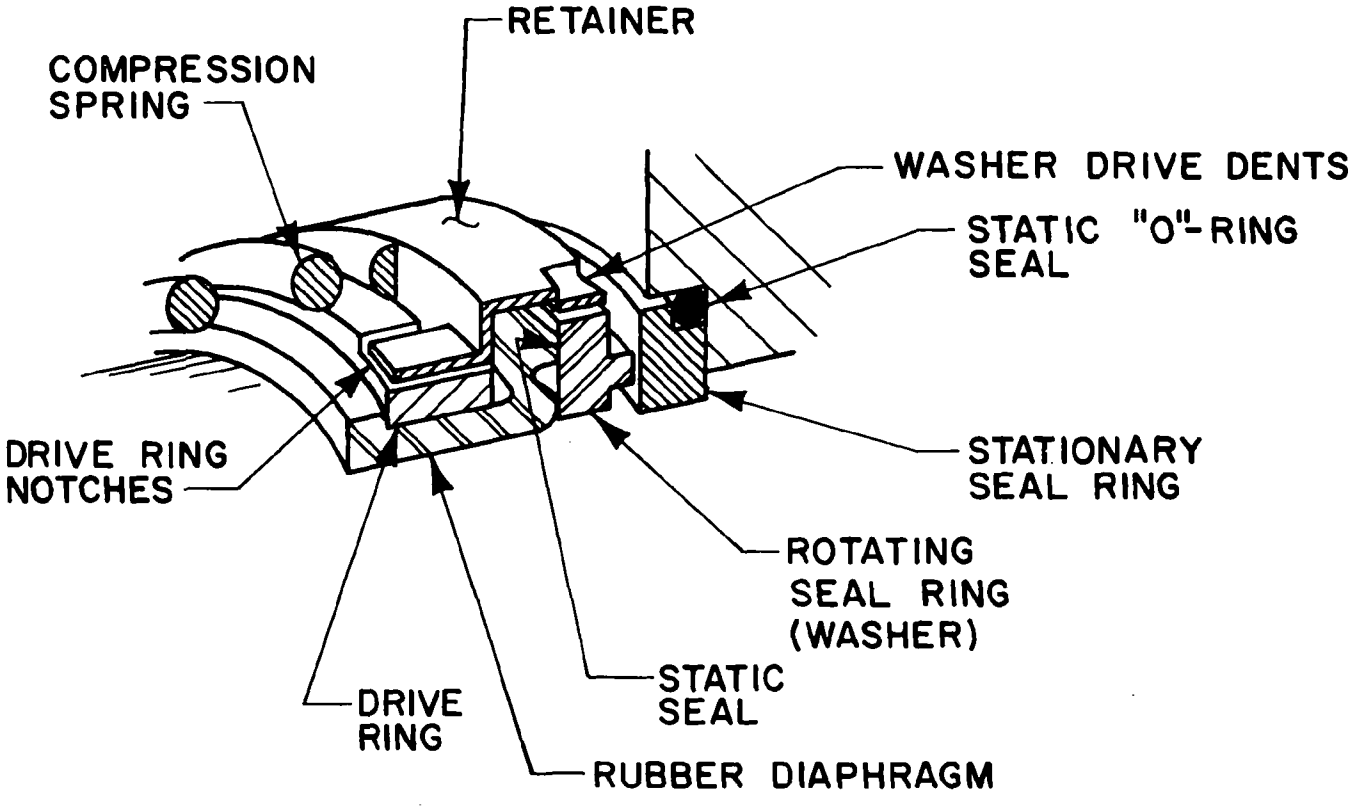

Figure III-6. Detail View Showing Crane Seal Drive Method.

seal type, with one of these test stands constructed for continuous dynamic testing and the other constructed with controls permitting testing over an on-off duty cycle. Photographs of three of the test stands are illustrated in Figure III-7. The major components of each of the test stands are:

a. Seal housing
b. Shaft housing with bearings
c. Shaft
d. Working fluid chamber
e. Isothermal bath container
f. Buffer fluid container

Most of these components are shown in Figure III-8.

Organic pressure on the crankshaft side of the inboard seal was maintained by use of a reservoir of the organic working fluid immersed in a constant temperature bath. The organic pressure was thus controlled by the temperature of the constant temperature bath.

The seal housing and shaft are different for the two seals. The Chicago Rawhide seal design requires a step in the shaft, whereas the Crane seal is mounted on a straight shaft. The only other differences in the seal housing and shaft are those associated with the particular working dimensions unique to each seal design.

The working fluid chamber is located at the end of the shaft which houses the seal assembly. The entire chamber is within the isothermal bath container which is filled with a heat transfer fluid. The bath fluid used is Union Carbide UCON, basically a polyalkylene glycol fluid.

The buffer fluid reservoir used in each of the test units is shown in Figure III-9. The reservoir contains the inventory of buffer fluid and an extended rod within a sight glass is used for measurement of the buffer fluid liquid level in the reservoir. The chamber utilizes a rolling diaphragm to separate the buffer fluid chamber from the air pressurizing chamber. A constant pressure of air is kept in the pressurizing chamber to give the desired buffer fluid pressure level in the seal cavity. Figure III-10 is a photograph showing the isothermal bath container with its heat transfer fluid; in the upper left of the picture can be seen the buffer fluid reservoir.

An unbalanced shaft, attained by placing holes in one side of it, was used to simulate vibration effects and shaft movement within the engine bearings. The shaft of the seal test assembly is directly coupled to a constant speed motor. Figure III-11 is a photograph showing the drive motor coupled to the shaft and the housing for the seal and shaft. The seal and shaft housing is located directly to the rear of the constant temperature bath.

Other important components of the test stand system are the control equipment, monitoring devices, and other accessories. This equipment can be listed as follows:

1. Buffer fluid and crankcase liquid level gauges for measuring leakage rates.
2. Isothermal bath control
   a. Mixer
   b. Heating element
   c. Water cooling system
   d. Temperature controller

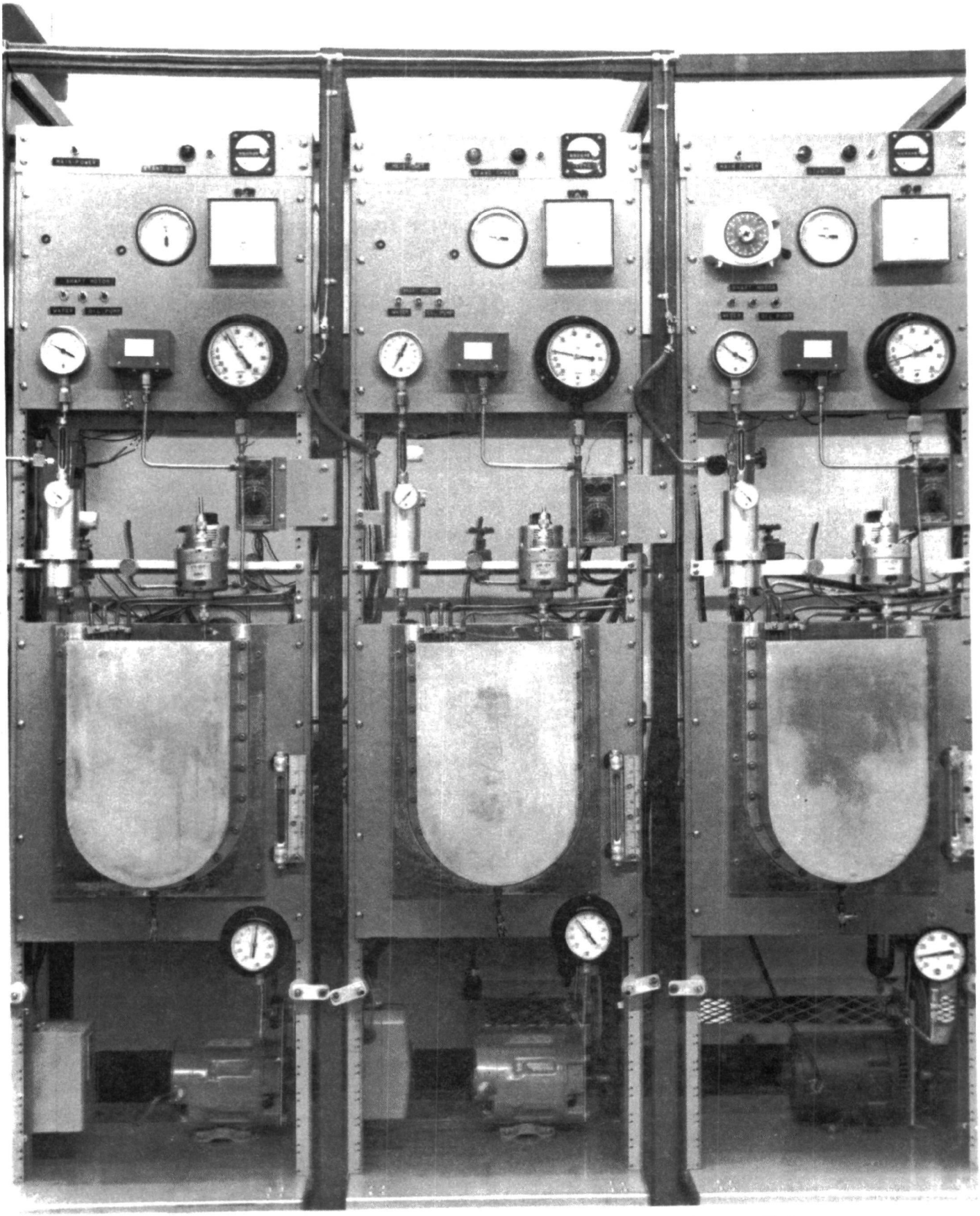

Figure III-7. Front View of Rotary Shaft Seal Test Units.

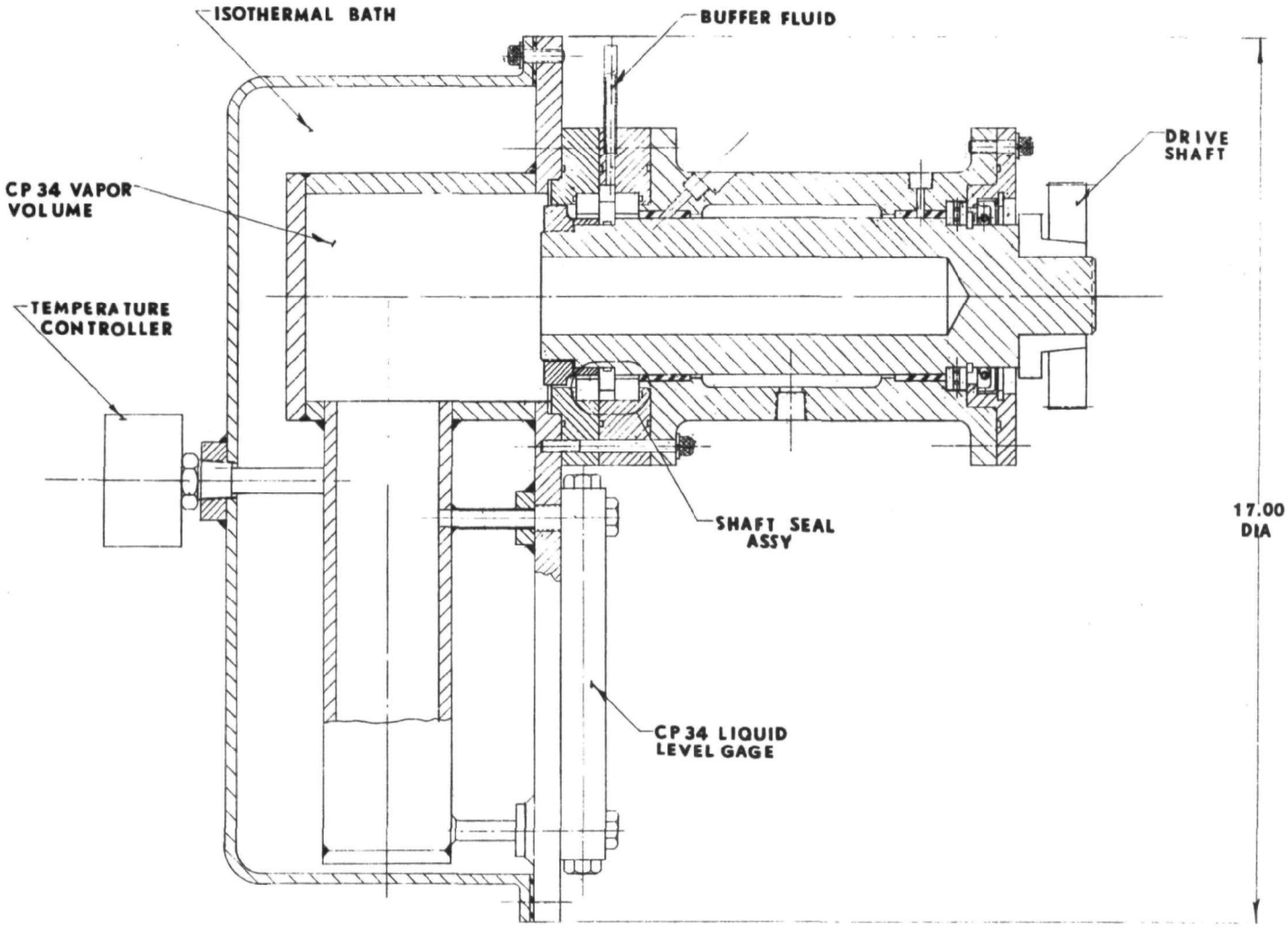

Figure III-8. Seal Test Apparatus.

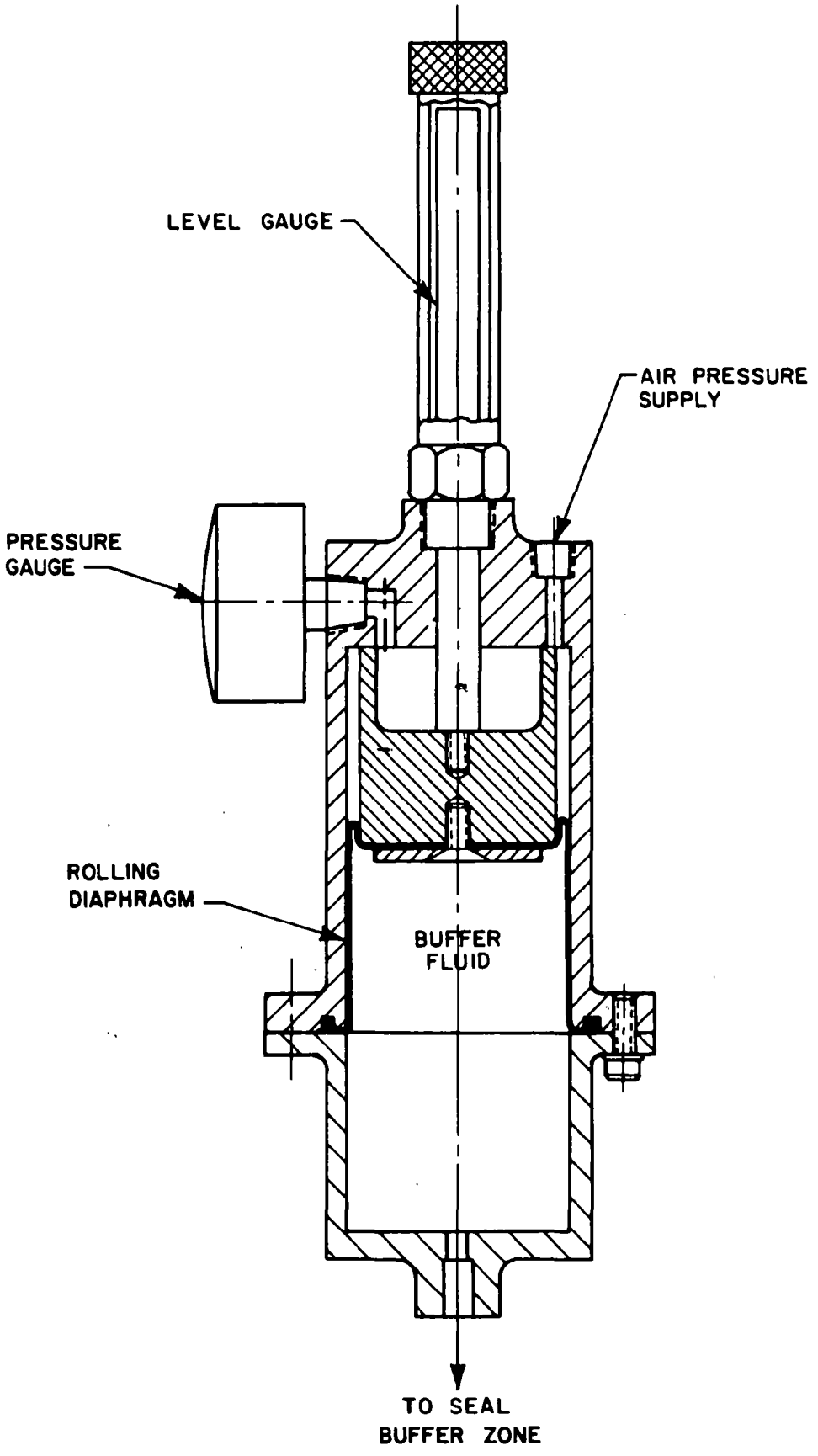

Figure III-9. Buffer Fluid Reservoir.

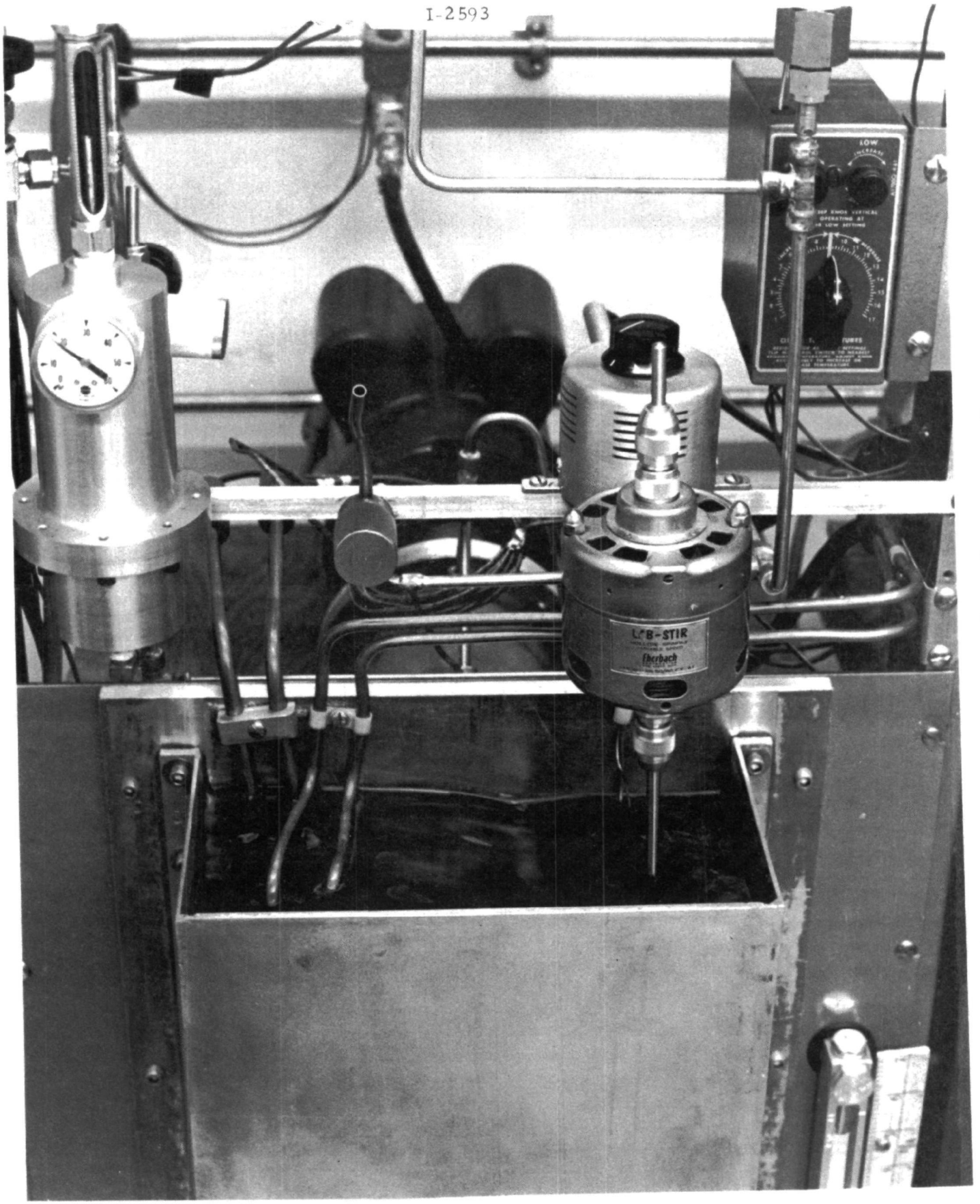

Figure III-10. View of Isothermal Bath and Buffer Fluid Reservoir.

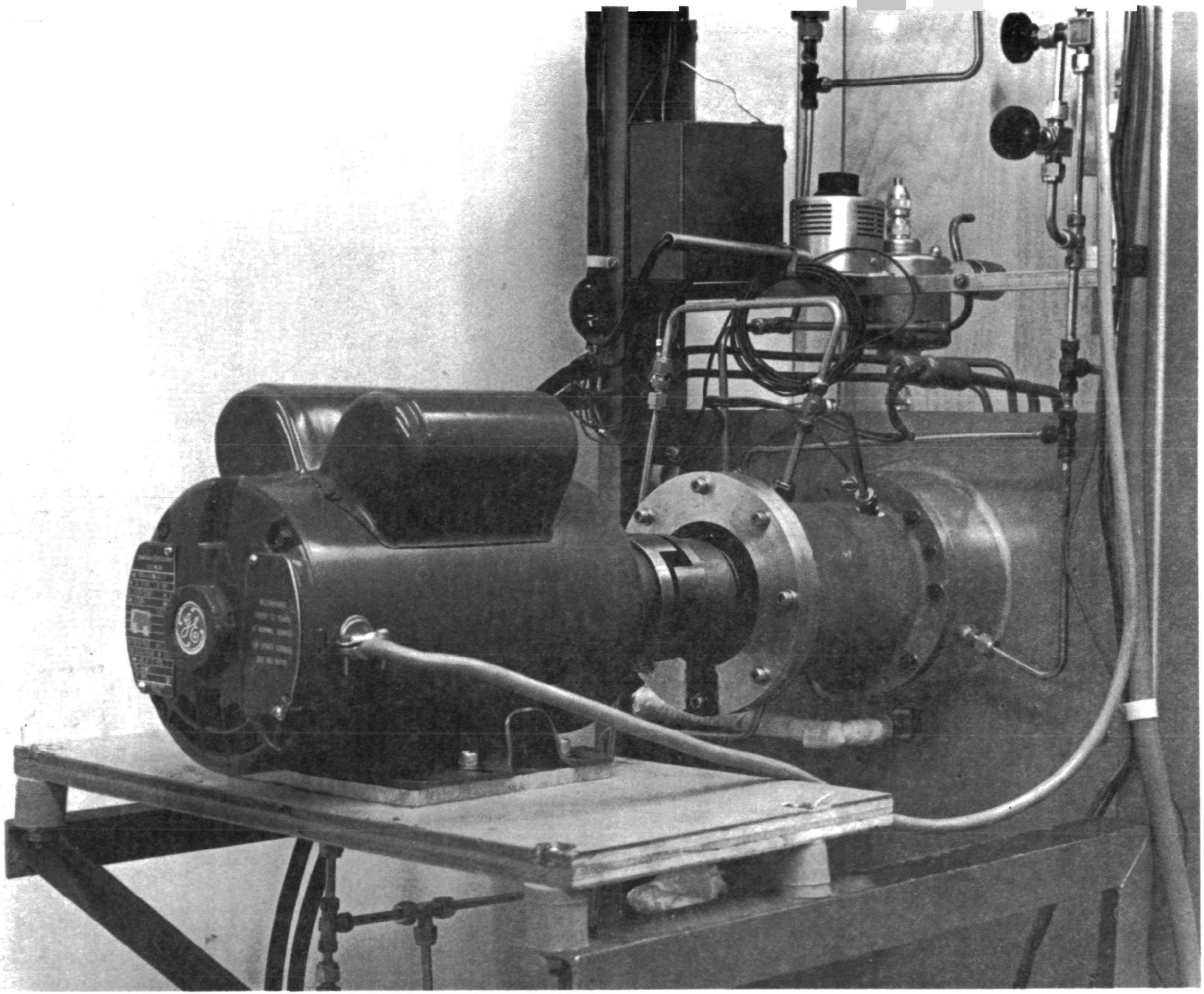

Figure III-11. View of Drive Motor and Seal Housing.

3. Twenty-four hour cyclic timer and total elapsed run time indicator
4. Shaft lubrication system
5. Seal housing and bath temperature measuring instruments
6. Buffer and crankcase pressure gauges
7. Safety devices.
   a. Over temperature cut-off
   b. Over pressure cut-off (pressure switch)

Most of the control and monitoring equipment can be seen in the close-up view of the test stand panel in Figure III-12.

The most important monitoring devices are the fluid level gauges used for measuring the seal leakage rates. One is mounted, as mentioned before, on the top of the buffer fluid reservoir. It consists of a rod connected to the piston plate of the reservoir and is visible through a sealed sight glass tube. The sight glass is graduated and the volume displacement of fluid is directly correlated to the linear travel of the piston and, therefore, measuring rod. The volume displacement per linear inch travel of the rod is 51.5 cc/inch. This fluid displacement is a direct measure of the leakage by both the crankcase and outboard seals - that is, the total leakage by both seal faces. The other level gauge is located on the working fluid chamber. A sight glass merely displays the fluid inventory in the chamber at any given time. This level gauge gives the leakage of buffer fluid past the crankcase seal face only. The calibration factor for this fluid level gauge is also 51.5 cc/inch.

The isothermal bath is used to maintain the proper temperature conditions in the simulated crankcase. During the dynamic mode of

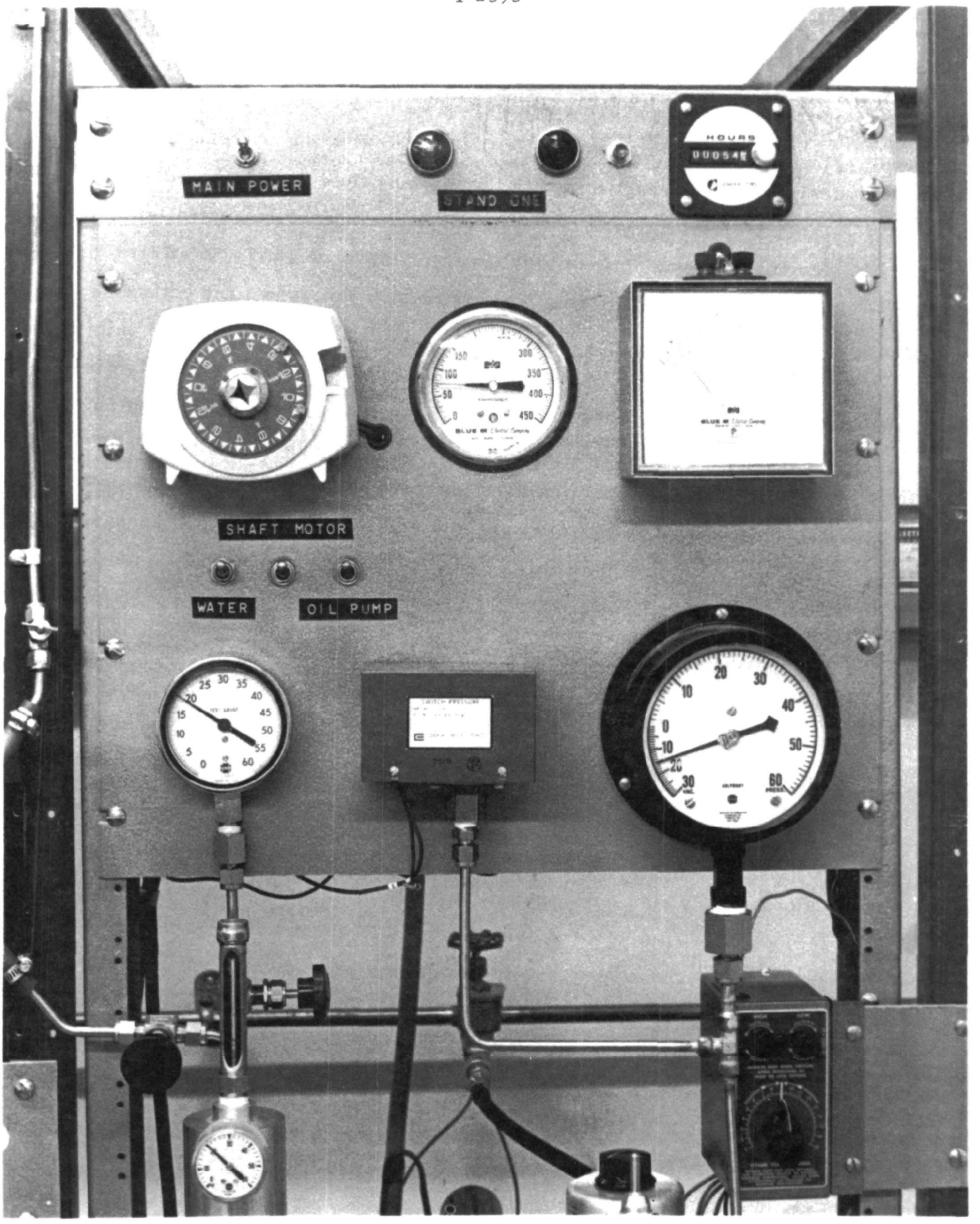

Figure III-12, Photograph of Rotary Shaft Seal Test Unit Control Panel.

operation, the pressure conditions within the crankcase are set by maintaining the temperature of the bath to give the corresponding desired vapor pressure within the working fluid chamber. A heating element within the bath is regulated by a temperature controller which automatically maintains the temperature level to ±5°F. A stirrer provides complete agitation and circulation throughout the entire liquid mass of the bath. Also submerged in the bath of the two units operating on a cycle is a water cooling coil, which automatically circulates water upon transition from the dynamic to static mode of operation. This circulating water helps to cool the system down rapidly to ambient conditions during the shutdown period. The ambient temperature and, therefore, vacuum conditions within the crankcase are more quickly achieved for the time cycle at static conditions.

One other important subsystem of the seal test stands is the lubrication system for the shaft bearings. As can be seen in the schematic of Figure III-13, the oil is pumped to the bearings, allowed to drain from the shaft area to a reservoir cylinder at atmospheric conditions, and subsequently recirculated to lubricate the shaft bearings.

Incorporated into the control system are certain safety features. The first of these features is an over-temperature switch, which will automatically shut down the entire system if, for some reason, the temperature controller should fail to maintain the desired temperature level. The second safety device is a pressure switch set to "trip" at a pre-set pressure level if there is an over-pressure in the crankcase. This pressure switch also completely de-energizes the system. Another pressure switch communicates with the lubricating system for the bearings and shaft. If the oil pressure drops below

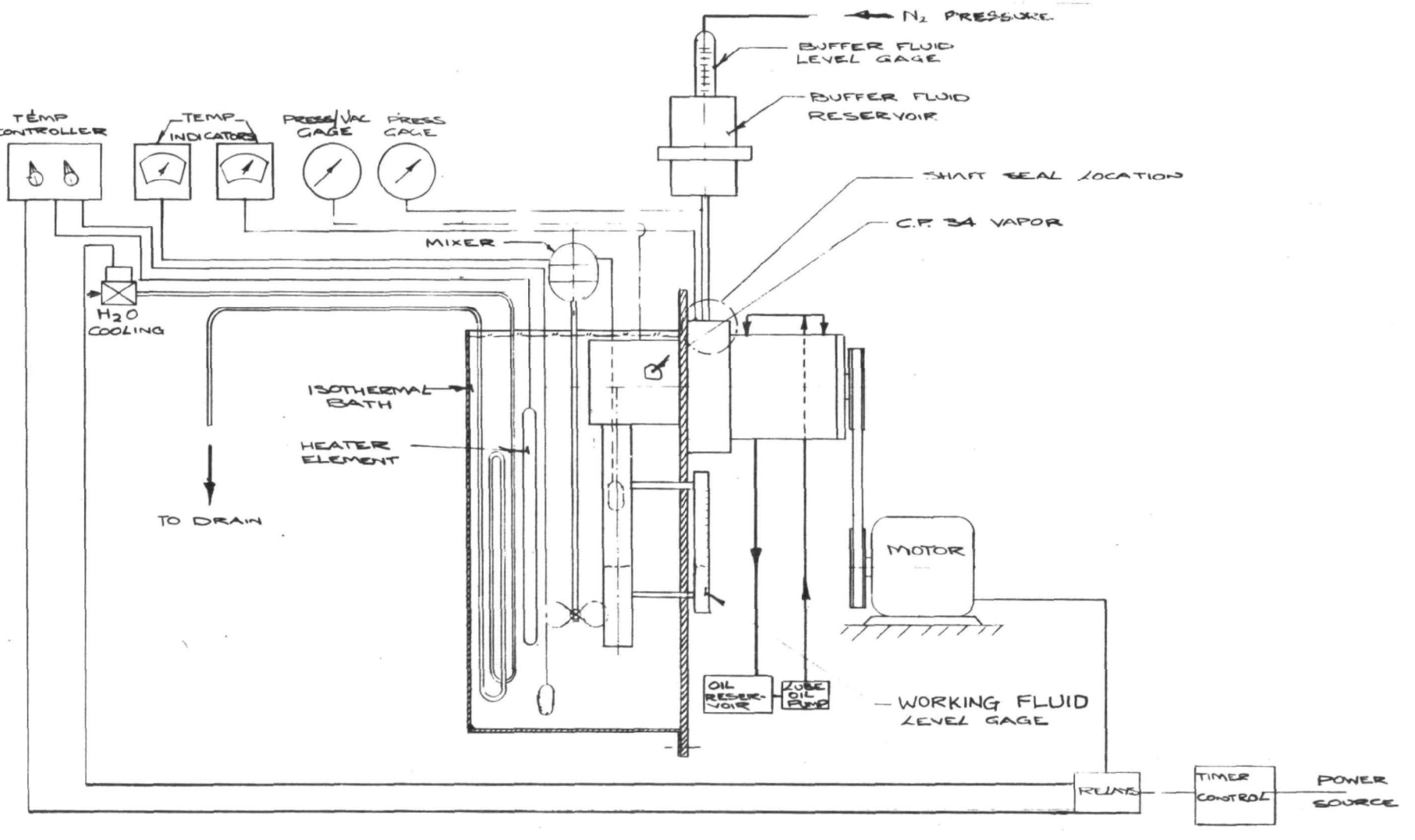

Figure III-13. Rotary Shaft Seal Test Setup.

the pre-set pressure level and, therefore, indicates stoppage or reduction of lube oil flow, then the switch will send a signal to de-energize the system and put the test in a static condition.

1. Procedures

When the testing work was started, thiophene with GE F-50 silicone lubricant was used for all four test stands. In January, 1971, midway through the testing, the decision was made to use Fluorinol-85 working fluid in the system with a lubricant currently used in refrigeration compressors. The two continuous dynamic test stands were then converted to Fluorinol-85 and Suniso 3GS lubricant. The two test stands operating on a cycle were not converted to Fluorinol-85 and continued to operate with thiophene and GE F-50 for the entire test period.

In Table III-1, the range of operating conditions is presented for the rotary shaft seal tests. The isothermal bath temperature was maintained at a level required to give a measured pressure of 23 - 25 psia in the organic chamber during dynamic testing. The buffer oil pressure was maintained at 33 - 35 psia during both dynamic and static testing, providing a positive 10 psi differential between the buffer fluid and the organic chamber during dynamic testing. During static testing, the organic pressure was reduced to 1 - 3 psia by reducing the isothermal bath temperature so that a negative pressure differential of ~33 psia existed between the buffer fluid and the organic chamber. These conditions were selected as representative of the average operating conditions for the seal.

TABLE III-1

RANGE OF OPERATING CONDITIONS
FOR ROTARY SHAFT SEAL TESTS

A. Thiophene Working Fluid and GE F-50 Silicone Oil Buffer Fluid. Testing Carried Out on Test Stands 1, 2, 3, and 4.

Mode of Operation	Dynamic	Static
Isothermal Bath Temperature (°F)	230 - 250	60 - 70
Organic Chamber Pressure (psia)	23 - 25	1 - 3
Buffer Oil Pressure (psia)	33 - 35	33 - 35
Shaft Speed (rpm)	1800	0

B. Fluorinol-85 Working Fluid and Suniso 3GS Buffer Fluid Testing Carried Out on Test Stands 3 and 4.

Mode of Operation	Dynamic
Isothermal Bath Temperature (°F)	190 - 210
Organic Chamber Pressure (psia)	23 - 25
Buffer Oil Pressure (psia)	33 - 35
Shaft Speed (rpm)	1800

The shaft speed used for all dynamic testing was 1800 rpm, the maximum speed expected for the expander. Leakage rates normally decrease as shaft speed decreases. However, measurements were made only at 0 rpm and 1800 rpm.

The two dynamic test stands (test stands No. 3 and 4) were operated continuously, 24 hours/day, 7 days/week. On the two test stands operating over an on-off cycle (test stands Nos. 1 and 2) a 24-hour duty cycle was used, with 19 hours of dynamic testing followed by 5 hours of shutdown (static mode of operation), providing 80% of dynamic test time and 20% static test time. During the static mode, there was no shaft rotation, the isothermal bath heaters were off, and the bath temperature was lowered automatically to ~60°F by water flowing through cooling coils immersed in the bath.

During the initial testing, a learning period occurred with only short operation of the seals before unacceptable leakage occurred. Changes were incorporated in the seal assembly and in the tolerances in the seal housing and bearing assembly to reduce the leakage to acceptable levels and to give long seal life. The shaft axial movement tolerance (end play) was 0.020 inch on the initial seal test units; the manufacturer's tolerance on end play was specified as 0.040 inch. Initial testing with the 0.020 inch end play resulted in unacceptable leakage. The test units were then modified to maintain end play at 0.005 inch with acceptable leakage. In the design of the expander, this tolerance has been maintained on the crankshaft end play.

Premature failure of an initially acceptable seal is primarily dependent on the initially "as received" condition of the seal and the care and procedure used in assembly of the seal. Premature failure of a seal can be caused by:

a. Excessive abrasives in the system such as wear debris from mechanisms, dirt, or other foreign matter.

b. Excessive heat, which can induce thermal shock or cracking of the carbon ring faces and cause sludging of the oil buffer fluid, thus restricting free movement of the carbon rings.

c. Dry operation of the seal, which can result in rapid failure.

d. Failure of the "as delivered" seal to meet specifications due to imperfections in the seal faces such as scratches and chips.

e. Improper installation of seal, resulting in scratches on the seal surfaces, insufficient cleaning, non-maintenance of required tolerances, and dry (non-lubricated) assembly of seal.

To eliminate these effects, the following procedure was followed in initiating a seal test.

a. Tolerance Inspection - The seals as received were inspected to insure adherence to specifications.

b. Seal Surfaces Inspection - Seal faces were closely inspected under illuminated magnification for imperfections such as excessive chips in the carbon faces or deep scratches or burnish lines which were directional, excessive in magnitude and number, and spanned with width of the sealing interface.

c. Cleaning of Seal Surfaces - All seal surfaces as well as the entire seal and housing were carefully cleaned. The seal faces were lightly wiped with a solvent fluid to insure elimination of all foreign particles from the seal surface.

d. The sealing faces were lubricated with a thin film of the buffer fluid before assembling the seal components.

e. The double seal configuration was pre-assembled within the flanged housing subassembly for a pre-run static check.

f. The flanged seal subassembly was then put on a static bench test, with the buffer zone loaded with oil and pressurized with nitrogen. After a period of time, leakage by the seal faces was checked as well as leakage elsewhere in the unit, such as by the static seal locations.

g. After satisfactorily checking the seal subassembly, it was then placed into the test stand unit and the seal was then ready for operational testing.

After preliminary testing was completed, long duration runs were started on all the units. The results of these experiments are described in the following section.

2. Leakage Test Results

The complete test results for all four test stands are summarized in Table III-2. Total testing time on all four test stands is in excess of the contract requirement of 3000 hours, with about 6000 hours total test time on the two continuous test stands. On test stands 3 and 4, the final runs were 3187 hours and 5325 hours, respectively, without disassembly of the seals and with total average buffer leakage rates

TABLE III-2

SUMMARY OF ROTARY SHAFT SEAL TESTS

Seal Test Unit No.	Seal Type	Type of Operation	Total Hours on Test Unit	Total Hours on Seal Set	Run No.	Elapsed Time (Hours)			Average Leakage Rate			Remarks
									Total (Buffer)	Crankcase	Outer	
						Total	Dyn.	Static	Pints/ 1000 hrs	Pints/ 1000 hrs	Pints/ 1000 hrs	
1	Chicago Rawhide	Cyclic	3303	80	1	48	38	10	0.275	0	0.275	
						80	64	16	4.44	0	4.44	Terminated Test
				3223	2	1600	949	651	1.03	0.29	0.74	Inspected Seals
						2110	1373	737	1.70	0.38	1.32	Restored Spring Force
					3	605	562	43	1.91	0.855	1.055	Restored Spring Force
					4	508	508	–	1.08	0.64	0.44	End of Test
2	Crane	Cyclic	3082	3082	1	150	–	150	0	0	0	Initial Static Test
					2	191	146	45	3.03	1.23	1.80	Terminated Test
					3	72	52	20	3.30	2.83	0.47	Leakage Too High
					4	1200	726	474	1.97	0.84	1.13	Inspected and Cleaned Seals
					5	1469	1405	64	1.92	0.342	1.578	End of Test
3	Chicago Rawhide	Continuous	5810	248	1	200	200	–	0.76	0.45	0.31	Terminated Test (Leakage continued to go up)
						248	248	–	1.35	0.74	0.61	
				283	2	283	283	–	1.92	0.24	1.68	Buffer Leakage Did Not Level Off
				817	3	117	117	–	2.91	1.97	0.94	Seal Ring Not Seated Properly
					4	633	633	–	2.29	0.494	1.796	Terminated Test (Carbon Face Worn)
						700	700	–	3.00	1.81	1.19	
				4462	5*	1275	1275	–	0.213	0.138	0.075	Air Leak into Crankcase Lost F-85 Inventory
					6*	3187	3187	–	0.438	0.183	0.255	Still Running
4	Crane	Continuous	6112	471	1	180	180	–	2.11	0.028	2.08	Buffer Leakage Did Not Level Off
					2	210	210	–	0.822	0.126	0.696	Not Consistent
						239	239	–	1.19	0.455	0.735	
					3	52	52	–	4.18	0	4.18	Buffer Leakage Too High
				5641	4*	218	218	–	2.45	0.125	2.32	Not Consistent
					5*	98	98	–	4.70	1.39	3.31	Shaft Seal Boot Crimped
					6*	5325	5325	–	0.323	0.054	0.269	Still Running

*These tests using Fluorinol-85 as working fluid and Suniso 3GS oil as lubricant.

of 0.44 pints/1000 hours and 0.32 pints/1000 hours, respectively. All leakage data given in the test results are average leakage rates determined by the full amount of leakage over the full time period being considered. A review of the testing results on each test stand will now be presented.

a. Test Stand No. 1

The tests performed on this seal test stand were run under cyclic operating conditions. All the tests were run with thiophene organic fluid in the vapor volume, with GE F-50 silicone oil used in the buffer zone and as the lubricant.

A total of two Chicago Rawhide double face seals were tested during the course of the 3000-hour experiment. The first set of seals ran a total of 80 hours during actual testing time (Run No. 1). Since this seal set was the first to be used in the experiment, it was assembled and disassembled more than once during the initial start-up and "debugging" period. As a result, the faces developed scratches that spanned the entire seal contact area; subsequently, there was early seal failure. Handling and assembly procedures were initiated during this early stage of testing to avoid damage to any of the seal components upon installation.

Run No. 2 was the best run of this series. The buffer and crankcase leakage rates over the entire test period of 2110 hours are presented in Figure III-14. For approximately 1600 hours, the seal was fairly consistent in performance, with a buffer fluid (total) leakage rate of 1.03 pints/1000 hours and a crankcase leakage rate (inboard) of 0.29 pint/1000 hours. This run was ended

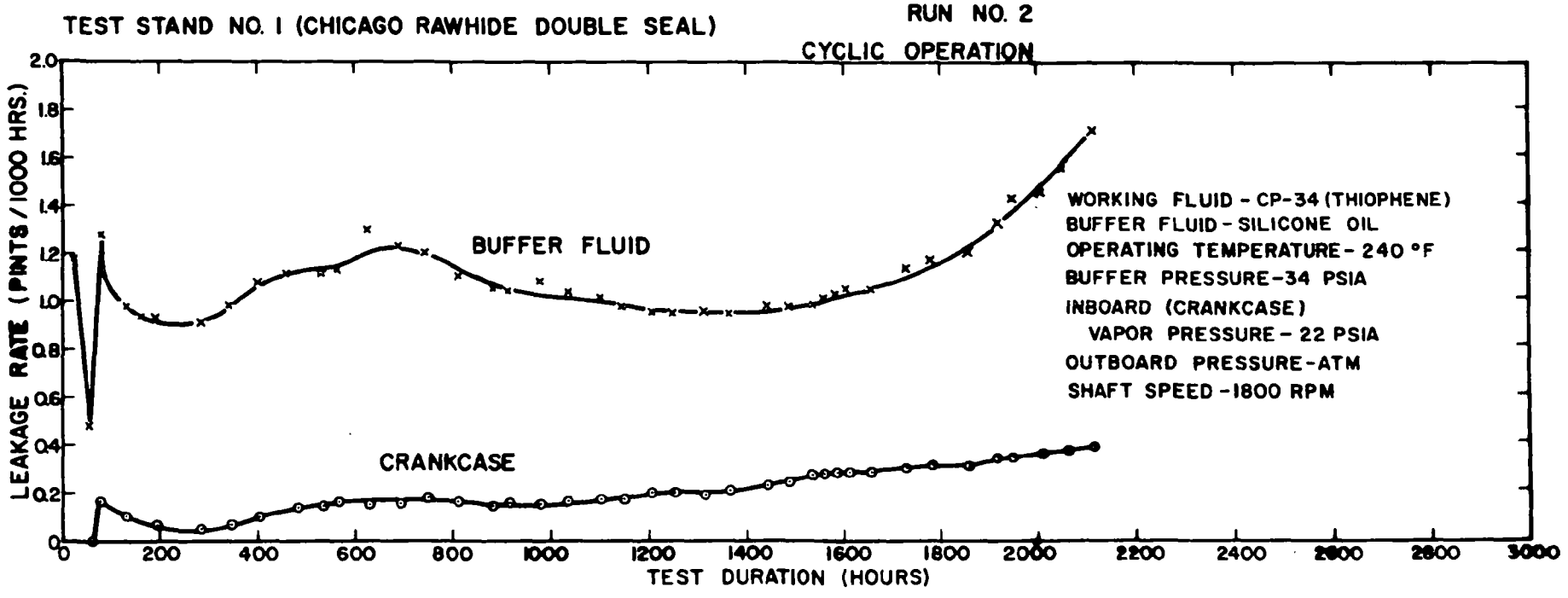

Figure III-14. Seal Leakage Rate versus Time, Test Stand No. 1.

at 2110 hours when the leakage rates continued to go up to the values seen in Figure III-14.

Upon examination of the seals following Run No. 2, it was found that the carbon ring within the cartridge was not properly seated and that the spring force was not uniform around the seal face. Since the spring and carbon ring are contained within the seal cartridge, it was not possible to determine the exact cause of the improper seating without destroying the entire seal. In an attempt to restore the seal, it was cleaned and flushed with a solvent until the carbon ring did reseat within the cartridge. Since the seal faces exhibited no excessive wear and there was no evidence of any other malfunctions, the seal set was reinstalled and tested once again as Run No. 3.

Run No. 3 was stopped after 605 hours of testing; inspection indicated the same carbon ring seating problem. Once again, the cartridge was flushed out and cleaned until the carbon re-seated itself. Run No. 4 with this same seal set accumulated 508 hours to the conclusion of the experiment on this test stand and displayed reasonable leakage rates with buffer (total) leakage rate equal to 1.08 pints/1000 hours and the crankcase leakage rate equal to 0.64 pint/1000 hours.

A more accurate measurement of the leakage rate was made periodically during the tests by taking a sample of the fluid from the organic chamber and analyzing it for oil content. At the 1300-hour mark of Run No. 2, a sample was taken and analyzed. The average leakage rate determined from the sample was 0.19 pint/1000 hours as compared to the measured leakage rate

into the crankcase of 0.20 pint/1000 hours (see Figure III-14). The agreement is within 0.5% and other such checks made during testing on all test stands were good, agreeing within 10%.

b. Test Stand No. 2

A Crane double face seal was used on this test stand, and only one seal set was used for the entire experiment. This Crane seal was tested in the cyclic mode of operation with thiophene as the working fluid and GE F-50 silicone oil as the buffer and lubricating oil for the entire testing period of this test stand.

A total of 5 runs were made on this seal set, with Runs 4 and 5 being the long-duration tests of the series. Run 1 was an initial static test of 150 hours duration with no measurable leakage (see Table III-2). The cyclic tests were begun with Run 2, which ran for 191 hours. The leakage in this run was more than desirable, so the seal set was inspected at this point. There was no damage visible to the seal faces; the seal set was once again installed and tested. Run 3 was terminated when the rear oil seal on the shaft of the test rig failed and all the lubricating oil to the bearings was lost, causing damage to the bearings, which then had to be replaced, Again, when inspected the seal set did not show any damage and the seal set was installed for Run No. 4. Figure III-15 shows the leakage rate versus time for Run 4. After 600 hours of running with a buffer leakage rate of 1.0 pint/1000 hours and a crankcase leakage rate of 0.6 pint/1000 hours, the buffer and crankcase leakages increased to 1.97 pints/1000 hours and 0.84 pint/1000 hours, respectively, at the 1200-hour mark; at that time, the run

was stopped. After inspecting and cleaning the seal set, no apparent damage was present. The seal set was reinstalled; Run No. 5 was started and was run for 1469 hours to the completion of the experiment. The final buffer and crankcase leakage rates for this run were 1.92 and 0.34 pint/1000 hours, respectively.

In this series of cyclic tests, the average ratio of dynamic to static leakage was better than 5 to 1. While the total buffer leakage rate in the dynamic mode was 2.0 pints/1000 hours, the static leakage rate over the test period was measured at 0.3 to 0.4 pint/1000 hours. This dynamic-to-static ratio was also applicable to the crankcase leakage rate.

c. Test Stand No. 3

Four sets of Chicago Rawhide seals were used in the testing on Test Stand 3. Three sets were used with thiophene working fluid and silicone oil as the buffer and lubricating oil on Runs 1 - 4 inclusive; the other set was used with Fluorinol-85 working fluid and Suniso 3GS as the buffer fluid and lubricant. All runs in this series were continuous in the dynamic mode of operation.

The initial runs of this series were short duration tests. The seal set used in Run 1 developed a sludge coating in the seal contact area, while the mating ring in the seal set used in Run 2 had some doubtful scratches on one of its mating faces. Runs 3 and 4 utilized a new seal set; the leakage rate results and problems encountered are summarized in Table III-2.

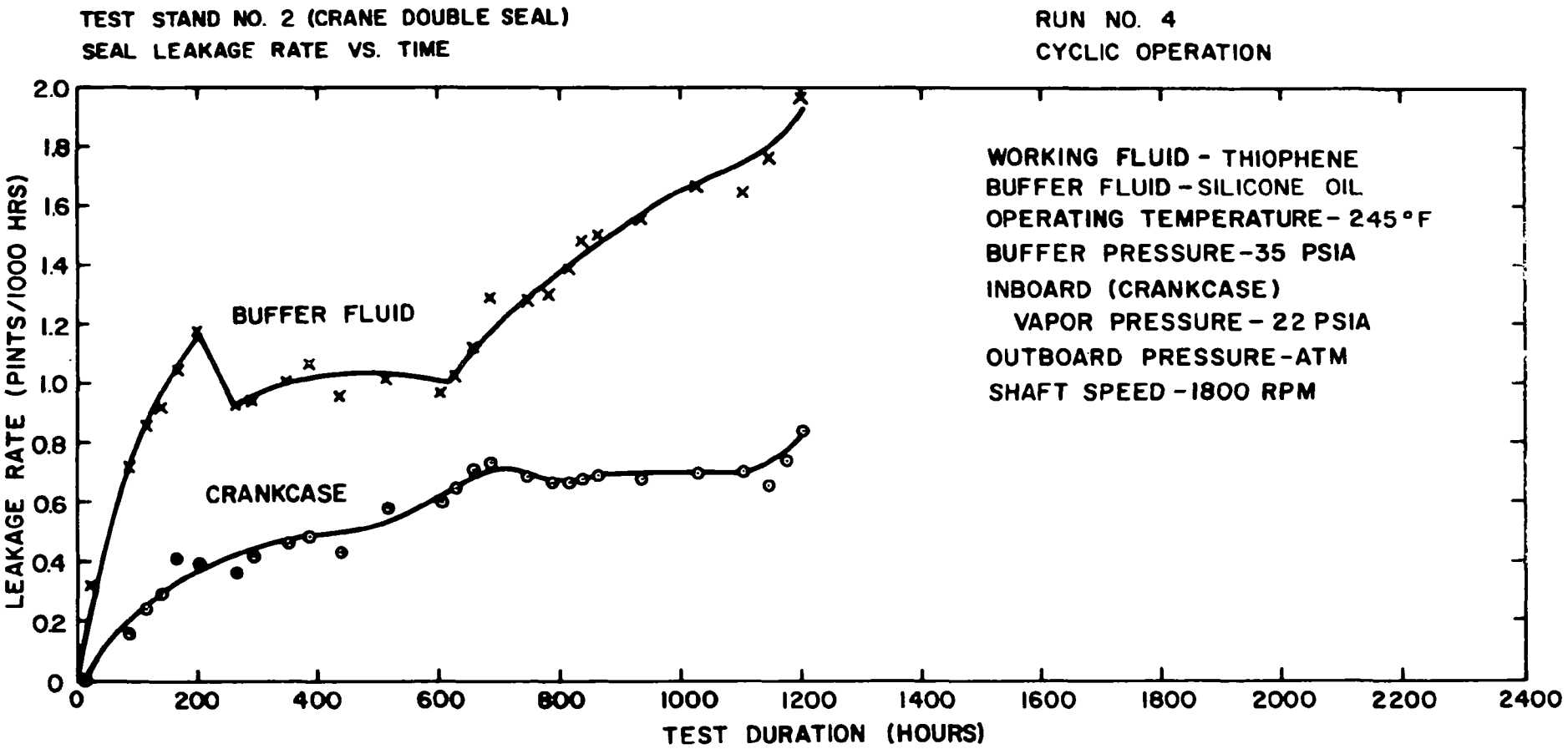

Figure III-15. Seal Leakage Rate versus Time, Test Stand No. 2.

It was decided at this point to change working and buffer fluids for Run No. 5 to Fluorinol-85 and Suniso 3 G55, respectively. The system was thoroughly cleaned and flushed out, and was subsequently charged with the Fluorinol-85 working fluid and Suniso 3 GS buffer and lubricating oil. A new seal set was installed; the results showed buffer and crankcase leakage rates of 0.213 pints/1000 hours and 0.138 pint/1000 hours, respectively, up to the 1275-hour mark (see Figure III-16). At this point, a leak developed in the organic chamber sight glass and the Fluorinol-85 fluid in the organic chamber was lost. The system was shut down and the seal set removed for inspection. The seal set was in good condition and was therefore re-installed for Run No. 6. After displaying a "break-in" period, as seen in Figure III-17, the leakages settled out to acceptable rates of 0.438 pint/1000 hours (total) and 0.183 pint/1000 hours (crankcase) at 3187 hours of Run No. 6.

d. Test Stand No. 4

Test Stand No. 4 was used to test two sets of Crane seals in the continuous mode of operation. The first three runs on the first seal set used thiophene and GE F-50, and totalled 471 hours. These initial runs, as shown in Table III-2, gave high and inconsistent leakage rates. Although one of the carbon rings had a chip in it, the same seal set was used for these three runs until it was determined that the width of the chip protruded too much into the contact area and should be replaced.

At the time the second Crane seal set was put into the system, the working and buffer fluids were also changed to Fluorinol-85

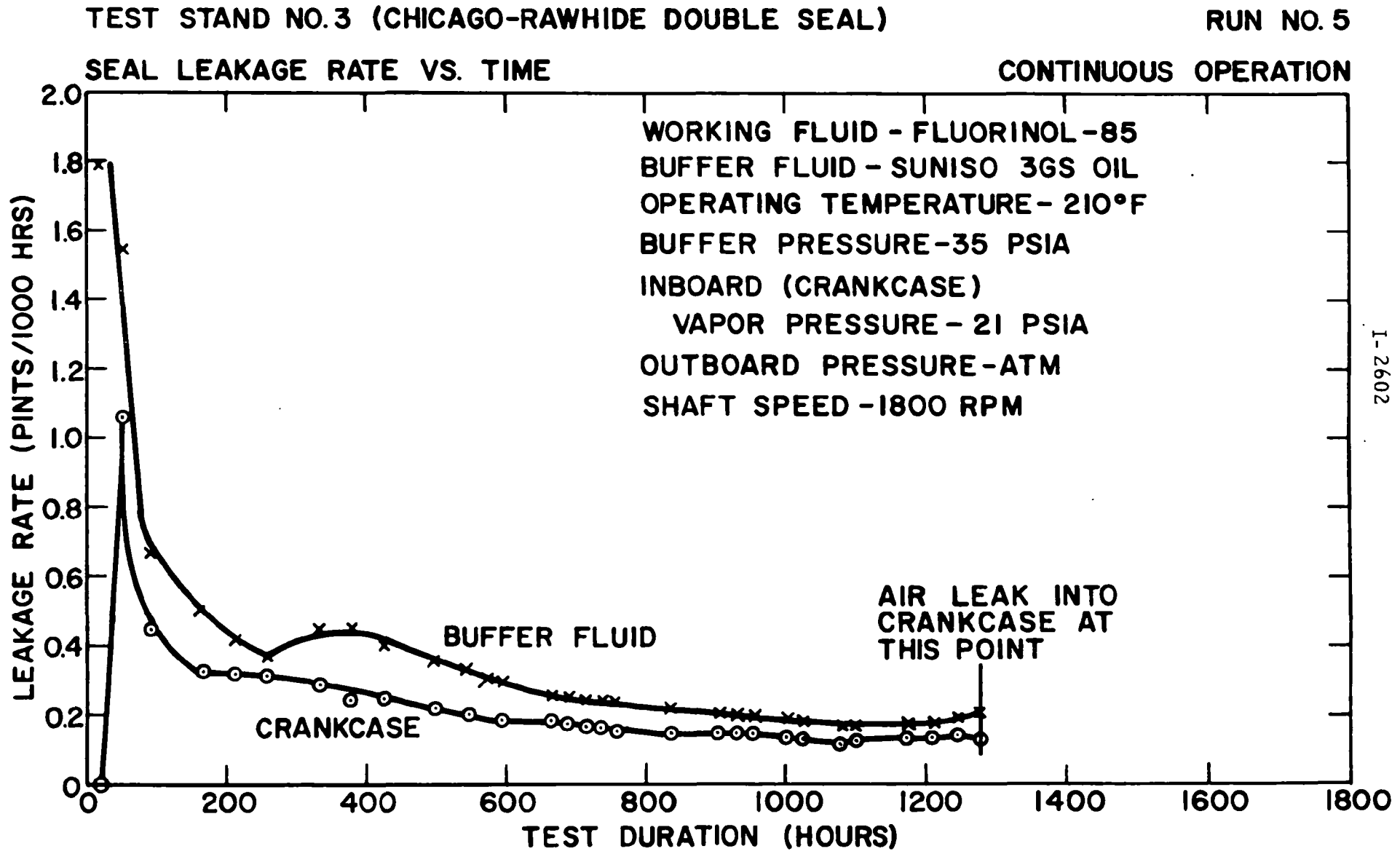

Figure III-16. Seal Leakage Rate versus Time, Test Stand No. 3.

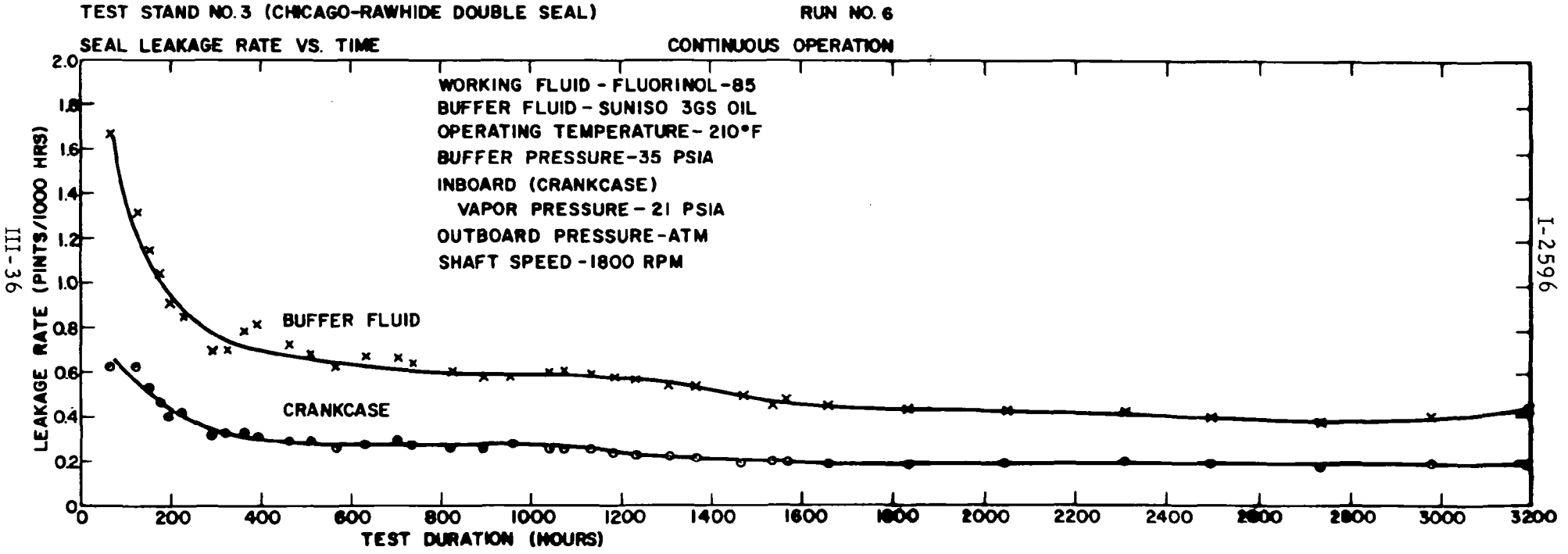

III-36

I-2596

Figure III-17. Seal Leakage Rate versus Time, Test Stand No. 3 .

and Suniso 3 GS oil, respectively. Runs 4 and 5 with the new seal set and working fluid gave unacceptable results. It was discovered after Run No. 5 that the rubber diaphragm on the shaft was crimped, causing leakage by this area. After this problem was remedied, Run No. 6 was begun; it has run for 5325 hours. This run was the most successful of all tests performed, showing a buffer leakage rate of 0.323 pint/1000 hours and a crankcase leakage rate of 0.054 pint/1000 hours over more than 5000 hours of test. Figure III-18 is a plot of the leakage rate as a function of running time for Run No. 6.

An analysis made on a sample of working fluid from an earlier run in this series for oil content showed good agreement once again with the level gauge measurement of leakage. For the same time period, the level gauge indicated a crankcase leakage rate of 0.455 pint/1000 hours, while the analyzed sample gave a leakage rate of 0.482 pint/1000 hours. Because of the good agreement between the two methods of leakage measurement, the liquid level gauges were used as the basis for measuring all leakages, with periodic analysis of the working fluid for oil content performed as a check.

e. Power Requirements

Some measurements were made on the shaft seal units to determine the power necessary to run the seals. A watt-meter was used with the drive motor characteristics to measure the power requirements for the seal units at dynamic operating conditions. From the measurements, it was determined that the net power required to drive the Chicago-Rawhide seals at

16.0 rpm was approximately 100 watts and for the Crane seals was approximately 150 watts.

D. DISCUSSION AND EVALUATION

Based on the experimental results, it is apparent that use of Fluorinol-85 with Suniso 3GS buffer fluid gives much more reliable seal operation than use of thiophene with GE F-50 buffer fluid. The leakage rates were the lowest when using the Fluorinol-85, and low leakage rate was maintained on both the Chicago Rawhide and Crane seal sets. Several characteristics are believed responsible for these more favorable results with Fluorinol-85. First of all, the Fluorinol 85-Suniso 3GS combination is immiscible, whereas the thiophene-GE F-50 combination is miscible. Even though the buffer fluid is under pressure in the seal cavity, in the latter case there is a tendency for the thiophene to diffuse into the oil film between the faces, diluting the oil film and affecting its lubricating properties. This factor, coupled with the superior lubricating properties of the Suniso 3 GS relative to the GE F-50, could lead to seal ring wear and, more important, local overheating. A second factor is the greater tendency for the thiophene-GE F-50 combination to form sludges which, particularly for the Chicago Rawhide seal set resulted in binding of the carbon seal rings. The thiophene-GE F-50 combination at a given operating temperature, particularly with air present, is not nearly as stable as the Fluorinol-85-Suniso 3GS combination. An additional factor was the greater potential for local hot spots with the thiophene-GE F-50 combination because of its poor lubricating properties, which thereby accelerates sludge formation.

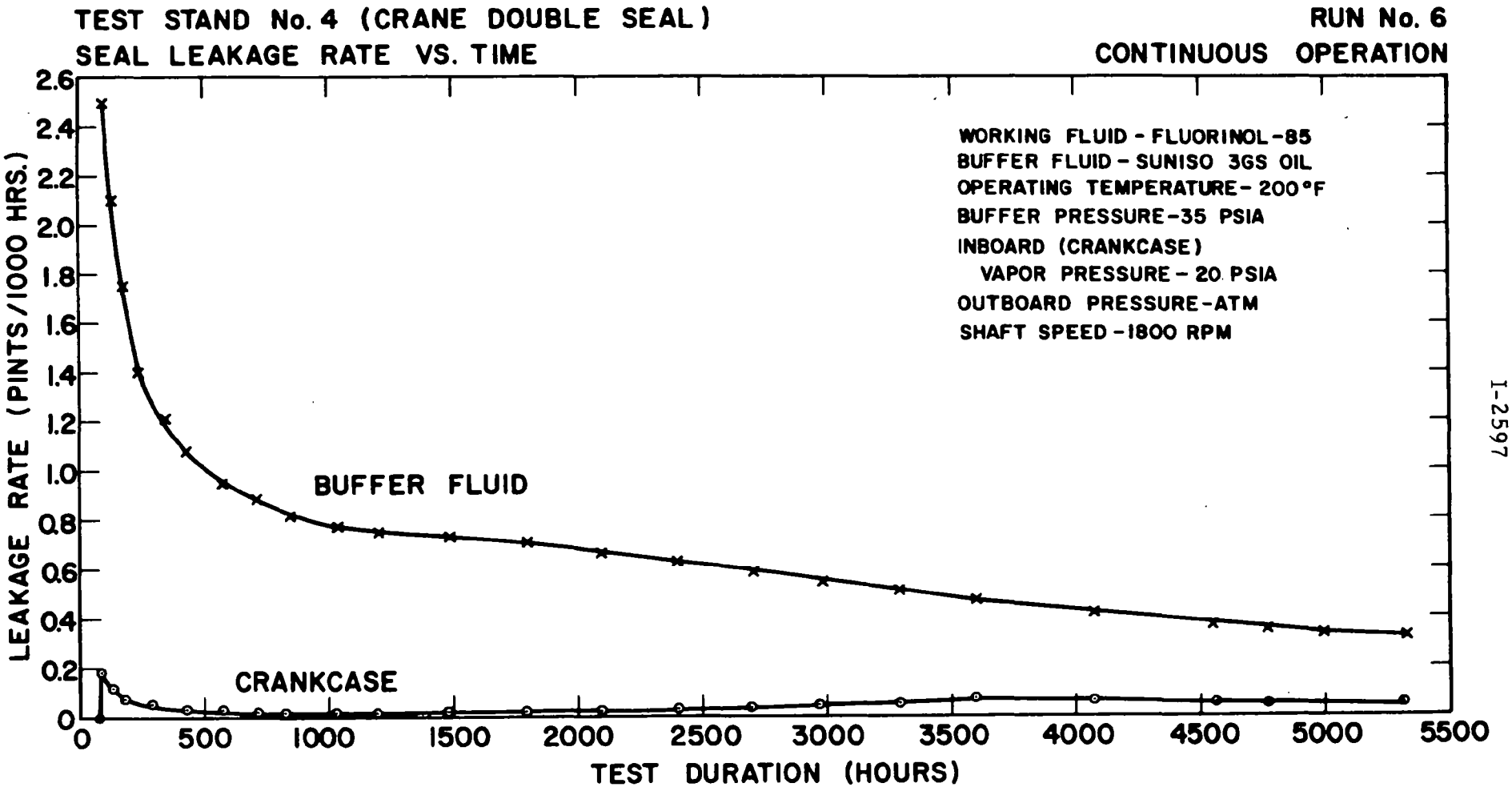

Figure III-18. Seal Leakage Rate versus Time, Test Stand No. 4.

With the Fluorinol-85-Suniso 3 GS combination, the results on test stands 3 and 4 indicate that both the Chicago Rawhide seal set and the Crane seal set should be suitable for use in the system. Both seal sets gave acceptable leak rates over a running time of more than 3000 hours. The shutdown leakage rates of both types of seal were also very low, in general unmeasurable on the test rig to a factor of 5 less than the dynamic leak rate. All testing with the Fluorinol 85-Suniso 3GS combination was carried out continuously, however, and additional cyclic testing would be useful to establish the seal behavior under conditions simulating those which will be encountered in actual practice. The cycling should not introduce problems; the cycling tests with the thiophene-GE F-50 combination were as successful in general as the continuous tests.

With the exception of Run No. 4 on Test Stand 3, wear of the carbon faces has not been a problem and in general has not been measureable. Where leakage has developed during a test, it has been due to causes other than carbon ring wear.

The testing had indicated that care must be used in inspection and assembly of the seals if acceptable results are to be obtained. Scratches extending across the seal faces or chips extending a fraction of the way across the seal faces will result in unacceptable leakage. Care must be used in assembly to insure cleanliness of the seal faces, to insure that the seal faces are not scratched in assembly, to insure that all dimensions are within tolerance, to coat the seal faces with lubricant before assembly, and to leak test the seal assembly statically before use to insure that there are no leaks through either the seal faces or the static seals in the assembly. If these precautions are followed,

one can expect the seal to operate satisfactorily with a high confidence level, particularly if the Fluorinol-Suniso 3GS combination is used.

The power required for the seal is approximately 100 watts (0.13 hp) for each type of seal.

In selecting the seal type to be used on the expander, the following characteristics are important for each seal type:

a. Chicago Rawhide Seal

(1) This seal requires a stepped shaft which leads to dimensional dependence on other components in the expander assembly. Dimensional tolerances become additive and therefore more critical.

(2) This seal requires a minimum axial length on the shaft and leads to a minimum overall length of the expander.

(3) The carbon seal cartridge is completely enclosed with an integral spring and is therefore easier to assemble and install. The enclosed carbon ring-spring assembly has closer tolerances, however, and is more susceptible to binding if sludge occurs than is the Crane seal.

b. Crane Seal

(1) The Crane seal fits on a shaft of uniform diameter. Dimensional tolerances and tolerance buildup is therefore not as critical as for the Chicago Rawhide seal.

(2) Because of the large diameter spring, a longer axial length is required for the seal unit, leading to a longer overall length of the expander.

(3) The spring in this seal gives a more uniform load over the seal contact area.

(4) The seal components are not contained in an enclosure and are much less susceptible to binding because of sludge formation or other contamination of the buffer fluid. Failure due to binding was not encountered on any of the tests with the Crane seal.

In conclusion, the test results indicate a high confidence level that both types of seals will perform satisfactorily in the system. Additional testing, particularly cyclic testing with the Fluorinol-85 - Suniso 3GS combination, should be carried out to complete the testing as well as to gain additional experience in assembly and installation of the seals in a manner which insures acceptable leakage. It should be pointed out that the double-face seal approach is used on the 5.5 hp systems under test at Thermo Electron Corporation (3/4 inch diameter shaft). On three systems tested for a total of about 650 hours, with numerous on-off cycles as well as extended shutdown periods, no seal failure has occurred.

APPENDIX IV

EVALUATION OF A BALL MATRIX AS AN EXTENDED SURFACE

A. INTRODUCTION

Ball matrix surfaces offer a very high heat transfer area per unit volume, and thereby have the potential of yielding a very compact heat exchanger, provided this area can be used effectively. Much research has been carried out to evaluate the heat transfer in porous media and in randomly packed sphere beds. Most of the previous applications involved the use of a ball matrix in cyclic heat exchangers; therefore, the question of surface (or fin) effectiveness did not arise. Based on the data reported for packed beds, a comparison of ball matrices with other heat transfer surfaces on an equal area basis and an equal volume basis is shown in Figures IV-1 and IV-2. From these plots, the ball matrix surface appears attractive for a very compact exchanger. Thus, the ball matrix was used in the third stage of the boiler designed under Contract CPA 22-69-132, as described in the final report issued in June, 1970[1]. In the current study, further evaluation of the ball matrix surface as an extended surface for heat exchanger applications has been made using experimental measurements. In the light of the information obtained, the preheat stage of the boiler design with ball matrix has been revised and compared with a conventional finned tube heat exchanger.

B. DESCRIPTION OF TEST UNIT

A test unit was designed to represent the third stage of the boiler in the conceptual design prepared under Contract CPA 22-69-132[1]. The unit consists of five steel tubes 1.315" O.D., with center-to-center spacing of 2.125". The flow of gas is normal to the tubes (i.e. cross-flow); the depth of the brazed ball matrix mounted between the tubes in the direction of gas flow is 1/2". All of these dimensions are identical to those used in the reference boiler design. A schematic of the test unit is shown in Figure IV-3 and a photograph of the test unit used in the experimental measurements is presented in Figure IV-4. The ball matrix consists of 3/32" diameter carbon steel burnishing balls brazed with pure copper. The overall dimensions of the test section are 11.25" x 13.7".

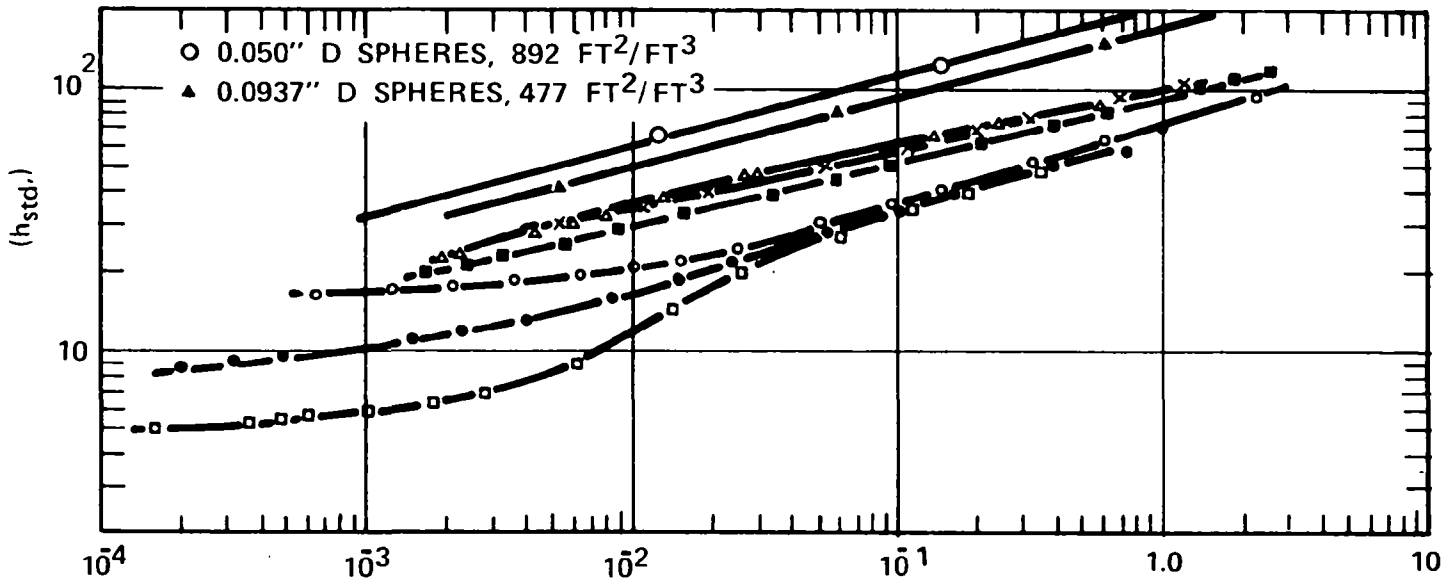

KEY	TYPE OF SURFACE	CODE NUMBER	β FT²/FT³
×	RUFFLED FINS	17.8 - 3/8 R	514
△	IN LINE PIN FINS	AP-2	244
■	LOUVERED PLATE FINS	3/8 - 11.1	367
○	PLAIN PLATE FINS	19.86	561
□	INSIDE CIRCULAR TUBES	ST-1	208
●	FINNED FLAT TUBE	9.68 - 0.87	305

Figure IV-1. Comparison of Compact Exchanger Surfaces on an Equal Area Basis Illustrating Compactness of Ball Matrix.

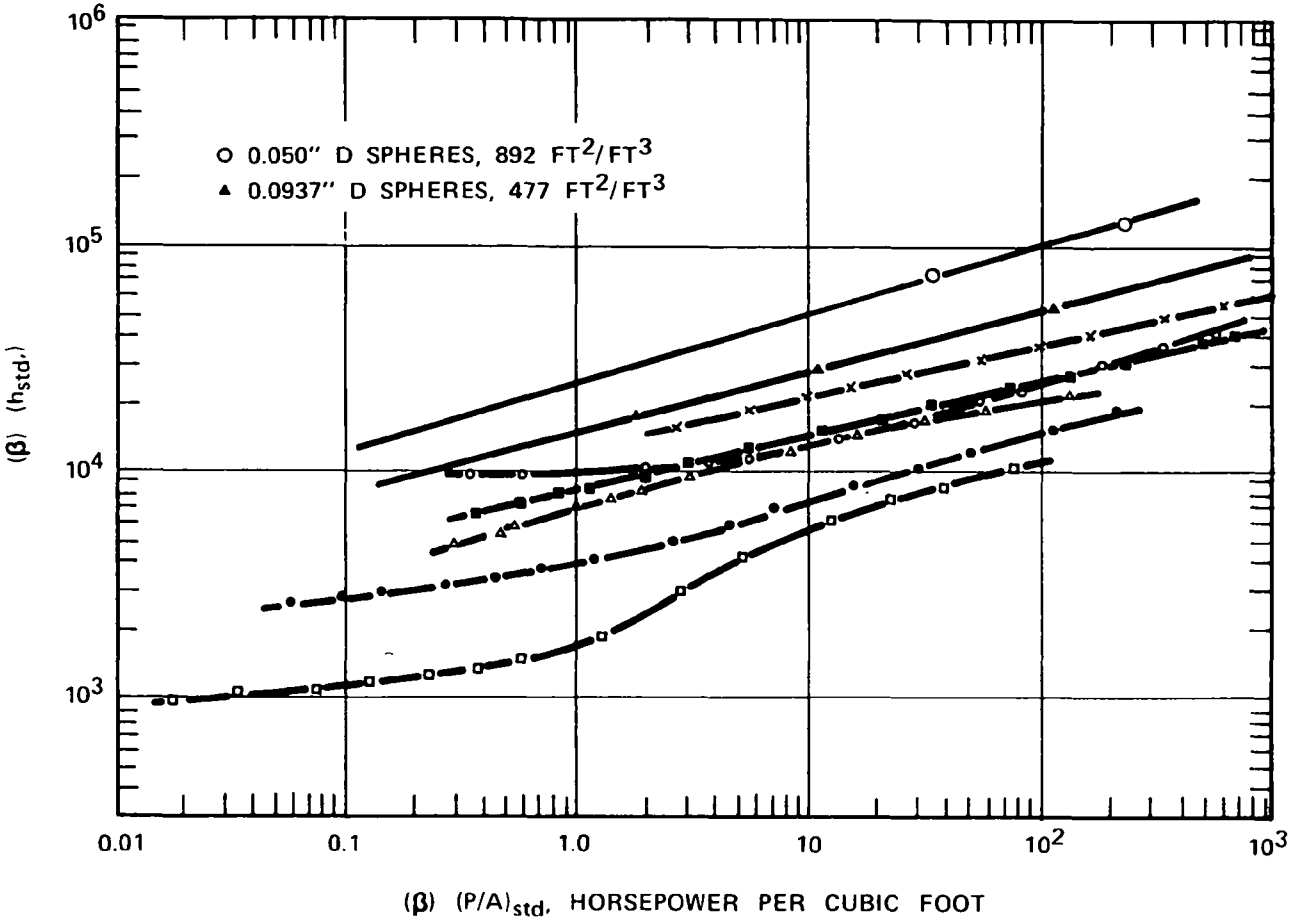

KEY	TYPE OF SURFACE	CODE NUMBER	β FT²/FT³
×	RUFFLED FINS	17.8 - 3/8 R	514
▲	IN LINE PIN FINS	AP-2	244
■	LOUVERED PLATE FINS	3/8 - 11.1	367
o	PLAIN PLATE FINS	19.86	561
□	INSIDE CIRCULAR TUBES	ST-1	208
●	FINNED FLAT TUBE	9.68 - 0.87	305

Figure IV-2. Comparison of Compact Heat Exchanger Surfaces on an Equal Volume Basis Illustrating Compactness of Ball Matrix.

8936

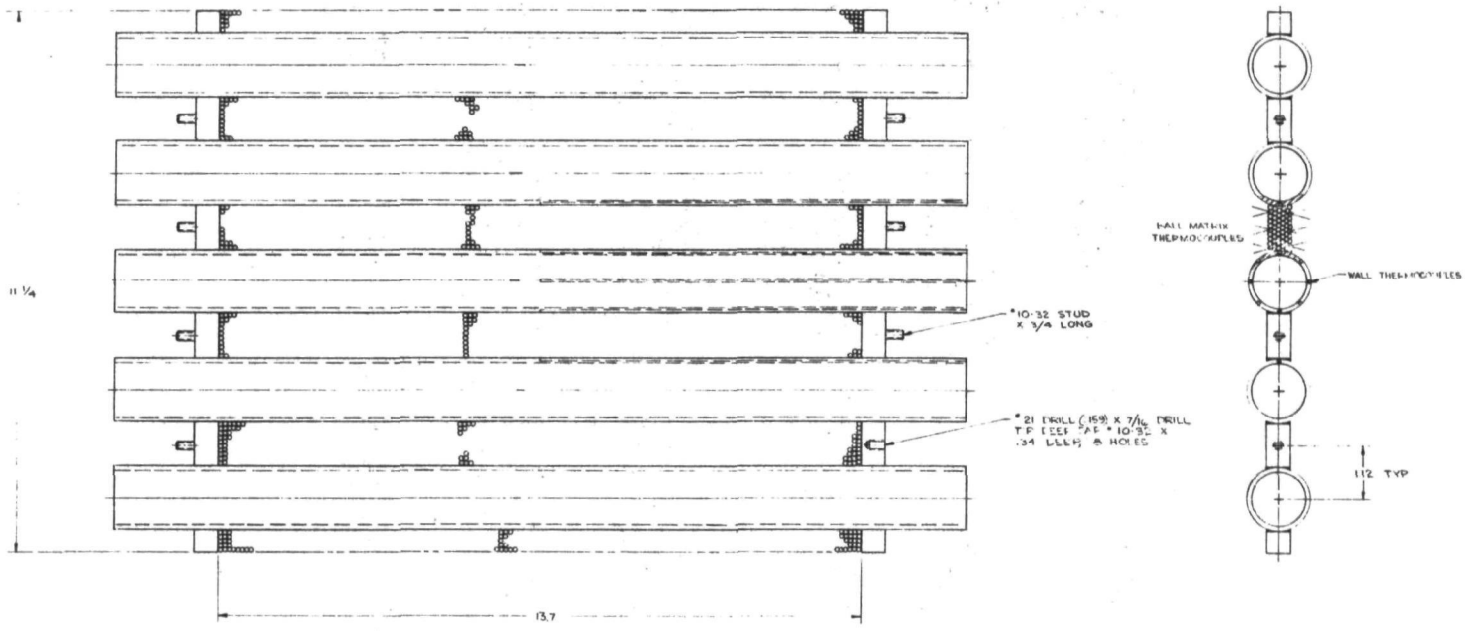

Figure IV-3. Test Section Ball Matrix.

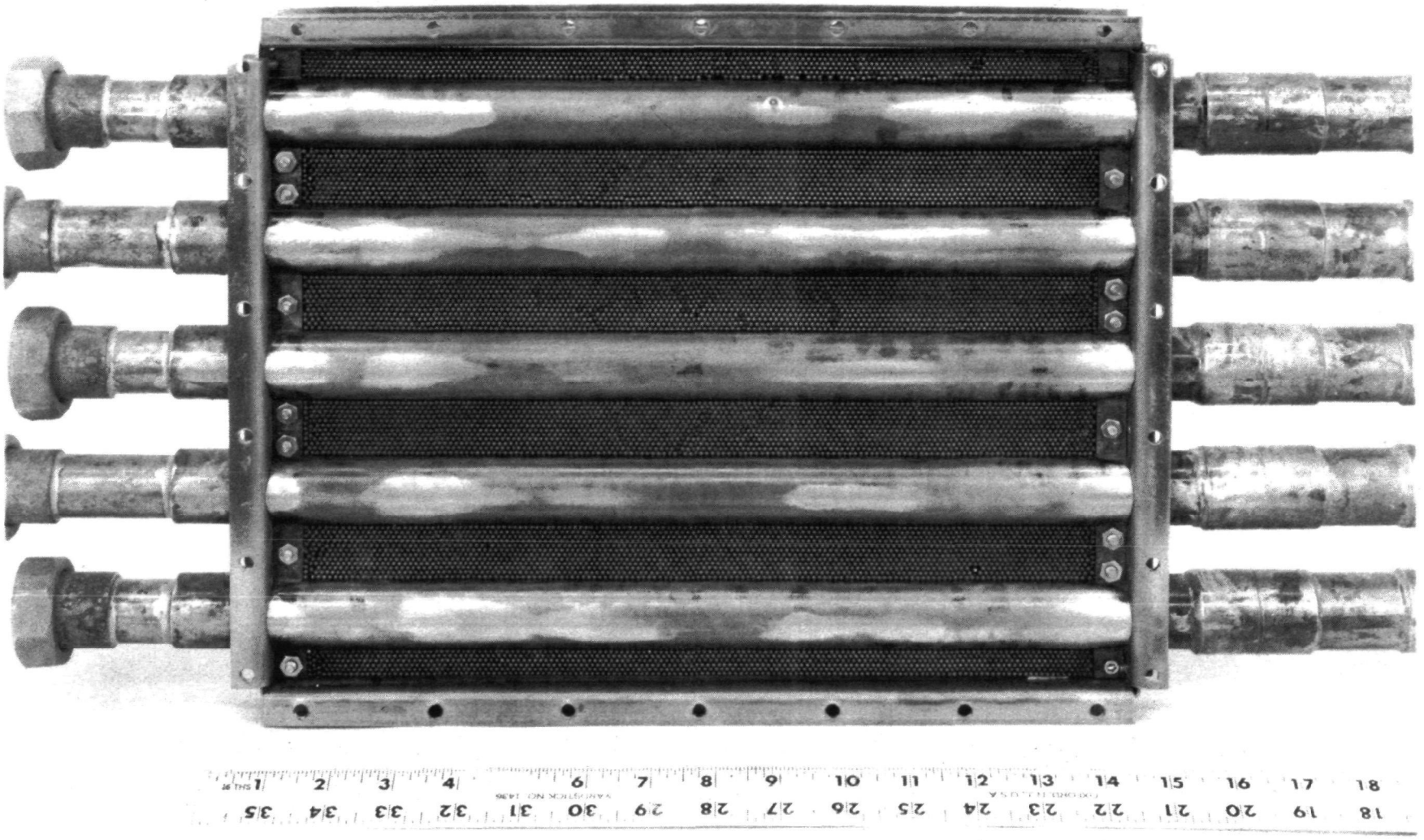

Figure IV-4. Photograph of Test Section.

C. FABRICATION OF TEST UNIT

As can be seen from Figure IV-4, the ball matrix surface in the reference design acts as an extended surface or fin. The process of heat transfer from a hot gas to a cold fluid inside the tube consists of two parts. First, heat is transferred from the gas to the balls by convection, in the same way as in a packed bed; this heat then is transferred to the tube carrying the cold fluid by conduction through the surrounding balls, since the ball matrix is used as a fin. In order to transfer the heat from the hot gas to the cold fluid effectively, a high overall thermal conductivity of the ball matrix is desirable. Perfectly round balls have only point-to-point contacts in a matrix, resulting in a very large constriction resistance and, therefore, low overall thermal conductivity of the packed bed. To improve the thermal conductivity of the bed, the balls are brazed together to provide a finite conduction path from one ball to the next. Copper was used as the bonding metal between carbon steel balls, because of its high thermal conductivity.

In fabricating the matrix for the test unit, the carbon steel tubes and the carbon steel balls were electroplated with a thin film of copper which served as the brazing material. The tubes and balls were then assembled in a special fixture for brazing; the fixture maintained pressure on the ball matrix during the brazing operation to insure maximum contact between the balls in the matrix and also between the tube wall and the ball matrix. Careful packing of the balls in the matrix region was essential to maximize ball-to-ball and ball-to-tube wall contact. In development of the brazing technique, a single tube module was used, as illustrated in Figures IV-5 and IV-6. This module was

also used in testing various "release" coatings to prevent brazing of the matrix to the brazing fixture.

In the development of the brazing technique using this single-tube module, the following parameters were found to be critical:

a. Copper Coating Thickness on Balls and Tube

An excessive copper-coating thickness resulted in plugging of the gas flow paths between the balls; too small a thickness resulted in incomplete brazing. The optimum coating thickness was determined experimentally to be 0.00033" - 0.00034". Complete brazing of all contact points was obtained with this thickness with no plugging of the test section, as illustrated in Figure IV-4. The average fillet diameter was 0.032" for 3/32" diameter balls. Because of the critical nature of the copper thickness, it was essential to have a uniform plate thickness on all of the balls making up the matrix. As shown in the photomicrograph of Figure IV-7, illustrating the coating thickness on three balls selected at random, no difficulty in the electroplating was encountered in obtaining a uniform coating on the balls and around the individual balls.

b. Heating Profile During Brazing

The temperature-time profile used in the furnace brazing operation is critical, particularly since some time is required for conduction of heat from the exterior of the test section to interior regions not directly in contact with the furnace gas. If the temperature is too high or maintained for too long, the copper evaporates, leaving insufficient material to form a good braze. If the temperature is not high enough or is not maintained for an adequate period, insufficient flow of the braze material

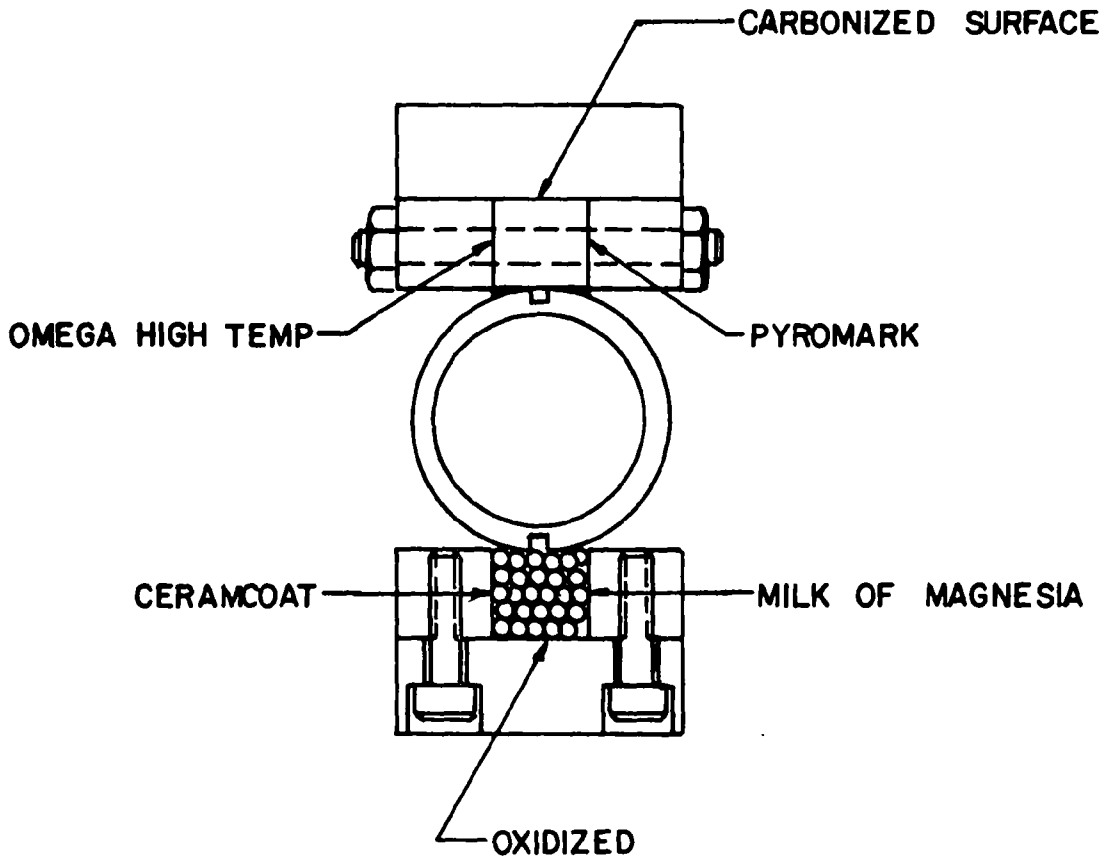

Figure IV-5. Brazing Checkout Module.

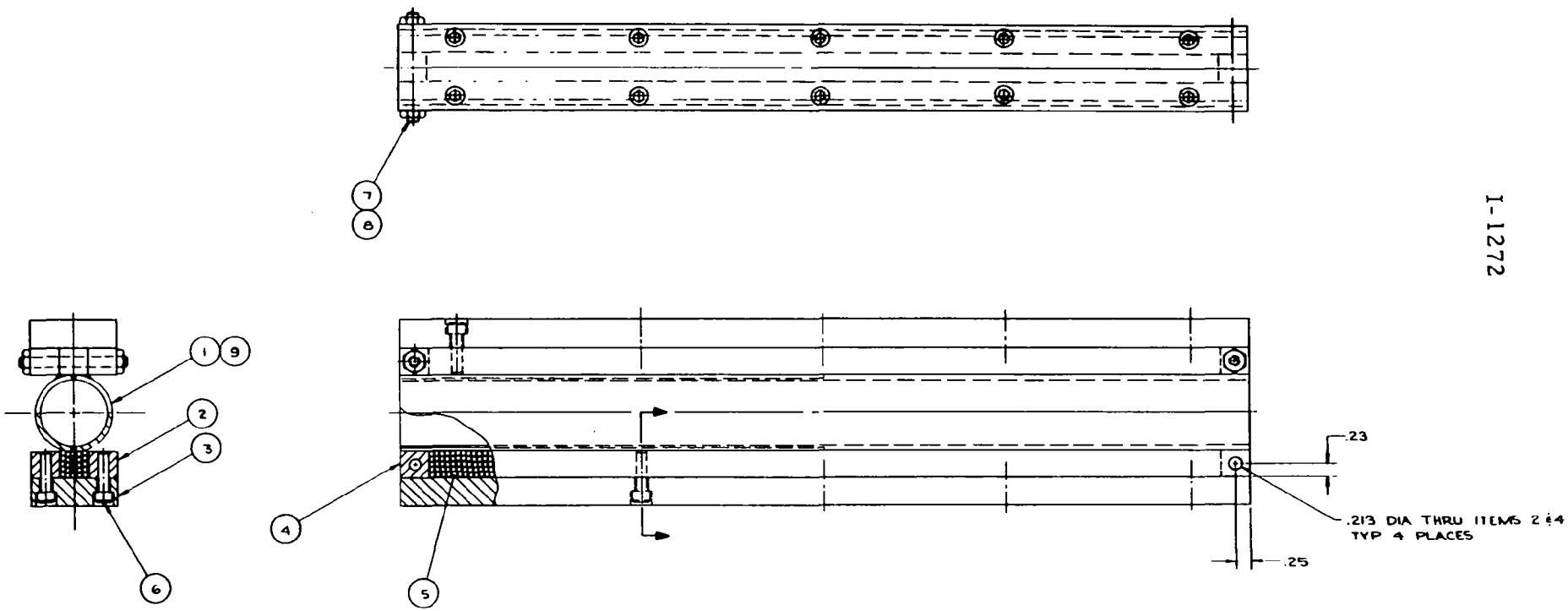

Figure IV-6. Boiler Matrix Brazing Checkout Module - Side View.

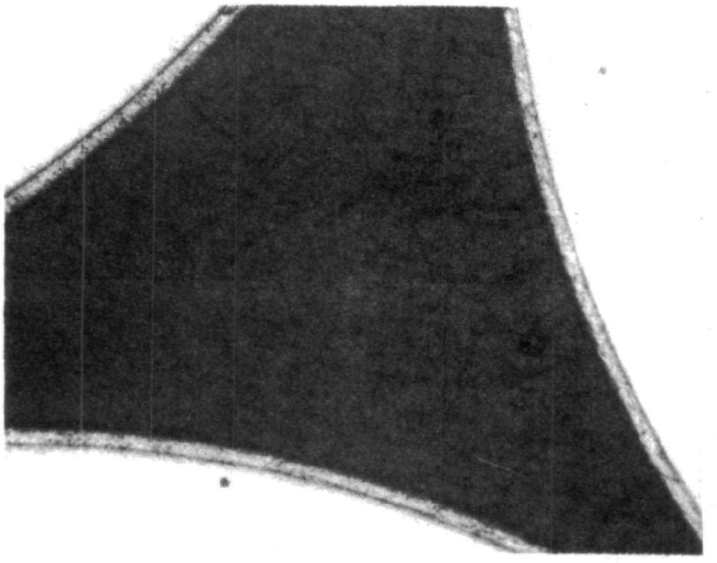

Figure IV-7. Copper Plated 3/32" Steel Balls, Magnification 150x. Thickness of Plating = .0006".

occurs again, resulting in a poor braze. After considerable experimentation, the temperature-time curve of Figure IV-8 provided satisfactory brazing. The furnace temperature was initially raised to 1920°F, just under the copper melting temperature of 1980°F, and allowed to soak thermally for 30 minutes to insure a uniform temperature through the test unit and brazing fixture. The furnace temperature was then raised to 2075°F and held at this temperature for 15 minutes, completing the brazing operation.

c. Design of Brazing Fixture to Maintain Pressure on Ball Matrix Elements During Brazing

During brazing, the flow of the copper braze to form fillets results in slight shrinkage of the matrix volume. The brazing fixture must, therefore, be designed to maintain force on the ball matrix section to insure ball-to-ball and ball-to-tube wall contact throughout the brazing operation. In Figure IV-9, an illustration is presented of tube wall separation and void formation in the matrix, which occur because of inadequate pressure during the brazing operation.

The brazing fixture was designed so that the volume of the balls was slightly greater than the volume formed by the test fixture walls. Bolting of the top cover plates (see Figure IV-5) in place then created a compression force on the ball matrix, eliminating this problem.

d. Release Coating on Test Fixture to Prevent Test Unit from Sticking to Brazing Fixture

Various release agents to coat the inside surfaces of the brazing fixture and to prevent sticking of the test unit to the brazing fixture were evaluated experimentally, as illustrated in Figure IV-5. Ceramacoat was found to yield the best results.

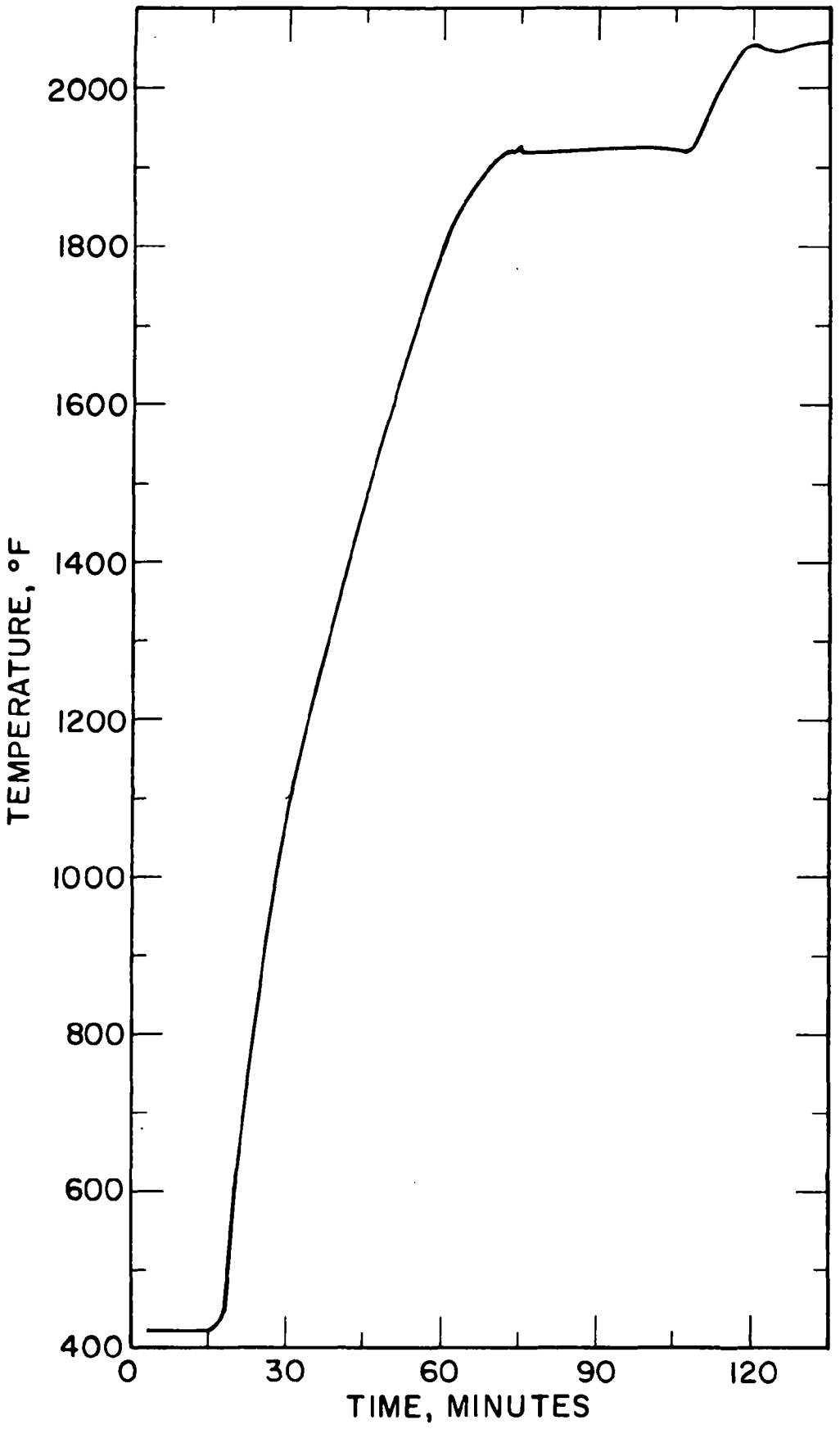

Figure IV-8. Brazing Temperature History.

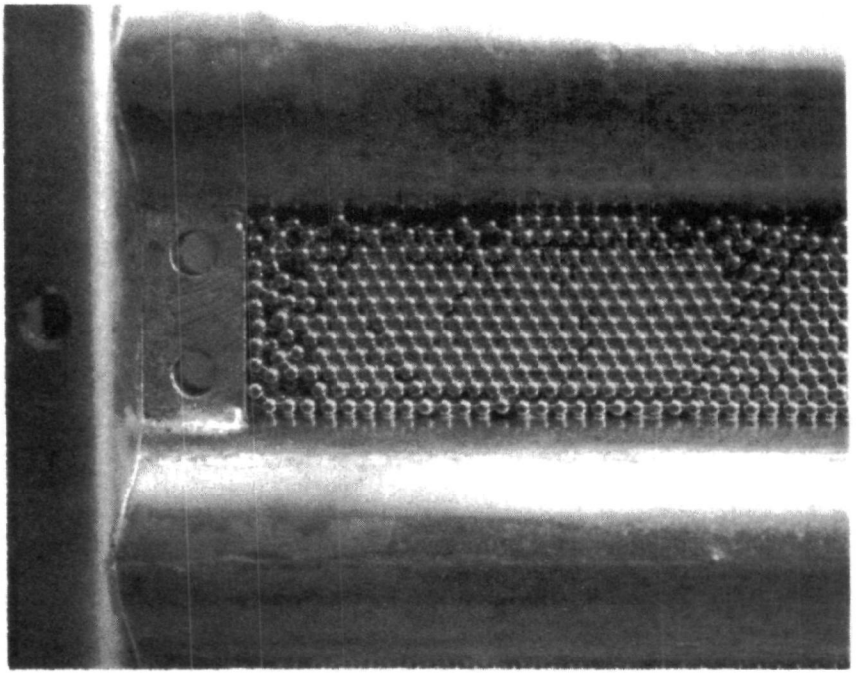

Figure IV-9. Braze Showing Ball Separation from Ball Matrix.

D. TEST LOOP

The flow schematic of the ball matrix test loop is shown in Figure IV-10. The test loop is comprised of two instrumented loops: a water loop and an air heating system. The water loop provides cooling water flow through the tubes of the test unit, and includes sufficient instrumentation for measurement of the heat transferred to the water in the test unit. The air heating system provides hot gas flow through the ball matrix sections of the test unit, and includes sufficient instrumentation both for measuring the heat transferred from the gas and for monitoring uniformity of the gas temperature at the inlet and outlet of the test unit.

The water loop consists of a circulating pump which drives water through a set of flowmeters (high flow or low flow). Two headers are installed at the entry and exit of the test section for proper distribution of water flow through the test section. All tubes in the test section carry the flow in parallel. The hot water coming out of the test section flows to a set of coolers which are cooled by city water. The city water flow rate is metered through a rotameter. An expansion tank and pressure relief valve are also part of this loop. The temperatures of the loop and city water are measured with copper-containing thermocouples at the inlet and exit of the heat exchangers.

All of the thermocouples were connected to ice junctions, with copper leads running from the junctions to a Honeywell potentiometer through a thermocouple selector switch. The potentiometer was capable of reading (Δ T) values within an accuracy of $\pm 0.2°F$. Extreme care was taken in the temperature measurement of loop water; the temperature rise of loop water could be as low as 5°F, allowing little

margin for error. The temperature level of the loop water was controlled by the city water flow rate. The loop water flow rate was generally kept constant at 10 gpm, whereas city water flow rate varied from 1 to 2 gpm.

The air heating system consists of an air and fuel supply to the combustor (Figure IV-11) and a dilution air supply to control the temperature of the gas entering the test section. The combustor performance is shown in Figure IV-12. The combustion chamber is ceramic-lined. A small compressor delivers the atomizing air to the atomizing nozzle. The fuel is pumped by aspiration by the atomizing air. The flow rates of both the atomizing air and the fuel flow are measured by rotameters.

Two air blowers were installed to supply combustion air and dilution air, respectively. Both combustion and dilution air rates were measured by using ASME standard orifices. Turning vanes were provided in the dilution air duct to improve mixing of the two streams. Mixing plates were also provided between the test section and the combustion chamber.

A set of radiation-shielded thermocouples (chromel-alumel type, stainless steel sheathed) were installed both in front and in back of the test section to measure the temperature profiles of the gas in the duct before and after the test section. A schematic of the thermocouple probe is shown in Figure IV-13. The temperature variation of the gas across the test unit was measured to be within 20° for all test conditions.

The loop was instrumented with manometers to measure the orifice ΔP and test section ΔP with an accuracy of 0.01 inch of water column

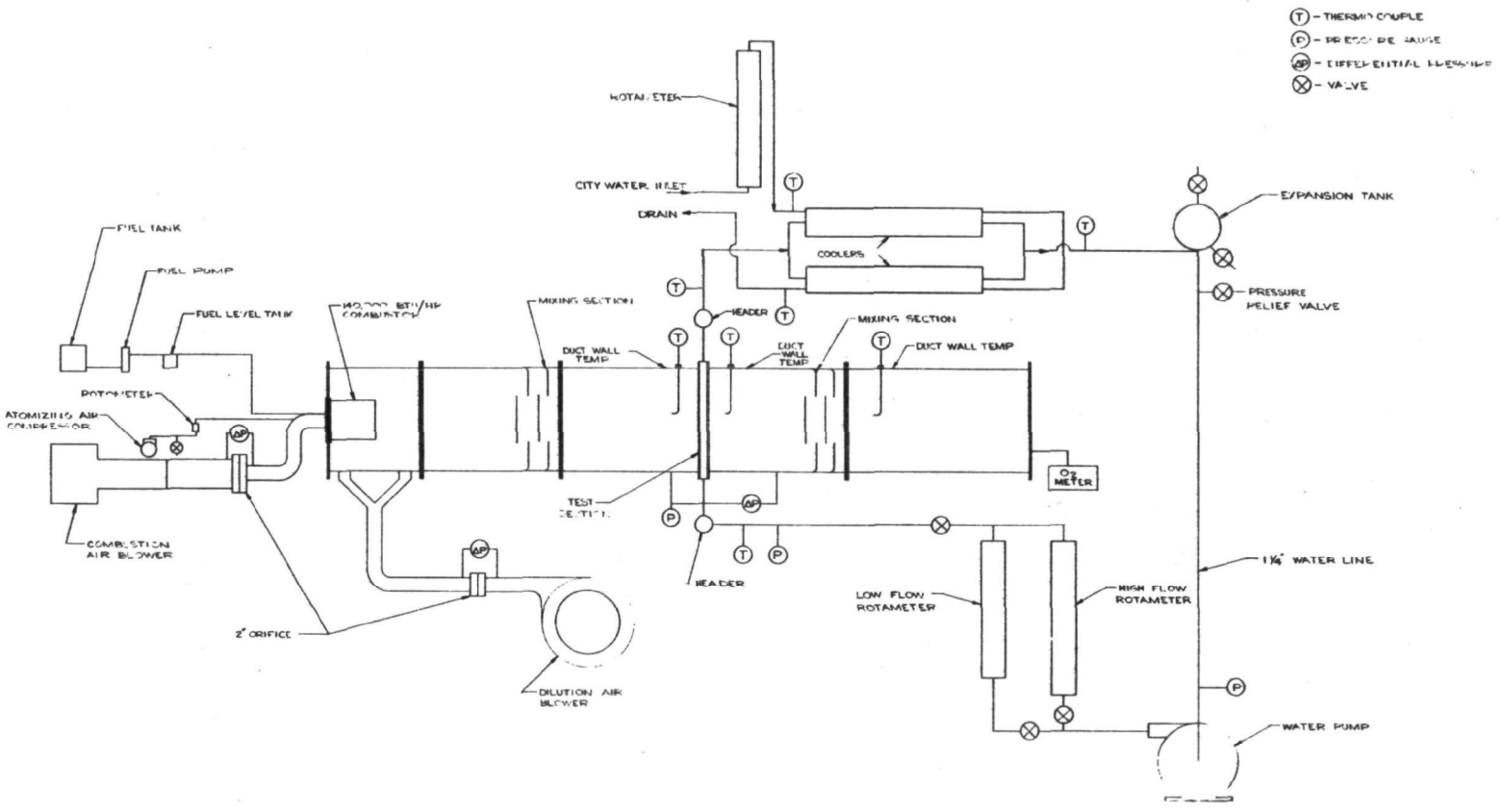

Figure IV-10. Flow Schematic-Boiler Matrix Test Facility.

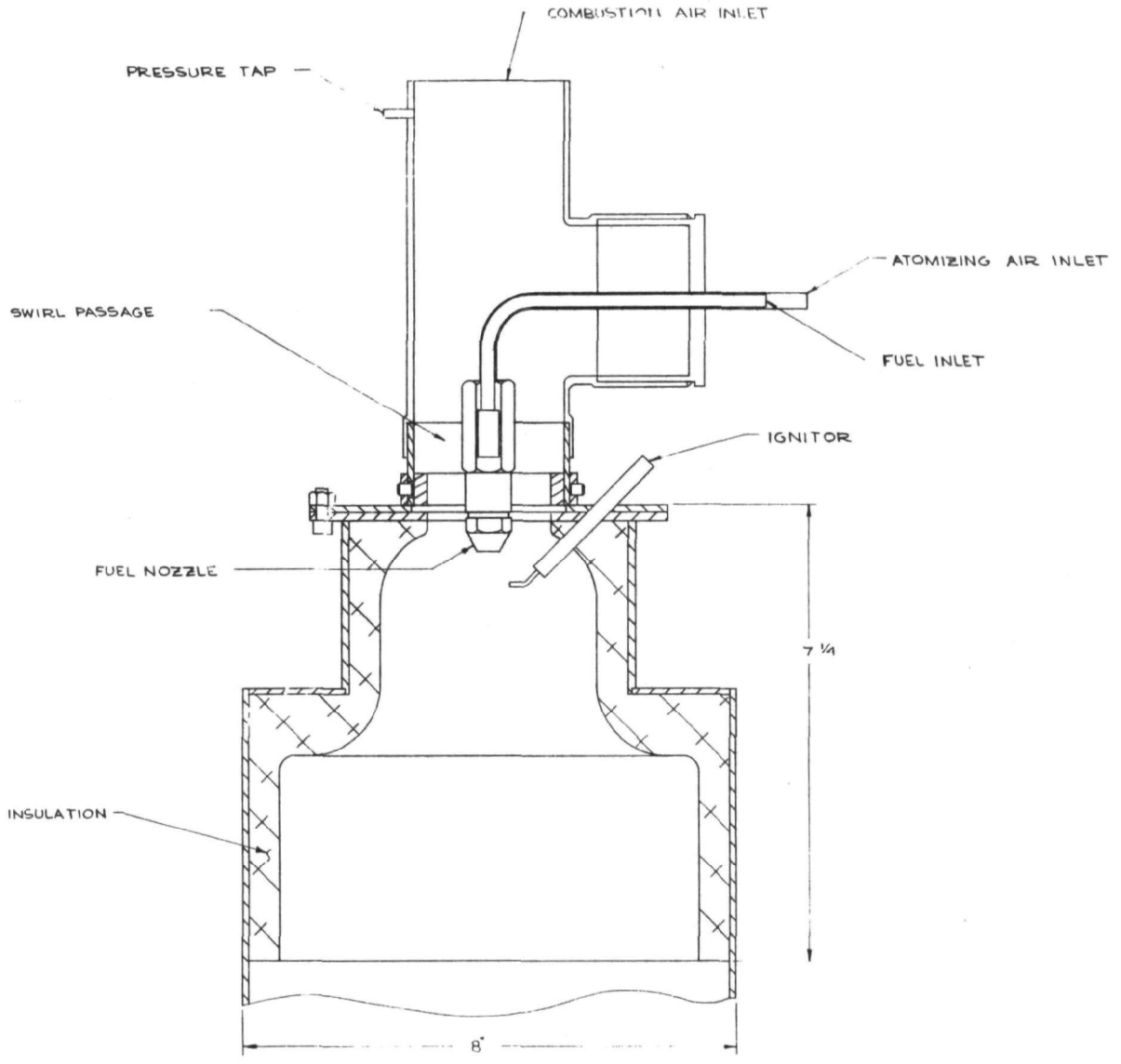

Figure IV-11. Combustor Used for Heating Gas Flow to Test Unit.

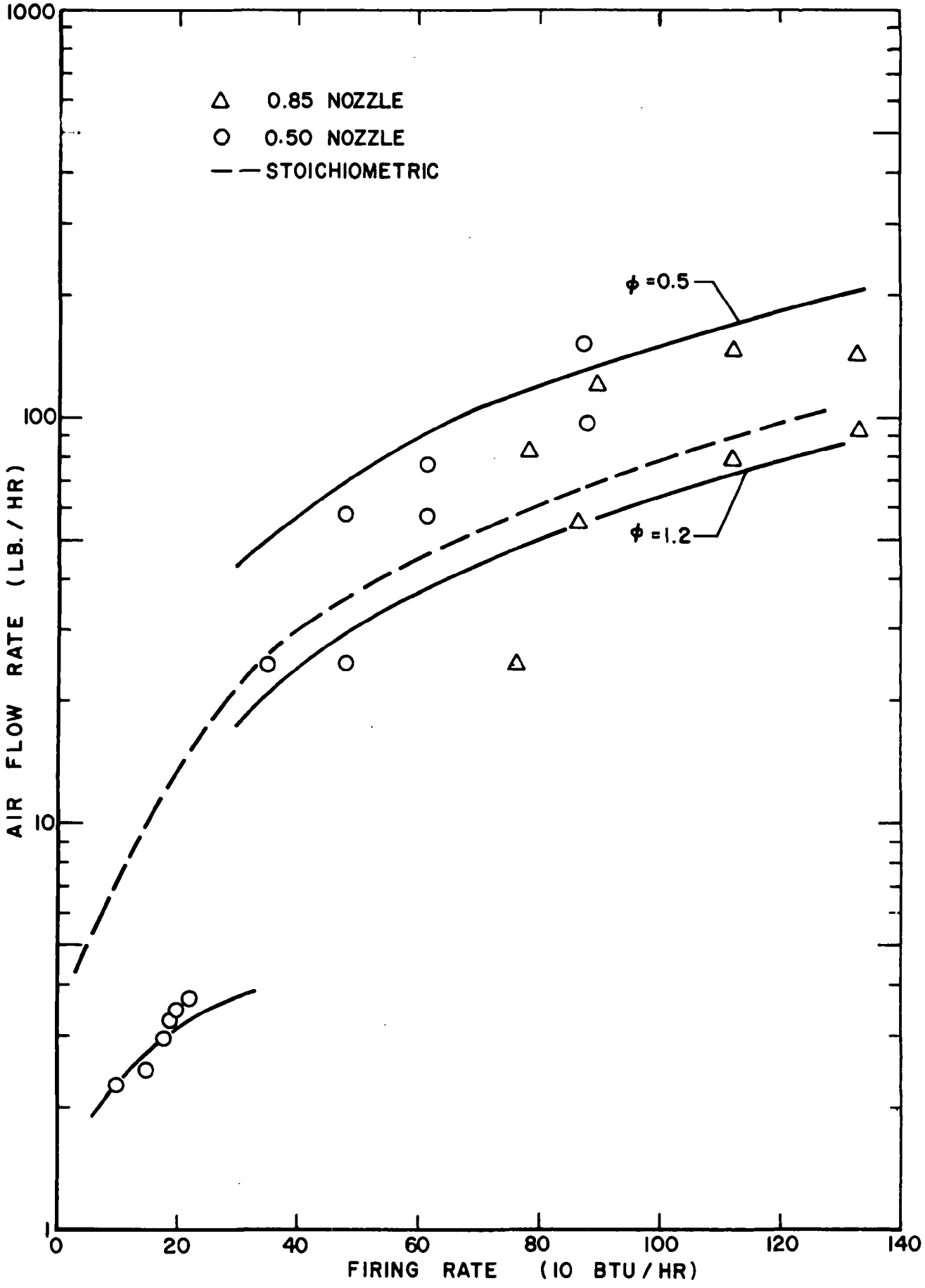

Figure IV-12. Combustor Performance.

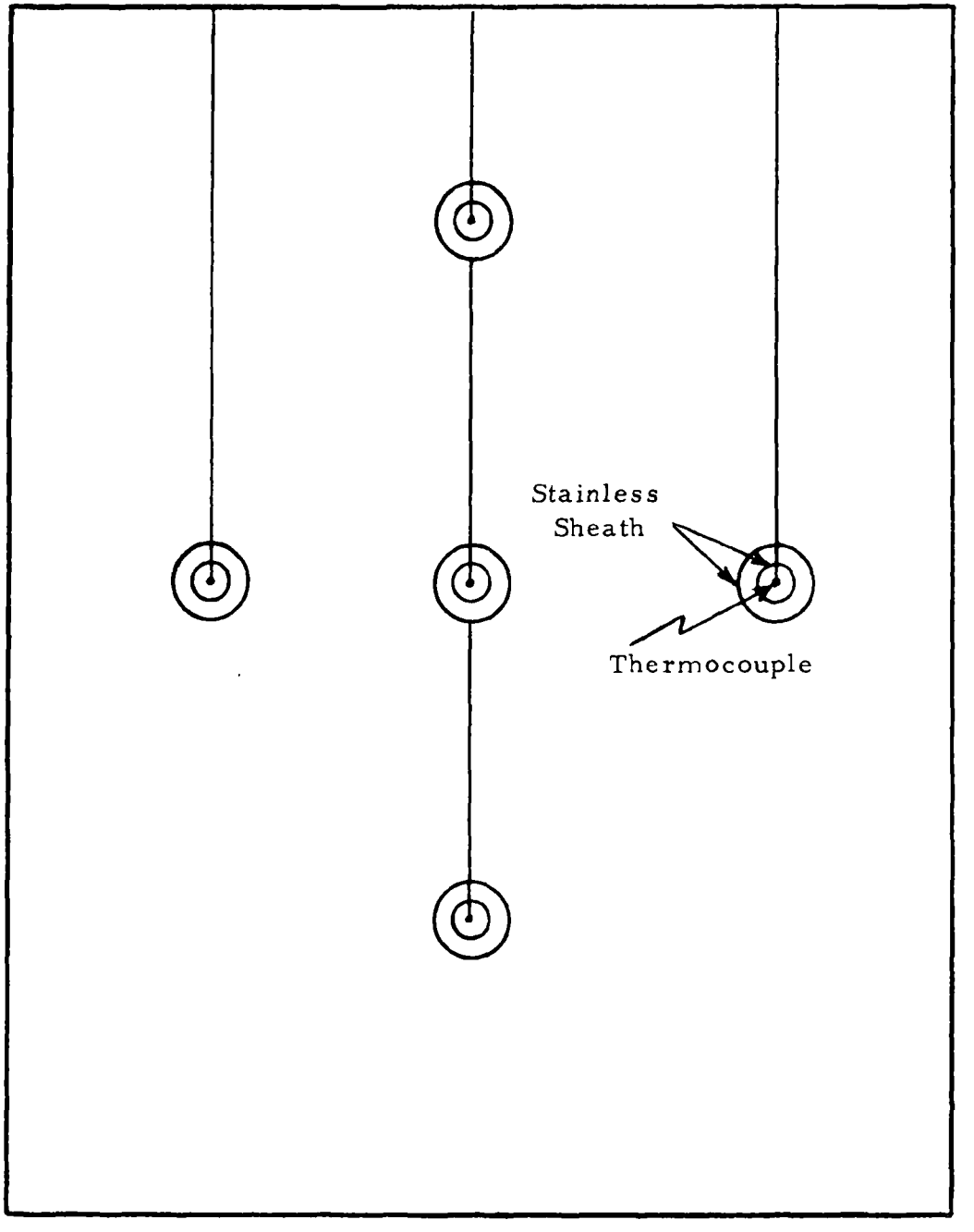

Figure IV-13. Five Probe Thermocouple Rake for Gas Temperature Measurements.

for readings up to 2" of water column (0.1" for higher values). A photograph of the instrument panel is shown in Figure IV-14. All the ducting and mixing plates were fabricated out of 304 stainless steel. The ducting was insulated with fiberfrax insulation to reduce the heat loss. A sight window was provided to view the flame. Figure IV-15 shows a photograph of the test loop.

E. MEASUREMENTS AND DATA REDUCTION

1. Porosity

Porosity of the ball matrix was measured by measuring the weight of the balls used to fabricate the test section. The volume occupied by the matrix was calculated; by comparing the effective density against the density of carbon steel, the porosity of the ball matrix was evaluated to be 0.377. This checks very well with the porosity of the randomly-packed balls, which is listed to range between 0.37 - 0.39[1,2].

2. Heat Transfer Area Correction Factor

Because of the presence of fillets between the balls, the heat transfer area of the ball matrix is modified. The portion of the ball surface area lost under the fillet joining the balls is replaced by the cylindrical surface area resulting from the fillet (see Figure IV-16).

The fillet diameter in the test section was measured with a machinist microscope to average 0.032" diameter. A visual inspection of the small samples of a ball matrix showed that the ball was contacted by approximately six other balls in three-dimensional space. This finding was substantiated by Wadsworth[3], from which Figure IV-17 is reproduced. Taking the number of contacting balls to be six and

the measured fillet diameter to be 0.032", an area correction factor was evaluated from solid geometry considerations. The value of the area correction factor, A_{cf}, was found to be 0.8743. Thus, in the present test section, 12.57% of heat transfer area is lost due to the presence of fillets. β, the heat transfer area/volume for an unbrazed ball matrix, is given by:[2]

$$\beta = \frac{6\,(1-\sigma)}{D}$$

where σ is the porosity of the unbrazed ball matrix and D the ball diameter. (In the present case, σ was measured to be 0.377.) For the present case, β will be given by:

$$\beta = A_{cf} \cdot \frac{6\,(1-\sigma)}{D} .$$

3. Measurement and Correlation of Pressure Drop

Even though the volume of copper used in the present test section is small (1.2% of total), it is expected to have a strong effect on the minimum flow area because most of the copper braze material settles in fillets, and thereby can raise the maximum velocity of the fluid in the ball matrix quite significantly. To take this factor into account, a pseudo porosity factor, σ^*, was introduced, which was correlated experimentally. Equation (2-26b) of Kays and London,[1] which was used to predict the pressure drop in the unbrazed ball matrix, is now modified to read:

$$\frac{\Delta P}{P_1} = \frac{G^2}{2g_c}\,\frac{v_1}{P_1}\left[(1+\sigma^2)\left(\frac{v_2}{v_1}-1\right) + f\,\frac{A}{A_m}\,\frac{v_m}{v_1}\right] \qquad \text{(IV-1)}$$

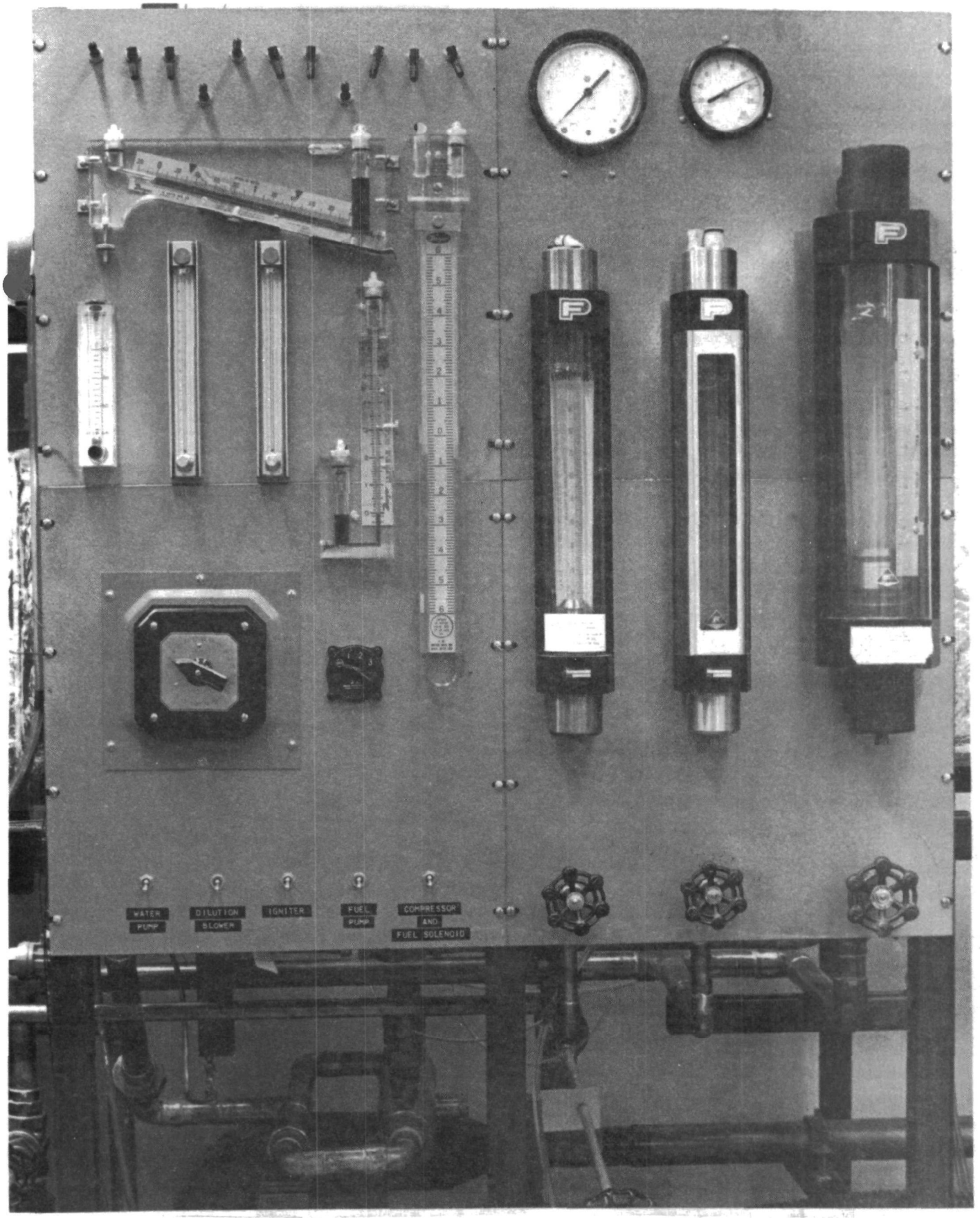

Figure IV-14. Photograph of Instrument Panel in Test Loop.

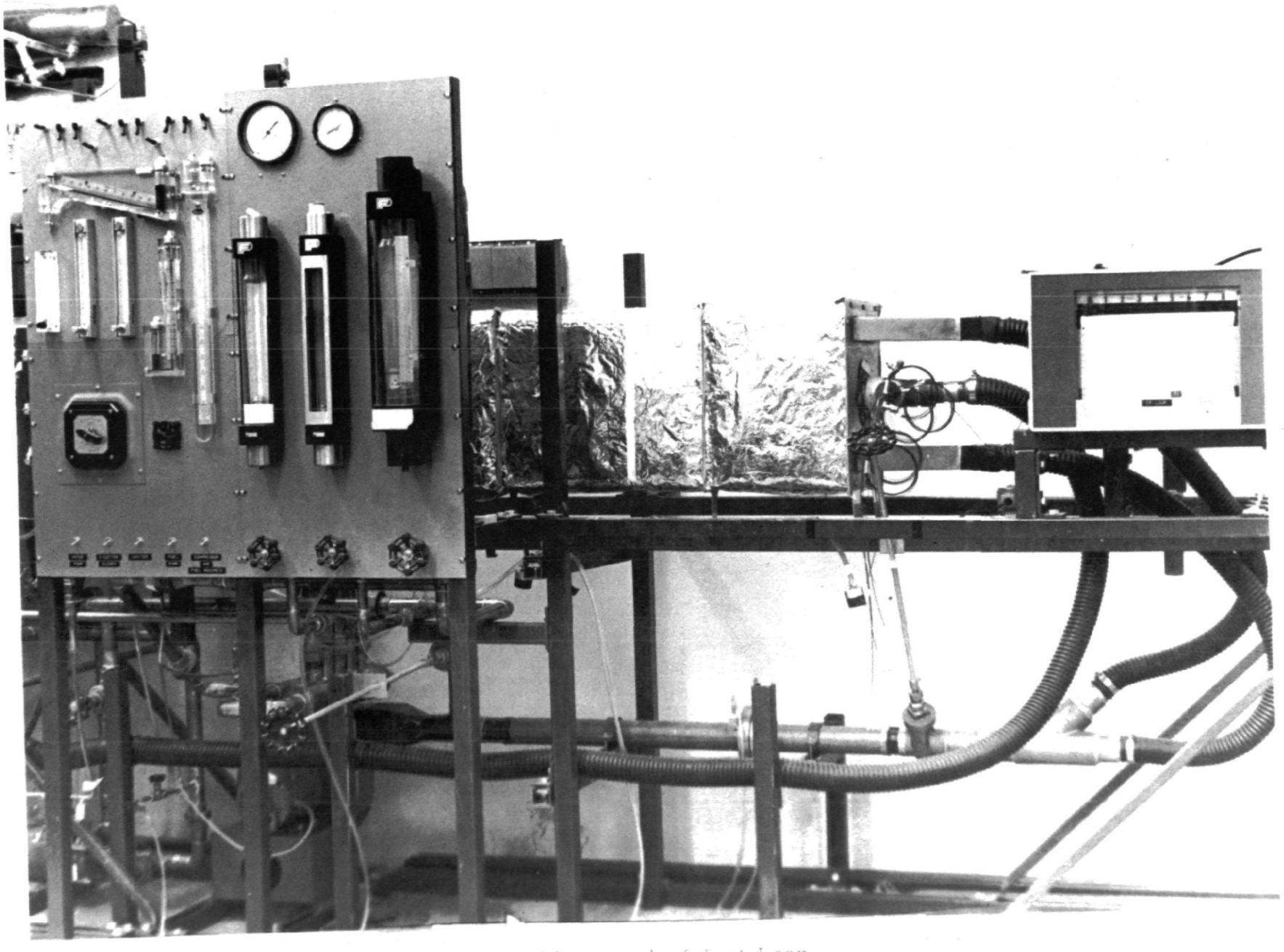

Figure IV-15. Photograph of Test Loop.

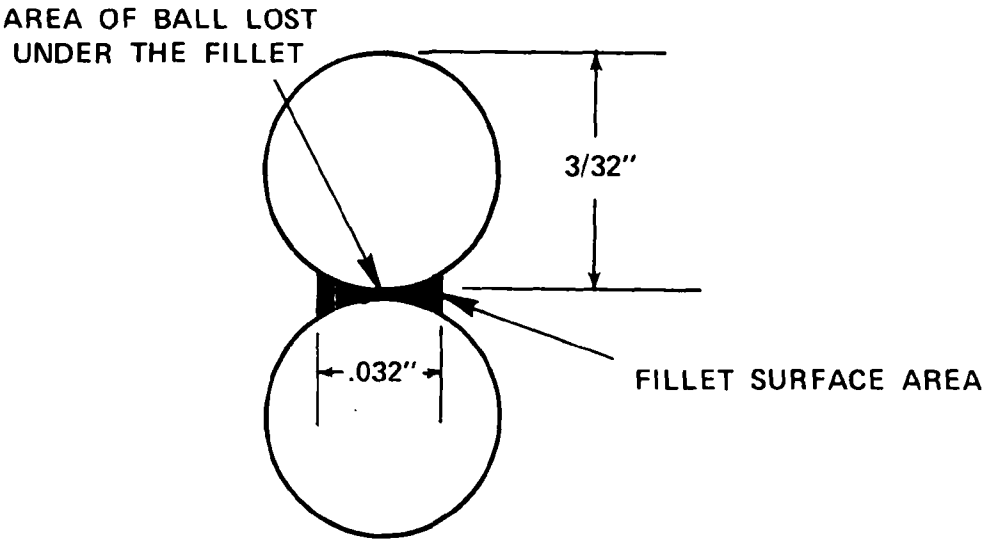

Figure IV-16. Effect of Fillets on Heat Transfer Area.

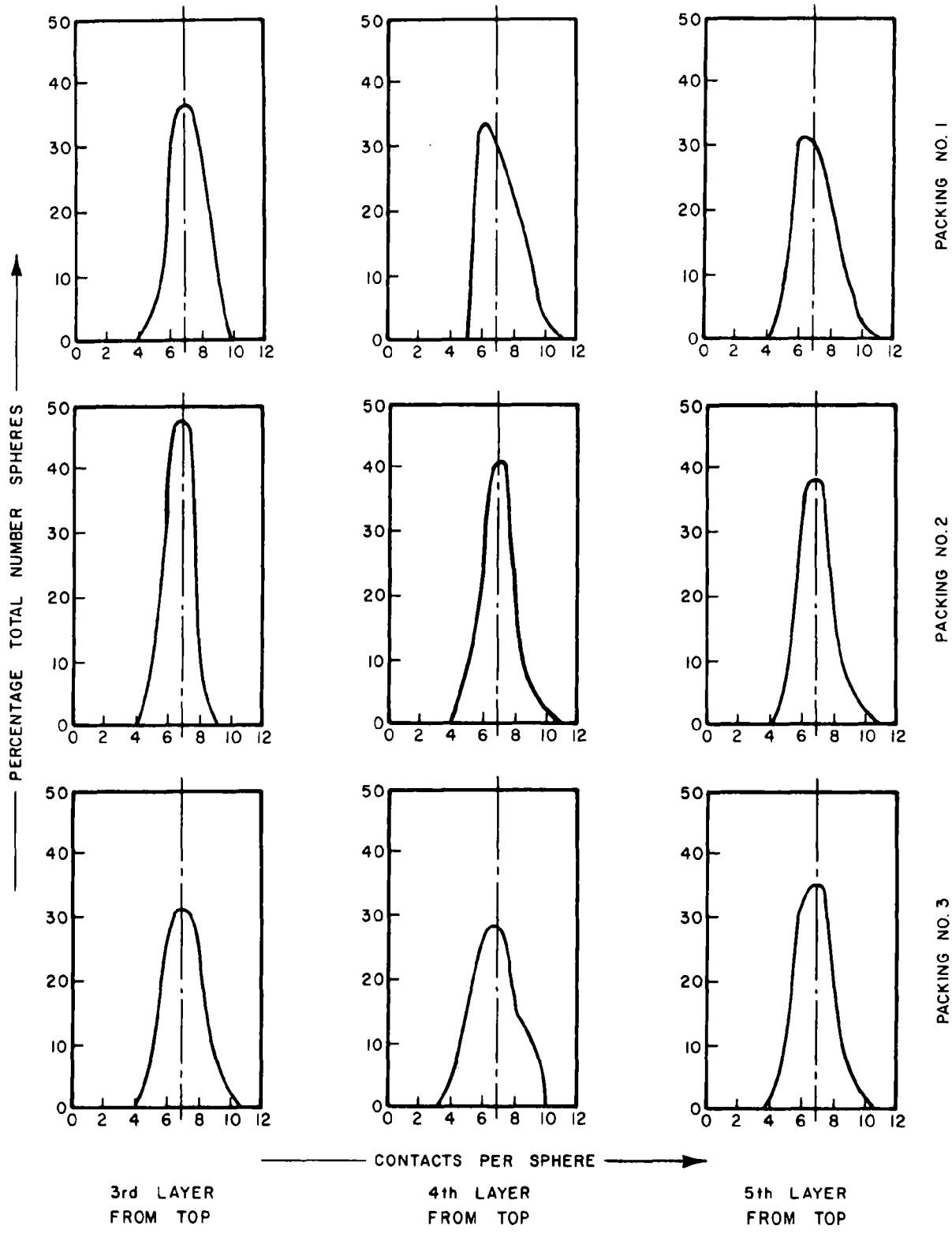

Figure IV-17. Observed Total Distribution of Contact Counts Across Horizontal Cross-Sections. Dia. container/Dia. sphere = 7.48

where

$$G = \frac{W}{A_m}$$

and A_m is the exchanger minimum flow area based on σ^*. The length of the passage is 0.5" in the present geometry. The friction factor, f, is assumed to be the same as that for the randomly packed beds.

In order to obtain the value of σ^*, pressure drop in the test section at various flow rates of air at room temperature was measured. This was correlated using Equation IV-1, which now reads

$$\Delta P = \frac{G^2 v_1}{2 g_c} \cdot f \cdot \frac{\beta V}{A_m} . \qquad \text{(IV-2)}$$

σ^* was treated as a correlating parameter and values of f were given by Figure IV-18 (which is the same as Fig. 7.10, Kays and London[1] where the Reynolds number, N_R, is given by

$$N_R = \frac{4 G r_h}{\mu} .$$

The results are plotted in Figure IV-19. The data correlate well for a value of $\sigma^* = 0.32$, and this value was used in Equation IV-1 to predict the pressure drop for high temperature runs. The results are shown in Figure IV-20. The data for these runs are listed in Table IV-1. The correlation predicts the pressure drop quite satisfactorily. A slight leakage in the ducting in the test loop during experiments could explain the slight dip in the data at higher flow rates.

4. Measurement and Correlation of Heat Transfer Performance

In performing a test run, the total mass flow rate of gas, the temperature of the gas at the entry and exit of the test section, the flow rate of loop water, and the temperature of loop water at the inlet and outlet of the test section were measured. These measurements provided a two-way heat balance which generally checked within 5%. The data were corrected for heat loss in the water tubing and radiation heat flux from gas ducting to the test section.

The gas transfers heat to the water at the bare tube and at the ball matrix. Though heat transfer to the bare tube is expected to be small, it was accounted for in the data reduction. The following equations were used in data reduction:

$$Q = U_b A_b (\text{LMTD}) \qquad \text{(IV-3a)}$$

$$= W C_p (\Delta T)_g \qquad \text{(IV-3b)}$$

$$U_o = \frac{1}{\frac{1}{h_c \eta_{oc} A_c/A_b} + \frac{r_o \ln(r_o/r_i)}{k_t} + \frac{1}{h_g \eta_g A_g/A_b}} \qquad \text{(IV-4)}$$

The bare tube and ball matrix are treated separately. Knowing the gas temperature at the entry and exit of the test section and the average loop water temperature, Equations IV-3 and IV-4 are used to evaluate the bare tube heat transfer. For bare tubes, we have $\eta_{oc} = 1$, $\frac{A_c}{A_g} = \frac{r_i}{r_o}$, and $\eta_g = 1.0$. The heat transfer coefficient on the coolant side, h_c, is calculated from McAdam's equation[1]. h_g is evaluated from single tube bank correlations given in Rohsenow and Choi[4]. Since the

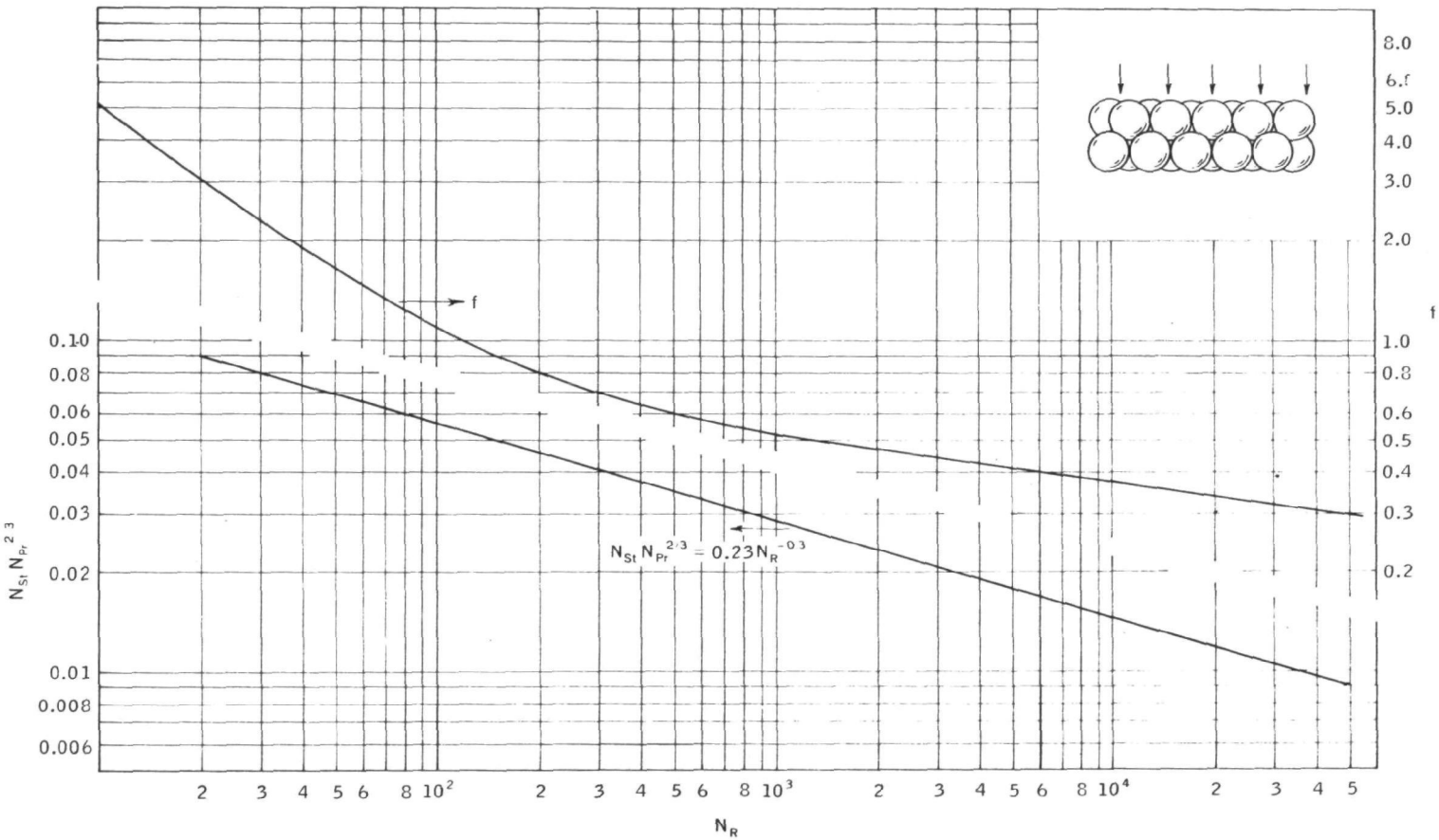

Figure IV-18. Gas Flow Through an Infinite Randomly Stacked Sphere Matrix. A correlation of experimental data with porosity varying from 0.37 to 0.39.

(Reproduced from Compact Heat Exchangers by Kays and London, McGraw-Hill Company, 1955)

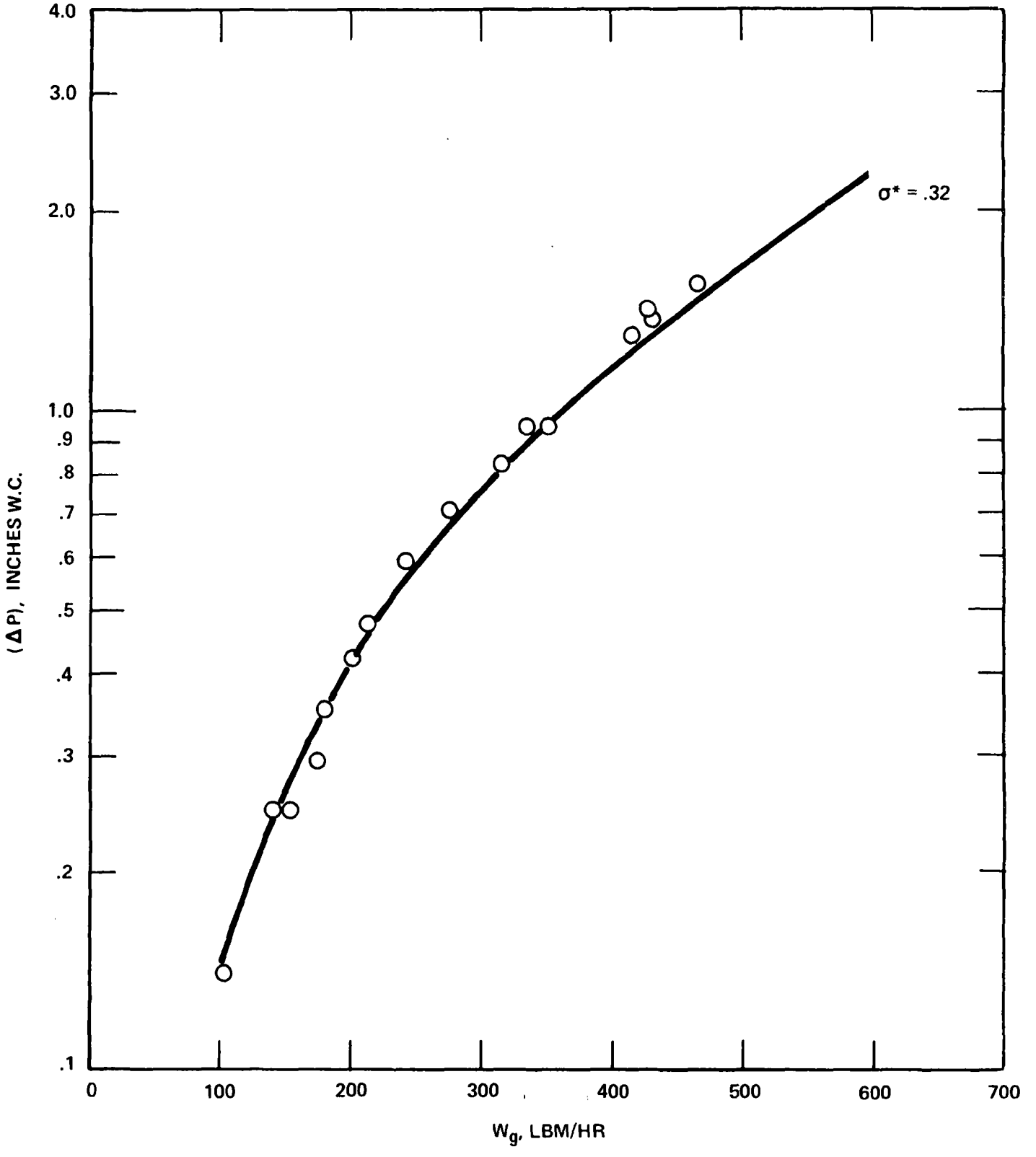

Figure IV-19. Measured Pressure Drop versus Flow Rate at Room Conditions.

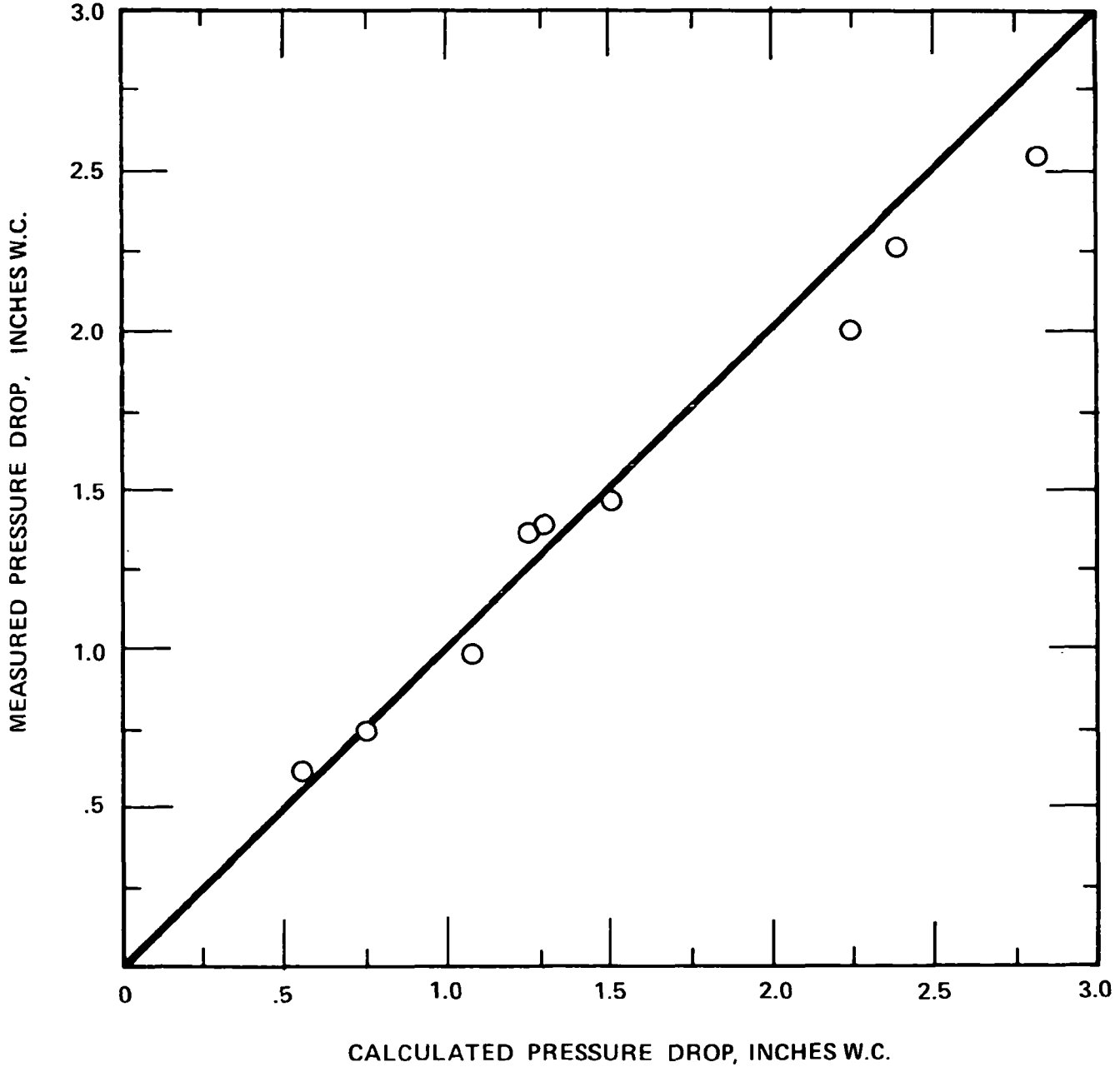

Figure IV-20. Predicted versus Measured Pressure Drop in Ball Matrix Test Section.

TABLE IV-1

DATA AND RESULTS

Test Run No.	Mass Flow Rate of Gas W_g (lbs/hr)	Average Loop Water Temp. (°F)	Gas Temperature		Rate of Heat Transfer Q (Btu/hr)	Gas Heat Transfer Coefficient h_g (Btu/hr ft^2 °F)	Fin Effectiveness	Measured Test Section Pressure Drop (inches w. c.)	Predicted Test Section Pressure Drop (inches w. c.)
			Inlet (°F)	Exit (°F)					
1	154	112	610	230	13723	24.76	.3185	.60	.55
2	183	117	621	251	17051	28.41	.3285	.72	.73
3	201	138	877	345	28581	31.67	.3241	.96	1.07
4	230	130	665	294	20576	33.33	.3046	1.07	1.10
5	257	135	653	308	20440	36.03	.283	1.37	1.30
6	283	135	634	318	21811	38.62	.278	1.46	1.49
7	305	158	966	433	39759	42.88	.302	1.99	2.25
8	350	162	996	473	44910	47.52	.291	2.57	2.83
9	362	148	742	372	30402	46.82	.278	2.25	2.42

temperature of the gas at the inlet and outlet of the heat exchanger is measured, the bare tube heat transfer can be evaluated and, hence, the net heat transfer to the ball matrix; the temperature of the gas at the inlet and outlet of the ball matrix part of the heat exchanger may also be deduced. The bare tube heat transfer rate was generally found to be 3 to 5% of the total heat transfer rate, so that this correction is small and any inaccuracies in evaluating heat transfer directly to the tube have a very small effect on the final results.

The ball matrix stage can be evaluated using Equations IV-3a, IV-3b, and IV-4. h_c is again evaluated using McAdam's equation. The fin effect on the coolant side is shown in Figure IV-21, and fin effectiveness η_{oc} is evaluated for the length of fin on the coolant side. A_g/A_b can also be evaluated, since the volume occupied by the ball matrix and heat transfer area/volume ratio, β, are known.

The fluid flow pattern in the brazed ball matrix is expected to be similar to that of unbrazed balls. Therefore, the same correlation for heat transfer was used as for the unbrazed ball matrix:[1]

$$N_{St} N_{Pr}^{2/3} = 0.23 N_R^{-.3} \qquad \text{(IV-5a)}$$

where

$$N_{St} = \frac{h}{C_p G}. \qquad \text{(IV-5b)}$$

Substituting the heat transfer coefficient from Equation IV-5 into Equation IV-4, the fin effectiveness of the ball matrix, η_g, can be calculated. The data and results of the experiment are summarized in Table IV-1.

5. Analytical Formulation for Prediction of Fin Effectiveness

An analytical model of the ball matrix extended surface was made to predict the fin effectiveness. In the present test section, the height of the ball matrix extended surface varies due to the curvature of the tube; since the variation of the height over the depth (which is 1/2" in the present setup) is small, the fin was modeled to be of constant height. An average height was calculated such that the volume of the ball matrix is kept constant. The equivalent fin is shown in Figure IV-22. The plane of symmetry between the tubes is considered to be adiabatic. The ball matrix surface is considered to be a homogeneous surface with known values of heat transfer area per unit volume, β, and effective thermal conductivity, k_{bm}. Heat balance over an element of the ball matrix results in the relation:

$$k_{bm} \frac{\partial^2 T_{bm}}{\partial x^2} + k_{bm} \frac{\partial^2 T_{bm}}{\partial y^2} = h_g \beta (T_{bm} - T_g). \qquad \text{(IV-6)}$$

The heat - balance on the gas results in

$$\frac{\partial T_g}{\partial x} = \frac{h_g \beta V}{W L C_p} (T_{bm} - T_g) . \qquad \text{(IV-7)}$$

In writing Equation IV-7, an assumption of constant mass velocity of gas over the fin was invoked. Equations IV-6 and IV-7 were solved numerically on an IBM 7094 computer. The coordinate axes and the grid used are shown in Figure IV-22.

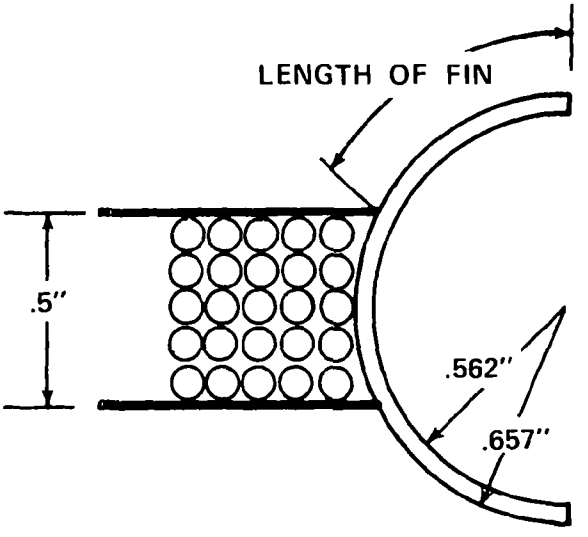

Figure IV-21. Fin Effect on Coolant Side.

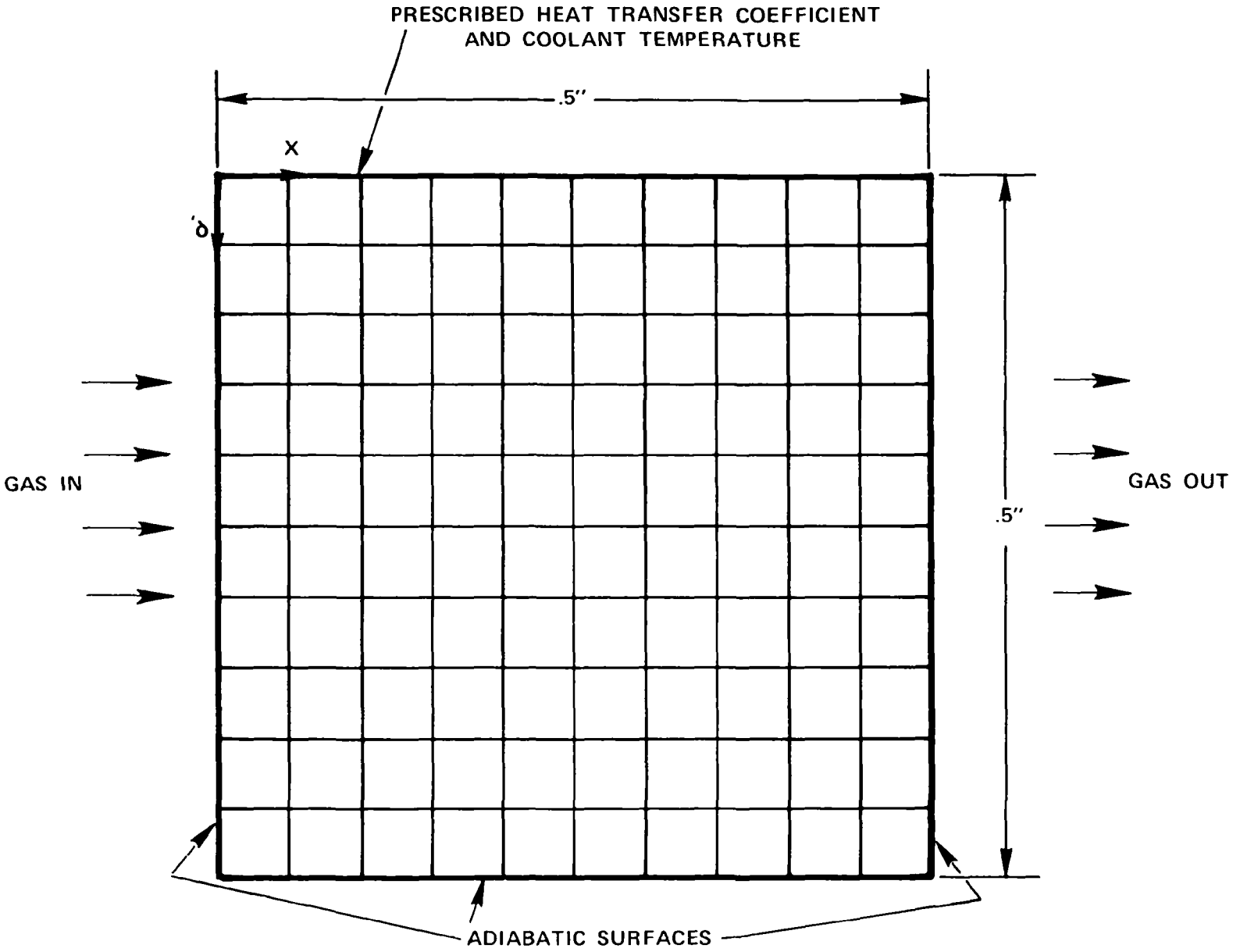

Figure IV-22. Analytical Model of Equivalent Ball Matrix Fin in the Present Test Section.

The following boundary conditions were imposed:

$$x = 0 \qquad T_g = T_{gi}, \qquad \frac{\partial T_{bm}}{\partial x} = 0 \qquad \text{(IV-8a, IV-8b)}$$

$$x = 0.5'' \qquad \frac{\partial T_{bm}}{\partial x} = 0 \qquad \text{(IV-9)}$$

$$y = 0 \qquad \frac{\partial T_{bm}}{\partial y} = \frac{h_c'}{k_{bm}} (T_g - T_c) \qquad \text{(IV-10)}$$

$$y = 0.5'' \qquad \frac{\partial T_{bm}}{\partial y} = 0 \qquad \text{(IV-11)}$$

The adiabatic conditions in Equations IV-8b and IV-9 are imposed since the value of β approaches zero at these boundaries.

For prescribed values of h_g, β, k_{bm}, W, C_p, T_{gi}, V, L, and T_c, Equations IV-6 and IV-7 are solved simultaneously using the boundary conditions in Equations IV-8 through IV-11. h_g was evaluated from equation IV-5. h_c' represents the combined conductance of the coolant and the tube wall, appropriately adjusted for area ratios.

6. Measurement of Thermal Conductivity of the Ball Matrix

Samples were made for measurement of the thermal conductivity of the brazed ball matrix with carbon steel balls. These samples were made with ball sizes of 1/16", 3/32", and 1/8" to study the effect of ball size. However, because of varying copper coating thickness on the 1/8" and 1/16" diameter balls, no valid conclusions could be drawn regarding the effect of ball diameter. Sample No. 4, made with 3/32" balls, had nearly the same porosity as the matrix in the test section,

and thus represented the test section quite well. The samples were 0.7" diameter and 1" long (Figure IV-23). The thermal conductivity of these samples was measured at 40°C and 167°C by Dynatech Corporation, using the Colora method; the results are listed in Table IV-2. The value of k_{bm} = 6.05 Btu/hr ft°F from Sample No. 4 was used in the computer program previously described. Equations IV-6 and IV-7 were then solved simultaneously on an IBM 7094 computer. The isotherms in the gas and the ball matrix are plotted in Figures IV-24 and IV-25 for one set of conditions. The heat transfer to the fin was calculated by numerical integration; Equations IV-3 and IV-4 were used to calculate the fin effectiveness. The resultant fin effectiveness and the measured fin effectiveness are shown in Figure IV-26. The data and theory check satisfactorily.

F. DISCUSSION OF RESULTS

The values of fin effectiveness predicted by the two-dimensional model are lower than those predicted by the crude one-dimensional model used in the conceptual boiler design[5]. The two-dimensional model predicts the effectiveness to be 27.7%, as opposed to the 42% predicted by the one-dimensional model at the design flow rate.

It was proposed that, by using a 50% copper/50% steel ball mixture, the thermal conductivity of the ball matrix would be improved to achieve the desired fin effectiveness. Three samples were made for thermal conductivity measurements: 100% copper, 75% copper/25% steel, and 50% copper/50% steel balls, respectively (Figure IV-27). Because 3/32" diameter copper balls were unavailable, 1/16" diameter copper and steel balls were used. The fillet width was measured with a machinist microscope to average .026", resulting in a fillet cross-

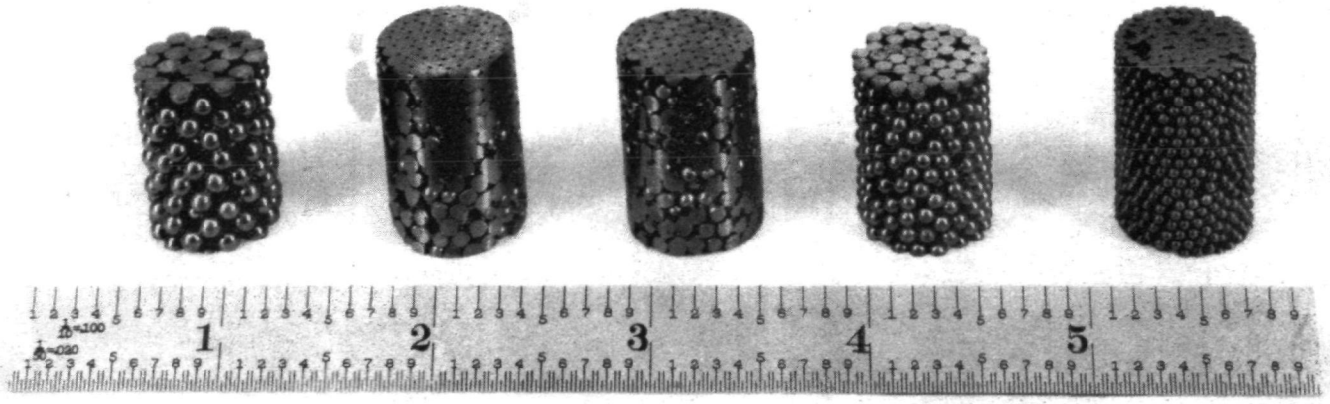

Figure IV-23. Photograph of Ball Matrix Samples for Measurement of Thermal Conductivity.

TABLE IV-2

THERMAL CONDUCTIVITY OF BALL MATRIX SAMPLES
CARBON STEEL BALLS, COPPER BRAZED

Sample No.	Ball Diameter (inches)	Dimensions (mm)		Weight (gm)	Apparent Density (Kg/m^3)	Porosity	Thermal Conductivity at 40°C (Btu/hr ft °F)	Thermal Conductivity at 167°C (Btu/hr ft °F)
		dia.	length					
1	1/16	17.38	25.54	29.18	4820	.381	5.5	5.9
2	3/32	17.71	25.40	33.05	5280	.324	6.95	6.45
3	3/32	17.73	26.03	35.94	5590	.284	6.65	6.2
4	3/32	17.31	23.38	25.69	4690	.400	6.21	6.05
5	1/8	17.25	23.23	25.08	4620	.408	7.2	7.1

W_g = MASS FLOW RATE OF GAS = 300 LBM/HR
T_{g_i} = TEMPERATURE OF GAS IN = 1190°F
W_c = MASS FLOW RATE OF COOLANT (WATER) = 5000 LBM/HR
T_c = TEMPERATURE OF COOLANT = 150°F
Q = RATE OF HEAT TRANSFER = 50,800 BTU/HR
h_g = HEAT TRANSFER COEFFICIENT OF GAS = 42.8 BTU/HR FT^2
k_{bm} = APPARENT THERMAL CONDUCTIVITY OF BALL MATRIX = 6.05 BTU/HR FT °F
η_h = FIN EFFECTIVENESS = .297

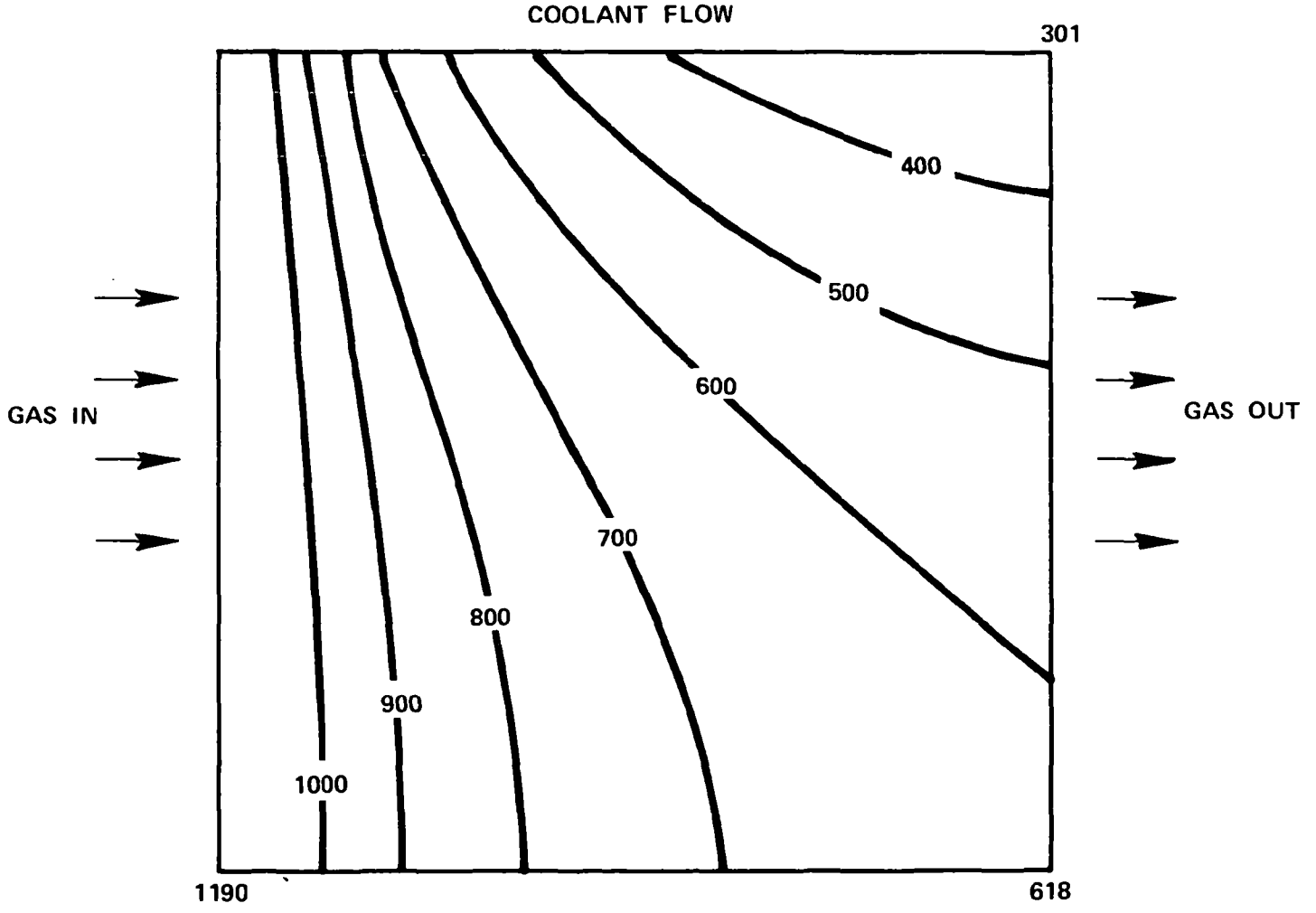

Figure IV-24. Isotherms in the Gas Passing Through Ball Matrix Extended Surface.

W_g = MASS FLOW RATE OF GAS = 300 LBM/HR
T_{g_i} = TEMPERATURE OF GAS IN = 1190°F
W_c = MASS FLOW RATE OF COOLANT (WATER) = 5000 LBM/HR
T_c = TEMPERATURE OF COOLANT = 150°F
Q = RATE OF HEAT TRANSFER = 50,800 BTU/HR
h_g = HEAT TRANSFER COEFFICIENT OF GAS = 42.8 BTU/HR FT^2
k_{bm} = APPARENT THERMAL CONDUCTIVITY OF BALL MATRIX = 6.05 BTU/HR FT °F
η_h = FIN EFFECTIVENESS = .297

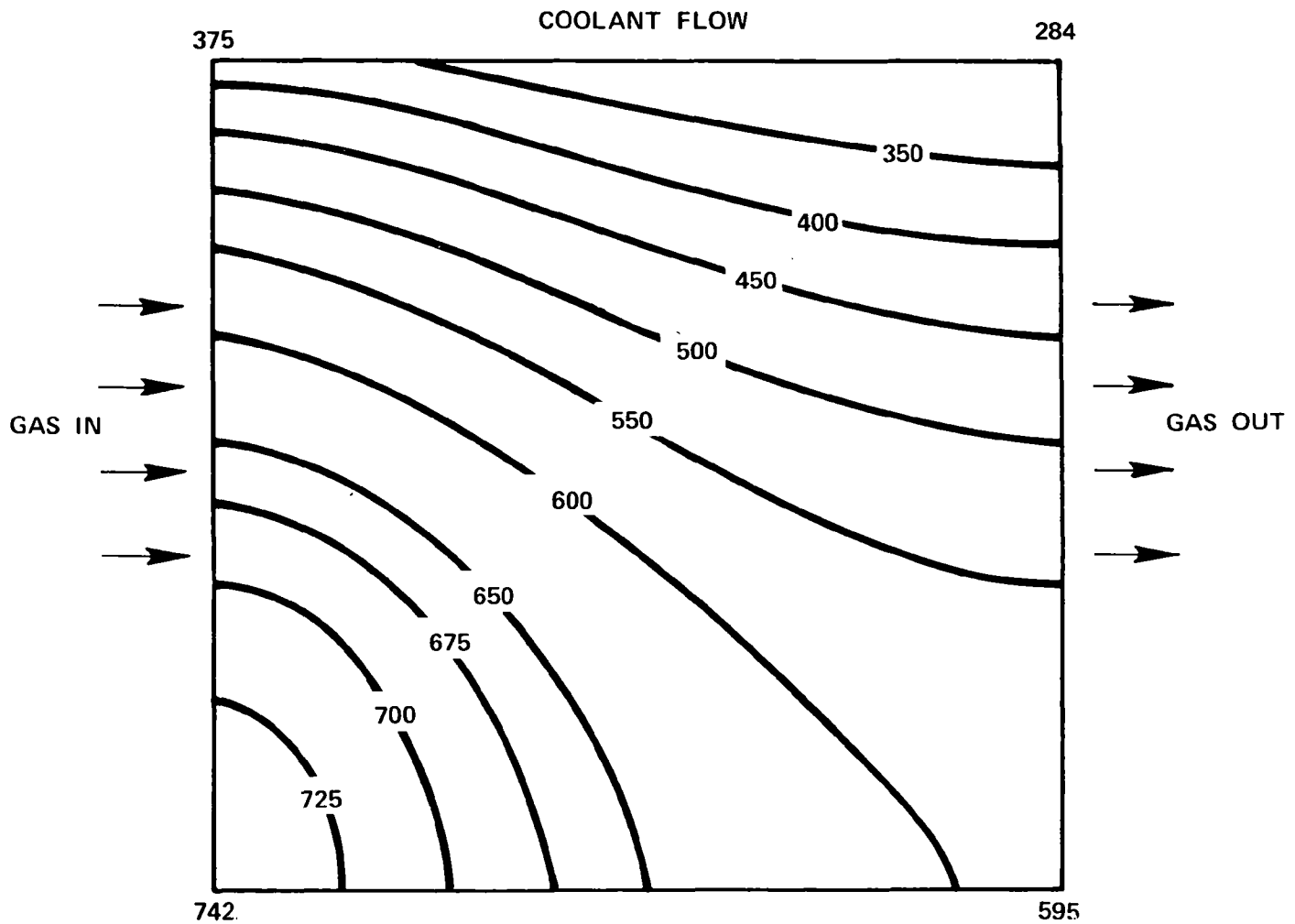

Fig IV - I er n F Ma E de fa

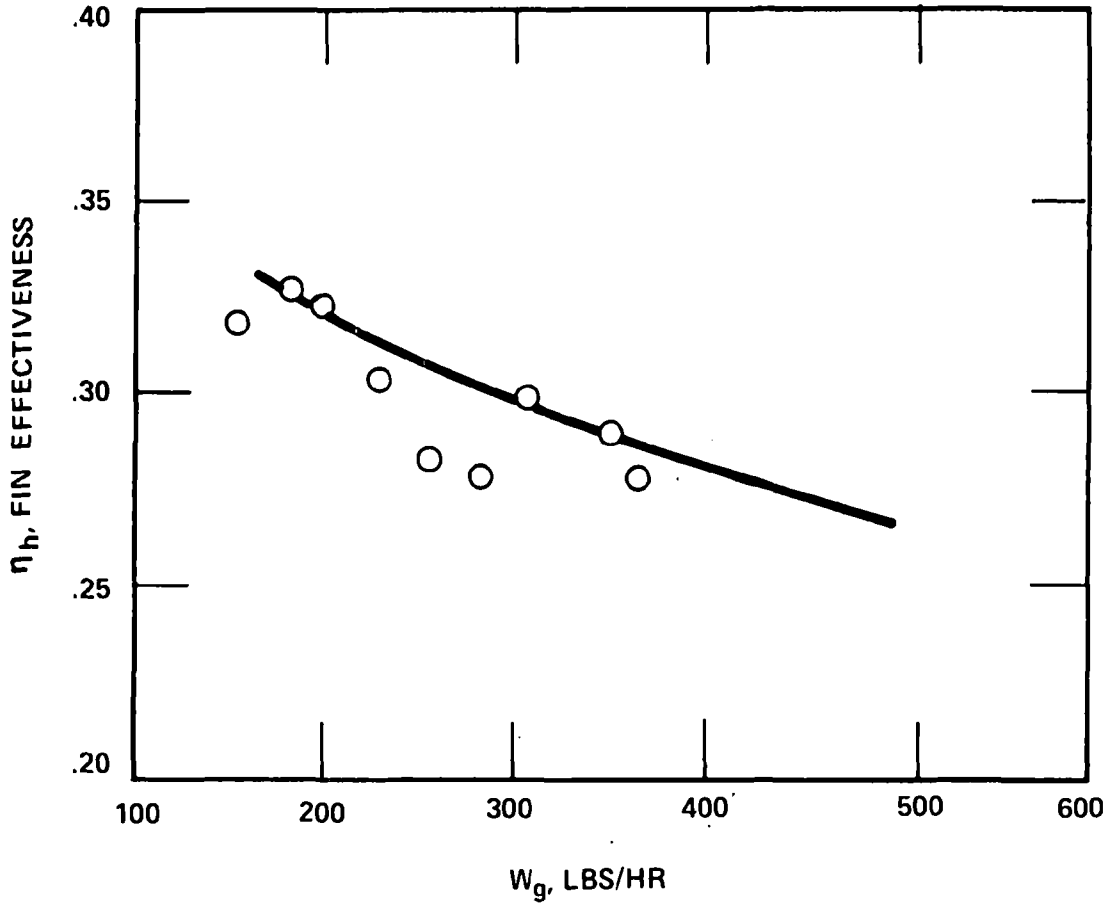

Figure IV-26. Predicted and Measured Fin Effectiveness versus Gas Flow Rate.

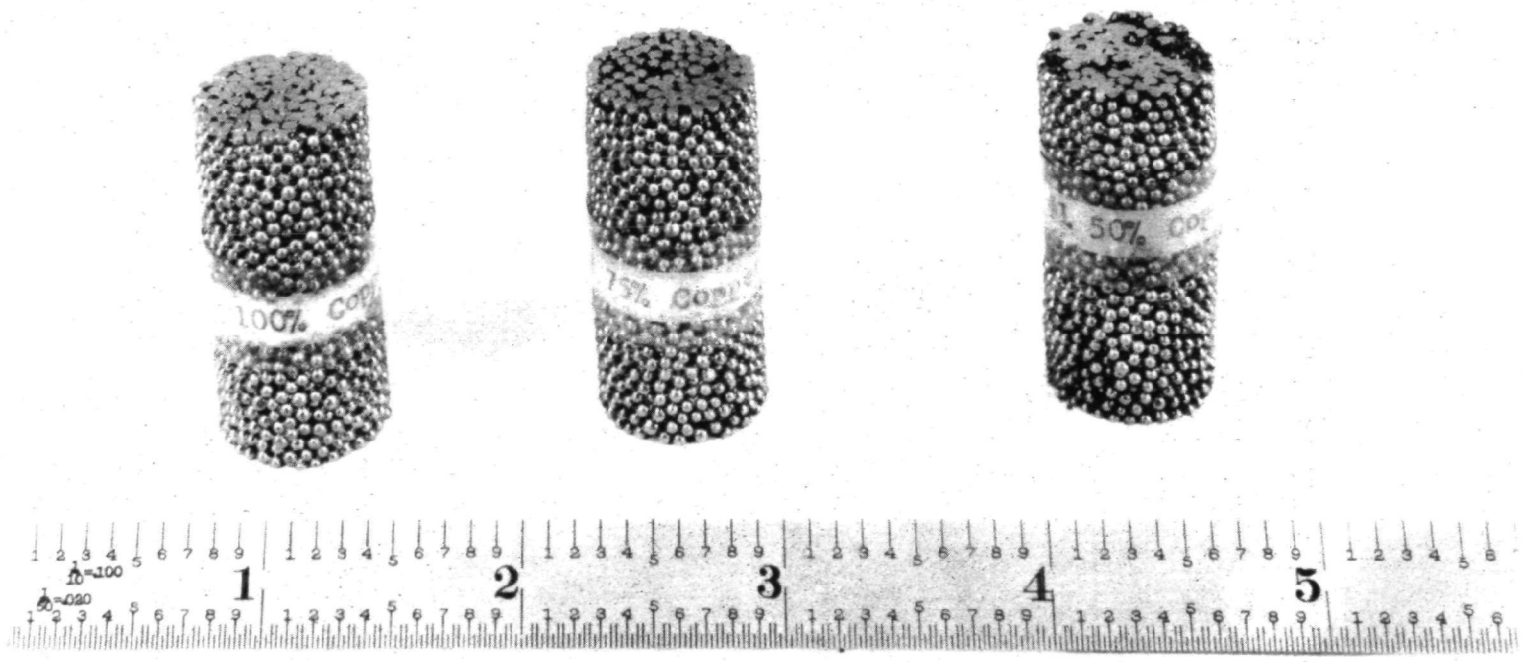

Figure IV-27. Photograph of Copper and Steel Ball Mixture Samples for Measurement of Thermal Conduct

section area-to-ball cross-section area ratio of 17.4% (as opposed to 10.8% in the present test section). Therefore, it is expected that the thermal conductivity measured with these samples would be somewhat higher than that obtained with 3/32" balls. The results are listed in Table IV-3. Using the two-dimensional computer results for these higher matrix thermal conductivities, the fin effectiveness for a 50% copper/50% steel ball mixture is projected to be 40.1%.

G. CONCLUSIONS AND RECOMMENDATIONS FOR BOILER PREHEAT STAGE

During the current study, the boiler design was changed because of packaging considerations to a flat configuration. Since the temperature of the combustion gas to the preheat stage is low (maximum of 1100°F), and the organic liquid is at a low temperature, the probability of overheating the organic in the preheat stage is low; the buffer fluid is not included in the preheat stage, to reduce the boiler weight and size. To provide a direct comparison of the ball matrix with various other extended surface exchangers, several designs for the flat preheat stage were developed, with the design for the ball matrix section based on the experimental results and analytical prediction method described in this Appendix. The results for a conventional finned tube preheat stage are presented and compared here with a preheat stage using the ball matrix. The preheat stage size is based on a 100 shp system.

In Table IV-4, the requirements for the preheat stage are outlined. The ball matrix preheat stage design is presented in Table IV-5 and Figure IV-28 and the finned tube design is presented in Table IV-6 and Figure IV-29. The same face area is used for both designs. Comparison of the two designs shows that the ball matrix design, with a

TABLE IV-3

THERMAL CONDUCTIVITY OF BALL MATRIX SAMPLES

Sample No.	Description		Dimensions (mm)		Weight (gm)	Porosity	Thermal Conductivity at 167°C (Btu/hr ft^2 °F)
	Copper (%)	Steel (%)	dia.	length			
1	50	50	18.85	40.39	58.81	.378	13.1
2	75	25	18.87	40.79	60.32	.386	18.3
3	100	0	18.88	40.87	62.51	.385	24.5
1*	0	100	17.38	25.54	29.18	.381	5.9

*This sample is the same as Sample No. 1 listed in Table IV-2.

TABLE IV-4

PREHEAT STAGE SPECIFICATIONS

Rate of heat transfer	303,000 Btu/hr
Mass flow rate of combustion gas	2018 lbs/hr
Temperature of gas in	1072°F
Temperature of gas out	531°F
Air fuel ratio	19.8 (by mass)
Mass flow rate of Fl-85	7760 lbs/hr
Temperature of Fl-85 in	290°F
Temperature of Fl-85 out	355°F
Pressure of Fl-85	700 psia
Face area of heat exchanger	2.842 ft^2

TABLE IV-5

BALL MATRIX DESIGN FOR PREHEAT STAGE

Ball diameter	3/32"
Ball matrix fin height	.5"
Ball matrix fin depth	.37"
Ball matrix fin effectiveness	.53
Face area	2.842 ft^2.
Number of parallel passes on liquid side	5
Tube dimensions (outside)	.37" x .25" (rectangular)
Pressure drop on gas side	2.73" w.c.
Pressure drop on Fl-85 side	11.65 psi

Material: Carbon steel balls and tubes. A copper plating of .00033" on balls is specified before brazing.

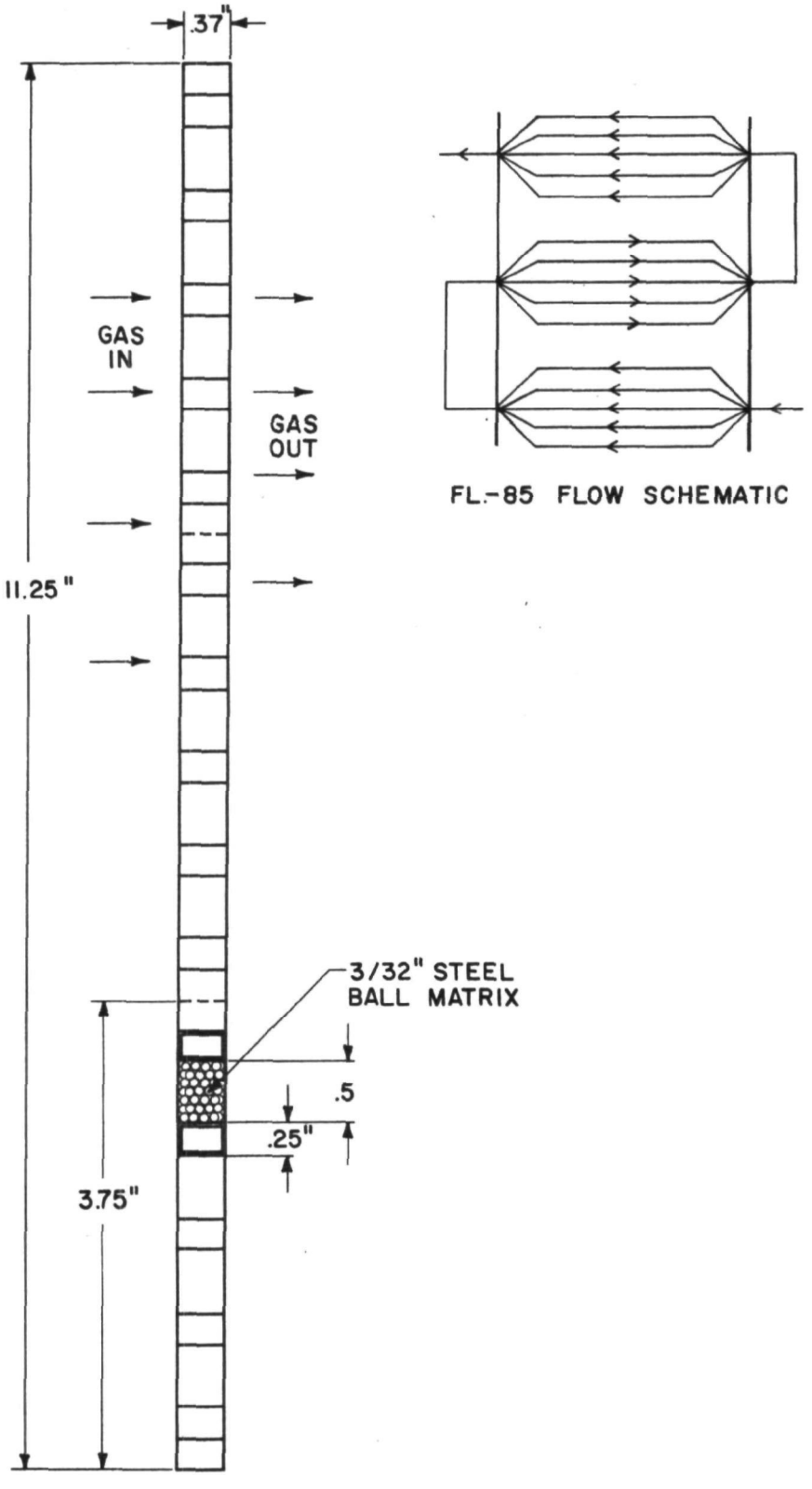

Figure IV-28. Ball Matrix Section III Stage Boiler Design with 5 Parallel Passes.

TABLE IV-6

FINNED CIRCULAR TUBE DESIGN FOR PREHEAT STAGE

Face Area	2.842 ft^2
Number of rows	2
Number of parallel passes	2
Tube O. D.	5/8" - .035" wall
Center-to-center tube spacing	1.50"
Center-to-center row spacing	1.50"
Fin pitch	14 fins/inch
Fin depth	2.88"
Fin thickness	.0095"
Pressure drop, combustion gas side	.06" w. c.
Pressure drop, Fl-85 side	5 psi

Material: Carbon steel for both tubes and fins. Rippled fins are proposed.

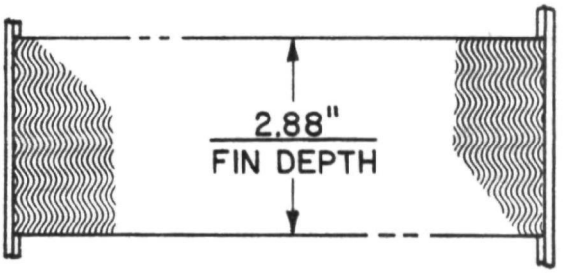

FL-85 FLOW SCHEMATIC

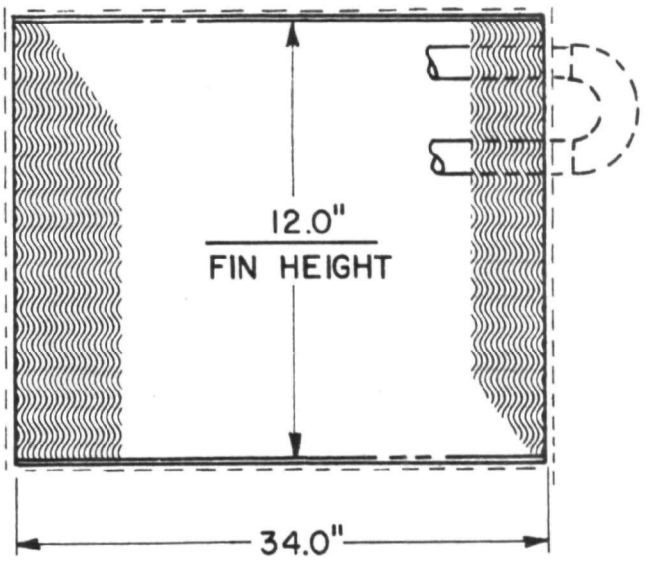

Figure IV-29. Rippled Finned Tube Preheat Stage.

thickness of 0.37", is much more compact than the finned circular tube design which has a thickness of 2.88". The ball matrix design has a much higher gas-side pressure drop (2.73" W.C.) than the finned tube design (0.06" W.C.). This difference results from the higher f/j ratio for the ball matrix as compared to the finned tube; also, the ratio of free flow area to frontal area is lower for the ball matrix. The compactness of the ball matrix exchanger results from the much higher j factor and β (i.e., heat transfer area per unit volume). While the pressure drop with the ball matrix is higher, it is still in an acceptable range for the boiler design.

The boiler design presented in Chapter 5 of this report uses a finned preheat stage. The choice of the finned design over the ball matrix design was based on the following factors:

- Sufficient space was available to permit use of the finned tube design.
- The gas-side pressure drop is smaller.
- The finned tube design is readily available commercially, since it is similar to exchangers now produced by various heat exchanger manufacturers. The ball matrix design would require special fabrication and considerable development on the fabrication technique.
- The weight of the finned tube design is less.
- The finned tube design is less susceptible to plugging by soot and other particulates resulting from burner malfunction, by the ash content of the fuel, or by hard particulates in the combustion air.

H. NOMENCLATURE

A	Heat transfer area
A_{cf}	Area correction factor
A_m	Minimum free flow area based on σ^* (i.e. = σ^* x minimum face area on ball matrix side)
C_p	Specific heat of gas
D	Ball diameter
f	Friction factor
g_c	Conversion factor
G	Mass velocity based on A_m
h	Heat transfer coefficient
h'_c	Combined conductance of coolant side and tube wall.
j	Heat transfer factor
k_{bm}	Apparent thermal conductivity of ball matrix
k_t	Thermal conductivity of tube metal
L	Depth of ball matrix fin
LMTD	Log mean temperature difference
N_{Pr}	Prandtl number
N_R	Reynolds number
N_{St}	Stanton number
P	Pressure
Q	Rate of heat transfer
r_o	Outer radius of tube
r_i	Inner radius of tube
r_h	Hydraulic radius $\left(\frac{A_m L}{A}\right)$

T	Temperature
U_b	Overall heat transfer coefficient based on "A_b"
V	Volume occupied by ball matrix
v	Specific volume
v_m	Mean specific volume
W	Mass flow rate
x	Coordinate axis
y	Coordinate axis

Greek Symbols

β	Heat transfer area/volume
ΔP	Pressure drop
ΔT	Temperature drop
μ	Viscosity
η_{oc}	Overall effectiveness on coolant side
η_g	Fin effectiveness on gas side
σ	True porosity
σ^*	Pseudo porosity (section 5.3)

Subscripts

b	Base area under the ball matrix fin
bm	Ball matrix
c	Coolant
g	Combustion gas side
1	Inlet
2	Outlet

I. REFERENCES

1. W. Kays and A. L. London, "Compact Heat Exchangers," McGraw Hill Book Co. (1964).

2. A. P. Fraas and M. N. Ozisik, "Heat Exchanger Design," John Wiley and Sons, Inc. (1965).

3. J. Wadsworth, "Experimental Examination of Local Processes in Packed Beds of Homogeneous Spheres," National Research Council of Canada, NRC-5895, February 1959.

4. W. M. Rohsenow and H. Y. Choi, "Heat, Mass and Momentum Transfer," Prentice-Hall Inc. (1961).

5. Morgan, D. T., and Raymond, R. J., "Conceptual Design, Rankine-Cycle Power System with Organic Working Fluid and Reciprocating Engine for Passenger Vehicles," Report No. TE 4121-133-70, June 1970, Thermo Electron Corporation, Waltham, Massachusetts.

APPENDIX V

ENGINE BEARING-LUBRICANT TESTING FOR RANKINE-CYCLE RECIPROCATING EXPANDER

Prepared under Subcontract No. 4134-07

By

Monsanto Research Corporation
800 N. Lindbergh Boulevard
St. Louis, Missouri 63166

Authors

Frank S. Clark
David R. Miller
Edward O. Stejskal

Final Report Submitted to
Thermo Electron Corporation
On
15 April 1971

FOREWORD

This is the final report on Thermo Electron subcontract #4134-07, titled Engine Bearing Lubricant Testing for Rankine-Cycle Reciprocating Expander. This subcontract was executed under a prime contract between Thermo Electron and the National Air Pollution Control Administration of HEW (prime contract No. EHS70-102). Research for the subcontract was done between May 18, 1970, and January 22, 1971. Contract work was terminated on the latter date at the request of Thermo Electron Corporation.

ABSTRACT

Various blends of General Electric Versilube^{R} F-50 silicone oil with Monsanto CP-34 (thiophene) were tested as journal bearing lubricants in s specially designed rig. This rig simulated both connecting rod journal bearings of a Rankine-cycle reciprocating expander. The silicone oil is a candidate lubricant and the thiophene a candidate working fluid for this engine. Initial wear studies established useful lubricant-fluid dilution ratios. Coefficients of friction and failure loads for the resulting test fluids were measured under continuous rotation at 200°F and 250°F. Densities and kinematic viscosities were also evaluated at these temperatures. This allowed calculation of bearing moduli for these mixtures. Analysis of the results led to the conclusion that F-50 should not be used as a journal bearing lubricant when diluted with more than 20% CP-34. This is because the load carrying ability drops rapidly above this concentration. However, conditions are defined under which higher dilutions are possible.

A. INTRODUCTION AND BACKGROUND

At the beginning of this (CP-34) phase of the development in June, 1970, the reference working fluid was thiophene and the lubricant was GE F-50 silicone oil, a chlorinated phenyl methyl silicone oil. Since this lubricant-working fluid combination is completely miscible, the crankcase lubricant is generally diluted with the working fluid during shutdown of the system. The startup procedure with this combination must therefore include provision for drying of the lubricant to insure adequate lubrication of the expander and feedpump bearings before cranking is started. This drying is accomplished by preheating the lubricant-working fluid mixture in the crankcase so that the working fluid is boiled out of the lubricant; the crankcase is normally vented to the condenser.

The purpose of this program was to determine the effect of thiophene concentration on the lubrication properties of the thiophene-GE F-50 mixture. This information could then be used in synthesis of the startup sequencing to insure proper drying of the lubricant before initiation of the cranking of the expander-feedpump. The test program was based on use of journal bearings in the expander.

Approximately midway through this phase of the development, the decision was made with EPA approval to switch to Fluorinol-85 as working fluid, with a hydrocarbon oil as lubricant. Since this combination is almost completely immiscible, drying of the lubricant during startup is no longer required, and this program was terminated. In this appendix, the experimental results obtained before termination are presented as a matter of record. The information may be of benefit if new and advanced working fluids are used with a miscible

lubricant. The research for this program was done between May 18, 1970, and January 22, 1971.

Four tasks defined the framework of the contract research. These were:

Task I The absolute viscosity will be measured at temperatures of 32°F, 100°F, 212°F, and 300°F, on each of four fluid lubricant combinations specified.

Task II From the viscosity obtained and the design requirements of the expander designed in contract CPA-22-69-132, Thermo Electron Corporation will specify the range of bearing moduli for both rotary and reciprocating motions which are applicable for each fluid lubricant combination.

Task III The rotary bearing lubricant test will be conducted over the range of values specified for bearing modulus for each of the four fluid lubricant ratios. The data should determine the plot of the friction factor values over the range of bearing moduli. In addition, the bearing modulus will be lowered until incipient scuffing of the bearing surfaces occurs and a point recorded.

Task IV The reciprocating motion bearing tests will be conducted over operating conditions approximating wrist-pin loading as closely as possible for each of the four fluid lubricant ratios. The friction factor will be measured over this range and the point of incipient scuffing determined. The same machine (with the addition of the oscillating crank) and the same essential test program will be used for

Task IV as was used for Task III.

The contractor shall make recommendations on the maximum temperature of the lubricant, and on a desirable operating range. If desirable, additional tests can be made to support these recommendations.

Discussions at the beginning of this subcontract between Thermo Electron Corporation (TECO) and Monsanto Research Corporation (MRC) led to:

a. Selection of the test metallurgy.

b. Definition of probable lubrication problems.

c. Agreement on the use of a Monsanto designed and built lubricant test machine.

d. Agreement on an initial series of friction and wear tests using the Monsanto tester. These tests employed opposing conforming rub blocks radially loaded against a 1-1/2 inch diameter ring; they were used in specifying the F-50/CP-34 concentrations to be used for more detailed study.

B. TASK I: VISCOSITY MEASUREMENTS

The absolute viscosity data obtained under this task are needed to define the bearing modulus. This is a design parameter having the dimension of length. It relates to the frictional stress on a bearing and is defined as:

$$\text{bearing modulus} = M = \frac{\eta \times \nu}{P}$$

where:

η = absolute viscosity (poises)

ν = sliding velocity (in./min.)

P = average bearing pressure (p.s.i.)

At sufficiently low values of the bearing moduli, scuffing and metal seizure occur.[1]

Table V-1 lists the kinematic viscosities of the test F-50/thiophene (CP-34) blends (0, 10, 20, 30 and 50 wt.% CP-34). These data are shown graphically versus temperature in Figure V-1. The viscosities at 300°F were not measured prior to contract termination. They can be closely estimated by extrapolation of the lines in Figure V-1.

---

[1] Many tests use a "dimensionless" parameter ZN/P (Z is absolute viscosity, N is journal speed in revolutions/min., P is unit load). For example, see P. Freeman, Lubrication and Friction, Pitman Publishing Corp., London, 1962, pg. 71; M.D. Hersey, Theory and Research in Lubrication, John Wiley and Sons, Inc., New York, 1966, Chapter 5; and A. Cameron, Principles of Lubrication, John Wiley and Sons, Inc., New York, 1966, pg. 7-11 and chapter 12.

TABLE V-1

KINEMATIC VISCOSITY (η_K, CENTISTOKES) AND DENSITY (ρ, gm cm^{-3})
AT SEVERAL TEMPERATURES (°F)
FOR SEVERAL SOLUTIONS OF MONSANTO CP-34
IN GENERAL ELECTRIC F-50 VERSILUBE

Dilution % (w/w) CP-34 in F-50	Temperature					
	32°		100°		210°	
	η_K	ρ	η_K	ρ	η_K	ρ
0	147.4		52.49	1.028	17.45	0.976
10	52.32	1.0599	23.4	1.031*	8.8	0.977*
20	24.31	1.0635	11.9	1.031	5.4	0.975
30	14.71	1.0662	7.6	1.033	3.8	0.974
50	8.38	1.0693	4.7	1.035	2.35	0.973

These data are shown graphically in Figures V-1 and V-2.

* Believed in error. Extrapolated values of 0.980 at 200°F. and 0.955 at 250°F. were used in all calculations.

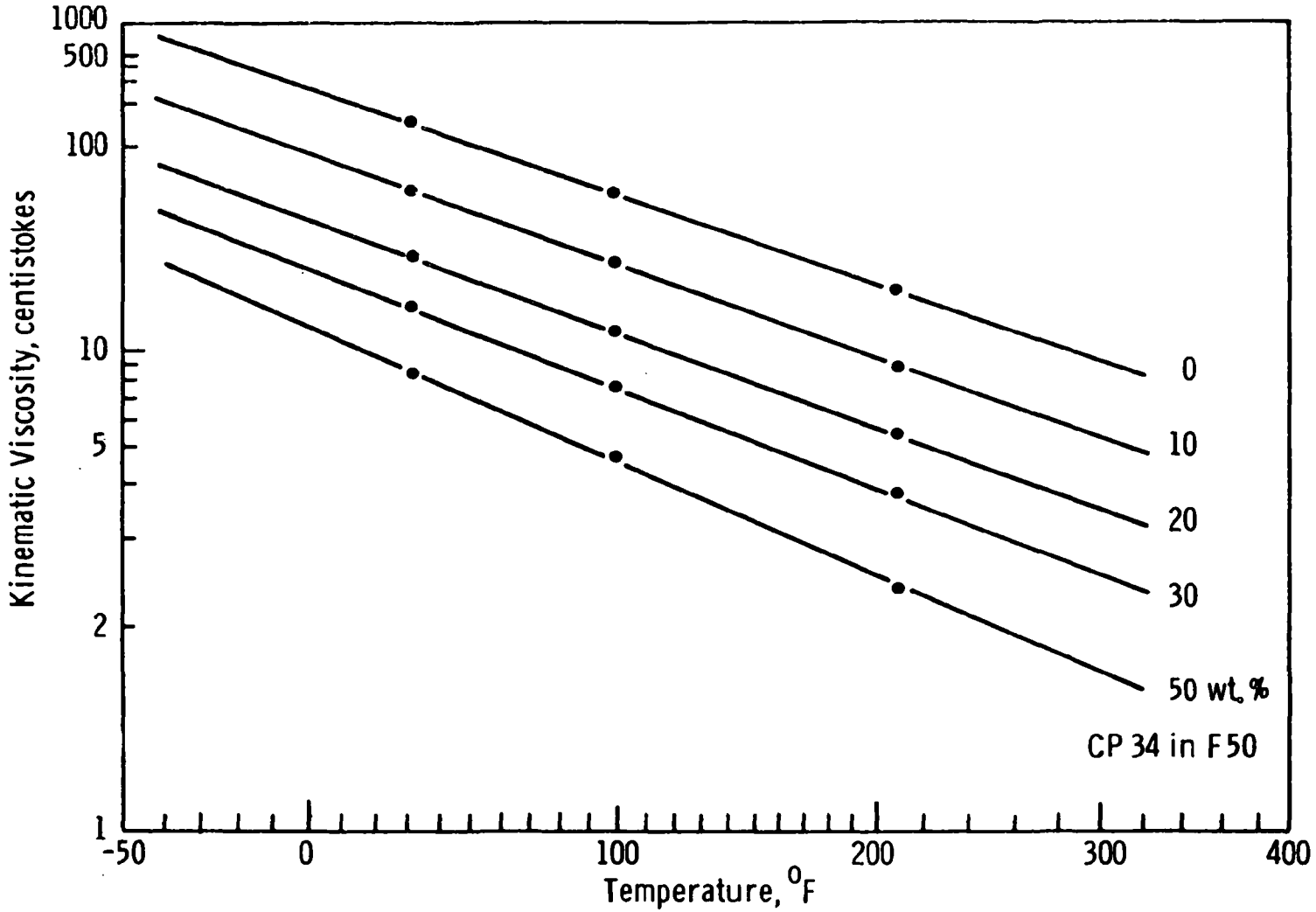

Figure V-1. Kinematic Viscosity vs. Temperature for Several CP-34 Blends.

The densities of the F-50/CP-34 blends needed to convert kinematic to absolute viscosities are also listed in Table V-1. The room temperature values were obtained with a Westfall balance; those at 100°F and 210°F were obtained by a closed pycnometer. Densities at 200°F and 250°F were found by extrapolation and interpolation as in Figure V-2. The experimental values for 10% are not in agreement with the other figures. We have assumed these values are in error and assigned the 10% solution a value between that of 0% and 20% CP-34. Contract termination prevented rechecking the 10% density values.

The absolute viscosities of the silicone blends are given in Table V-2.

The volatility of thiophene (b.p. = 84°C) necessitated designing a closed viscometer. Actually, two closed viscometers were used. The first is shown in Figure V-3. A Cannon-Manning semimicro viscometer tube is loaded in a normal way. The head is then joined to the tube with heat shrinkable FIT tubing. The height of the fluid in either arm of the tube is controlled by the gas piston and the stopcock.

This apparatus was satisfactory at room temperature and at 100°F. However, leakage of CP-34 became quite pronounced at 210°F. After 21 hours all of the CP-34 in a 10% blend evaporated and/or leaked from the system. A new design (Figure V-4) improved the sealing and reduced the volume above the test mixture. Thus volatility errors were minimized. A Cannon-Manning semimicro viscometer tube is loaded with the test fluid kept in the narrow arm

above the bulb. The stopcock is closed and joined to the viscometer tube with Vinethane tubing. Both tubing connections are tightened with hose clamps. After a short temperature equilibration in the bath (1 to 3 minutes), the stopcock is opened and the viscosity measured. This apparatus gave reasonable reproducibility. Some evaporation of CP-34 still occurred at 210°F as there was condensation in the viscometer tubes.

C. TASK II: MODULI SPECIFICATIONS

This task involved deciding how to simulate realistically the Rankine cycle journal with the Monsanto friction and wear tester. Bearing lubrication variables include:

- metallurgy
- surface roughness
- fluid viscosity
- fluid pressure-viscosity coefficient
- fluid interfacial tensions
- fluid composition
- atmosphere
- load
- temperature
- sliding speed
- oil feed
- geometry
- degree of oscillation

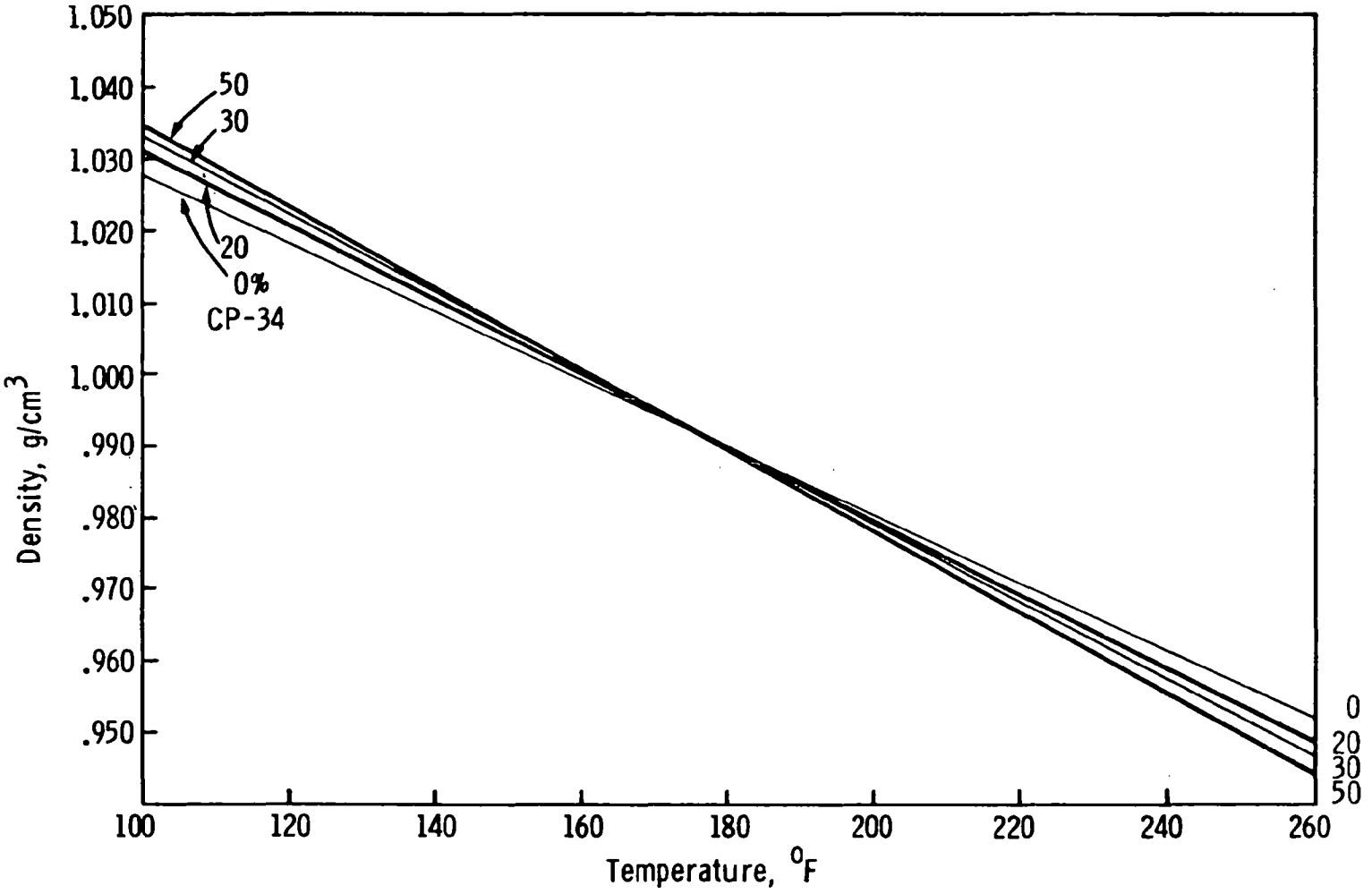

Figure V-2. Variation of Density with Temperature for Various Solutions of CP-34 in F-50.

TABLE V-2

ABSOLUTE VISCOSITIES (η POISES) AT 200°F AND 250°F
FOR SEVERAL SOLUTIONS OF
MONSANTO CP-34 IN GENERAL ELECTRIC F-50 VERSILUBE

Dilution % (w/w) CP-34 in F-50	200°F.	250°F.
0	0.194	0.136
10	0.097	0.073
20	0.058	0.046
30	0.040	0.033
50	0.026	0.021

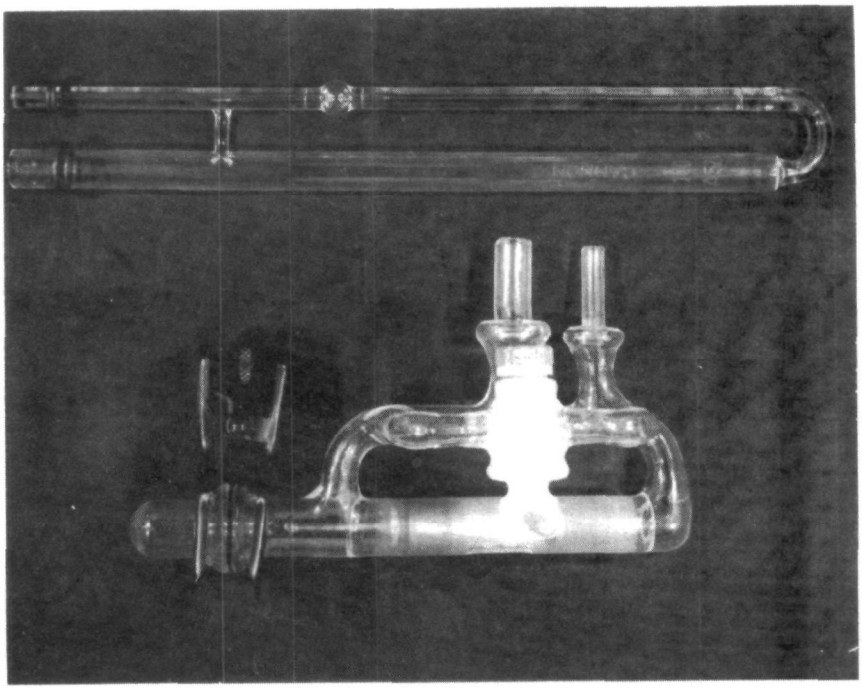

Figure V-3. Closed Viscometer Used at 100°F.

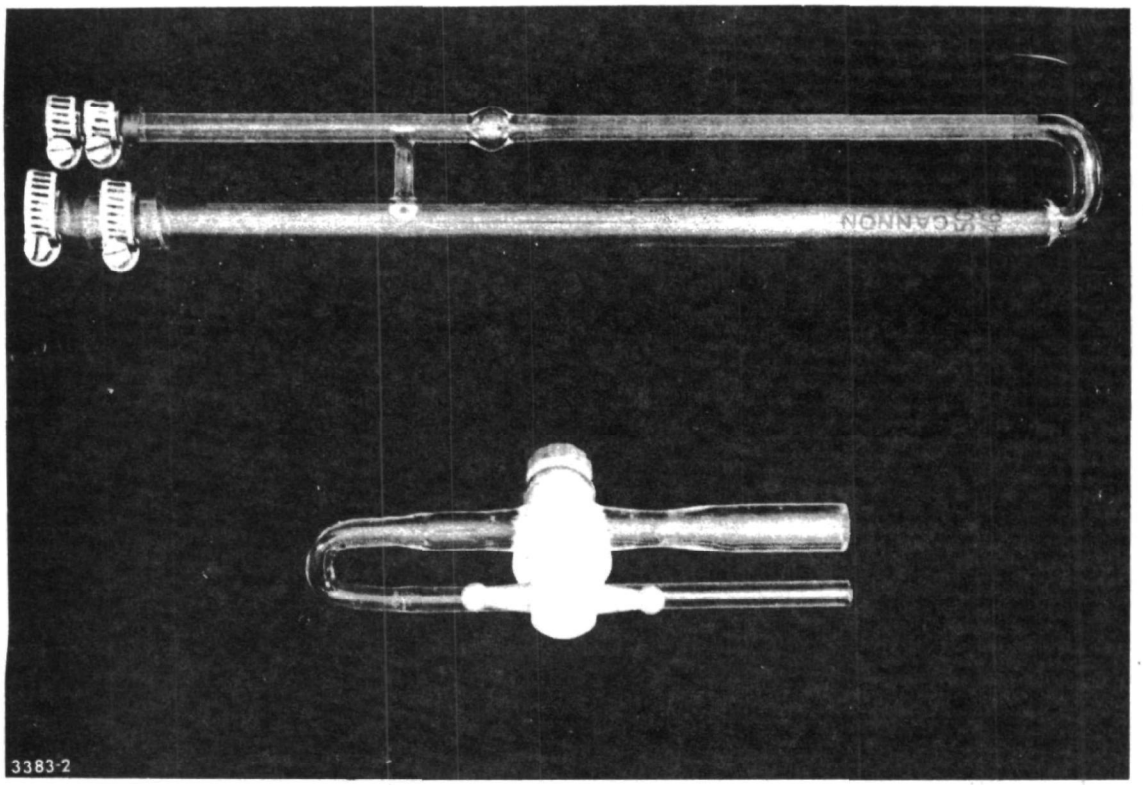

Figure V-4. Closed Viscometer Used at 210°F.

Test duplication of all these variables is not feasible. Effective simulation requires identical materials (metals and fluids), atmosphere control, surface speed, loads, temperatures, degree of oscillation, and load pulsation.

For comparison, some characteristics of the engine are given below:

Crankshaft end bearing: 3.0" dia. x 0.75" width

Wrist-pin end bearing: 1.5" dia. x 1.0" width (30° oscillation)

Diametral clearances: ~ .002-.003"

Speeds: 300-2000 rpm

Loads: 7450 lbf maximum

Internal oil feed: @ 50 psig

Temperatures: 300° to -40°F; normal operating temperature of 250°F

The specifications set for the test machine are described below:

1. Metallurgy and Initial Surface Roughness

   a. Inner, Rotating Element

      Hardenable cast iron (from a Ford camshaft casting), hardened to a Rockwell C of 50 to a depth of more than 25 mil, ground in the opposite direction from that in which it will operate, and polished to 8 to 12μ in rms in the operating direction.

   b. Outer, Stationary Bearing Sleeve

      Cast bronze, SAE specification No. 660, finished to better than 30μ in rms. The final choice of engine metallurgy has not been made, but it will approximate the above

combination. This metal pair is similar to the one now used in Ford internal combustion engines.

2. Atmosphere

CP-34 vapor from degassed fluid samples in a vacuum. The expander was to be pumped to 50 microns and charged with degassed fluids.

3. Sliding Speeds

2800 to 18,800 in./min. This range comes from the journal design. The diameter of the crankshaft end bearing of the expander is 3 in. The ring diameter in the wear machine is 1-1/2 in. Therefore, to get equivalent surface speeds, the rpm of the wear machine is twice that of the expander journal. It was considered more important to duplicate sliding speed than frequency.

4. Loads

Up to 3400 p.s.i. (based on the design of the crankshaft journal Rankine-cycle expander).

5. Fluid Temperature

Friction studies to be done at 200°F and 250°F. The higher temperature is the design temperature of the journal. The lower temperature approximates the lower operating ranges such as would occur shortly after starting the engine.

6. Fluid Compositions

Pure F-50

F-50 + 10, 20, 30, and 50 wt.% CP-34

Initial wear tests showed:

10% CP-34 - load capacity about equal to pure F-50

25% CP-34 - fair load capacity

50% CP-34 - very low load capacity

Consequently, 10% and 50% seemed logical lower and upper limits of dilution. The 20% and 30% values bracket the intermediate area.

7. Degree of Oscillation

Task III would involve only continuous rotation; Task IV would cover reciprocating motion.

Differences in geometry and lubricant feed between the engine journal and the wear tester are very important. These differences must be recognized to correlate correctly and any wear data with lubricant performance in the journal. This is discussed further in Section F.

D. TASK III: SLIDING FRICTION STUDIES

1. Apparatus (Figures V-5 and V-6)

A Monsanto designed friction and wear instrument was used for the sliding friction measurements. As required, this machine is equivalent to or will exceed the performance of the Hohman A-6. It was felt necessary and desirable to employ a special design to overcome the low maximum pressure limitation of the A-6, especially when dealing with volatile fluids such as CP-34. (For the most realistic assessment of friction and wear behavior, the test temperature should approximate operating temperatures. The use of the

bearing modulus to compensate for temperature should not be pushed too far.) At temperatures above 150°F, CP-34 has such a high vapor pressure that, in the A-6, it would distill rapidly from the test fluid reservoir to the cold walls of the test chamber. Were it practical to heat the entire test chamber of the A-6 hot enough to prevent this, the pressures that would be developed at temperatures above 200°F would be too much for the large, flat sides of the A-6 "kiln". Finally, the dead weight loading system of the A-6 is located inside the test chamber and can be changed only by opening the test chamber, which would cause considerable inconvenience at the higher temperatures.

The specifications of the special test machine are listed below. For comparison, the corresponding specifications of the A-6 (from a recent brochure) are given parenthetically.

Load: 2 to 1600 lbf; continuously variable from outside the test chamber (A-6: 80-1600 lbf, in 80-lb. increments; necessary to open the test chamber to change load).

Temperature: Fluid reservoir to 650°F; entire test chamber to 350°F. (A-6: fluid reservoir to 1500°F; test chamber not heatable.)

Speed: 100 to 3390 rpm, 5 hp motor giving shaft speeds from 30 to 10,000 rpm with suitable pulleys. (A-6: 50 to 3000 rpm at 1 hp standard; other drives available as required.)

Reciprocating Drive: 0° to 45° adjustable. (A-6: same.)

Sample Geometry: Two rub-blocks on rotating ring. (A-6: same.)

Data Available: Friction, wear, test-specimen temperature continuously available during operation. (A-6: same, except wear measurable after completion of test.)

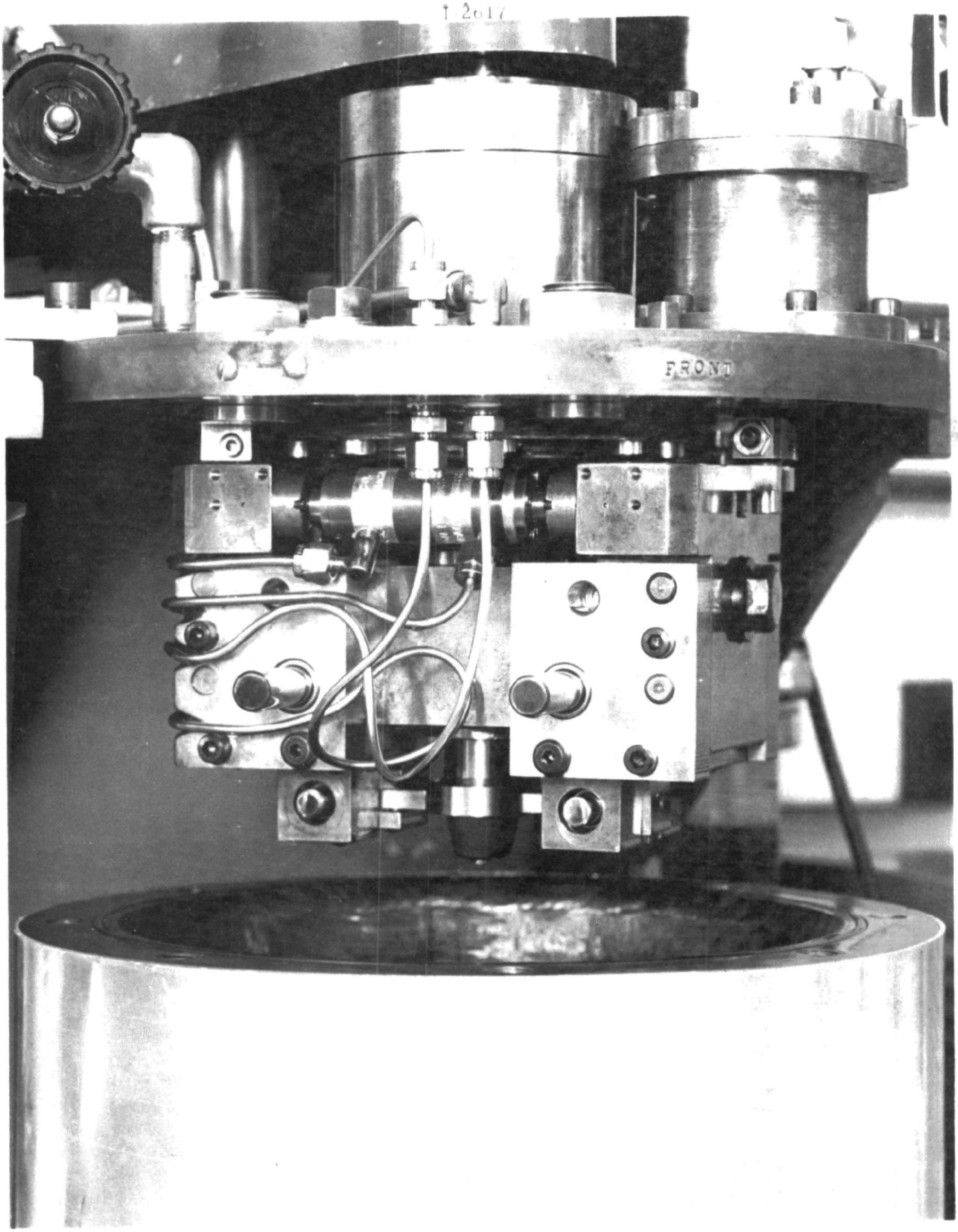

Figure V-5. Internal Mechanism of the Monsanto Wear Tester.

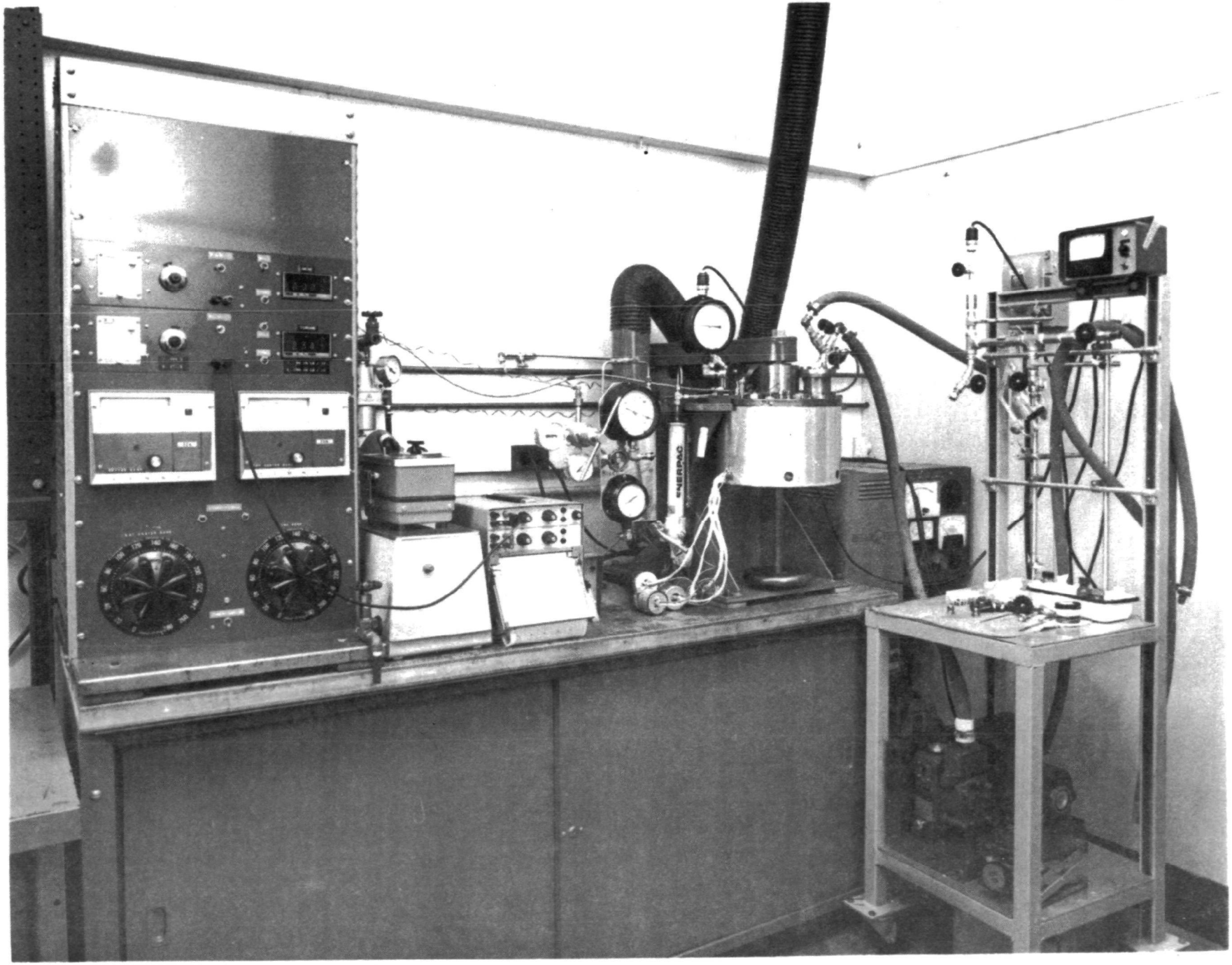

Figure V-6. Overall View of the Monsanto Wear Tester.

2. Typical Procedure

A typical friction run consisted of:

a) Strain gauge calibration
b) Charge of pure F-50
c) Degassing the F-50
d) Run-in on pure F-50
e) Friction measurements on F-50 if desired
f) Addition of degassed CP-34 to desired concentration
g) Friction measurements
h) Addition of more degassed CP-34

Alternatively, premixed solutions of CP-34 in F-50 were added to the test vessel. Then the procedure was:

a) Strain gauge calibration
b) Run-in
c) Friction measurements

This technique saved considerable time, particularly at high concentrations of thiophene. It was used on runs containing 30% and 50% CP-34.

3. Initial Runs

The first test program on silicone blends at 200°F defined the concentrations of CP-34 for further study. As mentioned before, 10% CP-34 was comparable to pure F-50, while 50% CP-34 was markedly inferior to F-50 and 25% CP-34 was intermediate. The load capacity data is given in Table V-3. We selected concentrations of 0, 10, 20, 30, and 50% CP-34 for lubrication testing.

Figure V-7 is a graph of typical raw data from these early runs. It is a plot of torque vs. bearing surface load for pure F-50. Since stick-slip causes a range of torque values, each load is represented by a line depicting that range.

There are no origin corrections in Figure V-7. The plotted load is the average bearing load plus extra pressure in the loading system due to instrumentation and due to overcoming any gas pressure in the vessel. The correction to get the bearing load can be read from the graph itself. The actual values of bearing load are 80 p.s.i. less than plotted. Load corrections for blends of F-50 and CP-34 can likewise be found from their torque-load plots, or they can be calculated from the vapor pressure of CP-34 (see Section G and Table V-4).

The torque values must be relative to the torque reading when the specimens are not in contact. Although this does not allow for the torque due to the viscous drag of the fluid on the rotating specimens, the error is small and may be ignored. The correction can be seen on the torque-load plots (e.g. 0.6 in.-lb. in Figure V-7) or eliminated by alterations of the base lines on the raw data charts.

4. Run-in Procedures

Without careful run-in, subsequent torque vs. load plots were not reproducible. Apparently the specimen surface finish is a variable of the first importance. Thus we had to define reliable run-in procedures to maximize load carrying ability and stabilize friction values.

TABLE V-3

INITIAL RUNS: LOAD CARRYING CAPACITY
(AVERAGE PSI BETWEEN TEST SPECIMENS)
SAE 660 BRONZE ON HARDENED CAST IRON AT 200°F.

Various Sliding Speeds and Various Concentrations of
Monsanto CP-34 in General Electric F-50 Versilube.

Sliding Speed (in./min.)	% (w/w) CP-34			
	0%	10%	25%	50%
18800	3400	3400	3400	500(900)
9400	3400	3400	2100(2500)	300
4700	2600	2000	1200	200
2800	1500	1000	600	200

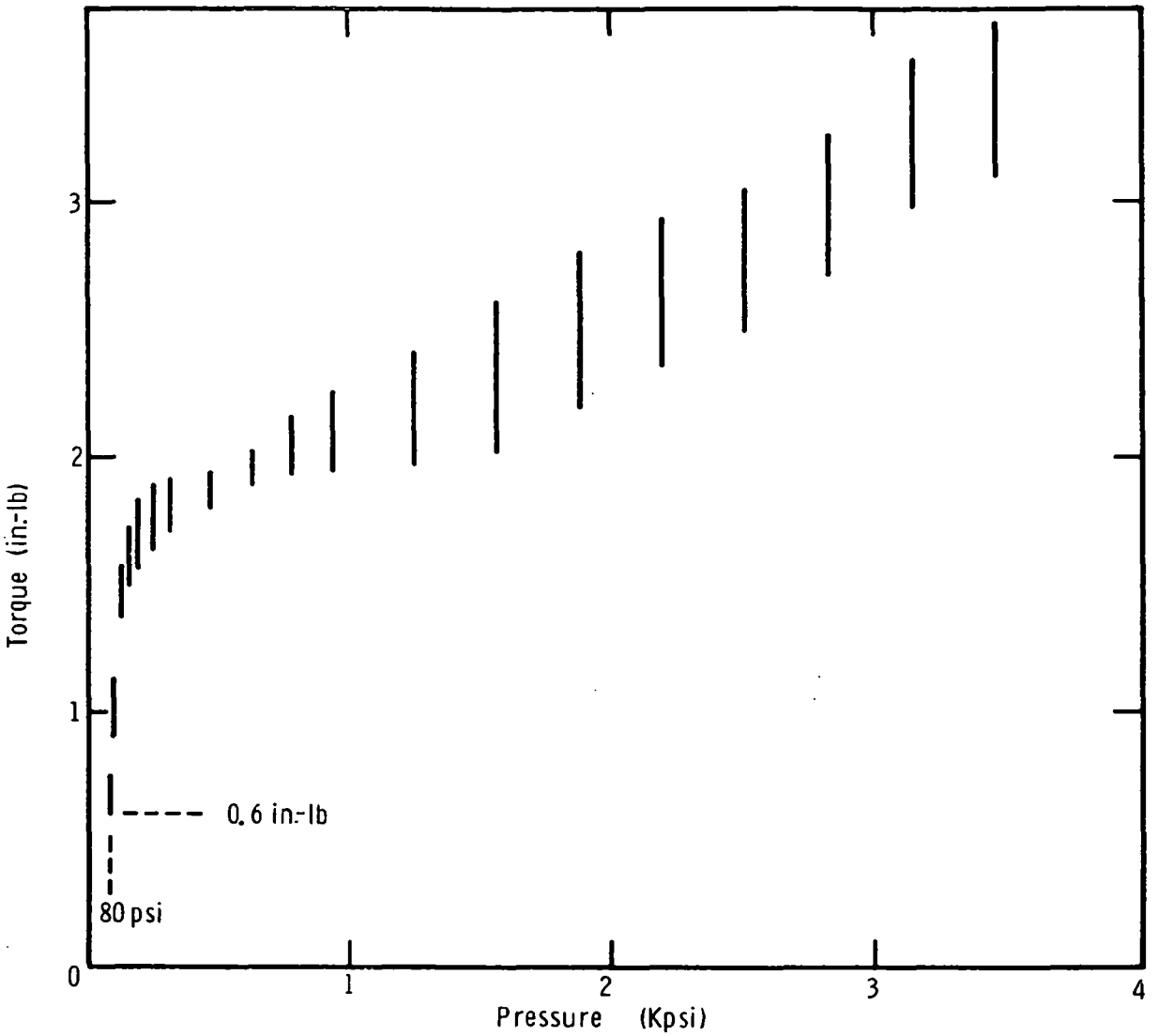

Figure V-7. Torque (in. -lb) vs. Bearing Load (Kpsi). SAE 660 Bronze on Hardened Cast Iron. 200°F., Pure F-50, 18800 in./min.

TABLE V-4

CONVERSION OF GAUGE PRESSURE (PSI) TO AVERAGE BEARING PRESSURE (PSI) FOR THE TEST BLENDS OF CP-34/F-50

P = (gauge pressure) x π - correction for instrumentation and gas pressure

The corrections were:

% CP-34	200°F.	250°F.
0	-80	-80
10	-90	-105
20	-95	-115
30	-110	-147
50	-130	-180*

* Estimate based on an extrapolation of the nomograph pressure lines.

A satisfactory run-in technique is as follows:

> A hardened cast iron ring and two conforming SAE 660 bronze rub-blocks (surface finishes as specified by Thermo Electron) were loaded at 200°F in pure F-50. The break-in began at low speed (2800 in./min.). The load was increased carefully in small increments, allowing plentiful time for the friction to stabilize at each load. After excessive stick-slip which refused to go away with further running in was encountered, the load was removed and the speed increased. This process was repeated at 4700, 9400, 14000 and finally at 18800 in./min. after which the specimens were declared ready for use.

For the data in this report a simpler, time-saving run-in procedure was used.

> Beginning with pure F-50 and fresh test specimens, without applying heat to the test chamber, the run-in was started at 600 rpm. After the load had been slowly pushed as high as practical without failure, the speed was increased to 4000 rpm and the load increased slowly again, this time to 3400 psi before stopping.

This completed the new run-in.

Finally, we found that run-in at 250°F is better than at 200°F. Contract termination prevented incorporation of this into a standard procedure.

Additional effort was spent on finding a quicker run-in method. It appears that run-in is necessarily a slow process and attempts to

hurry it are risky. Several conclusions based on this work are:

a. Wear particle generation is not desirable during run-in although very minute amounts do not seem detrimental.

b. Any transfer of bronze to the disc is reason to reduce load--if transfer does not disappear, further run-in is fruitless.

c. The high speed run-in must not produce particles--fluid agitation suspends them and causes more wear.

5. Interpretation of Data

Friction data were obtained on all test concentrations at four speeds and two temperatures (200°F and 250°F). The raw data values used to characterize each run are given in Table V-5. Various summarizes and plots of these data include:

a. Table V-6 - Load Capacities and Failure Bearing Moduli at 200°F and Table V-7 - Load Capacities and Failure Bearing Moduli at 250°F

These summaries show failure or maximum loads, as well as the corresponding bearing moduli and coefficients of friction for various CP-34 concentrations at different speeds. The failure load (load capacity) is the highest load at which a two minute run was completed without failure or signs of incipient failure. Note that failure occurred for values of the bearing modulus in the range of 1.25 to 0.11 (200°F) and 1.47 to 0.13 (250°F).

b. Load Capacity vs. CP-34 Concentration

The failure or maximum bearing loads at 200°F are plotted against concentration in Figure V-8. At the two fastest speeds,

load carrying decreases above 30% CP-34. The initial load decrease occurs at lower concentrations at the lower speeds. Figure V-8 also shows the corresponding plot for 250°F. The load carrying ability of the blends holds up fairly well to 20% CP-34. When a decrease in bearing load occurs at higher concentrations, it is a sharper and quicker drop than at 200°F. By 30% CP-34, the load carrying is very low except for the fastest speed. Surprisingly, 50% CP-34 at 18800 in./min. carries the load to 2646 p.s.i.

c. Coefficient of Friction vs. Bearing Modulus

Normally, the experimental friction coefficient is plotted against a bearing modulus.[4] However, the geometry of the block on the ring in the test instrument allows a certain self-alignment by the block. This in effect makes the test bearing resemble a tilting pad journal bearing.[5] For such a bearing in the hydrodynamic regime, the coefficient of friction is proportional to the square root of the bearing modulus.[6]

Since ho varies with both $\sqrt{M}$ and μ, their ratio should be constant. This is so at the boundary transition through 30% CP-34.

% CP-34	Ratio $\sqrt{M}/\mu \times 10^{-2}$
0	2.7
10	2.7
20	1.7
30	1.7

[4] A. Cameron, p. cit., pg. 8
[5] Ibid, pg. 4 and Chapter 5
[6] Ibid, pg. 115

TABLE V-5

RAW FRICTION DATA

Speed (ν, in./min.), absolute viscosity (η, poises), torque (L, in.-lb.), average bearing pressure P, psi), bearing modulus ($\eta\nu/P$, M, poises in. min.$^{-1}$ psi^{-i}), $M^{1/2}$, and coefficient of friction (μ) for all points used in data interpretation. (The initial F-50 run, Fig. V-7, is not included.)

% CP34	Temp. °F.	ν	η	L	P	M	$M^{1/2}$	μ
0	200	2800	.194	.12	77	7.04	2.65	.0052
				.76	862	.63	.79	.0034
				1.77	1490	.36	.60	.0042
				2.11	1647	.33	.57	.0045
		4700		.18	77	11.76	3.42	.0084
				.79	862	1.06	1.03	.0032
				1.24	1490	.61	.78	.0029
				1.78	2118	.43	.66	.0030
				2.22	2432	.38	.61	.0031
				2.51	2589	.35	.59	.0034
		9400		.20	77	23.81	4.88	.0090
				.98	862	2.11	1.45	.0040
				1.46	1490	1.22	1.10	.0035
				1.78	2118	.86	.93	.0029
				2.22	2746	.66	.81	.0029
				2.66	3374	.54	.74	.0028
		18800		.42	77	47.6	6.90	.0194
				1.45	862	4.22	2.05	.0059
				1.96	1490	2.44	1.56	.0047
				2.52	2118	1.72	1.31	.0042
				2.80	2746	1.32	1.15	.0036
				3.33	3374	1.07	1.04	.0035
10	200	2800	.097	.084	67	4.05	2.01	.0045
				.224	224	1.21	1.10	.0036
				2.128	381	.71	.845	.0046
				.952	538	.51	.71	.0063
				.490	853	.32	.56	.0089
		4700		.35	67	6.80	2.61	.019
				.38	224	2.04	1.43	.0060
				.95	852	.53	.73	.0039
				1.20	1170	.39	.62	.0037
				1.75	1480	.31	.55	.0042
				2.52	1794	.25	.50	.0050
		9400		.53	67	13.51	3.68	.028
				1.06	853	1.07	1.03	.0044
				1.44	1480	.62	.79	.0035
				1.82	2108	.43	.66	.0031
				2.20	2736	.33	.58	.0028
				3.14	3364	.27	.52	.0033

TABLE V-5 (cont.)

% CP34	Temp. °F.	ν	η	L	P	M	$M^{1/2}$	μ
10	200	18800	.097	.43	67	27.03	5.20	.023
				1.26	853	2.14	1.46	.0052
				1.64	1480	1.23	1.11	.0039
				2.02	2108	.86	.93	.0034
				2.39	2736	.66	.82	.0031
				2.86	3364	.54	.74	.0030
20	200	2800	.058	.23	62	2.62	1.62	.013
				.40	219	.74	.86	.0065
				.94	376	.43	.66	.0088
				1.42	533	.31	.56	.0095
				1.86	847	.19	.44	.0078
		4700		.32	219	1.24	1.11	.0052
				.93	847	.32	.57	.0039
				1.23	1161	.23	.48	.0038
				1.50	1475	.18	.42	.0036
				2.25	1789	.15	.39	.0045
		9400		.60	219	2.49	1.58	.0097
				1.08	847	.64	.80	.0045
				1.40	1475	.37	.61	.0034
				1.67	2103	.26	.51	.0028
				2.10	2731	.20	.45	.0027
				2.90	3359	.16	.40	.0031
		18800		.72	219	4.97	2.23	.012
				1.32	847	1.29	1.14	.0055
				1.79	1789	.61	.78	.0036
				2.22	2731	.40	.63	.0029
				2.50	3359	.32	.57	.0026
30	200	2800	.040	.38	204	.55	.74	.0066
				.69	361	.31	.56	.0068
				1.10	518	.22	.46	.0075
				1.24	675	.17	.41	.0065
				1.55	832	.13	.37	.0066
		4700		.30	204	.92	.96	.0052
				.52	518	.36	.60	.0036
				1.62	1146	.16	.40	.0050
				1.93	1460	.13	.36	.0047
				2.50	1774	.11	.32	.0050
		9400		.42	204	1.82	1.35	.0073
				.75	832	.45	.67	.0032
				.94	1460	.26	.51	.0023
				1.38	2088	.18	.42	.0023
				2.10	2716	.14	.37	.0027
				2.28	3030	.12	.35	.0027

TABLE V-5 (cont.)

% CP34	Temp. °F.	ν	η	L	P	M	$M^{1/2}$	u
30	200	18800	.040	.57	204	3.70	1.92	.0099
				.96	832	.90	.95	.0041
				1.22	1460	.51	.72	.0030
				1.38	1774	.42	.65	.0028
				1.84	2716	.27	.52	.0024
				2.13	3344	.22	.47	.0027
50	200	2800	.026	.40	27	2.70	1.64	.052
				1.10	58	1.25	1.12	.67
		4700		.24	27	4.55	2.13	.032
				.68	184	.67	.82	.013
				.94	341	.36	.60	.0098
				1.16	498	.25	.50	.0082
				1.31	577	.21	.46	.0080
		9400		.40	27	9.09	3.02	.053
				.93	184	1.33	1.15	.018
				1.34	341	.72	.85	.014
				1.72	498	.49	.70	.012
				2.15	655	.37	.61	.012
		18800		.43	27	18.18	4.26	.057
				.71	184	2.62	1.62	.014
				1.28	341	1.44	1.20	.013
				1.95	1440	.34	.58	.0048
				2.38	1754	.28	.53	.0048
0	250	2800	.136	.32	77	4.95	2.22	.015
				.45	234	1.63	1.28	.0068
				1.28	862	.44	.67	.0053
				1.67	1176	.32	.57	.0050
				1.81	1333	.29	.53	.0048
		4700		.40	234	2.70	1.64	.0061
				.93	862	.74	.86	.0038
				1.43	1490	.43	.66	.0034
				1.92	2118	.30	.55	.0032
				2.70	2746	.23	.48	.0035
		9400		.54	234	5.56	2.36	.0082
				1.64	1490	.85	.92	.0039
				2.58	3060	.42	.65	.0030
				2.78	3374	.38	.62	.0029
		18800		.75	234	10.87	3.30	.011
				2.00	1490	1.72	1.31	.0047
				3.04	3060	.83	.92	.0035
				3.40	3374	.76	.87	.0036

TABLE V-5 (cont.)

% CP34	Temp. °F.	ν	η	L	P	M	$M^{1/2}$	μ
10	250	2800	.073	.25	209	.98	.99	.0042
				1.06	523	.39	.63	.0071
				1.10	837	.24	.49	.0047
				1.53	1151	.18	.42	.0047
		4700		.21	209	1.64	1.28	.0037
				.80	837	.41	.64	.0034
				1.14	1465	.23	.48	.0027
				1.77	2093	.16	.40	.0030
				1.95	2407	.14	.38	.0028
		9400		.63	209	3.33	1.83	.011
				1.38	837	.82	.91	.0059
				1.73	1465	.47	.69	.0041
				1.90	2093	.32	.57	.0032
				2.14	2721	.25	.50	.0028
				2.75	3349	.20	.45	.0029
		18800		.48	209	6.67	2.58	.0082
				1.25	837	1.64	1.28	.0053
				1.96	1465	.93	.97	.0047
				2.15	2093	.65	.81	.0036
				2.50	2721	.51	.71	.0033
				2.91	3349	.41	.64	.0031
20	250	2800	.046	.12	42	2.63	1.62	.010
				.50	199	.56	.75	.0089
				1.00	356	.31	.56	.010
				1.13	513	.22	.47	.0078
		4700		.41	199	1.09	1.04	.0073
				.65	513	.42	.65	.0045
				1.00	827	.26	.51	.0043
				1.88	1141	.19	.44	.0058
				2.40	1455	.15	.39	.0058
		9400		.43	199	2.17	1.47	.0076
				.87	827	.52	.72	.0037
				1.30	1455	.30	.55	.0032
				1.68	2083	.21	.46	.0029
				2.29	2711	.16	.40	.0030
				2.84	3339	.13	.36	.0030
		18800		.91	827	1.04	1.02	.0039
				1.65	1769	.49	.70	.0033
				2.10	2711	.32	.57	.0027
				2.45	3339	.26	.51	.0026
30	250	2800	.033	.30	10	9.09	3.02	.106
				.94	89	1.04	1.02	.037
				2.58	167	.55	.74	.055

TABLE V-5 (cont.)

% CP34	Temp. °F.	ν	η	L	P	M	$M^{1/2}$	μ
30	250	4700	.033	.56	89	1.75	1.32	.022
				.91	167	.93	.97	.019
				1.65	246	.63	.79	.024
				2.49	324	.48	.69	.027
		9400		.24	89	3.45	1.86	.0096
				.50	167	1.85	1.36	.011
				.75	324	.96	.98	.0082
				1.10	481	.65	.80	.0081
				2.25	795	.39	.63	.010
		18800		.41	167	3.70	1.92	.0087
				.88	795	.78	.88	.0039
				1.41	1423	.43	.66	.0035
				2.00	2051	.30	.55	.0035
				2.28	2365	.26	.51	.0034
50	250	2800	.021	.2	8	7.14	2.67	.088
				.37	40	1.47	1.21	.033
				1.42	71	.83	.91	.071
		4700		.42	40	2.43	1.56	.037
				.87	71	1.39	1.18	.044
				1.52	103	.96	.98	.052
		9400		.23	40	5.00	2.23	.020
				.48	71	2.78	1.67	.024
				.64	103	1.92	1.39	.022
				.88	134	1.47	1.21	.023
		18800		.42	762	.52	.72	.0020
				.88	1390	.28	.53	.0022
				1.50	2018	.20	.44	.0026
				2.00	2646	.15	.39	.0027

TABLE V-6

LOAD CARRYING CAPACITY

(Average p.s.i. between test specimens) SAE 660 Bronze on Hardened Cast Iron at 200°F. Various Sliding Speeds (in./min.) and Various Concentrations (w/w %) of CP-34 in F-50. Bearing Moduli ($\eta\ \nu/P$, M, poise in. min.$^{-1}$ p.s.i.$^{-1}$) are shown parenthetically beneath the values of concentration and load carrying capacity respectively. The second parenthesis is the coefficient of friction.

Sliding Speed in./min.		Concentration (w/w %)				
		0	10	20	30	50
2800	psi	1647	852	847	832	58
	M	(.33)	(.32)	(.19)	(.13)	(1.25)
	μ	(.0045)	(.0089)	(.0078)	(.0066)	(.67)
4700	psi	2589	1794	1789	1774	655
	M	(.35)	(.25)	(.15)	(.11)	(.21)
	μ	(.0034)	(.0050)	(.0045)	(.0050)	(.0080)
9400	psi	>3374	>3364	>3359	3030	655
	M	(.54)	(.27)	(.16)	(.12)	(.37)
	μ	(.0028)	(.0033)	(.0031)	(.0027)	(.012)
18800	psi	>3374	>3364	>3359	>3344	1754
	M	(1.07)	(.54)	(.32)	(.22)	(.28)
	μ	(.0035)	(.0030)	(.0026)	(.0027)	(.0048)

> No failure occurred, no signs of incipient failure.

TABLE V-7

LOAD CARRYING CAPACITY

(Average p.s.i. between test specimens) SAE 660 Bronze on Hardened Cast Iron at 250°F. Various Sliding Speeds (in./min.) and Various Concentrations (w/w %) of CP-34 in F-50. Bearing Moduli ($\eta\nu/P$, M, poise in. min.$^{-1}$ p.s.i.$^{-1}$) are shown parenthetically beneath the values of concentration and load carrying capacity respectively. The second parenthesis is the coefficient of friction.

Sliding Speed in./min.		Concentration (w/w %)				
		0	10	20	30	50
2800	psi	1333	1151	513	167	71
	M	(.29)	(.18)	(.22)	(.55)	(.83)
	μ	(.0048)	(.0047)	(.0078)	(.055)	(.071)
4700	psi	2746	2407	1455	324	103
	M	(.23)	(.14)	(.15)	(.48)	(.96)
	μ	(.0035)	(.0028)	(.0058)	(.027)	(.052)
9400	psi	>3374	>3349	>3339	795	134
	M	(.38)	(.20)	(.13)	(.39)	(.147)
	μ	(.0029)	(.0029)	(.0030)	(.010)	(.023)
18800	psi	>3374	>3349	>3339	2365	2646*
	M	(.76)	(.41)	(.26)	(.26)	(.15)
	μ	(.0036)	(.0031)	(.0026)	(.0034)	(.0027)

> No failure occurred, no signs of incipient failure.

* Seizure after 30 sec. at 2960 p.s.i.

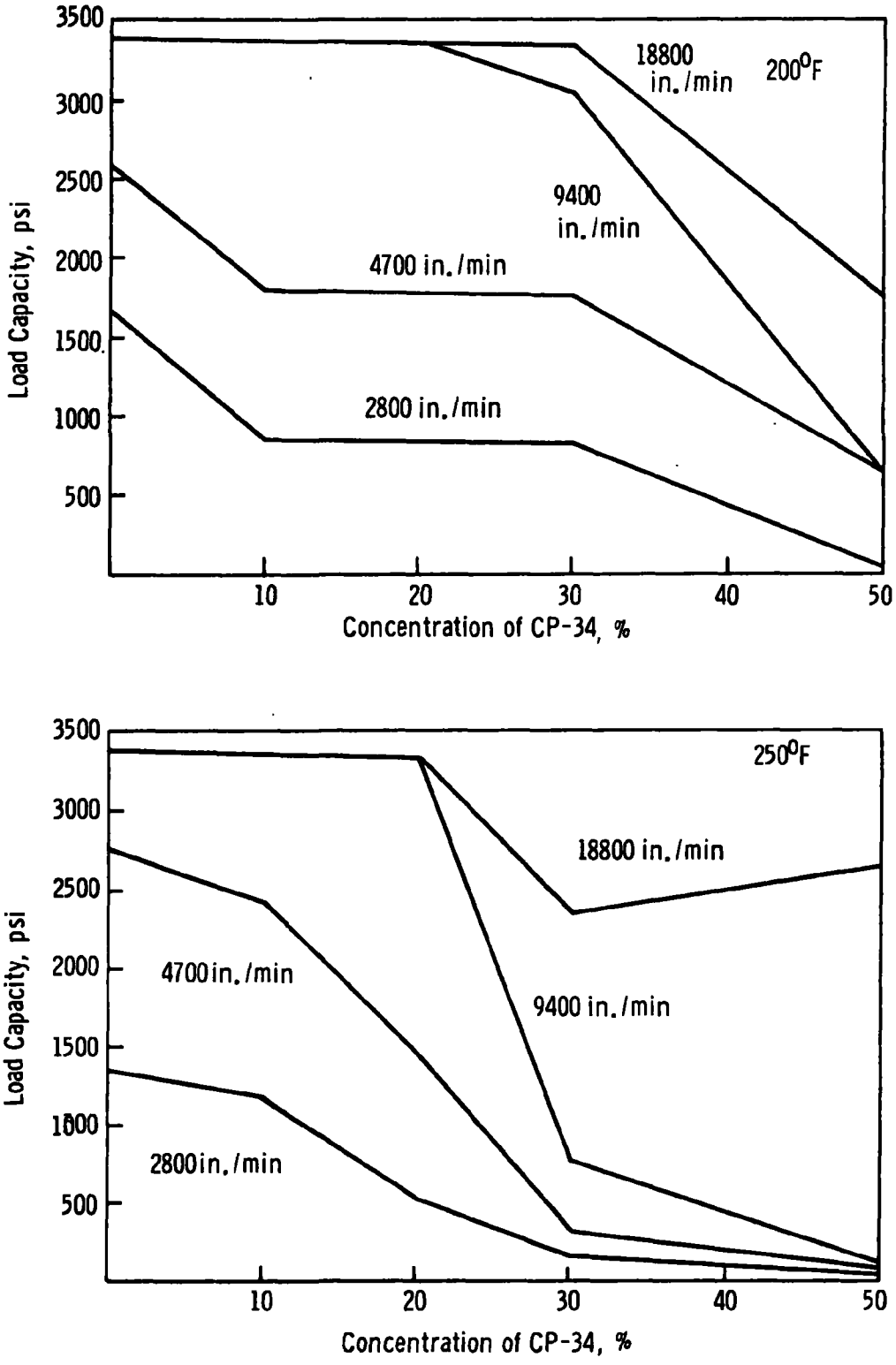

Figure V-8. Maximum Load Capacity as a Function of CP-34 Concentration. The top graph is at 200°F., the bottom at 250°F.

$$\mu \alpha \sqrt{\eta} \times v/P^{*}$$

Also, the minimum film thickness (ho) is proportional to the square root of the bearing modulus,[7] and so for any geometry $\mu \alpha$ho.

The plots of μ vs. $\sqrt{\text{bearing modulus}}$ at 200°F are shown in Figures V-9 through V-13. For many of the curves there is a fairly quick failure after μ begins to rise. Any differences in the film thickness of the various blends at the hydrodynamic-boundary transition will show up in differences of $\sqrt{M}$ or μ at the transition. The averaged values of $\sqrt{M}$ and μ at the minimum of the modulus curves are given below. These figures neglect curves with obvious friction spikes. These jumps are probably transitory boundary spots. Within experimental error, there is no difference in ho for the various silicone-thiophene blends through 30% CP-34. This is easily shown graphically. Apparently initial contact occurs at a limiting film thickness regardless of composition through 30% CP-34. The limiting film thickness will vary with surface roughness.[8]

% Thiophene	Transition, $\sqrt{M}$	Transition, μ
0	0.8	0.003
10	0.8	0.003
20	0.5	0.003
30	0.5	0.003
50		

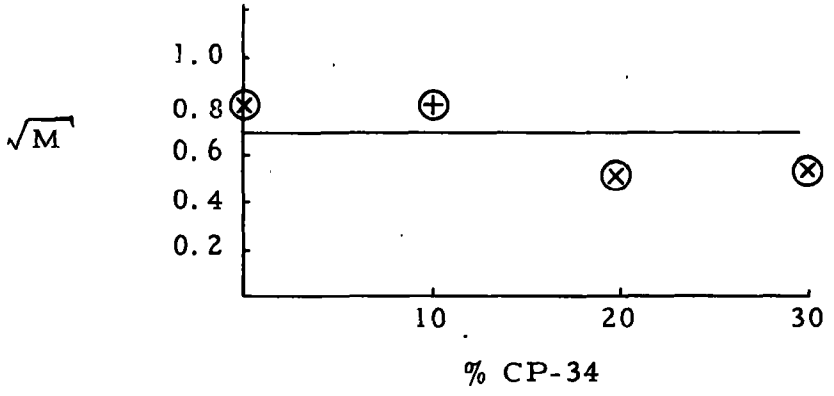

*Note that the speed term above has units of in/min instead of the more common rev/min.

[7] Ibid., p. 110.

[8] Ibid., p. 126.

Since ho varies with both $\sqrt{M}$ and μ, their ratio should be constant. This is so at the boundary transition through 30% CP-34.

% CP-34	Ratio $\sqrt{M}/\mu \times 10^{-2}$
0	2.7
10	2.7
20	1.7
30	1.7

The data for 50% thiophene is much more fragmentary (Figure V-13) and there is no attempt at interpretation of the curves.

A constant ratio of $\sqrt{M}/\mu$ occurs at 250°F for the 0, 10, and 20% blends. The curves are in Figures V-14, V-15 and V-16. The ratios are:

% Thiophene	$\sqrt{M}/\mu \times 10^{-2}$
0	1.7
10	1.7
20	1.6

At 30% and 50% dilution, the family of lines separates (see Figures V-17 and V-18). There is a wide friction variation with speed; high coefficients occur at low speeds and the curves have unusual shapes. The high volatility of thiophene (b. p. = 84°C) may affect the spread of the data. Vapor bubbles can form vapor dams or layers which interfere with heat transfer to the lubricant and cause metal contact and ultimately metal transfer. This concept does not explain the relatively good load carrying at the highest temperature, speed, and thiophene concentration (250°F, 18800 in./min., 50% dilution). Vaporization should maximize at these conditions.

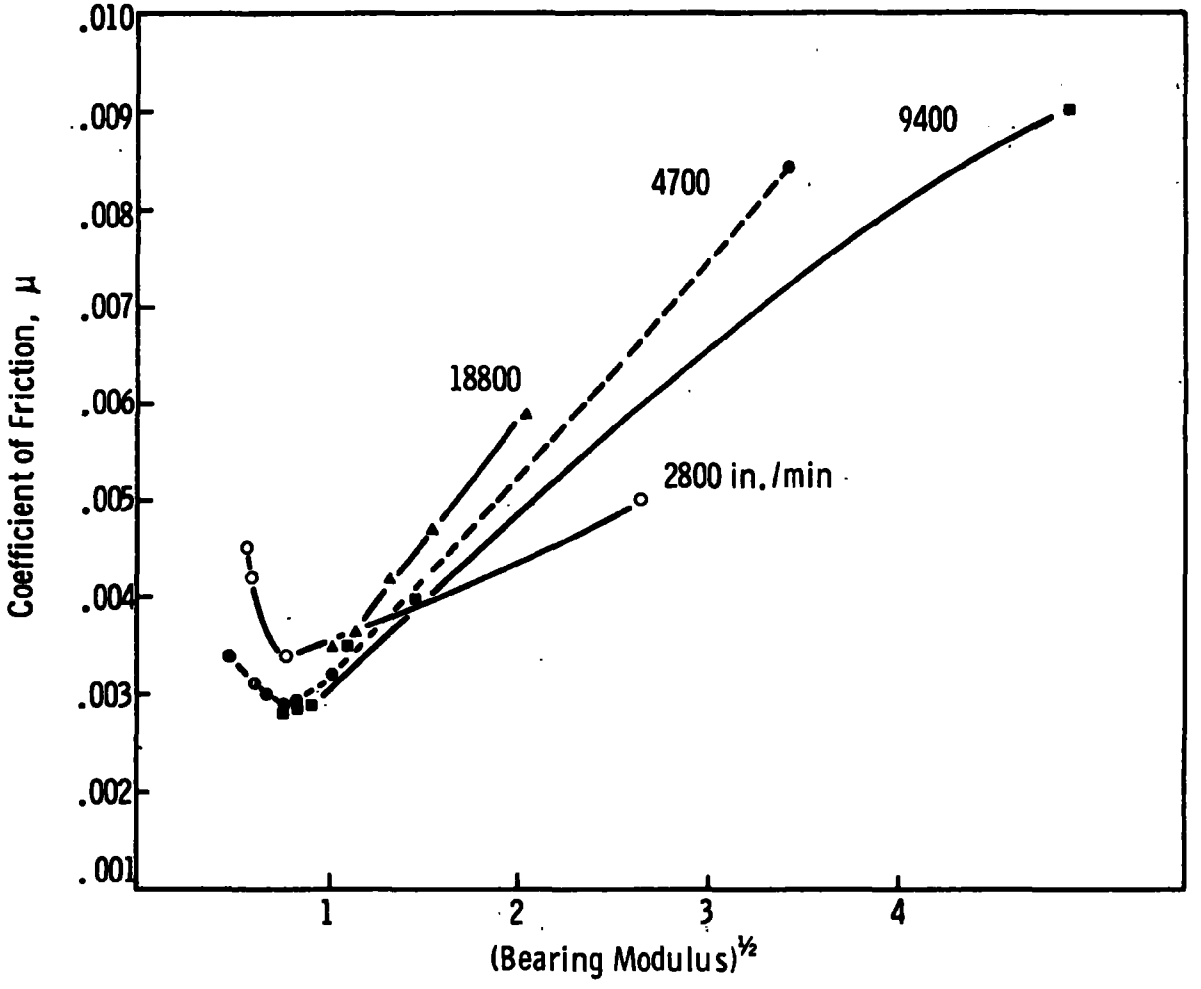

Figure V-9. Coefficient of Friction vs. √Bearing Modulus. F-50 Silicone. 200°F.

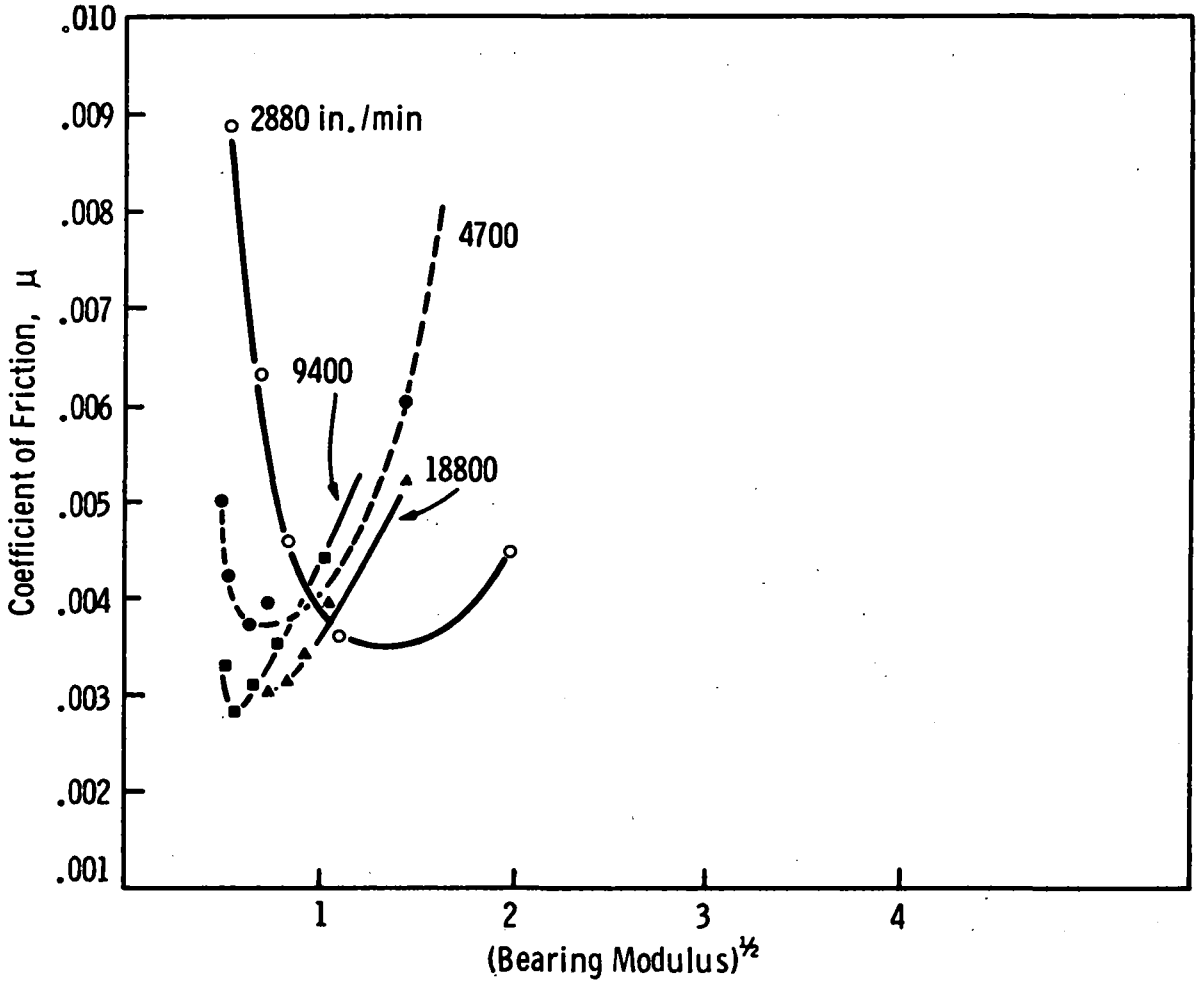

Figure V-10. Coefficient of Friction vs. √Bearing Modulus. 10% CP-34. 200°F.

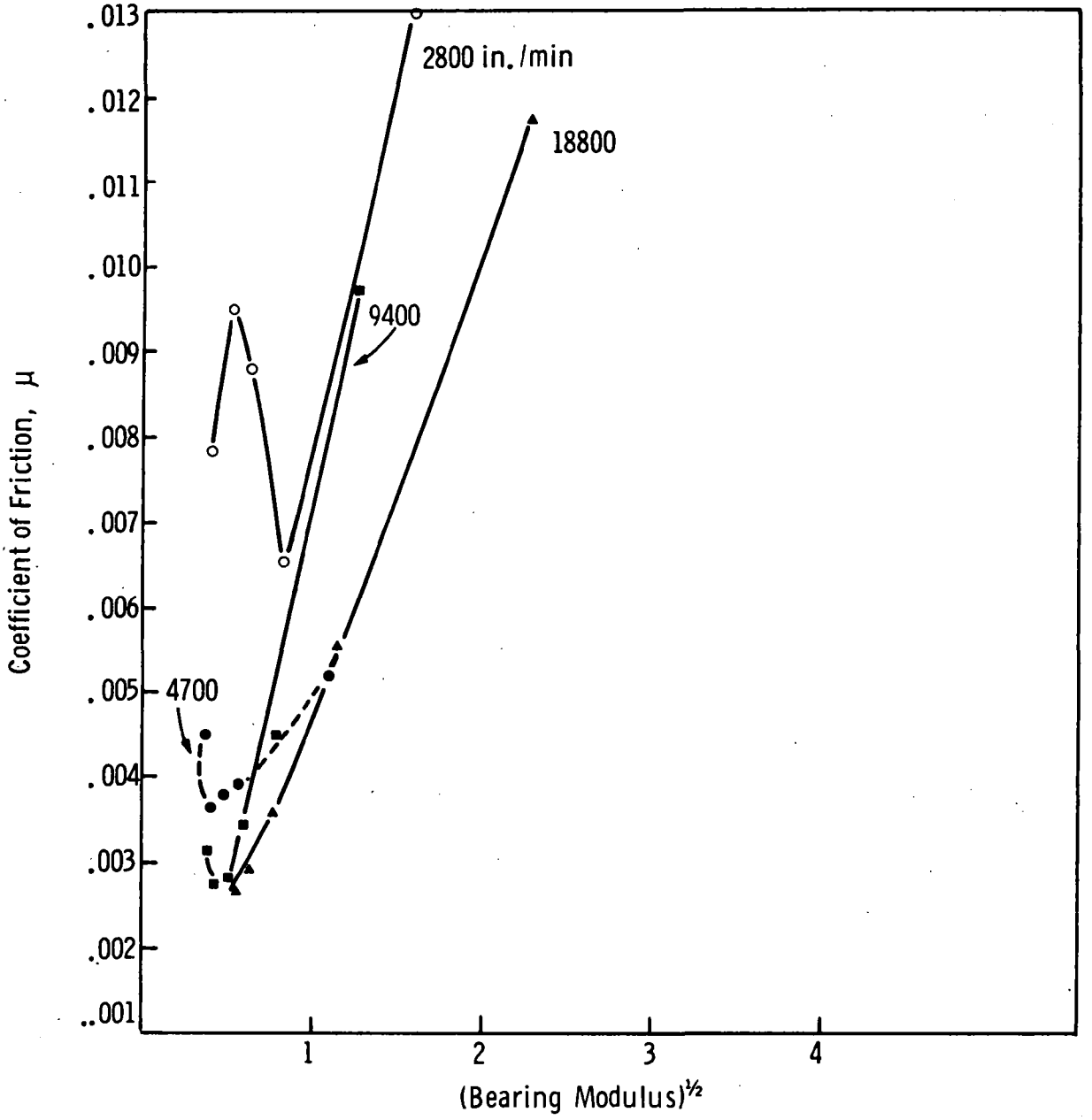

Figure V-11. Coefficient of Friction vs. √Bearing Modulus. 20% CP-34. 200°F.

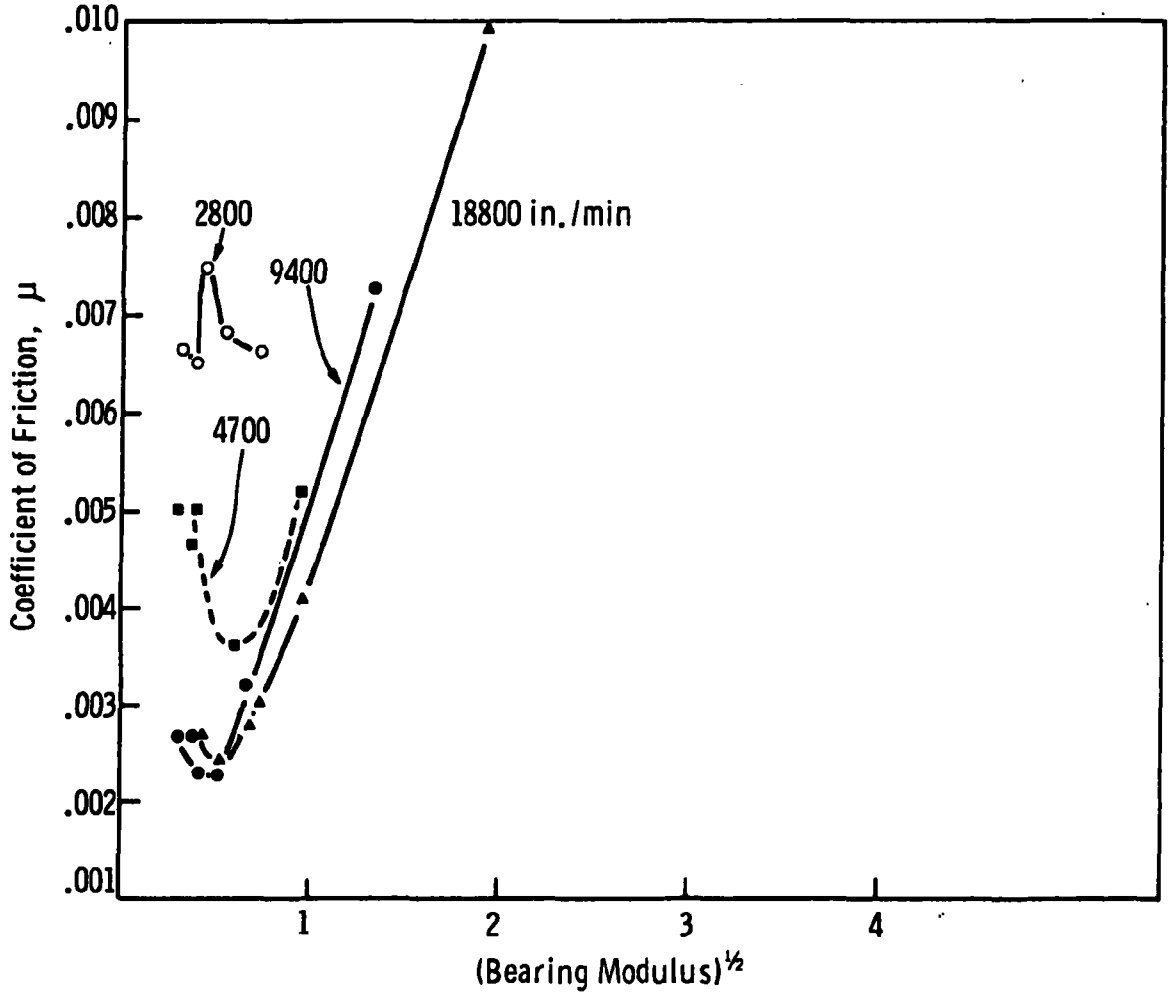

Figure V-12. Coefficient of Friction vs. √Bearing Modulus. 30% CP-34. 200°F.

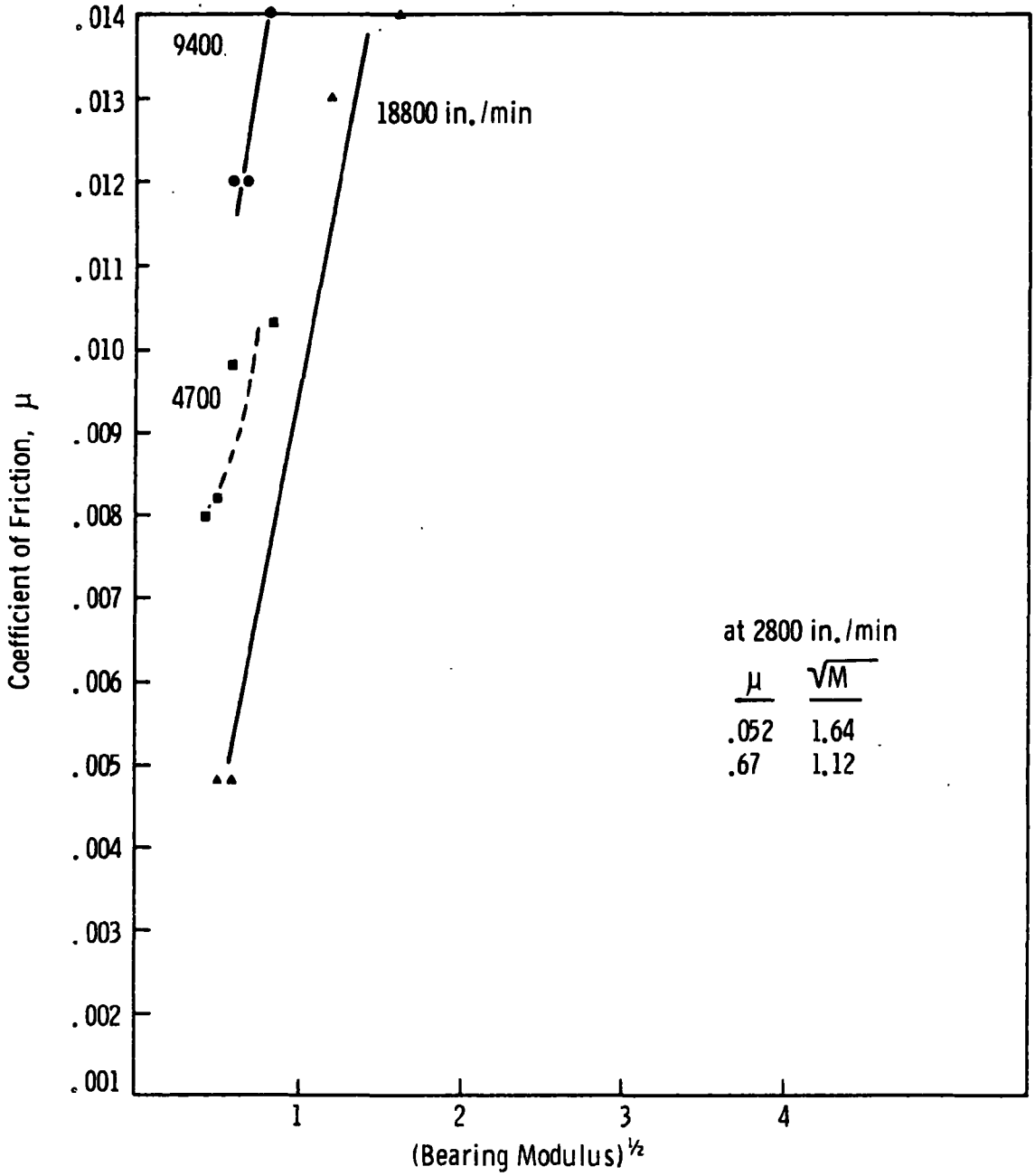

Figure V-13. Coefficient of Friction vs. √Bearing Modulus. 50% CP-34. 200°F.

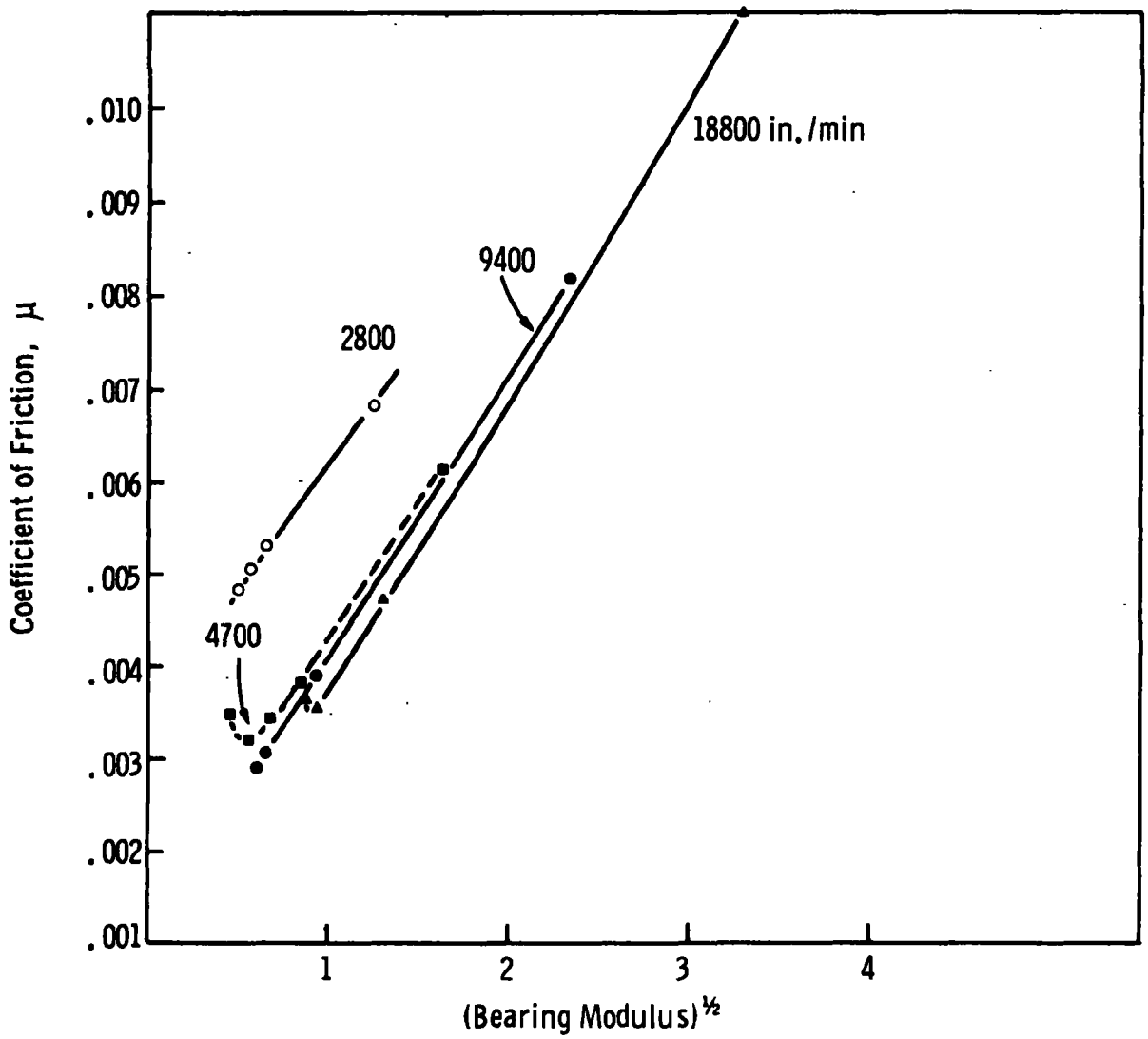

Figure V-14. Coefficient of Friction vs. √Bearing Modulus. F-50 Silicone. 250°F.

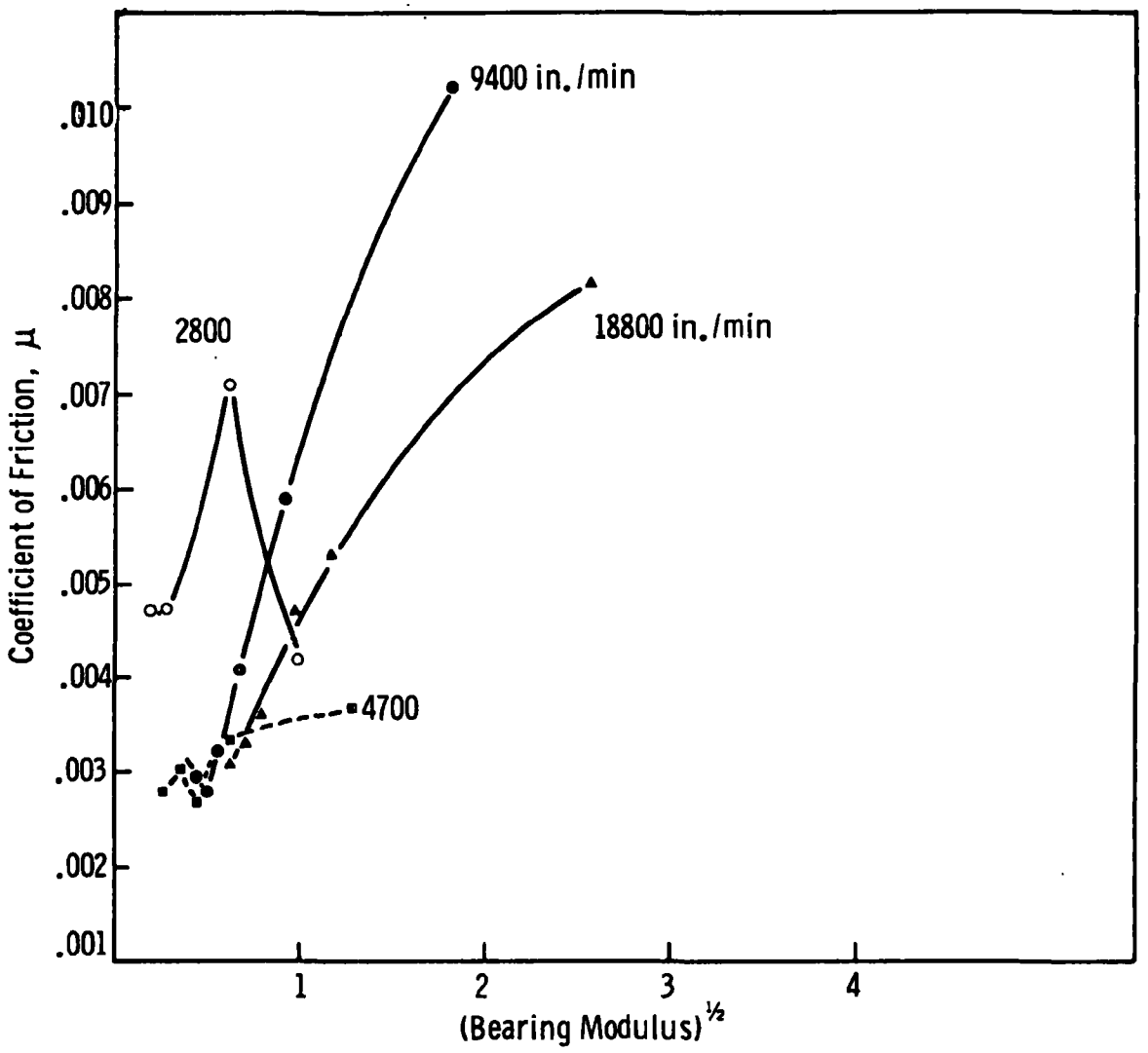

Figure V-15. Coefficient of Friction vs. √Bearing Modulus. 10% CP-34. 250°F.

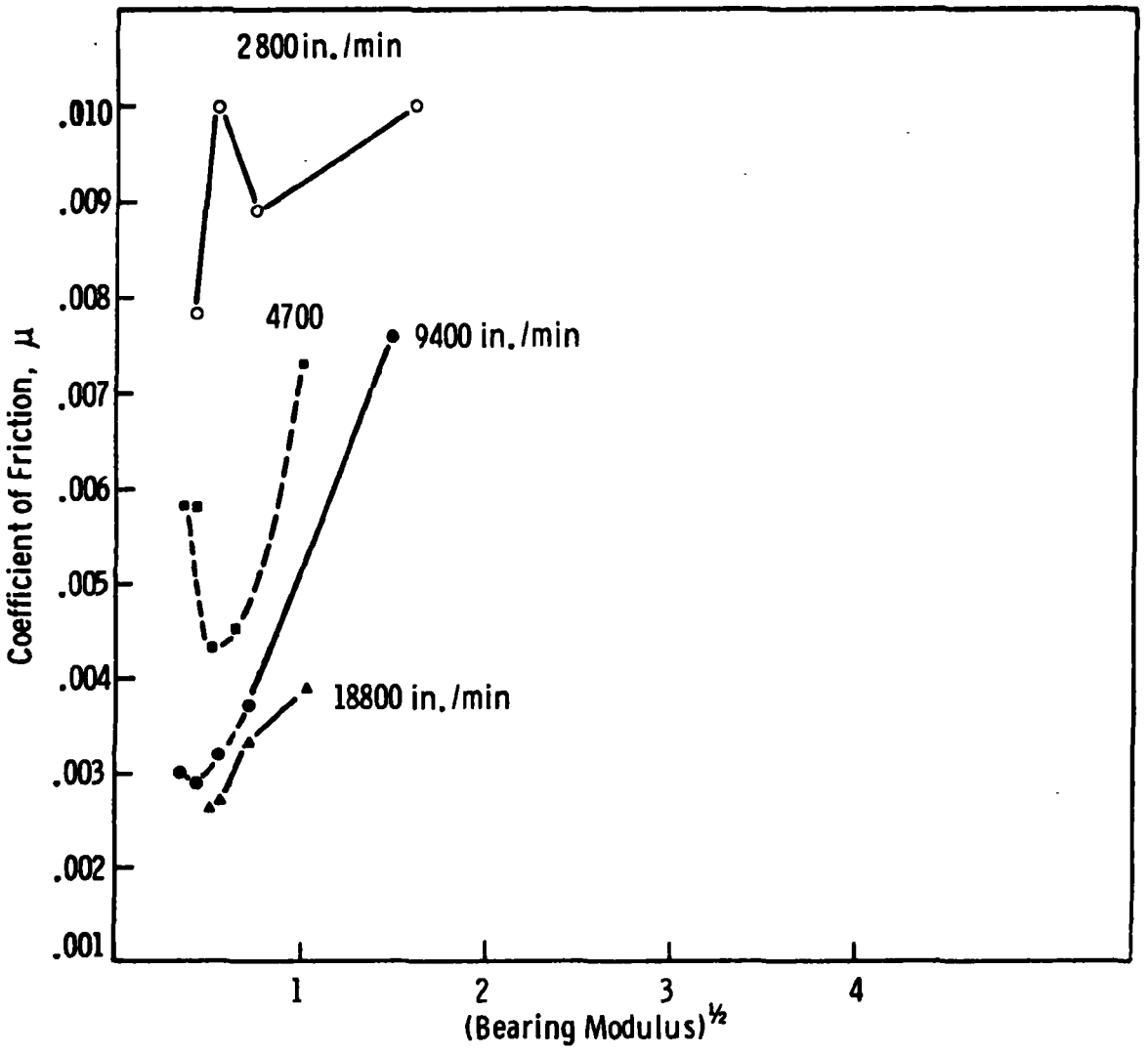

Figure V-16. Coefficient of Friction vs. √Bearing Modulus. 20% CP-34. 250°F.

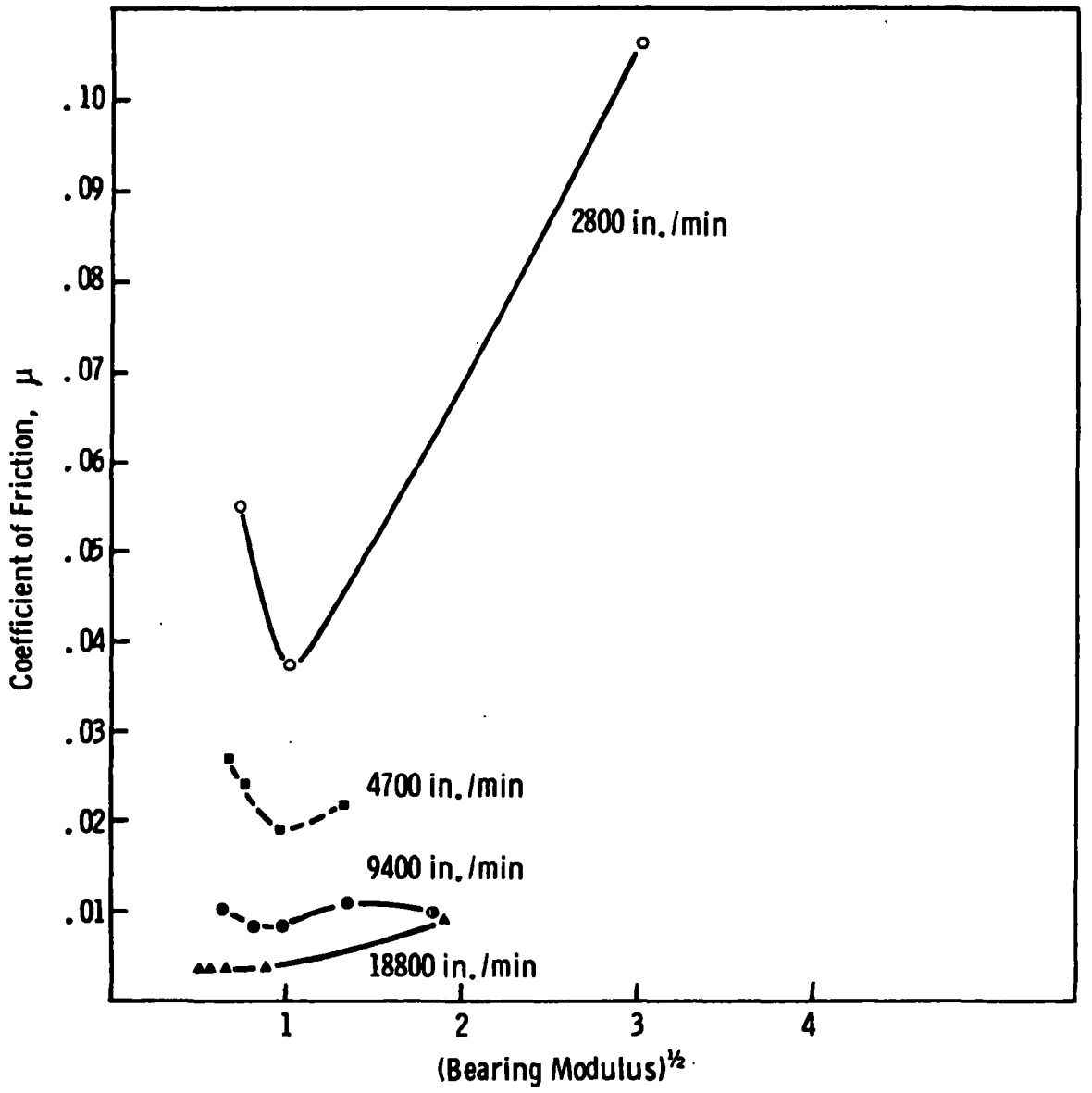

Figure V-17. Coefficient of Friction vs. √Bearing Modulus. 30% CP-34. 250°F.

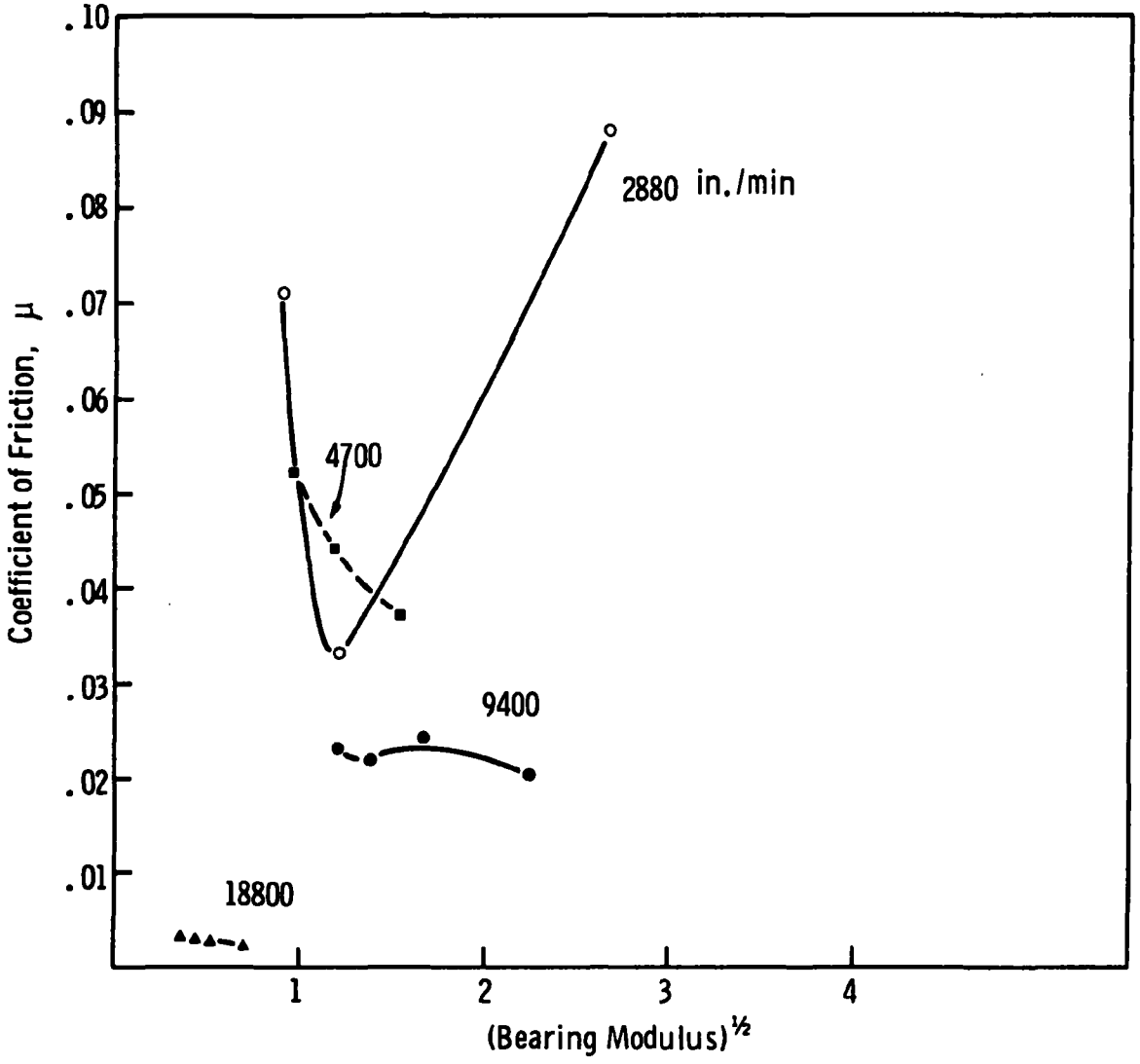

Figure V-18. Coefficient of Friction vs. √Bearing Modulus. 50% CP-34. 250°F.

d. Failure Bearing Moduli as a Function of Dilution: Boundary Lubrication of F-50/CP-34 Blends

While most of the previous analysis suggests hydrodynamic lubrication, the failed test specimens show metal transfer and smearing. The wear pattern is outward from the center of the block rather than backward along the face (Figure V-19). All of this is characteristic of boundary conditions. The bearing moduli at failure then reflect boundary lubrication. These failure moduli vary with concentration. This is shown in Figure V-20. The symbol ↓ means no failure occurred, so the actual failure modulus is less than the plotted value. These points are the dotted lines (unreal moduli) in the graph. The moduli minimum is at 30% for all speeds.

At 250°F the minimum for most of the curves is 10-20% CP-34 (Figure V-21). The exception is the fastest speed which has the lowest modulus at 50%.

Previous work[9] has shown that dilution of polydimethyl silicones with various solvents, such as benzene or methyl ethyl ketone, improves the boundary lubrication of the silicones. In fact, the lubrication of the mixture exceeds that of either component. Normally silicones exist in bulk in a helical configuration. The solvent molecules are believed to uncoil the silicone helix, producing a polymer which can form closely packed surface films. Perhaps the thiophene is assisting the boundary lubrication of F-50 silicone by this mechanism.

[9] S. F. Murray and R. L. Johnson, Natl. Advisory Comm. Aeronaut., Tech. Note No. 2788 (1952). See also Chem. Abst., 47, 40681 (1953).

The shaded areas in Figures V-20 and V-21 represent areas of acceptable bearing design. Lubrication failures should be minimized at these conditions of bearing moduli and concentration. If the value of the bearing modulus is sufficiently high, high concentrations (>20%) of thiophene can be tolerated. (Where a dashed line defines the apparent boundary of the shaded region, the permissible modulus may be quite a bit lower.)

In summary:

After the transition from hydrodynamic to boundary lubrication, the wear tester produces boundary failures. For such an environment, load carrying ability drops above 20% CP-34 at 250°F. Consistently poor lubrication occurs at 200°F with 50% CP-34. This is shown by low loads, high friction coefficients, and deviant bearing modulus curves.

E. TASK IV: RECIPROCATING STUDIES

Conditions were set for friction measurements under reciprocal motion. This motion approximates wrist pin loading. The conditions were: frequencies from 300 to 2000 cpm, up to 30° amplitude, bearing surface loadings up to 5000 psi (1-1/2 in. diameter test piece). We installed an oscillating drive on the rub-block tester and completed a few trial runs prior to contract termination.

This preliminary work showed that runs with an unheated, shallow, open reservoir were practical at any speed desired. This method allows observation of progress at any time and provides easy access to the test specimen. This is particularly valuable during run-in. Test speeds chosen were 300 and 2000 cpm. Several

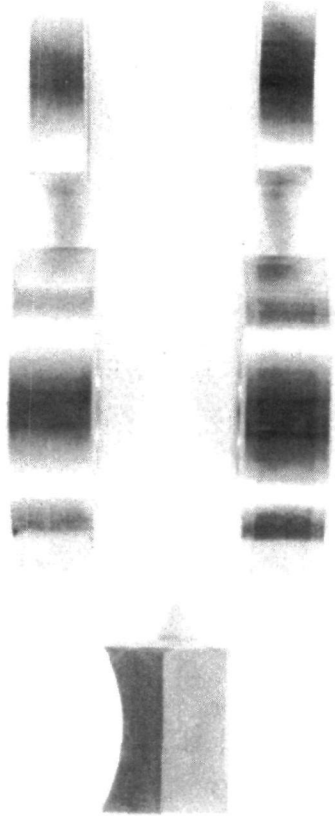

Figure V-19. Typical Worn Specimens. Set #6 on right and bottom compared with unused specimens on left.

NOTE: Bronze transferred to the ring, glazed, polished surface of the block, and discoloration of the block where unmasked by the block holder. (Streaks between polished areas are the original milling marks on the block surface. The polished streaks correspond on the ring and the blocks.)

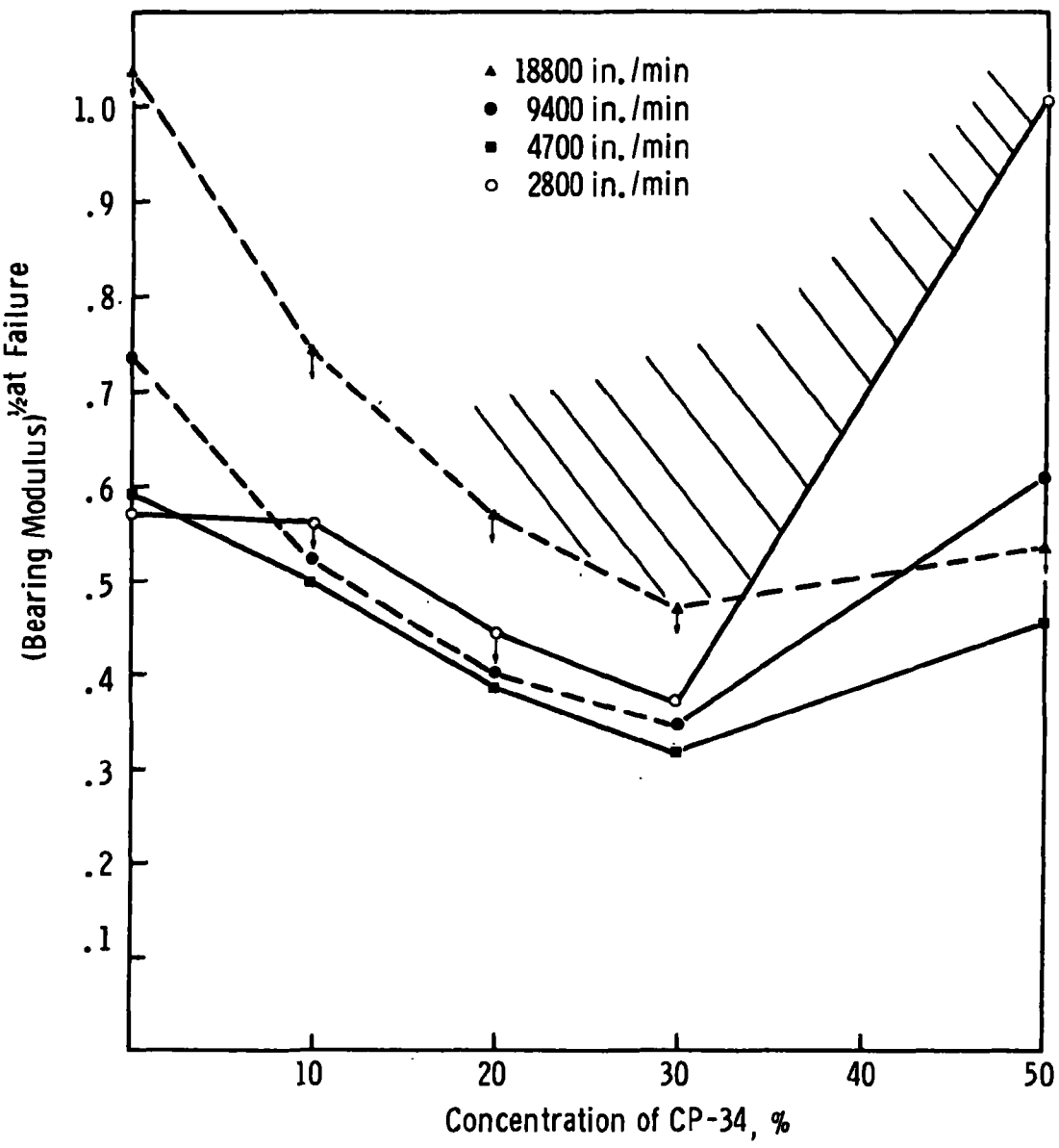

Figure V-20. $\sqrt{M}$ at Failure vs. CP-34 Concentration. 200°F.

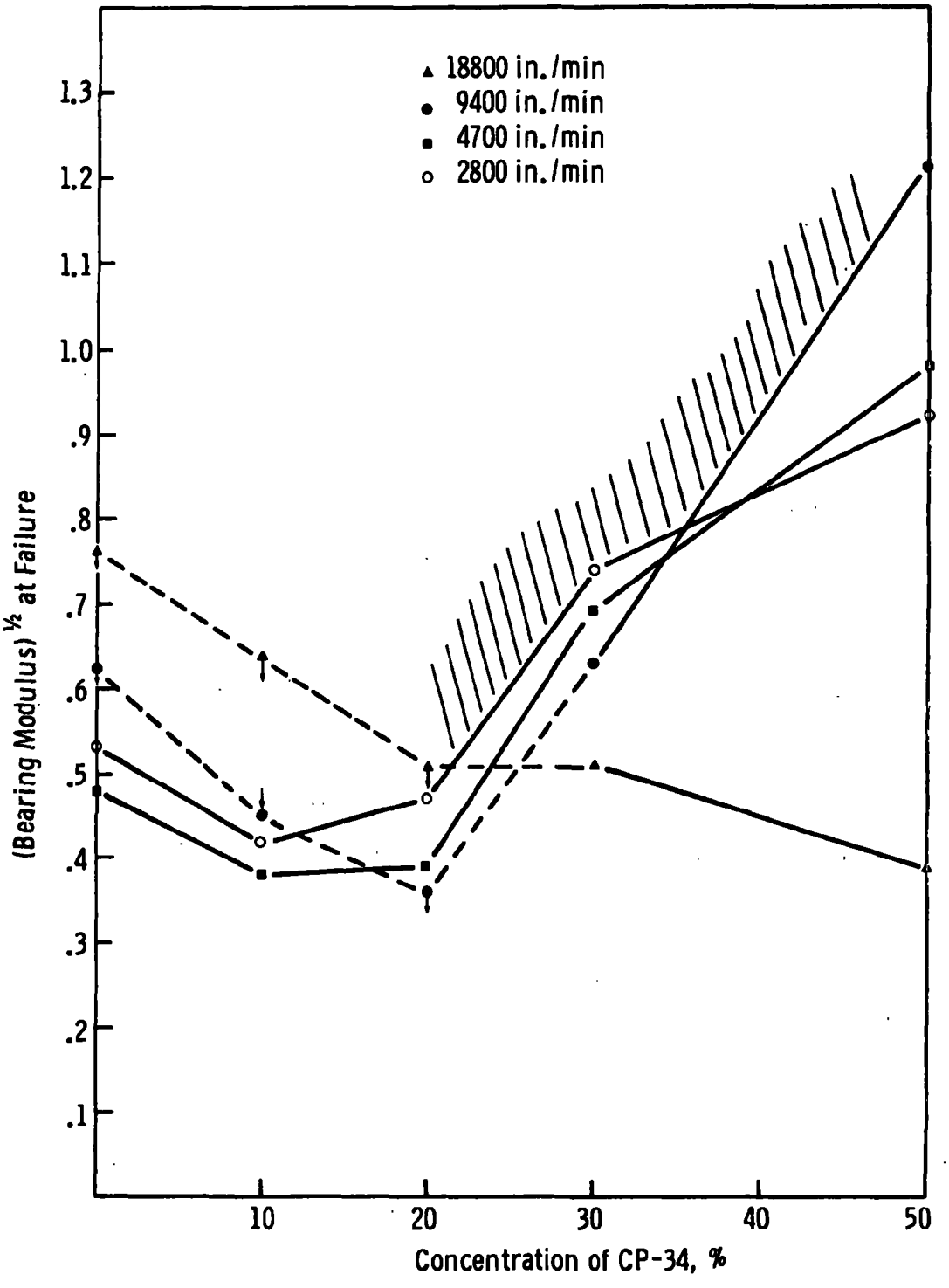

Figure V-21. $\sqrt{M}$ at Failure vs. Concentration of CP-34. 250°F.

attempts were made to run in a set of test specimens in F-50 with a limited amount of success. A maximum average bearing load of 1960 psi at 300 cpm was attained--then speed was changed to 2000 cpm and a maximum of 2270 psi was reached at which time the blocks scored after about 5 minutes run. F-50 temperature at that time was about 150°F. Inspection of the blocks immediately before the 2000 cpm run showed 80-90% of the surface polished. Thus the advisability of further low speed run-in may be indicated. Further attempts with these specimens were unsatisfactory.

F. SUGGESTIONS FOR FUTURE WORK

Future journal lubrication studies on silicones might include:

a. Use of a profilometer to monitor surface finishes (especially during run-ins).

b. Simulation of the connecting rod journals by using pulsed loading or alteration of ring-block geometry in the tester.

Each cycle of the journal bearing causes introduction of a heavy oil film between the bearing surfaces. Preferably the wear tester should simulate this cyclic oil wedge. One approach would be pulsed loading controlled by a solenoid valve. Continuous fresh oil feed to the contact is also possible by curving the leading edge of the block. As now designed, this edge scrapes the oil off the ring. Alternatively, the diameter of the ring could be made slightly smaller relative to the block diameter.

c. Wear studies on reference petroleum lubricants. This would aid the interpretation of Task III. These petroleum oils should have

known bearing performance and the same physical properties as the various test silicone mixtures. In particular, viscosity, bulk modulus, and pressure-viscosity coefficient would be matched as much as possible. Presumably, then, the hydrodynamic flow and lubrication of the paired oils in a journal would be roughly equivalent. If the oil pairs were to give similar wear in the rub-block tester, their boundary lubrication would also be equivalent and their total bearing performance similar. If their wear properties in the screening test were unequal, a comparison would be possible of the boundary lubrication of the silicones vs. the hydrocarbons.

d. Use of a slice of a bearing liner as the block edge in the tester. This would insure correct metallurgy, correct finish, and ease of replacement.

e. Use of a thermocouple in the block close to the contact surface. This will allow recording of the true fluid temperature in the contact (skin temperature plus flash temperature).

f. Studies of the chemical effects of F-50/thiophene blends on the contact surfaces. Dimethyl silicones are known to form varnishes on copper surfaces.[10] These aid boundary lubrication. Surface analysis would show if F-50 forms such films and, if so, whether CP-34 assists or inhibits the varnish formation. There was no visible evidence for such films in the completed wear runs.

---

[10] R. F. Willis, Tribology, 2, 175 (1969).

G. CALCULATION OF PRESSURE AND TORQUE CORRECTIONS

1. Pressure

Plots of torque vs. load give these corrections. This is the point where the curve drops vertically to the abscissa. The correction for pure F-50 from Figure V-7 is -80 p.s.i. This is an instrumentation correction since there is no gas pressure with F-50. When there is pressure in the pot, it opposes the hydraulic system pressure (which is π^{-1} times the average bearing pressure) and must be allowed for. The correction for any CP-34/F-50 mixutre can be found graphically as in Fig. V-7 or calculated from the pot pressure. Both methods were used at 200°F and gave reasonable agreement. The gas pressures at 250°F were calculated from the pressure at 200°F using a nomograph.

A sample calculation to find the correction for 10% CP-34 at 250°F is:

Correction for the vapor pressure at 200°F = Total correction minus the correction for instrumentation = 90-80 or 10 p.s.i.

10 p.s.i. on the bearing is $10/\pi$ p.s.i. piston pressure

= 164.7 mm. @ 200°F

= 407 mm. @ 250°F (nomograph reading)

= 7.86 p.s.i. piston pressure

This is 7.86 x π or 25 p.s.i. gauge pressure.

2. Torque Corrections

These were made directly on the friction base lines on the raw data charts.

H. INTERRELATION OF INSTRUMENT VARIABLES

Observed quantities:

p, hydraulic system pressure, net (psi)

L, torque generated, net (in-lb)

f, rotational frequency (rpm)

System constants:

r, radius of ring (= 0.75 in)

a, loading piston (one) area ($=\pi/4^2=0.1963$ in^2)

A, projected contact area between one block and ring ($=0.1875$ in^2)

Derived parameters:

F, load between specimens (lb)

P, average bearing pressure (psi)

μ, effective coefficient of friction between specimens

ν, sliding speed (in/min)

dE/dt, power dissipated between specimens (hp)

Calibration parameters:

w, calibration weight (lb)

l, lever arm to strain gauge calibration tie point (=3.36 in)

Relationships

$F = 2pa(3/2) = 0.589p$

$P = F/A = 5.33F = 3.14p\ (=\pi p)$

$\mu = (L/r)/(2F) = 1.131\ L/p = 3.55L/P$

$\nu = 2\pi rf = 4.71f$

$dE/dt = (L/r)(2\pi rf)/(12 \times 33000) = (1.54 \times 10^{-5})Lf$

to calibrate $\sim L = lw = 3.36w$

I. NOMENCLATURE (see also Section H).

η, absolute viscosity

η_K, kinematic viscosity

ρ, density

ν, sliding velocity

μ, effective coefficient of friction

P, average bearing pressure

M, bearing modulus

ho, minimum film thickness

(See also Section H)

APPENDIX VI

STEADY-STATE AND TRANSIENT EMISSION MEASUREMENTS FROM AUTOMOTIVE RANKINE-CYCLE BURNER

A. INTRODUCTION

A program was carried out at Thermo Electron to obtain emission data on full-size combustion chamber designs to be used in the 100 shp Rankine-cycle propulsion system being built at Thermo Electron.

Initially, a combustion loop was designed and constructed to test different combustion chamber designs under steady-state combustion conditions. The emission data from a number of combustion chambers which had low emissions were fed into a computer program designed to take steady-state emission data and to calculate the burner performance over a simulated urban driving cycle using calculated system performance data. At the conclusion of these tests, a control system was installed, allowing the combustor to be operated under transient urban driving cycle conditions, and the exhaust was collected in a constant volume sampler. This allowed transient emissions to be both measured and realistically compared to the current Federal Emission Standards, following the exact Federal test procedure.

B. STEADY-STATE MEASUREMENTS

1. Steady-State Combustor Test System

The combustion loop used for taking steady-state emission data is shown in Figure VI-1. Combustion air was supplied to the burner with a variable speed blower connected to a 4-inch diameter orifice line. Various orifice plates were used in this line, allowing accurate measurement of the air flow going into the burner. The fuel nozzle used on this combustion rig was an air-atomizing type. The shop air supply was used to supply atomizing air to the nozzle through two rotameters for measurement of the atomizing air flow rate. Fuel was pumped from a tank through different size rotameters to the fuel nozzle. With this test set-up, accurate measurement of air and fuel going into the combustion chamber could be made.

A secondary air loop capable of pumping air from the boiler exhaust through a 3-inch diameter orifice line was also used in the tests with exhaust gas recirculation. The burner exhausted directly into a water-cooled boiler, thus cooling the combustion products before taking exhaust samples for emission analysis.

The emission equipment used was:

- Beckman Model 109 FID Hydrocarbon Analyzer.
- Beckman Model 315A NDIR CO_2 Analyzer.
- Beckman Model 315AL NDIR CO Analyzer.
- Thermo Electron Chemiluminescent NO_x Analyzer.

A photograph of the emission test bench is shown in Figure VI-2.

2. Steady-State Combustion Data

Various combustion chambers were tested by varying the air-fuel ratio and measuring emissions. The tested burners were all designed for a 100 shp system with a peak burning rate of 1.05×10^6 Btu/hr (two burners operating in parallel are used for the system). The three configurations which are reported here are shown in Figures VI-3 through VI-5. Four different tests were run on the three configurations: A-1 and B-1 were tested with exhaust gas recirculation; chambers B-1 and H-1 were run without recirculation.

Emission data from configuration B-1 without recirculation are shown in Figure VI-6. Also indicated in Figure VI-6 are the pollutant concentrations corresponding to the 1976 Federal Standards with a fuel consumption of 10 miles/gallon; these levels should be used only for qualitative indication, since the emission levels apply to a specific cycle covering a wide range of burning rates. The CO and UHC data

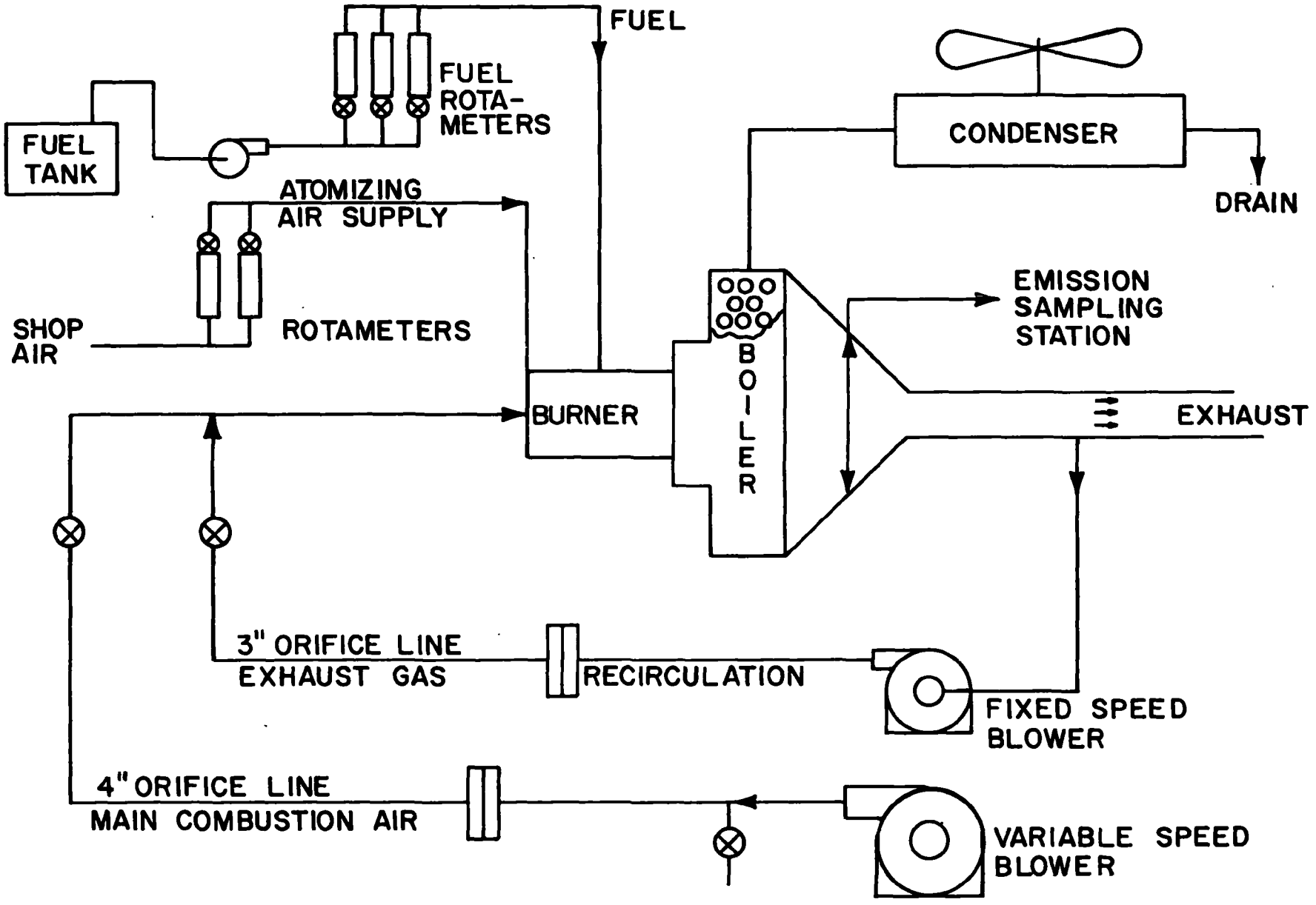

Figure VI-1. Steady-State Combustor Test System.

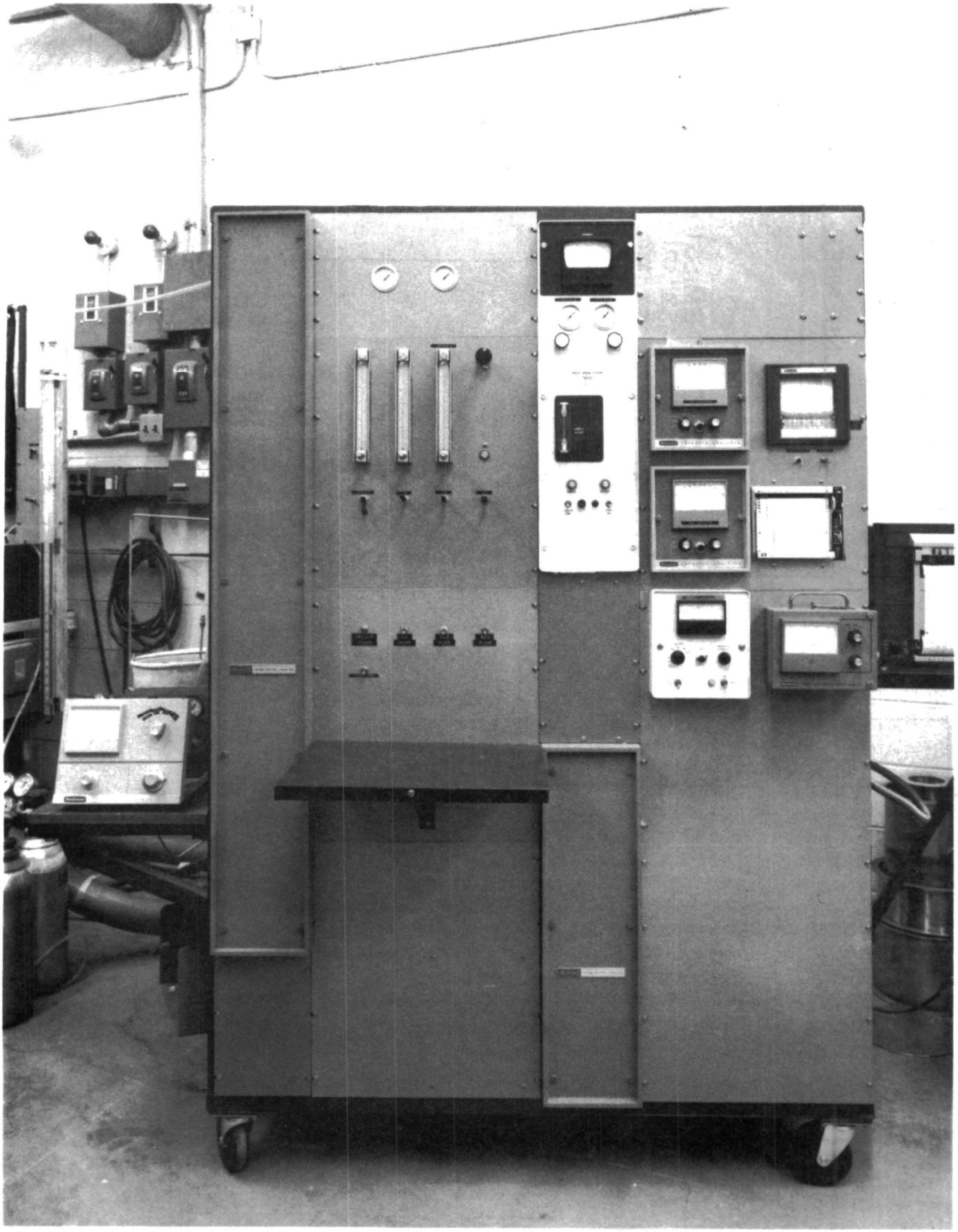

Figure VI-2. Emission Test Stand.

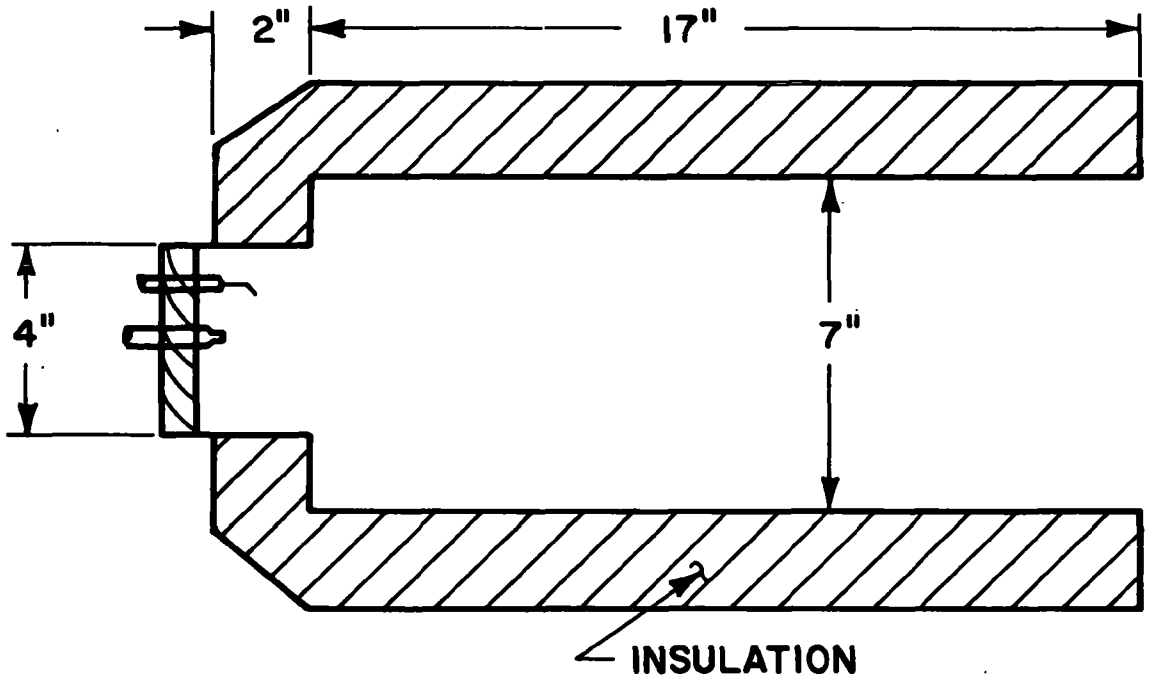

Figure VI-3. Configuration A-1.

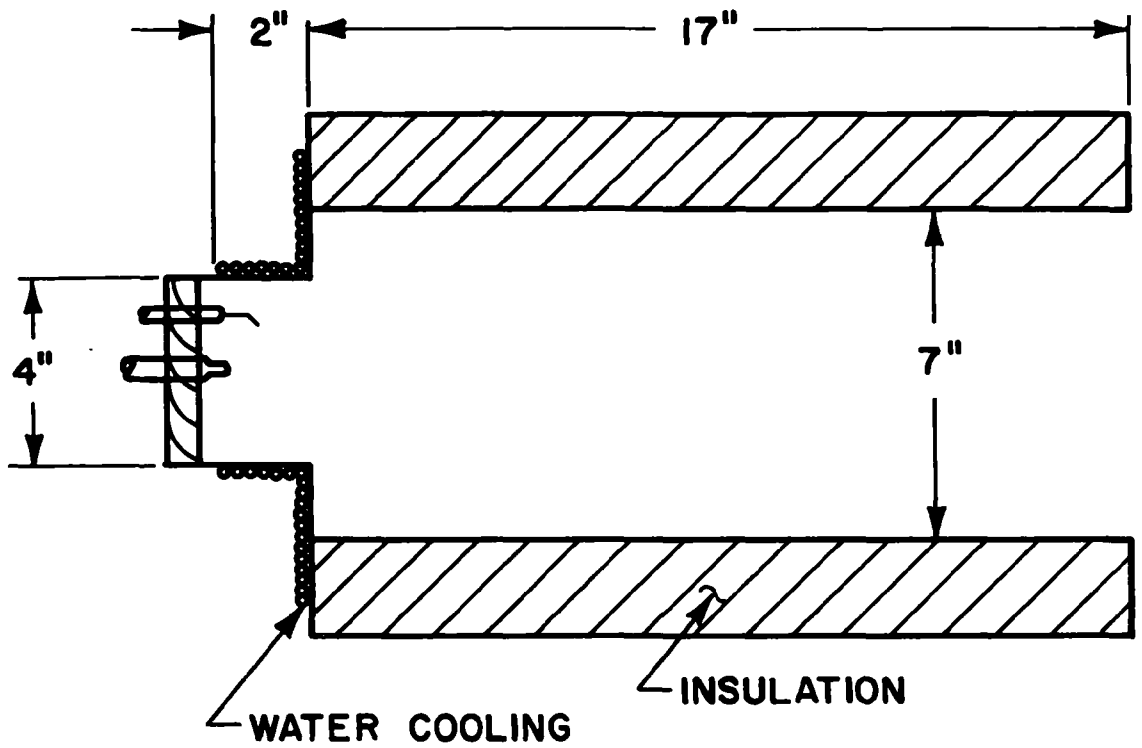

Figure VI-4. Configuration B-1.

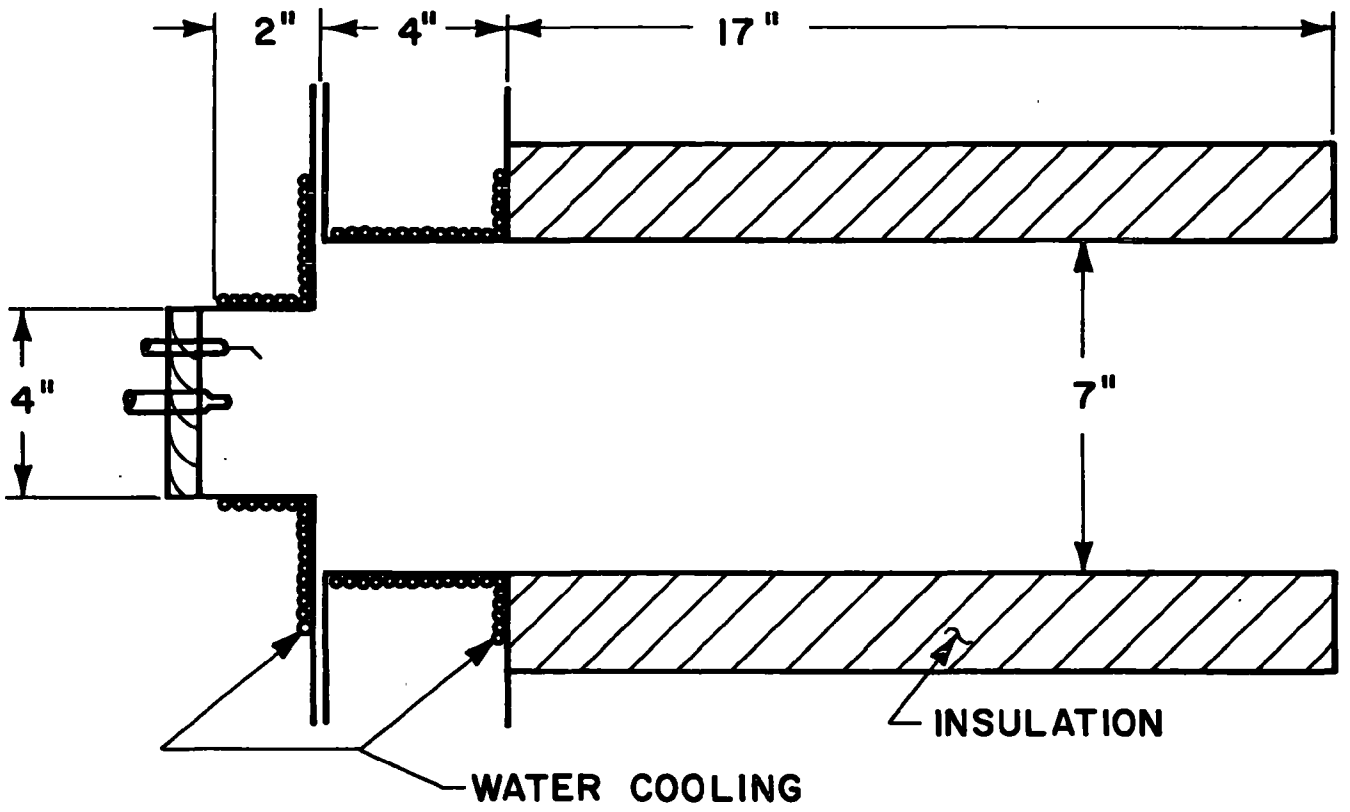

Figure VI-5. Configuration H-1.

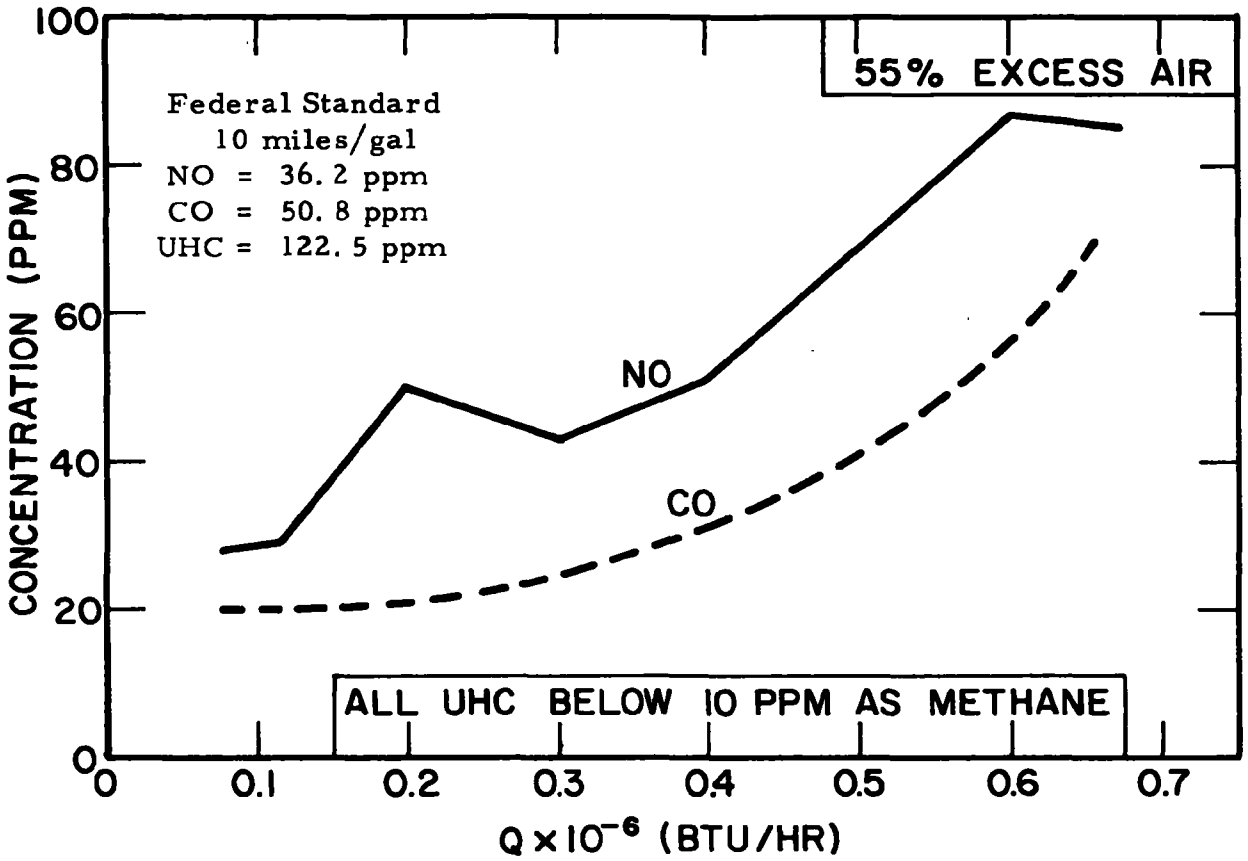

Figure VI-6. Emission Data for Configuration B-1.

are well below the 1976 Federal Standard. The NO is below the standard up to a burning rate of 150,000 Btu/hr; it then goes above the standard. The burner configuration for which the data of Figure VI-6 were obtained is that used in the CVS test discussed in a later section.

Initial testing indicated that a burner having 4% of the wall area cooled (configuration B-1) had a pronounced effect on NO emission relative to the adiabatic chamber (configuration A-1); wall cooling was thus extended to 26% of the wall area in configuration H-1. NO data taken with this configuration are shown in Figure VI-7. The NO data for configuration H-1 was 30% lower at the low firing rates and 12% lower at the higher firing rates. The CO and UHC data are not shown, but the CO was lower for chamber H-1 while the UHC were approximately double the levels obtained with chamber B-1.

Exhaust gas recirculation data using an adiabatic combustor chamber (A-1) are shown in Figures VI-8 through VI-10. The data taken using both recirculation and cooling (B-1) are plotted in Figures VI-11 through VI-13. Exhaust gas recirculation resulted in a significant reduction in NO emissions for both chambers.

The fuel used in all these tests was JP-4.

3. Calculation of Emissions Over Urban Driving Cycle

The urban driving cycle is a schedule of miles/hr versus time (seconds) specified in the Federal Register, November 10, 1970, Appendix A, for the emission testing of vehicles. This was converted to firing rate (Btu/hr) versus time (seconds) using the system and

vehicle performance prediction programs. A computer program was written and the steady-state data (including start-up) were used to predict the emission levels over the urban driving cycle of the various combustion chambers tested. Figures VI-14 and VI-15 show the predicted emission levels. The recirculation runs with and without wall cooling were well within the Federal Standards for all emittants. The chamber run without recirculation but with wall cooling passed the CO and UHC standards, but NO levels were high except at high excess air rates. The data without recirculation are included, since program hardware commitments made early in the program established this chamber as the only one which could be run under transient conditions. The air-fuel control as constructed for the transient test was not adaptable to the exhaust gas recirculation running mode. Subsequent performance programs have indicated the urban driving cycle results in a gas mileage of 11 rather than 12.1 mpg, so the emission levels in Figures VI-14 and VI-15 are 10% low.

C. TRANSIENT EMISSION MEASUREMENTS OVER URBAN DRIVING CYCLE USING FEDERAL PROCEDURE

A CVS test system was built so that a burner could be run over the urban driving cycle exactly as specified in the Federal Register (see Figure VI-16). The firing rate schedule calculated from the urban driving cycle was pre-plotted on a conductive chart at 1 second intervals. This chart was installed in a data tracking device which electrostatically followed the curve. The output from the Data Track was an electrical signal which in turn was converted to a pneumatic pressure used to operate the air-fuel control over the firing rate schedule. All of the burner exhaust was piped into a standard

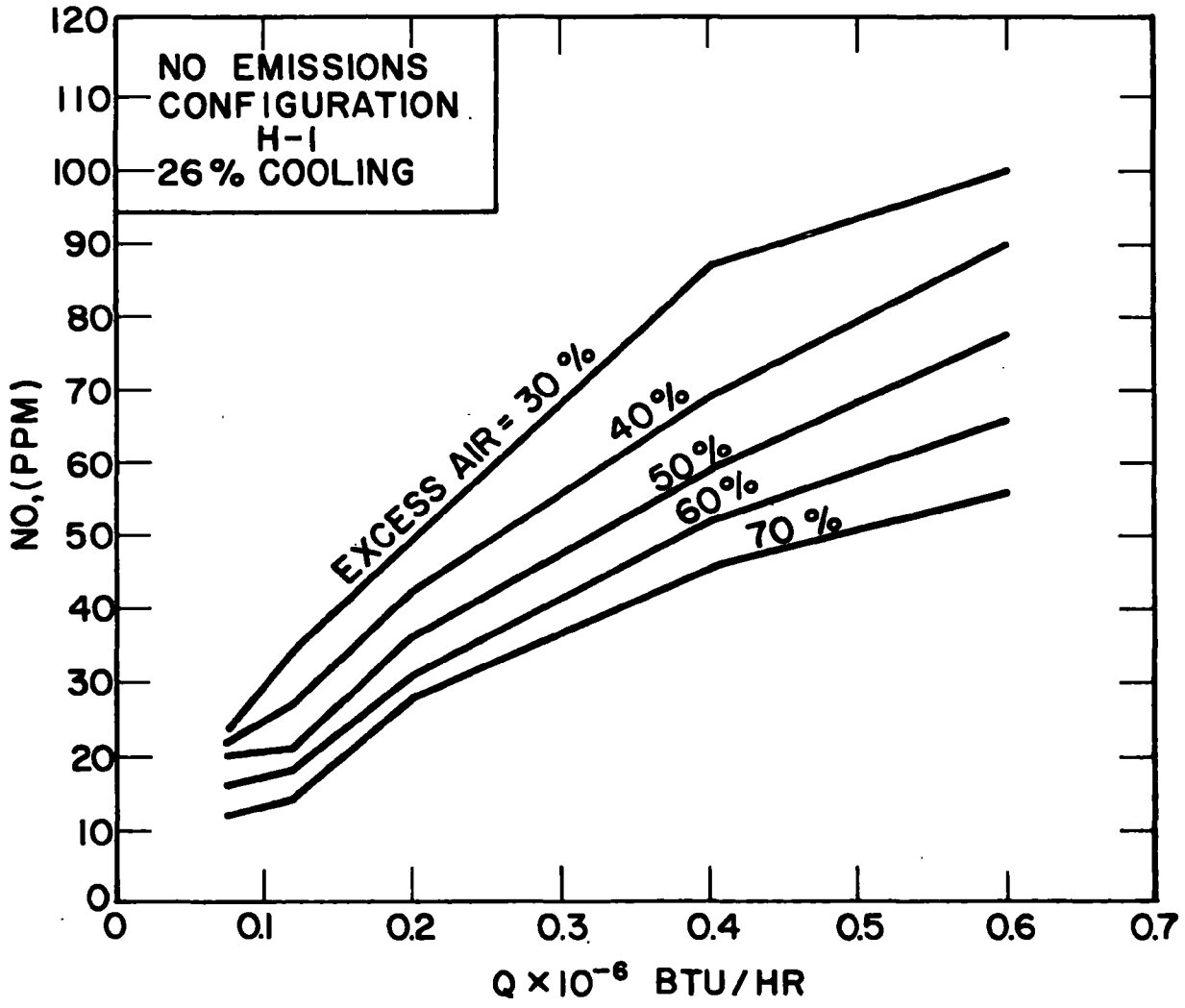

Figure VI-7. NO Emissions for Configuration H-1.

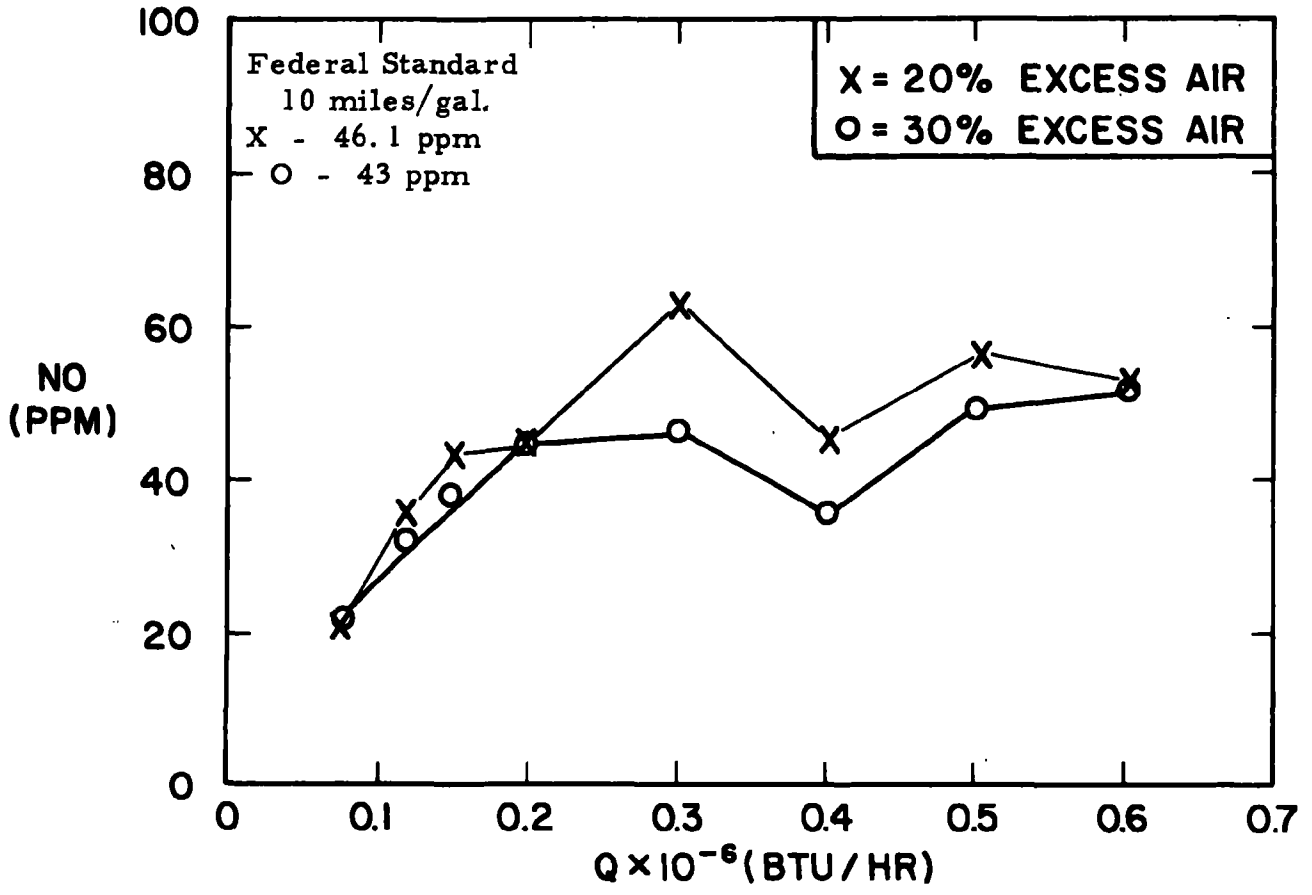

Figure VI-8. Adiabatic Combustion Chamber, 20% EGR.

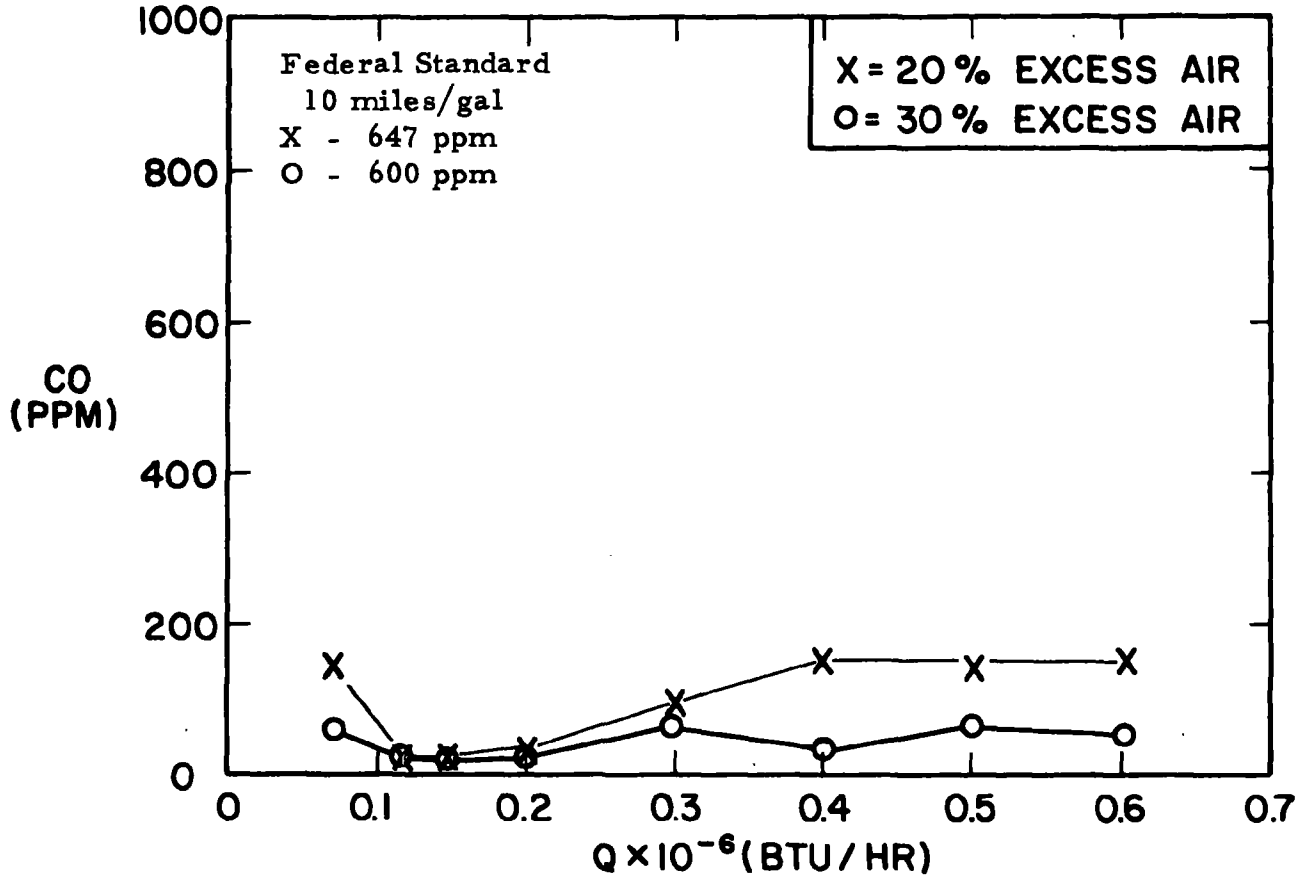

Figure VI-9. Adiabatic Combustion Chamber, 20% EGR.

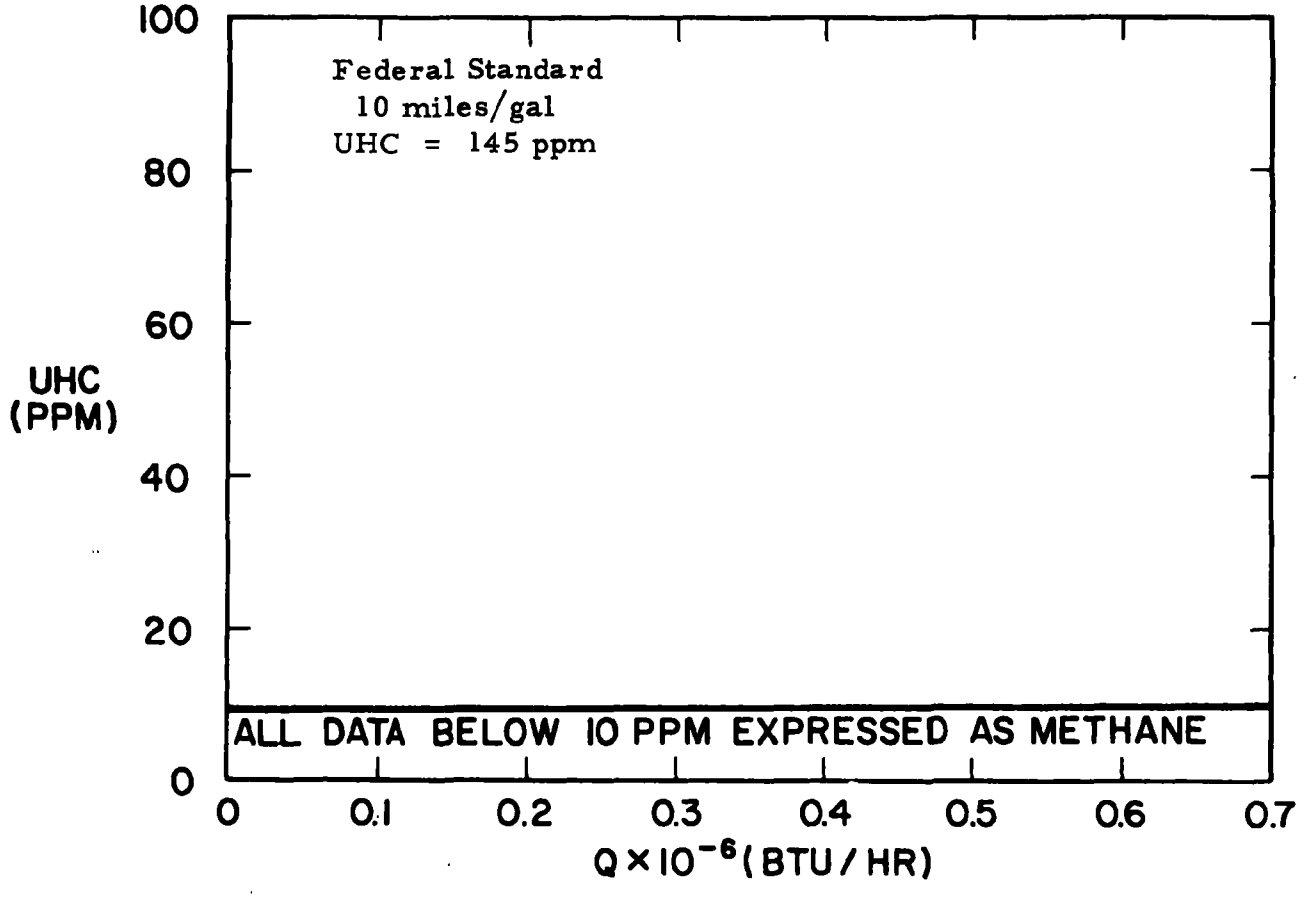

Figure VI-10. Adiabatic Combustion Chamber, 20% EGR.

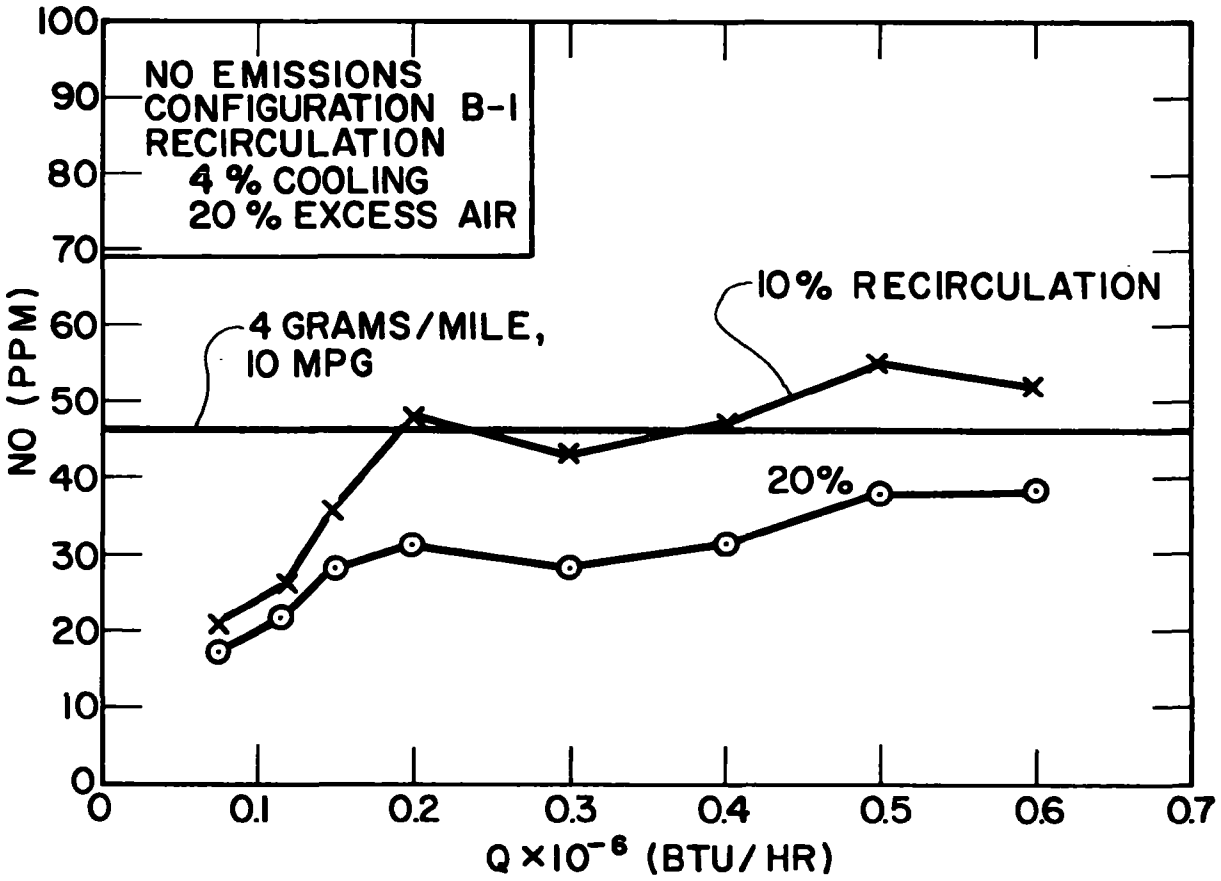

Figure VI-11. NO Emissions for Configuration B-1.

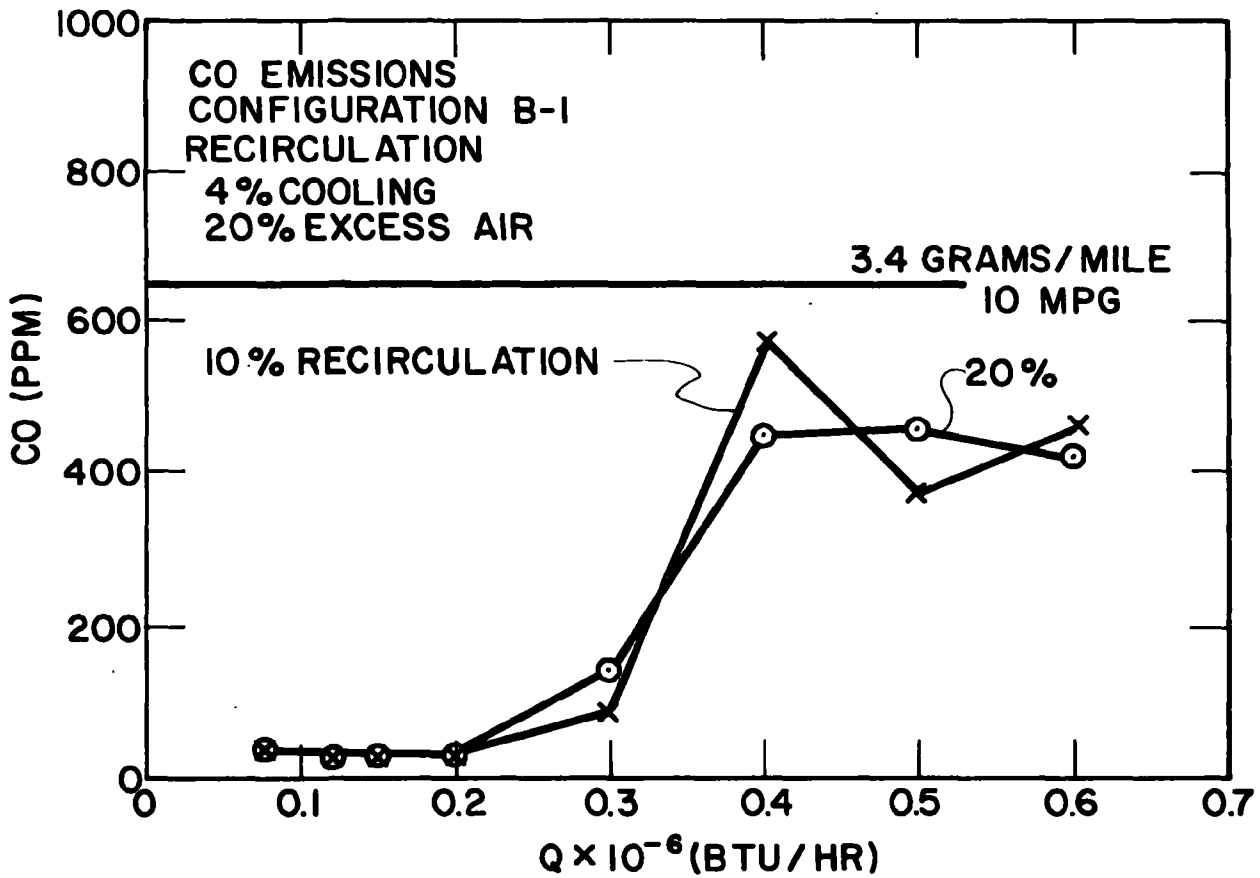

Figure VI-12. CO Emissions, Configuration B-1.

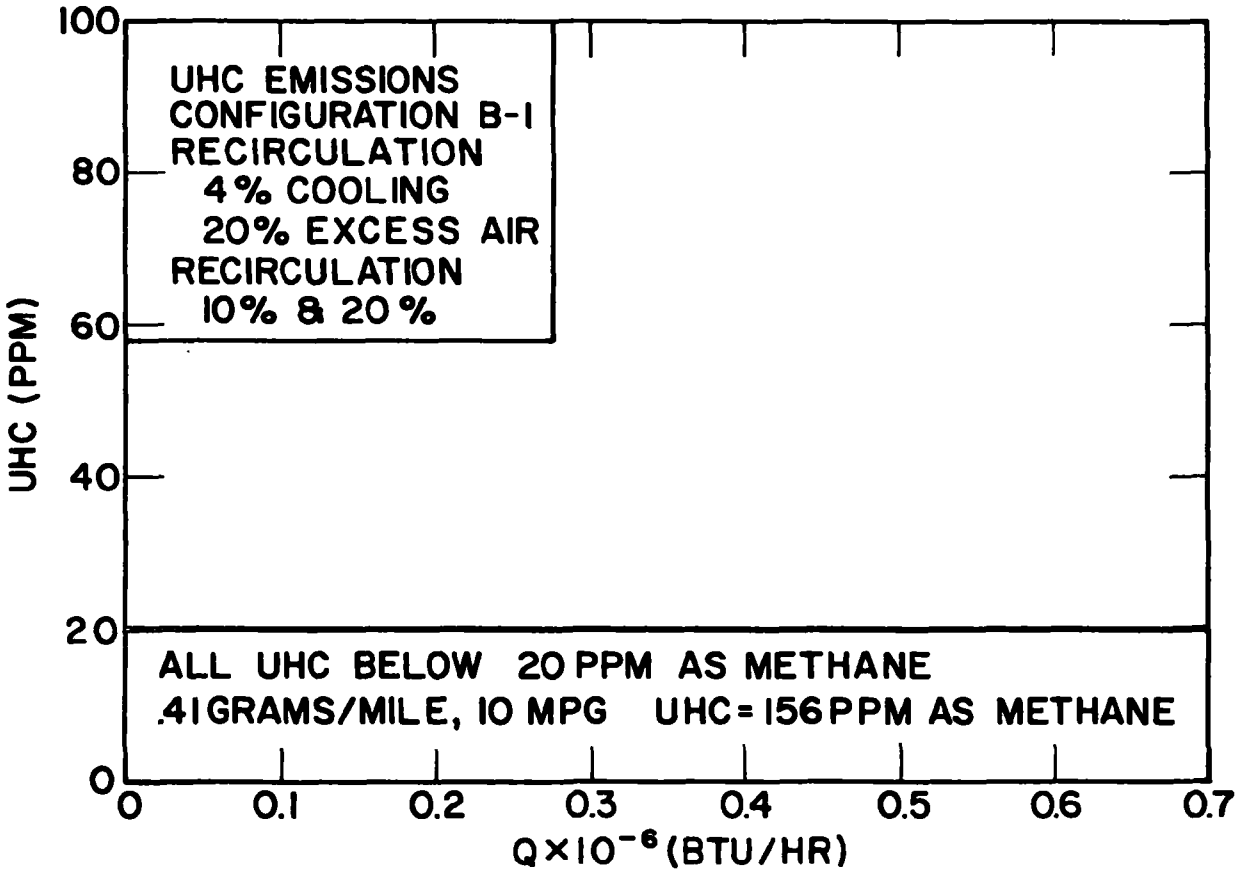

Figure VI-13. UHC Emissions, Configuration B-1.

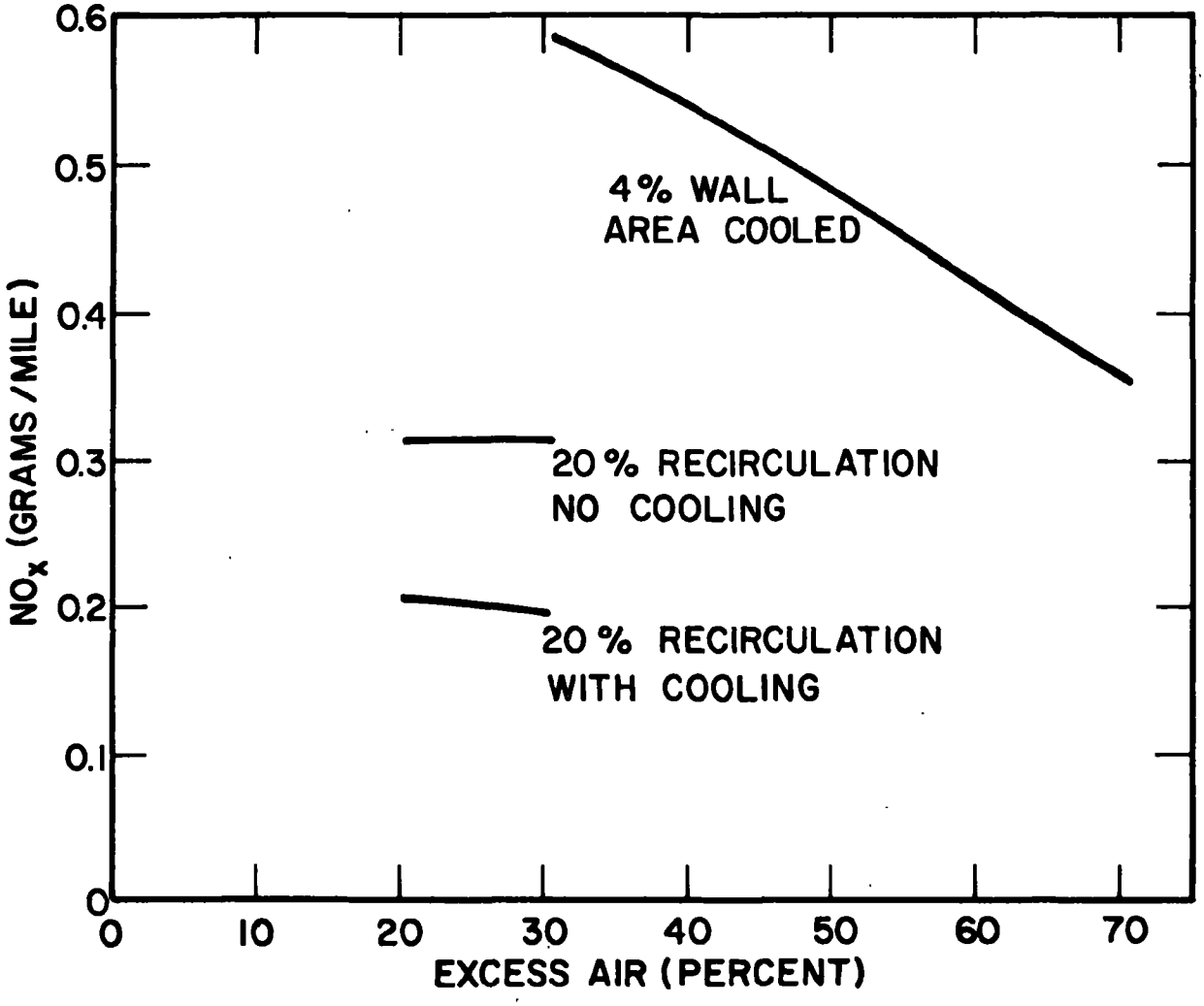

Figure VI-14. Urban Driving Cycle Generated With a Computer Program Using Steady-State Combustion Data (12.1 mpg).

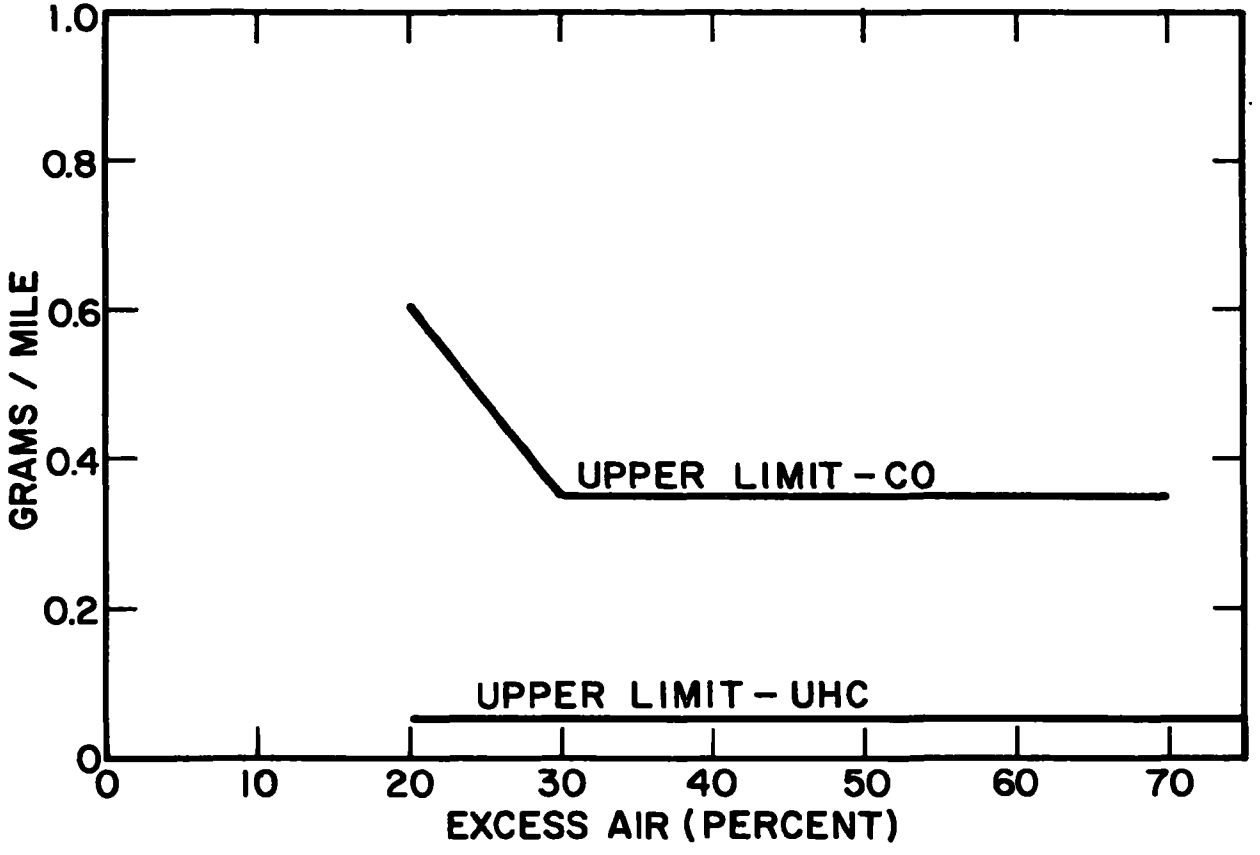

Figure VI-15. Urban Driving Cycle Generated with a Computer Program Using Steady-State Combustion Data (12.1 mpg).

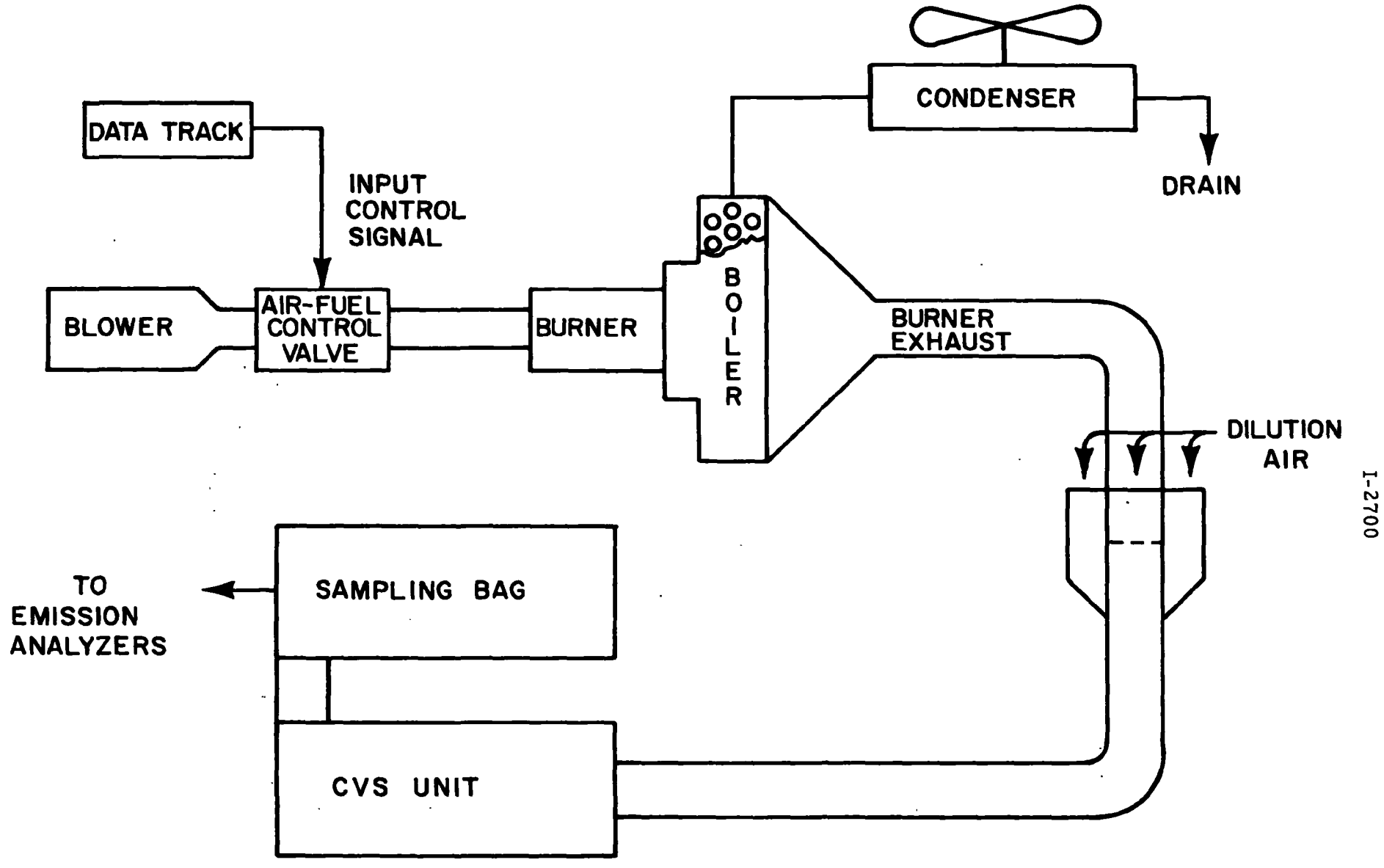

Figure VI-16. Transient Burner Test System.

300 CFM Scott Research Laboratory Constant Volume Sampler. A photograph of the test facility can be seen in Figure VI-17. The fuel/air control operated similar to that proposed for use in the system, with the organic orifice ΔP simulated by the pneumatic pressure.

The CVS test was run with burner configuration B-1 without exhaust gas recirculation. The test procedure used was that outlined in the Federal Register, July 2, 1971, Part I. It included collection in three dilute exhaust bags and two background air bags for emission measurements. In order to simulate a start, the heat required to produce enough boiler pressure to run the expander was calculated and the burner was run long enough to produce this heat before starting the transient portion of the CVS cycle.

The emission samples collected were as follows:

1. Minimum 12 hour cold soak
   - Bag 1. Cold start plus first 505 seconds of cycle.
   - Bag 2. Remainder of cycle plus shut down plus 5 seconds
2. 10 Minute Wait
   - Bag 3. Hot Start plus first 505 seconds of cycle.

The results of two such tests are shown in Table VI-1. The tests indicated that all emission levels were significantly below the 1976 Federal Standards, the ratio of Federal Standards/measured emission rate being 1.40 for NO_x, 15.4 for CO, and 2.87 for UHC (Test 2). It is expected that use of exhaust gas recirculation will significantly reduce the NO_x emission rate.

One problem encountered in running the combustion chambers was momentary flame-out following a long idle. For a long idle period, backheating of the nozzle occurred, resulting in vaporization of the fuel at the nozzle tip. When rapid excursion to a high power level occurred following a long idle, the air flow would respond immediately; the fuel flow would momentarily lag while it overcame the vapor blockage, resulting at times in a flame-out. This did not occur during every test, and the two tests in Table VI-1 compare the emission levels with and without a flame-out.

Continuous recordings were also taken during CVS runs, and transient emissions were observed. In general, the fuel-air control maintained the proper fuel/air mixture during transients. There were no emission peaks, and the NO simply rose toward its steady-state value with no sharp transients. During the cycle, the NO never reached its steady-state value at the higher firing rates, since the high power transients for the Federal emission driving cycle are of short duration and the burner wall never reaches temperatures corresponding to steady-state operation at the equivalent firing rates. Effective cooling of the combustion gases by the burner walls thus occurs during these short, high power transients with a resulting reduction in the NO emission levels relative to the steady-state measurements. Comparison of the transient test with the calculated result based on steady state measurements (Figure VI-14) indicated the importance of this effect, the transient value being 0.29 gms/mile compared to 0.45 gms/mile for the emission level calculated from steady-state measurements. Hydrocarbons and CO peaks occurred only at start-up and shutdown. The range encountered for these peaks is illustrated in Table VI-2.

Figure VI-17. Thermo Electron Combustion Facility.

TABLE VI-1

TRANSIENT EMISSION TEST
RESULTS

CONFIGURATION B-1

11 MPG**

Emissions (grams/mile)	Test 1	Test 2	Federal 1976 Standard
NO_x	0.297	0.29	0.4
CO	0.341*	0.22	3.4
UHC	0.594*	0.14	0.41

* Momentary flameout at idle.

** Actual gas mileage used for tests was 12.1 mpg. The latest performance calculation predicts 11 mpg for the CVS cycle and the emission levels were increased by 10% to reflect the change in fuel economy.

TABLE VI-2

RANGE OF TRANSIENT PEAKS OBTAINED ON START-UP AND SHUTDOWN DURING TRANSIENT EMISSION TESTING

Condition	UHC	CO
Start-up	200 - 350 ppm	70 - 80 ppm
Shutdown	800 - 1500 ppm	~350 ppm

The accuracy of the peaks is limited by the instrument time response since a long path NDIR was used to obtain a 0 - 100 ppm range for the CVS tests; this slow response thus gave "average peaks" as opposed to instantaneous peaks.

APPENDIX VII

DANA TRANSMISSION

The Dana Corporation of Toledo, Ohio, developed a transmission design for the Thermo Electron Rankine-cycle powerplant. It is a two-speed automatic design that uses a hydraulically-controlled slip clutch to permit the expander to idle at zero vehicle speed. The clutch also slips at low vehicle speeds when the driveshaft speed is less than that of the expander idle speed. Above a vehicle speed of 8.3 mph, where the driveshaft speed equals the expander speed, the clutch locks up and operates as a direct coupling except during shifting operation. This procedure gives a high efficiency for the transmission and takes advantage of the low-speed, high-torque characteristics of the Rankine-cycle expander.

The overall layout of the transmission is illustrated in Figure VII-1 and the control schematic in Figure VII-2. Due to the many system tradeoffs and the possibility of wishing to make gear ratio changes in the future, the transmission design was developed so that gear ratio changes could be easily made without major modifications to the transmission. A countershaft transmission, rather than an earlier planetary concept, was selected primarily for this reason. As illustrated in the drawing, the clutches are at the front end of the transmission. One clutch is for direct drive with a 1:1 speed ratio and is used for starting and low vehicle speed operation. The other clutch has a 0.584:1 overdrive ratio and is used for cruising at relatively high vehicle speed. The gear ratios were selected so that the standard Ford rear axle with 2.79:1 ratio and the standard propeller shaft could be used. This rear axle with 7.75 x 14 tires (778 rev per mile) will give 95 mph vehicle speed at 2000 rpm expander speed.

The design uses a two-way sliding spline collar for forward, neutral, and reverse selection. This collar is shifted only when the vehicle is stationary. A park mode is also provided.

Operation of the transmission is as follows:

1. Standard Start - Forward

With engine running at 300 rpm idle speed, the operator manually selects forward speed, which engages the splined clutch collar with the 1:1 ratio and moves the hydraulic selector valve from neutral to forward position. The operator then depresses the accelerator pedal, transferring control of the expander inlet valve from the governor to the operator and increasing intake ratio (IR) and torque potential beyond that required to idle the engine at 300 rpm. Simultaneously the IR control linkage operates the clutch pressure regulator in the Dana transmission causing hydraulic pressure, now valved to the direct drive clutch at the front of the transmission, to rise in concert with the IR ratio and engine torque. The clutch is now picking up the drive and the car begins to move forward while the clutch is slipping. At the minimum governed speed, the car will be traveling 8.3 mph with the clutch fully engaged. IR and clutch torque capacity (through hydraulic pressure control) will always be related by the IR control linkage throughout the whole spectrum of engine operation, thus making smooth shifts inherent and reducing pump horsepower at higher speeds where the expander torque is lower. The pump pressure will vary from 170 psi at 530 lbs. ft. torque to 91 psi at 270 lbs. ft. torque.

An input governor on the Dana transmission will perform two functions (see the control schematic of Figure VII-2). One is to close a normally open electrical circuit if the expander speed should drop

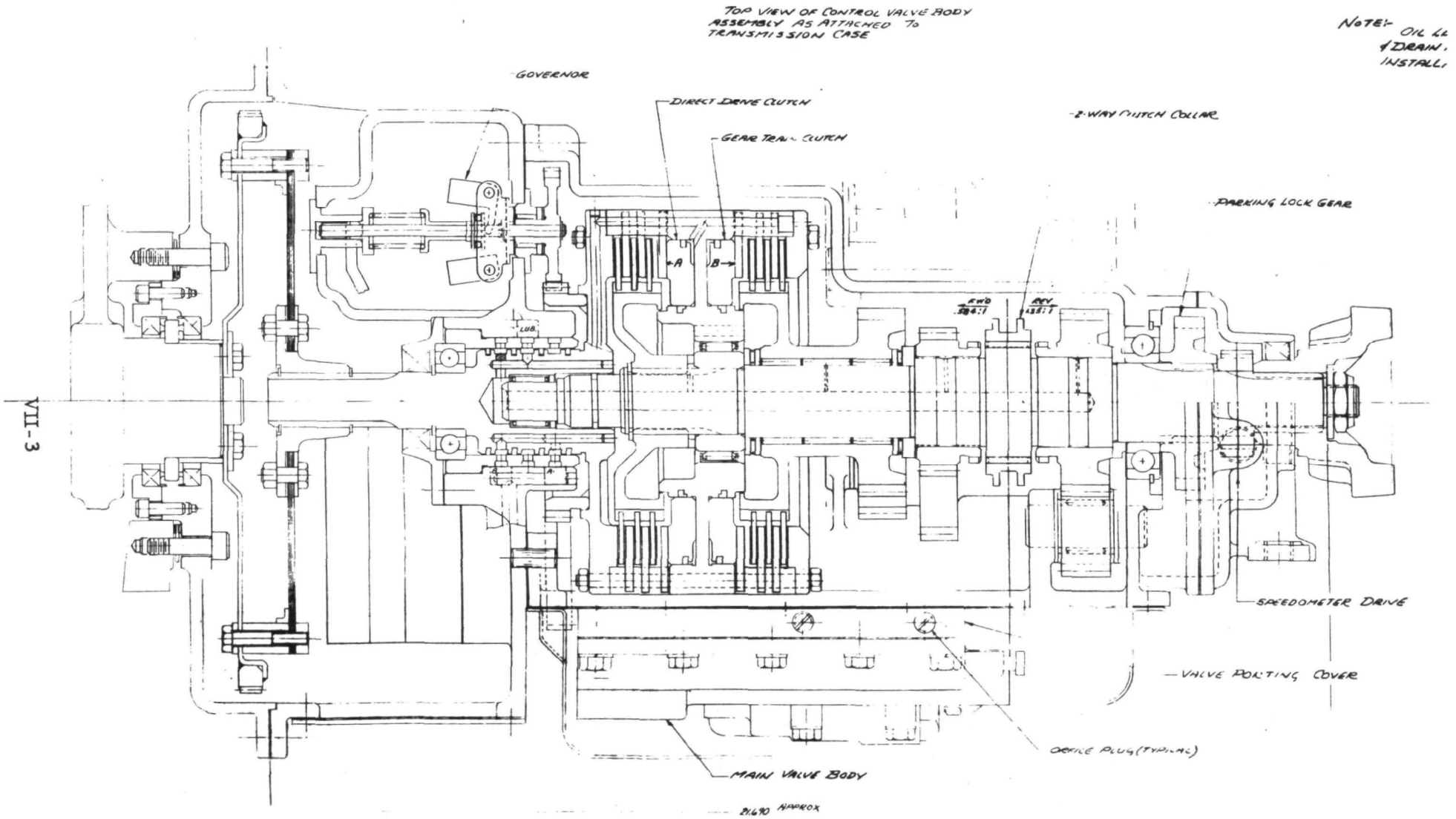

Figure VII-1. Layout of Dana Transmission.

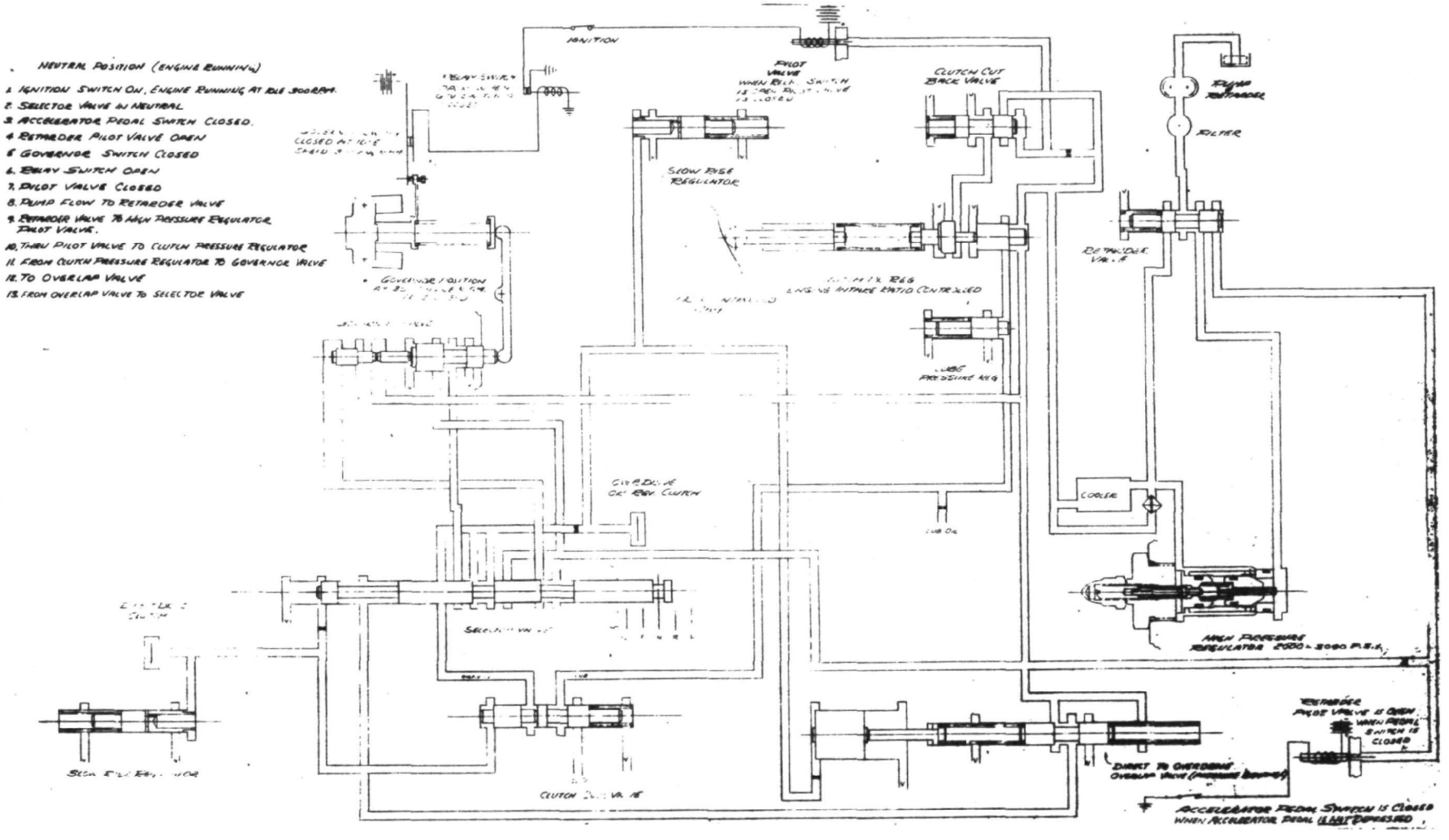

Figure VII-2. Control System for Dana Transmission.

below the idle speed of 300 rpm; this opens a solenoid-controlled vent which causes clutch pressure to drop slightly below the full starting torque capacity. This function prevents stalling of the expander when the operator floorboards the accelerator pedal. Function number two is to control shift from the 1:1 starting ratio to the .584:1 cruising ratio at appropriate combinations of expander speed and intake ratio. The upshift and downshift lines are illustrated in Figure VII-3.

The shifting control operates as follows: The transmission shifting control uses a spool valve to control application of hydraulic pressure to the appropriate clutches. The shift spool valve position is controlled by application of hydraulic forces controlled by the expander speed through the transmission governor and by the position of the intake ratio control on the expander. The shift control spool valve is forced in the direction of the 0.584:1 clutch port by the governor-generated pressure. An opposing force on the valve is provided by the IR generated pressure. Under wide-open-throttle acceleration (maximum IR), the 1:1 to 0.584:1 shift does not occur until the expander speed reaches 1800 rpm; the shifting operation then lowers the expander speed to 1100 rpm. Under part-throttle accelerations, this shift occurs at lower expander speeds, depending on the IR setting, down to a minimum expander speed of 1200 rpm; shifting at 1200 rpm lowers the expander speed to 700 rpm.

The 0.584:1 to 1:1 shift occurs when the system operating conditions cross the lower speed shift line. Thus, if the expander speed drops below 600 rpm at IR's below 0.10, this shift occurs, raising the expander speed to 1060 rpm. Depressing the accelerator pedal at expander speeds from 600 to 800 rpm can result in this shift.

Shifting at 800 rpm would raise the expander speed to 1370 rpm. Above 800 rpm and in the 0.584:1 ratio, complete depression of the accelerator pedal does not result in shifting.

2. Starting - Reverse

Same as forward except the manual selector lever is moved to the reverse position, engaging the two-way splined collar with the reverse gear while moving the selector valve to the reverse position where it will direct hydraulic pressure to the drive clutch (1:1 ratio) rather than to the gear train clutch.

3. Retarding Feature

For downhill retardation of the vehicle, the hydraulic pump in the transmission can be used with the absorbed power rejected through cooling the transmission fluid. The control system and hydraulic pump have been designed for this function. For retardation, an electrical circuit is employed to actuate a pilot valve which in turn operates the retarder valve, channeling the pump output to the high pressure regulator. This makes the pump work against this pressure as a retarder.

Retardation occurs when the accelerator pedal is fully released, closing a switch that completes the electrical circuit to cause the pilot valve that is normally closed to open. This, in turn, actuates the retarder valve.

The Dana transmission offers the following advantages relative to a conventional torque converter-three speed transmission.

- It has a higher efficiency at speeds above 8.9 mph, where the transmission locks and provides direct drive from the expander

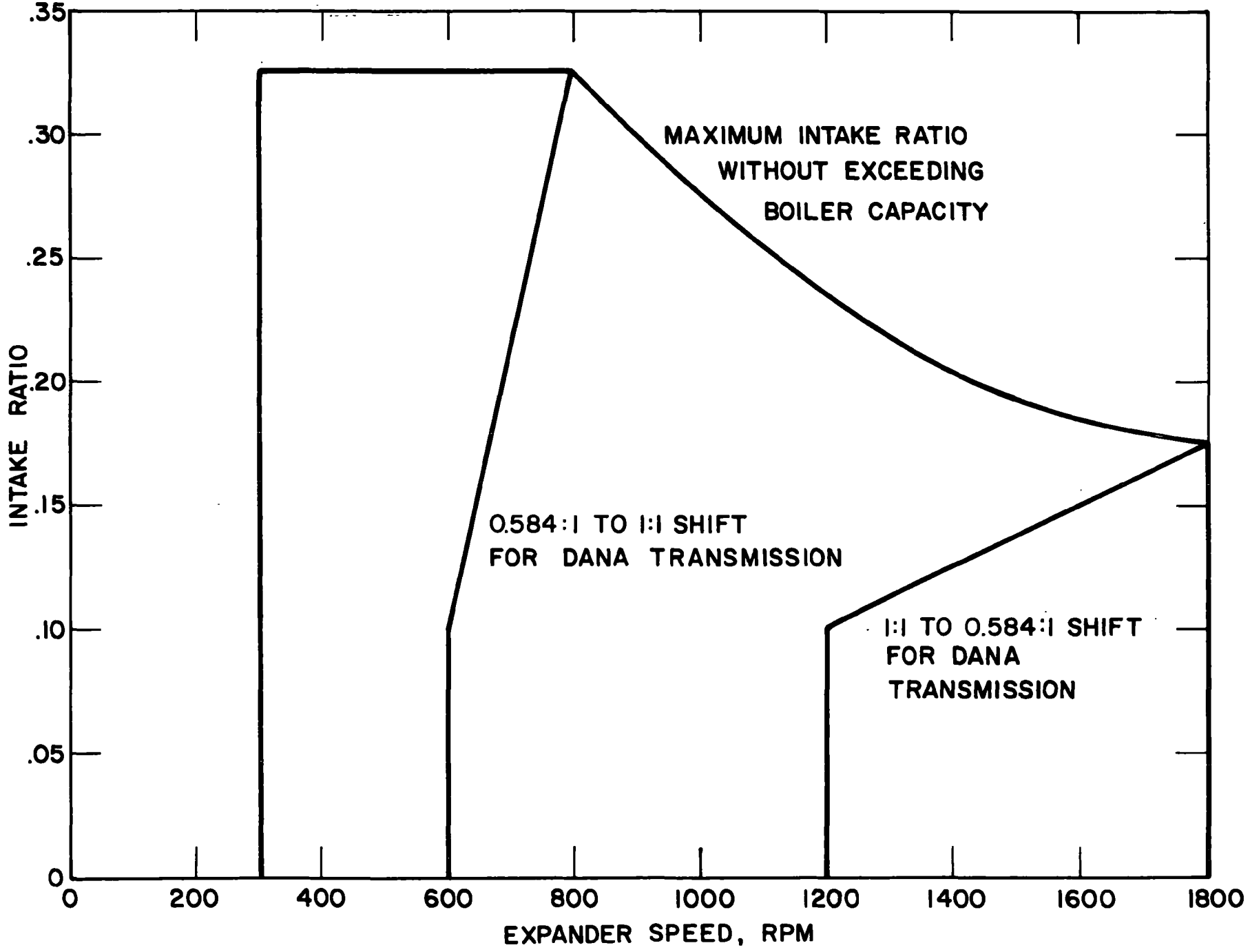
.35
.30
.25
.20
.15
.10
.05
0
INTAKE RATIO
MAXIMUM INTAKE RATIO
WITHOUT EXCEEDING
BOILER CAPACITY
0.584:1 TO 1:1 SHIFT
FOR DANA TRANSMISSION
1:1 TO 0.584:1 SHIFT
FOR DANA
TRANSMISSION
0
200
400
600
800
1000
1200
1400
1600
1800
EXPANDER SPEED, RPM

Figure VII-3.

to the propeller shaft. The only losses are gearing losses (when in the 0.584:1 ratio) and the hydraulic pump power required for operation of the transmission. This power varies from 0.1 hp at low torque to 0.95 hp at high torque conditions. Below vehicle speeds of 8.9 mph, the clutch slips and the transmission efficiency is correspondingly less.

The transmission is simpler and should be less expensive.

Retardation is easily incorporated in the transmission for downhill driving by using a larger hydraulic pump and cooling the transmission hydraulic fluid. The retardation characteristics can be optimized to provide the best vehicle drivability.

The Dana transmission would require considerable development; as a result, the decision was made to use a conventional three-speed transmission with torque converter coupling, as described in Chapter 5.

APPENDIX VIII

DEVELOPMENT SCHEDULE
AND
TASK BREAKDOWN

A. INTRODUCTION

A detailed program plan has been developed at Thermo Electron Corporation for the development of preprototype and prototype cars based on Thermo Electron's Rankine-cycle system. In preparing this plan, the engineers responsible for each component and for the overall system prepared detailed task breakdowns, manpowe r requirements, equipment and material requirements, and time requirements for the accomplishment of each task. These inputs were then integrated into an overall program plan which is broken into 174 separate sub-tasks. The preparation of the program plan has relied heavily on prior experience at Thermo Electron in development of the 3 kwe engine-generator prototypes. The plan is realistic and represents the tightest schedule that is practical for development of well-performing preprototype and prototype cars. In those areas with the greatest technical uncertainty and with the greatest impact on the system performance if design goals are not reached, such as the expander intake valving, concurrent development of both a primary and a secondary (or backup) approach is recommended. It is also expected that maximum utilization of the separate component technology programs sponsored by EPA (such as the condenser fin development) will be made.

B. PROGRAM PLAN

Table VIII-1 identifies the code used in the program plan of Figure VIII-1 and gives the description for each of the 174 elements and tasks into which the detailed program plan is divided.

1. Development Approach

The development approach is similar to that outlined to Thermo Electron by the EPA project office, with the modifications outlined below. The plan has been extended to include construction and testing of complete preprototype and prototype cars. In the component development phase, component designs to be tested would be suitable for integration into the selected vehicle.

Following testing of the separate components, the tested components from the component development phase would be integrated into a breadboard test of the complete engine as part of the preprototype development phase. This procedure provides the earliest possible test of the complete system. Since all of the major components would already be tested, the problems accompanying integration would be resolved in the breadboard testing. In parallel with the breadboard test, a vehicle chassis would be modified for the system. At the conclusion of the breadboard test, the components would be removed from the breadboard and installed in the vehicle; this step would be followed by chassis dynamometer testing and road testing of the preprototype car. Information from testing of the preprototype car would be used in the final installation of the prototype car so that any desirable modifications could be made during system installation.

Design of the prototype car would be initiated at the conclusion of the major component testing and would proceed in parallel with the breadboard testing of the preprototype system. This would not be a major redesign, but would include desirable modifications based on the component and breadboard testing. The prototype design would

also be closer to a production prototype, since the preprototype would be designed for greater flexibility in disassembly and making changes during the component testing. The complete prototype system would be installed in the breadboard test loop for confirmation testing and the tested system removed from the breadboard and installed in the vehicle chassis. Chassis dynamometer testing would again be carried out, followed by road testing and delivery to EPA. Additional prototype cars would be fabricated as required by EPA.

In the component preprototype development phase, two complete systems will be fabricated; one will be installed in the preprototype car. In the prototype development phase, three complete systems will be fabricated; one will be installed in the prototype car, one is for continuous breadboard testing, and one is for backup.

Key dates in the program are summarized in Figure VIII-1 as follows:

Design of Preprototype System Begins	November 1, 1971
Testing of All Major Components Begins	Dec. 1970-July 1972
Preprototype Engine Testing Begins	November 1972
Design of Prototype System Begins	November 1972
Decision to Install Preprototype System in Chassis	January 1973
Prototype Engine Testing Begins	July 1973
Testing of Preprototype Car Begins	July 1973
Testing of Prototype Car Begins	December 1973

2. Detailed Plan

The detailed plan is described in Figure VIII-1 and Table

VIII-1. The plan covers all components required for a system operating in a car.

TABLE VIII-1

TASK CODE USED IN DETAILED PROGRAM PLAN, FIGURE VIII-1

Task Description	Task Code
General	G
Single Cylinder Expander	S
Single Cylinder Valve (Bosch)	SV
Single Cylinder Test	ST
4 Cylinder Expander	E
4 Cylinder Expander Valve (Bosch)	EV
Breadboard Test	ET, BB
Regenerator	R, RT
Boiler and Test Loop	B, BT
Breadboard Loop	BB
Shaft Seal	SS
Feedpump	FP
System Performance Prediction	SP
Combustion System	CS
Controls	CN
Condenser and Fan	CF
Motor and Accessory Drives	M
Automotive Accessories	AX
Transmission and Driveline	TR
Vehicle Integration	V
Road Test Instrumentation	I
Chassis Dynamo Test Stand	CD
Preprototype Car	PC
Prototype Car	C, PC
Manufacturing Cost Estimate	CE
Boost Pump, Jet Pump, Reservoir	BP

TABLE VIII-1 (continued)

TASK CODE USED IN DETAILED PROGRAM PLAN, FIGURE VIII-1

Task Description	Task Code
General	
Project approval and goals	G1
Develop functional specs and ground rules	G3
Refinement of thermodynamic and heat transfer data and correlations	G4
4-Cylinder Expander	
Modifications and layout	E1
Detailed drawings	E2
Detailed drawings - continued	E3
Procure patterns, sample castings and revisions	E4
Machine in-house (2 sets)	E5
Purchase all other parts	E6
Assemble 2 units	E7
Define test program and requirements	ET1
Test on expander loop and debug	E8
Single-Cylinder Expander	
Preliminary engineering	S1
Design and layout drawings	S2
Detailed drawings	S3
Detailed drawings - continued	S4
Procure castings, patterns, etc.	S5

TABLE VIII-1 (continued)

TASK CODE USED IN DETAILED PROGRAM PLAN, FIGURE VIII-1

Task Description	Task Code
Single-Cylinder Expander	
Machine in-house	S6
Purchase all other parts	S7
Assemble one expander with primary valve mechanism	S8
Secondary or backup valving study and drawings	S9
Define test program and facility requirements	ST1
Test on expander loop and debug	ST5
Procure machine and assemble secondary valve mechanism	S10
Test on expander and evaluate secondary valve mechanism	S11
Performance improvement and life test	ST6
Performance improvement and life test - cont.	ST7
Expander Test Loop	
Design and select test unit components	ST2
Fabricate and procure system components	ST3
Test stand and loop fabrication	ST4
Regenerator	
Modify design and run performance program	R1
Detailed design and drawings	R3
Procure parts	R5
Fabricate and assemble 2 units	R6
Define test requirements	RT1

TABLE VIII-1 (continued)

TASK CODE USED IN DETAILED PROGRAM PLAN, FIGURE VIII-1

Task Description	Task Code
Boiler	
Modify design, transient and performance analysis	B2
Detailed burner-boiler unit design and drawings	B3
Procure parts	B5
Fabricate and assemble 2 units	B6
Test on boiler loop	BT4
Test on boiler loop - continued	BT6
Boiler Test Loop	
Define requirements and facility design	BT1
Procure parts and components	BT2
Fabricate facility	BT3
Breadboard Test Loop	
Design basic loop	BB1
Finalize loop design	BB2
Specify and purchase equipment	BB3
Modify major component designs for loop	BB4
Select, specify and buy instrumentation, including emission equipment	BB5
Construct loop	BB6

TABLE VIII-1 (continued)

TASK CODE USED IN DETAILED PROGRAM PLAN, FIGURE VIII-1

Task Description	Task Code
Breadboard Assembly, Installation, Checkout and System Testing in Breadboard Loop	
Install boiler and regenerator on breadboard loop	BB7
Install and test boiler, preliminary burner and control, regenerator in boiler loop	BT5
Install and test regenerator in boiler loop	RT3
Install system pump	BB8
Install expander on dynamometer	BB9
Install final combustion package	CS11
Install automobile condenser and drive	ET4
Install condenser ram air system	ET5
Test system	ET6
Install accessories and test	ET7
Final data reduction and programming	ET8
Shaft Seal and Static Seal	
Select rotary and static seals	SS1
Buffer pressure control - design	SS3
Buffer pressure control - fabricate	SS4
Incorporate in final expander design	SS6
American Bosch Valving	
Design, fabrication (valve actuator, high pressure supply, control and timer for single cylinder) and component tests	SV1

TABLE VIII-1 (continued)

TASK CODE USED IN DETAILED PROGRAM PLAN, FIGURE VIII-1

Task Description	Task Code
Performance and endurance test - first single cylinder unit	SV2
Performance and endurance test - second single cylinder unit	SV3
Design, fabrication and component tests (actuator, high pressure supply, control and timer for 4 cylinder expander)	EV1
Performance and endurance test - first four cylinder unit	EV2
Performance and endurance test - second four cylinder unit	EV2
Boost Pump, Jet Pump and Reservoir	
Design and drawings	BP1
Procure parts and build	BP2
Checkout test	BP3
Feedpump and Controls	
Design and layout	FP1
Detailed drawings	FP2
Procure parts, castings, etc.	FP3
Fabricate and assemble	FP4
Test and debug on current loop	FP5
Life and performance test and inspect	FP6
System Performance Prediction	
Burner-boiler controls, dynamic response prediction, program and study	SP1
Overall system performance prediction and optimization studies	SP2

TABLE VIII-1 (continued)

TASK CODE USED IN DETAILED PROGRAM PLAN, FIGURE VIII-1

Task Description	Task Code
Overall system performance prediction and optimization studies - continued	SP3
Combustion System (Burner, Blower, Fuel Pump and Compressor)	
Modify burner design and detail drawings	CS1
Modify current test facilities	CS2
Buy parts and build 2 burners	CS3
Preliminary burner test	CS4
Continue burner test	CS10
Select final fuel pump, blower and compressor	CS5
Procure final fuel pump, blower and compressor	CS6
Design, integrate and build combustion package (burner, components, controls, drives)	CS7
Test package	CS8
Fuel-Air Control System	
Combustion air system - concept and engineering analysis	CN1
Combustion air system - hardware design, specs and schematics	CN2
Fuel system - concept and engineering analysis	CN3
Fuel system - hardware design	CN4
Procure parts and components	CN5
Component assembly and instrumentation	CN6
Test, debug and analyze system	CN7

TABLE VIII-1 (continued)

TASK CODE USED IN DETAILED PROGRAM PLAN, FIGURE VIII-1

Task Description	Task Code
Condenser and Fan	
Condenser design and layout (By EPA condenser contractor)	CF1
Condenser detailed drawings (By EPA condenser contractor)	CF2
Fan design and layout (By EPA condenser contractor)	CF3
Fan detailed drawings (By EPA condenser contractor)	CF4
Fabricate and supply parts (By EPA condenser contractor)	CF5
Assemble and complete units (including frame, controls, mounts, drive)	CF6
Test in chassis mockup	CF7
Condenser Fan Controls	
Concept and eng.. analysis	CN8
Hardware design and specifications	CN9
Procure and fabricate parts	CN10
Assembly and instrumentation	CN11
Test and debug	CN12
Motors and Accessory Drives, Alternator, Battery, etc.	
Design and select components	M1
Detailed drawings	M2
Procure components and assemble 2 sets	M3
Efficiency tests	M4

TABLE VIII-1 (continued)

TASK CODE USED IN DETAILED PROGRAM PLAN, FIGURE VIII-1

Task Description	Task Code
Acceleration Control System	
Concept and hardware design	CN13
Procure parts (2 sets)	CN14
Assembly and instrumentation	CN15
Test and debug, install on breadboard loop	CN16
Safety and Startup Sequencing Controls	
Conceptual design	CN17
Hardware design and selection	CN18
Procure parts and assemble	CN19
Test for proper operation and install on BB loop	CN20
Automotive Accessories (Heater, Pressure Operated WW, P/S, A/C, etc.)	
Heating alternates and conceptual design	AX1
Detailed design of special components and selected standard components	AX2
Procure and/or fabricate	AX3
Test special components	AX4
Transmission and Driveline	
Finalize preliminary design of conventional transmission	TR1
Support detailed design effort by FOMOCO	TR2
Fabricate, assemble, test and modify as required	TR3

TABLE VIII-1 (continued)

TASK CODE USED IN DETAILED PROGRAM PLAN, FIGURE VIII-1

Task Description	Task Code
Transmission and Driveline (continued)	
Build and deliver units as required	TR4
Transmission and driveline analysis and optimization	TR5
Vehicle Integration and Mock-up	
Vehicle design and integration	V1
Layout drawings	V2
Detailed drawings, modifications, flow diagram and installation drawings	V3
Build mock-up	V4
Road Test Instrumentation	
Define requirements	I1
Design and layout	I2
Detailed drawings	I3
Procure parts	I4
Assemble and test as required	I5
Chassis Dynamometer Test Stand	
(including emission erupt. 1972 drive cycle)	
Procure equipment and instruments	CD1
Fabricate facility and install equipment	CD2

TABLE VIII-1 (continued)

TASK CODE USED IN DETAILED PROGRAM PLAN, FIGURE VIII-1

Task Description	Task Code
Preprototype Car (Breadboard Components)	
Procure (2 set) chassis, valves and other parts	PC1
Remove components from breadboard loop	PC2
Modify chassis and other components and integrate for car installation	PC3
Modify and install breadboard components and assemble complete car	PC4
Chassis dynamometer test	PC5
Limited road test and debug	PC6
Prepare operating manual	PC7
Prototype Car	
Incorporate modifications and improvements of various subsystems, detail design and drawings	C1
Procure parts for various subsystems, chassis and other parts for car (3 sets) (1 car, 1 spare, 1 BB test)	C2
Assemble subsystems, modify chassis and other components for car installation	C3
Install subsystems on breadboard loop	PC8
Test on breadboard loop	PC9
Remove components from breadboard loop	PC10

TABLE VIII-1 (continued)

TASK CODE USED IN DETAILED PROGRAM PLAN, FIGURE VIII-1

Task Description	Task Code
Prototype Car (continued)	
Modify and install subsystems in car and complete car assembly	PC12
Chassis Dynamometer Test	PC13
Limited Road Test	PC14
Report measured performance	PC15
Breadboard Test Prototype Components	
Install subsystems (second set) on BB loop	PC16
Test system	PC17
Test system - continued	PC18
Data reduction	PC19
Manufacturing Cost Estimate (of Prototype Design)	
Develop master material list	CE1
Determine make vs. buy items	CE2
Obtain quotes on buy items	CE3
Develop manufacturing strategy for make parts	CE4
Labor planning for make parts	CE5
Prepare direct and overhead cost estimates	CE6
Identify cost reduction opportunities	CE7.

PAGE NOT

AVAILABLE

DIGITALLY